Synthesis of Polymer Grafted Silica Nanoparticles: Effect of Grafting on Mechanical Reinforcement

Moussa Abrahim Saleh Khlifa

Submitted for the Degree of Doctor of Philosophy

Heriot-Watt University

School of Engineering and Physical Sciences

Institute of Chemical Sciences

August 2013

ABSTRACT

A series of polymer-silica nanocomposites were prepared by grafting poly(methyl methacrylate), poly(butyl acrylate), polystyrene and poly(styrene-*co*-acrylonitrile) from both aggregated silica nanoparticles and colloidally dispersed silica using atom-transfer radical polymerisation (ATRP). Cross-linking and macroscopic gelation were minimised by using a miniemulsion system. The grafted polymers silica nanoparticles were characterised using scanning electron microscopy (SEM), transmission electron microscopy (TEM), gel permeation chromatography (GPC), nuclear magnetic resonance (NMR), fourier transform infrared spectroscopy (FTIR) and elemental analysis.

The thermal and mechanical behaviour of the nanocomposites have been examined by differential scanning calorimetry (DSC) and dynamic mechanical thermal analysis (DMTA). Grafting polymers chains from the surface of the nanoparticles gave materials with a 10 ^{o}C higher glass transition temperature T_g (according to DSC and DMTA) compared to the pure polymers. DMTA measurements revealed that chain grafted nanocomposites showed an increased modulus and significantly lower high-temperature damping over the neat polymers. In contrast, samples prepared from colloidally dispersed silica nanoparticles exhibited a much less pronounced reinforcement effect than aggregated silica and also showed little change in T_g. Further information on the temperature dependence of the relaxation process was obtained using time temperature superposition.

A fast and efficient microwave-assisted method for ring-deuteration of polystyrene and poly(4-hydroxystyrene) using "superheated" C_6D_6 or D_2O in sealed microwave reaction vials has also been developed. The optimised procedure will make future work using neutron scattering possible.

Acknowledgments

I would like to express my sincere thanks to my research supervisors, Dr Valeria Arrighi and Dr Arno Kraft for their supervision, guidance, and constructive advices throughout the work. For technical assistance with this work, I thank Dr. Richard Langford (University of Cambridge) for SEM and TEM measurements and Professor Graeme Cooke at Glasgow University for GPC analyses.

Thanks are also due to Christina Graham for elemental analyses and Marian Miller for the SEM measurements. I would also like to thank Abdalslam Yossef, a fellow PhD student for his freely offered help in the synthesis of deuterated polymer.

Finally, I would like to thank my wife and my parents in Libya for their support and encouragements throughout my studies.

Table of Contents

Chapter 1 – Introduction

Contents

1.1 Preface

For polymeric systems, improved mechanical behaviour is traditionally achieved by the addition of fillers such as carbon black, clays, talc and silica. These composites have been widely studied and owe their success to their strength, light weight and low cost. The effect a filler material has on mechanical properties is easily apparent in rubber tyres. The first pneumatic tyres were made from crosslinked rubber but, unlike their modern counterparts, they did not contain any fillers, which even at low speed limited their service range to just a few thousand miles. The addition of up to 50% of carbon black improves the abrasion resistance of the rubber tyre tremendously. The nature of the reinforcement effect in polymer–filler composites has been extensively discussed in the literature. It is known that polymer–particle as well as particle–particle interactions play a very important role in determing the reinforcing ability of a composite. Particle pre-treatment is often a necessary step used to improve polymer–particle interactions.[1, 2] At high filler concentration, particle–particle aggregation may dominate the mechanical response with a consequent decrease in the level of improvement. Controlling the dispersion of fillers in a polymer matrix is crucial but not always straightforward: poorly bonded particles increase brittleness and lower the composite's resistance to crack growth.[3]

When filler particles are dispersed in a polymer, they can interact with polymer chains by hydrogen bonding and other intermolecular bonding forces such as dipolar interactions. Recently, surface functionalisation of filler nanoparticles with polymer brushes has gained attention.[4, 5] This route provides a unique opportunity to engineer the interfacial properties of these modified particles and increase their compatibility with a polymer matrix; also the thermal and mechanical properties of the matrices can be altered by covalently attaching the polymer to the filler nanoparticle. The preparation of polymer nanocomposites using sub-micrometer fillers with high surface–to–volume ratios is currently studied intensively in both industry and academia. Nanosize inorganic particles are known to produce larger improvements in mechanical properties compared to micron-sized fillers. Nanoparticles (i.e. particles having diameters of less than 100 nm) can be derived from metals (e.g. Au and Ag), metal oxides (e.g. TiO_2 and Al_2O_3), non-metal oxides (e.g. SiO_2), and semiconductors such as carbon nanotubes and graphene.[6-9] The presence of filler material restrains the mobility of the chains by introducing more physical cross-linking.[10, 11] While some filler materials are quite cheap

(typical examples being carbon black, talc and silica), others such as carbon nanotubes are much too expensive for use in all but specialty applications.[12]

New and reliable ways of making nanoparticles have led to an increasing interest in nanocomposites. Fillers influence the mobility of the polymer chains, and thus the glass transition temperature T_g, particularly in the vicinity of the filler's surface. This effect becomes even more pronounced for nanoparticles, particularly at high filler concentrations.

Silica nanoparticles have been shown to modify the properties of thermoplastic polymers and elastomers.[10, 13] Commercial applications of silica fillers range from tyres to shoe soles, from toothpaste to printing inks. Two recent developments have renewed the interest in cheap silica fillers. First, silica nanoparticles are commercially available both in aggregated and non-aggregated form, and their high surface–to–volume ratio promises excellent compatibility with many polymer matrices.[4] Second, new controlled radical polymerisation techniques have emerged for grafting polymers from the surface of silica and other nanoparticles which allow polymer and filler particle to become intimately linked to each other. From a chemical point of view, silica particles are relatively easy to functionalise and modify. In particular, a suitable surface treatment makes silica hydrophilic or hydrophobic, and thus helps to improve the filler's compatibility with the surrounding polymer matrix.

Several recent papers have demonstrated already that polymer chains can be grafted onto silica and alumina particles by controlled radical polymerisations.[14-16] Section 1.2 will describe the various types of silica nanoparticles that are available and of interest for this project.

Rühe first reported the successful attachment of polymers to silica nanoparticles by grafting an azo initiator to the silica surface, which was followed by a conventional radical polymerisation.[17-19] This and similar work will be discussed in **Section 1.3.1.** More recently, controlled radical polymerisation methods have been used to generate surface-grafted polymer chains. The general strategy involves the covalent linking of a suitable initiator onto the silica surface, followed by controlled radical polymerisation of a monomer. Contributions from termination reactions that are typical for conventional radical processes become, if not negligible, at least minimised in controlled radical polymerisations as the concentration of active radical species is

considerably reduced. This allows well-defined polymers to be synthesised with narrow molar mass distributions (M_w/M_n < 1.3) and predetermined degrees of polymerisation (DP = [monomer]/[initiator]). Most prominent amongst these are atom-transfer radical polymerisation (ATRP),[20, 21] nitroxide-mediated polymerisation (NMP)[22] and reversible addition–fragmentation–chain transfer (RAFT) polymerisation.[23, 24] The by far most popular method is atom-transfer radical polymerisation, which has the added advantage that the functionalisation of silica particles with a suitable initiator is straightforward and allows polymer chains to be grown from the silica surface in a narrow size distribution. For this reason, ATRP was used in this work and will be discussed in detail in **Sections 1.3.2** and **1.3.2.1**.

Atom-transfer radical polymerisation has been successful in controlling molecular weight and polydispersity of various surface-grafted polymers, such as polystyrene (PS), poly(methyl methacrylate) (PMMA), poly(butyl acrylate) (PBA) and poly(styrene-*co*-acrylonitrile) (PSAN),[18, 25-33] and even block copolymers.[15, 34] In contrast, nitroxide-mediated seems to be more restricted with regard to the choice of monomer and require a more elaborate synthesis for the surface initiating group.[22, 24]

1.2 Silica Nanoparticles

In general, silica plays an important role in nature and technical applications.[35] The most important advantage of silica is that different morphologies are commercially available or they can be prepared in the laboratory.

Colloidal silica is easy to make with precise control of the size and distribution.[36] Stöber *et al*.[37] reported a simple process to synthesise monodisperse spherical silica particles via hydrolysis of tetraethyl orthosilicate (TEOS), followed by condensation of silicic acid in an alcoholic solution and ammonia (catalyst) (**Figure 1.1)**. The resulting particles are in the range less than 0.05 μm to 2 μm in diameter. This process was improved later by many others.[38-43] Osseoasare and Arrigada[43] synthesised monodisperse silica particles in the range of 50 to 70 nm by controlled hydrolysis of TEOS in a non-ionic surfactant/ammonium hydroxide reverse microemulsion. This technique is extensively used to prepare silica nanoparticles.

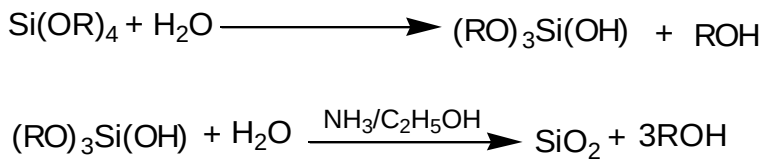

Figure 1. 1: Synthesis of silica particles by the Stöber process.

More recently, silica nanoparticles have become commercially available in both aggregated and non-aggregated form of varying sizes. The aggregated nanosilica is mostly produced in industry by the fuming method or the precipitation process. Fumed silica is manufactured by high–temperature hydrolysis of chlorosilanes ($SiCl_4$) vapour in an oxygen-hydrogen flame[44] (**Figure 1.2)**. It is a fine and tasteless amorphous powder. In the precipitation process, hydrated silica particles are obtained by treating silicates with mineral acids.[45] Even though aggregated silicas are more widely used, lack of particle stabilisation during preparation of the composites limits their application in polymer technology.[46] Therefore, non-aggregated silica nanoparticles have more recently attracted interest in many polymeric systems due to the precise control of particle size and distribution they offer. Commercial colloidal silica are often prepared in a sol form, with water or other solvents as the dispersing medium.[45]

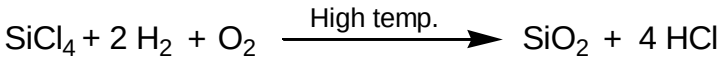

Figure 1.2: Synthesis of fumed silica particles by high-temperature vapour method.[44]

The surface of silica is usually terminated with three types of silanol groups at the time of manufacturing: isolated or free silanols, vicinal silanols (hydrogen-bonded) and geminal silanols (**Figure 1.3**).[4] The silanol groups on the surface of the silica have the ability to form hydrogen bonds which lead to the formation of aggregates. These hydrogen bonds hold the particles together and the aggregates remain intact even in the best mixing conditions.[9]

The dispersion of silica nanoparticles in a polymer matrix can have a significant impact on the performance of the material; however changes in rheology and mechanical properties are usually only observed when the nanoparticles are highly dispersed within the polymer matrix (**Figure 1.4**).[47, 48] The higher the surface area of the particles the higher the number of particle−polymer interactions that occur which leads to restriction of chain mobility. The interfacial interaction between polymer and silica

nanoparticles is the most important factor affecting the properties, e.g. mechanical reinforcement, of the resulting nanocomposites.[2] Absence of polymer−particle interactions leads to phase separation.

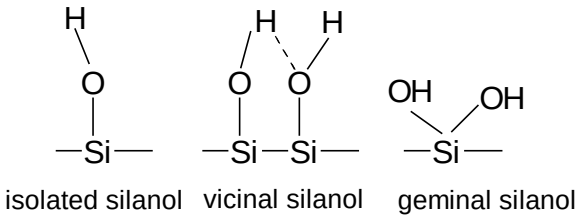

Figure 1.3: Schematic diagram showing possible surface groups in silica particles.[4]

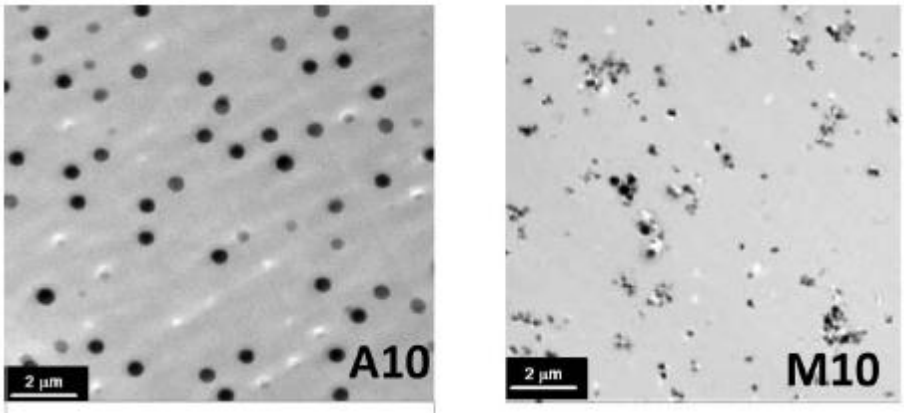

Figure 1.4: TEM images of (a) homogeneously dispersed silica nano-particles and (b) aggregated silica nanoparticles.[48]

1.3 Surface Modification of Silica Nanoparticles

In general, the modification of the surface of silica nanoparticles to enhance the compatibility between the silica and polymer can be carried out either via a chemical reaction or a physical process (physisorption).[49] Modification of the surface of silica nanoparticles by a chemical reaction is preferred since it leads to much stronger interactions between nanosilica and modifier. This method involves modification either with modifier agents (silane coupling agents) or by grafting polymer chains to the surface of silica. A highly popular method for surface functionalisation is the reaction of silanol groups with silane reagents in a suitable solvent such as toluene. The general formula of the coupling agents is $RSiX_3$, where X represents the hydrolysable group and R represents the organofunctional end group. The hydroxyl groups on the surface of silica can be reacted with the functional group X, while the alkyl chain reacts with the

polymer to obtain hydrophobic silica (**Figure 1.5**).[2] **Table 1.1** shows a selection of the wide variety of silane coupling agents used for modification of silica nanoparticles. One of the most commonly used is 3-methacryloxypropyl trimethoxysilane (MPS).[2] In addition, tolylene-2,4-diisocyanide (TDI),[50] glycidyl phenyl ether (GPE)[51] and epichlorohyrin[52] have also been reported as modifier agents.

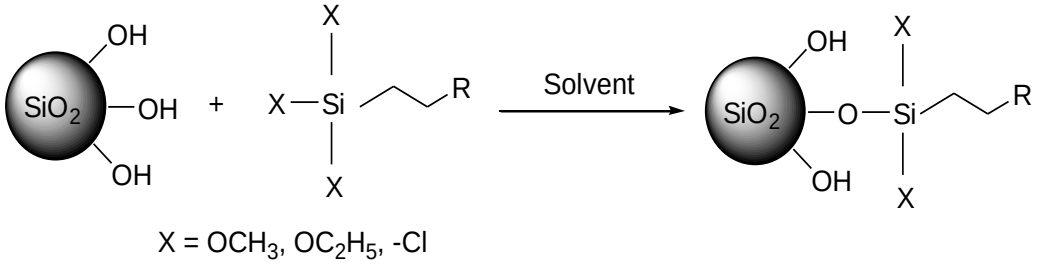

Figure 1.5: Schematic diagram of surface modification of silica particles.

Table 1.1: Typical silane coupling agents used for modification of nanosilica.

Name and abbreviation	**Ref.**
Aminopropyl methyldiethoxysilane (APMDES)	53
3-Aminopropyltriethoxysilane (APTEOS)	54
3-Aminopropyltrimethoxysilane(APTMOS)	23
(3-Acryloxypropyl)methyldimethoxysilane (APMDMOS)	55
3-Glycidoxypropyltrimethoxysilane (GPS)	22

Grafting polymer chains to the surface of silica is preferred to achieve maximum interfacial compatibility between the polymer and nanosilica. There are two main methods to chemically attach polymer chains to the surface of silica nanoparticles: the "grafting from" and "grafting to" methods. These methods create a much stronger adhesion between the polymer chains and the surface through covalent bonding. Without any modification, silica particles are agglomerated due to strong polar interactions between them. Therefore polymer chains attached to the modified silica reduce interactions between particles, achieving stable dispersions, while inhibiting further agglomeration due to the creation of a compatible interface (**Figure 1.6**).[56]

In the "grafting from" technique, which is also commonly called surface-initiated polymerisation,[56] the initiator is attached to the surface of the silica nanoparticles followed by polymerisation of the monomer (M), leading to the formation of the so-called " polymer brushes" (**Figure 1.7**). This method can be used to obtain thick polymer brushes with high grafted density on the silica surface. Various polymerisation techniques have been employed to synthesise polymer brushes via this method, including conventional free radical,[57, 58] controlled radical,[14, 15, 25] anionic,[59] cationic[60, 61] and ring opening polymerisation.[62] On the contrary, in the "grafting to" approach, end-functionalised polymers are first synthesised with end-capped groups or side chain groups and then reacted with the surface of the silica. This method has the drawback of producing low graft density due to steric crowding of reactive sites by already attached chains on the surface, which hinder diffusion of additional chains.[56] It has the advantage, however, that it is a simpler method and the polymer chains can be characterised before attaching them to the surface of the silica.

Mora-Barrantes *et al*.[56] studied ATRP of styrene from the surface of silica particles using both synthetic methods. They reported that the "grafting from" yields a dense layer covering the nanoparticle, and the "grafting to" method also provides a well-controlled polymer chain attached on silica but with a lower graft density.

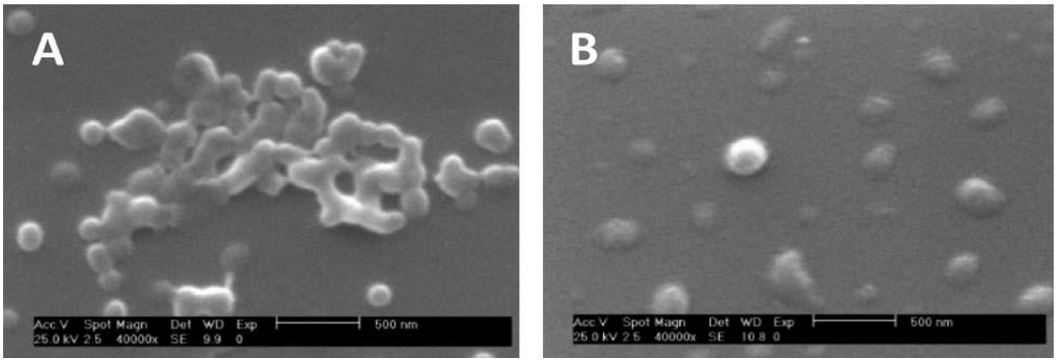

Figure 1.6: SEM micrographs of (A) unmodified fumed silica and (B) polymer/silica hybrid particles.[56]

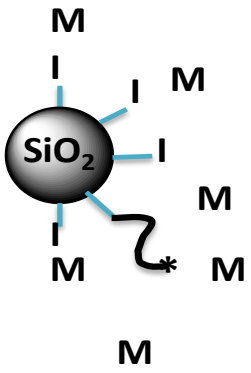

Figure 1.7: "Grafting from" technique for surface modification.[63]

Physical methods were also used to functionalise the surface of the silica nanoparticles with polymer chains by using either surfactants or macromolecules adsorbed onto the surface of the nanosilica. Surfactants reduce the interaction between the silica particles by reducing the physical attraction. This allows the modified nanosilica to be easily incorporated into a polymer matrix, resulting in an improved dispersion of the silica in the composites.[64] For instance, stearic acid[65] and oleic acid[66, 67] have been used widely as surfactants to improve the dispersion and the adhesion between the silica and polymer matrix.

To date, three major routes have been reported for the preparation of silica nanocomposites: blending, sol-gel and in-situ polymerisation processes (**Figure 1.8**).[4] The blending process is a simplified method for preparing silica nanocomposites by mixing the silica into the polymer. The mixing can be done either by solution blending and melt blending. The main difficulty in this method is always to achieve an effective dispersion of the silica into the polymer matrix, due to the strong trend of particles to agglomerate.[4] In the solution blending technique the composites are obtained by mixing silica nanoparticles and polymer in a solvent. This technique requires continuous stirring to avoid any agglomeration.[68] Its advantage is that it brings about a well molecular level of mixing and can overcome the limitations of the melt mixing method. The method works well for many polymers. However, solution blending has some disadvantages. For example, a suitable solvent is not always easy to find and it is essential to remove solvent completely after processing since it may act as a plasticizer.

Melt blending is done by mixing the polymer with the silica nanoparticles above the melting point of a semicrystalline polymer or above the glass-transition temperature

(T_g) of an amorphous polymer.[69] This method is most commonly used because of its efficiency and operability. Münstedt *et al*.[70] prepared PMMA composites with silica particles of different sizes through the blending method. Characterisation of the polymer composites by SEM and TEM showed that the silica particles were fairly well dispersed in the matrix. A series of PS/SiO_2 nanocomposites were also prepared by the melt mixing method.[71, 72] A good distribution of silica particles in PS matrix was observed in the SEM image. However, increasing the silica content in polystyrene nanocomposites was found to lead to larger agglomerates.

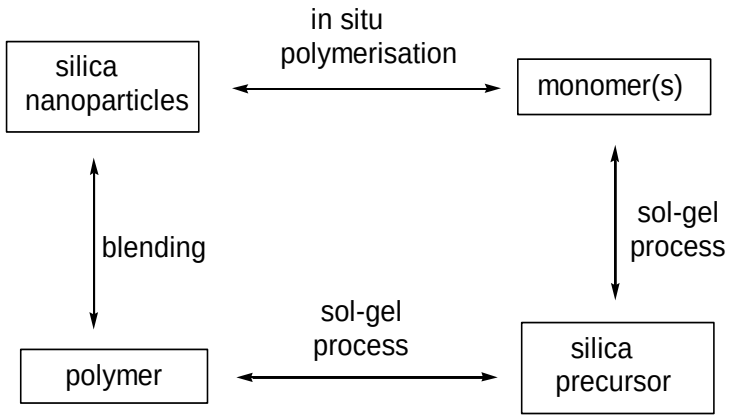

Figure 1.8: The three general approaches to prepare silica nanocomposites.

1.3.1 Surface Modification using Conventional Radical Polymerisation

Conventional free radical polymerisation is one of the most important methods of producing polymers. One of the major virtues of radical polymerisation is its tolerance to functional groups and impurities and its applicability to a wide range of monomers and under a wide range of conditions. Although controlled polymerisation techniques yield well-defined polymers with narrow polydispersities, problems such as limited choice of monomers, solvents, long reaction times to achieve high monomer conversions and the need to remove metal catalysts have restricted their use on a large scale. Since conventional radical polymerisation presents none of the problems associated with controlled polymerisations, it is the leading industrial process to produce polymers.

Radical polymerisation consists of four basic elementary stages:[73] initiation, propagation, termination and chain transfer. Initiation involves two steps: generation of initiator radicals and then reaction of these radicals with monomers. Typical initiators such as diazo derivatives and peroxides are used at concentrations between 1 to

0.01 mol%. Propagation occurs by the repetitive addition of a growing polymer chain radical to the double bond in the monomer. Termination occurs when two active chains combine. The fourth step is chain transfer. Chain transfer can occur to a monomer or to a polymer chain. If the transfer occurs to a polymer, branched, or in extreme cases crosslinked polymers will form. In practice, the polydispersity tends to be above 2.[74, 75]

Prucker and Rühe[17, 18] first reported the successful attachment of polystyrene to silica nanoparticles. In 1998 these authors attached an azo initiator **A** onto the surface of the silica particles and carried out conventional radical polymerisation using styrene as a monomer. The immoblisation of the azo initiator, onto the surface of the silica and the principles of the conventional radical-chain polymerisation of styrene are displayed in **Figure 1.9**. Their procedure led to high molecular weight polymer brushes with high graft density. However, half the PS produced was not covalently attached to the surface of silica, because of the formation of initiator radicals in the solution. The unattached polymer (free polymer) was removed by extracting the polymer-modified silica several times with toluene via centrifugation, until no precipitate formed when the supernatant solution was added to an excess of methanol. In this case about 5 − 10 cycles were sufficient to remove all free polymer.

Ueda *et al*.[75] investigated the radical polymerisation of styrene and MMA onto silica nanoparticles initiated by an azo and peroxycarbonate groups. The azo group was introduced by the reaction of surface amino groups with *4,4′*-azobis(4-cyanopentanoyl chloride) (ACPC). On the other hand, the introduction of peroxycarbonate group onto the silica surface was achieved by Michael addition of *t*-butylperoxy-2-methacryloxyethylcarbonate (MEC) to amino groups. Thus silica nanoparticles coated with an azo initiator and a peroxy initiator were prepared separately (**Figure 1.10**). The grafting efficiency onto the surface of silica was extremely high and formation of un-grafted polymer (free polymer) was reduced in comparison with Rühe's approach.

Polymers made by a conventional free radical polymerisation technique are generally characterised by a broad molecular weight distribution and poor control of end chain functionality. However, many of these drawbacks can be easily avoided by using controlled radical polymerisation.

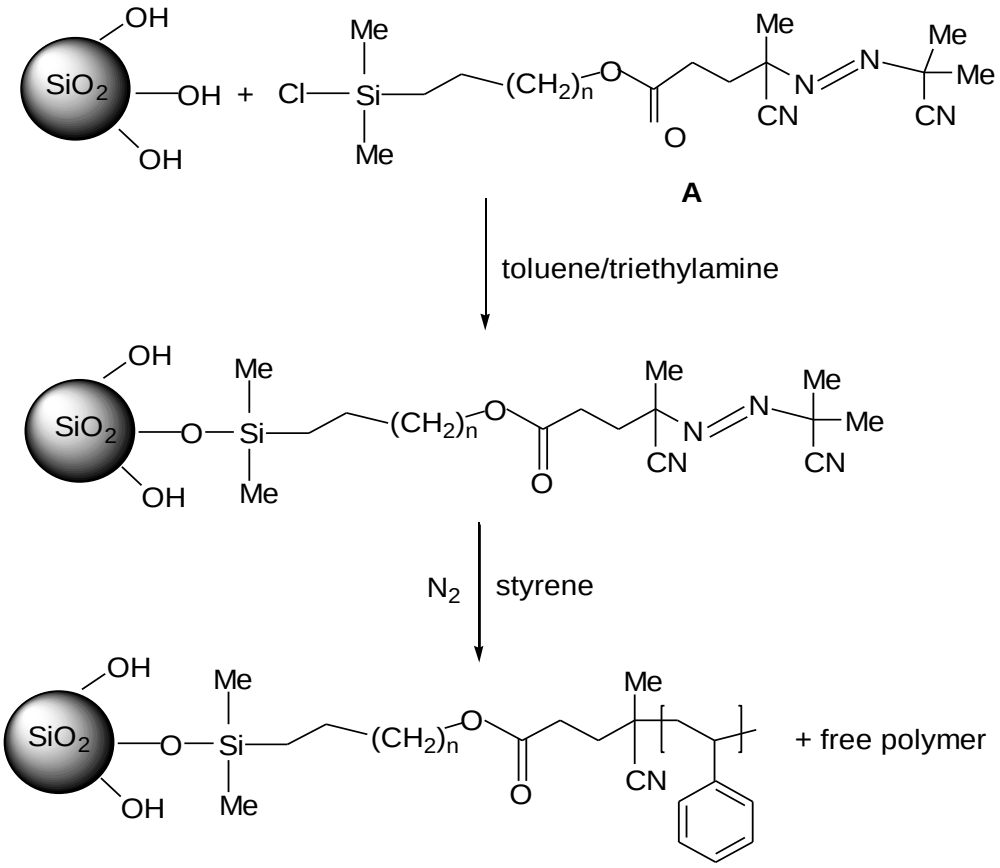

Figure 1.9: Reaction scheme for the synthesis of covalently attached PS on silica using surface immobilised azo initiator.

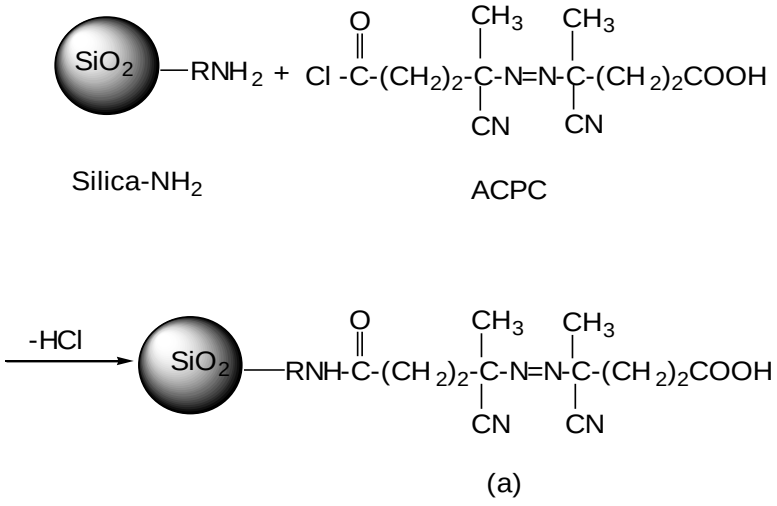

Figure 1.10: Nanosilica particles immobilised with free radical initiators: (a) Silica-azo and (b) silica-peroxy initiators.

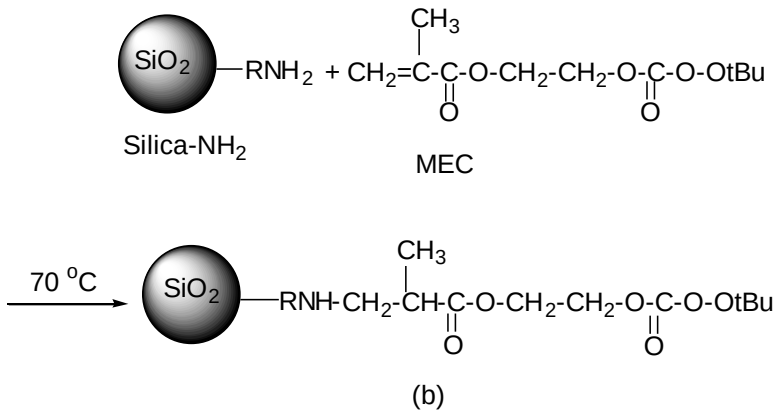

(b)

1.3.2 Surface Modification using Controlled Radical Polymerisation

Controlled/living radical polymerisations (LRP) have attracted a great deal of attention due to their ability to polymerise a wide range of monomers. In addition, experimental conditions are simple and easily adjustable to cover bulk, solution, suspension and emulsion polymerisations.[75] Unlike the conventional radical process, in controlled radical polymerisation the contribution of the inevitable and irreversible termination reactions are negligible. As a consequence, well-defined polymers can be synthesised with narrow molecular weight distributions.[76]

Recently, controlled radical polymerisations have been used to graft polymer chains from the surface of silica nanoparticles. This process is attractive for two reasons.[77] First, the silica surface onto which initiating groups are located confers a mobility barrier for termination. Second, only a limited amount of initiating groups need to be attached to the silica's surface, therefore the free active radical species present in the polymreisation process was reducing.

The main difference between controlled radical polymerisation and conventional radical polymerisation is that the steady concentration of free radical in an LRP is established by balancing rates of activation and deactivation, whereas in conventional radical polymerisation the rates of termination and initiation are balanced. For an LRP, the rate of initiation must be large, but the rate of propagation must be much lower. Finally, the rate of termination should be low (or virtually zero in ATRP). This allows initiation of all chains simultaneously and therefore control over various polymer architectures.

The most studied controlled radical polymerisations are nitroxide mediated polymerisation,[22, 78] reversible addition fragmentation chain transfer polymerisation,[24,

[53, 79] and atom transfer radical polymerisation.[20, 21, 29, 80] These three controlled radical polymerisation processes are being increasingly used nowadays to graft polymer chains from the surface of substrates such as glass or silica particles. ATRP is often preferred as the procedure is simple and initiators are easily made compared to RAFT and NMP.

1.3.2.1 Surface Modification using ATRP

ATRP is regarded as one the most successful techniques which has been applied to surface-initiated graft polymerisation on a variety of materials including fine particles such as silica and gold nanoparticles,[81-83] flat substrates[82] and porous materials.[83] ATRP is compatible with a variety of functionalised vinyl monomers (e.g. styrene, acrylates and methacrylates). However, some monomers are not suitable for ATRP (such as acrylamides, vinyl chloride, vinyl ethers/esters). The controlled character of the ATRP process yields polymers with a narrow polydispersity which are end functionalised and so can be used as macroinitiators for the synthesis of di-block and triblock copolymers.[49]

The first successful attempt at performing an ATRP was carried out by Matyjaszewski *et al.*[84] and Sawamoto *et al.*[85] in the mid 1990's. Since then ATRP has been a highly useful technique for the synthesis of different polymer architectures and morphologies (such as star, comb, branch, and cyclic polymers).[27, 86-88] Matyjaszewski's group carried out the first polymerisation of styrene, using an alkyl chloride (1-phenylethyl chloride), CuCl and *2,2'*-bipyridine (bpy) as initiator, catalyst, and ligand respectively. Sawamoto *et al.*[85] were able to achieve the polymerisation of MMA initiated with CCl_4 and $[RuCl_2(PPh_3)_3]$ as a catalyst with methylaluminum bis(2,6-di-tert-butylphenoxide), $MeAl(ODBP)_2$, as a ligand.

The transition metal catalyst in ATRP is used for activation and deactivation of the initiator. The polymerisation uses a copper(I) catalyst which gets oxidised to Cu(II). There are other less common catalysts such as Fe(II),[89] Ni(II),[90] and Pd(II)[91] that can also be used. The complex between a transition metal catalyst and a ligand (L) removes the halogen atom (X) from the alkyl halide initiator (or the dormant species P_n-X), generating a polymer radical ($P_n^{\bullet}$, active form), and a halogen-catalyst complex. The rate constant of activation k_{act} is generally much smaller than the rate constant of deactivation k_{deact}, thus ensuring that the equilibrium is very much on the side of the dormant radical species.

Propagation occurs when active chains $P_n^{\bullet}$ react with the monomer with rate constant of propagation, k_p. Termination occurs when two active chains combine with a rate constant of combination, k_t, and is minimised because the $P_n^{\bullet}$ concentration is deliberately kept very low so that the majority of chains are in the deactivated state at any given time (**Figure 1.11**).[80] The controlled nature of ATRP is a result of the reversible activation-deactivation reaction between a copper-ligand species and the growing polymer chains.[73, 74, 80]

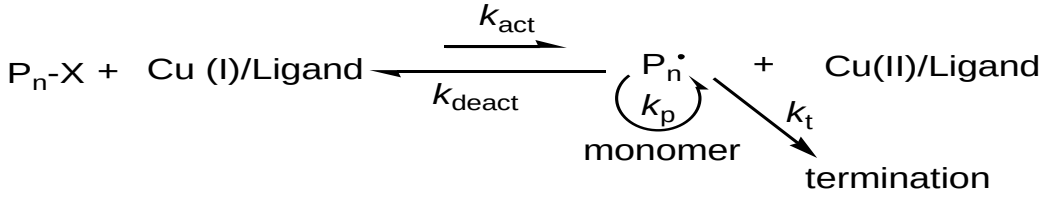

Figure 1.11: Schematic illustration of ATRP mechanism.[80]

Alkyl halides R-X (X = Cl, Br),[92-94] α-halo esters[95] or sulfonyl halides[96] serve most commonly as ATRP initiators for vinyl monomers such as styrene or methacrylates which are activated by the presence of metal catalyst salts. The ligand increases the solubility of the inorganic salt, thus facilitating the abstraction of halogen atoms from the initiator, P_n-X. The number-average molecular weight M_n of polymers synthesised by ATRP depends on the the monomer (M) to initiator (RX) ratio as well the monomer conversion:[97]

$$M_n = M_0 \; RX_0 \times Con \times M_w \; M \qquad (\mathbf{1.1})$$

where M_0 and RX_0 are the initial concentrations of the monomer and alkyl halide respectively, Con is the monomer conversion, and M_w(M) is the molecular weight of the monomer. The alkyl halide initiators can contain either one or more halogen atoms. The architecture from linear to star-like of the prepared polymers depends on the exact initiator structure and the number of the halogen atoms.

The facile polymerisation via ATRP and less stringent experimental conditions promoted the application to brush growth on nanoparticles, especially silica. Several groups investigated the synthesis of hybrid nanoparticles with different monomers. Tsujii *et al*. first succeeded in synthesising a dense brush of low polydispersity PMMA

via surface initiated ATRP with Cu^{I} ligand complexes. A commercially available silane-coupling agent, 2-(4-chlorosulfonylphenyl)ethyltriethoxysilane (CTS) was immobilised onto silicon surface to form a covalent bond by coupling with the silanol groups on the surface of the silicon.[98] Hedrick *et al*. prepared alkoxyamines and haloesters of silane coupling agents and successfully grafted MMA by surface initiated ATRP using a Ni complex.[95] The main advantage of using those initiators is that the alkoxyamine or R-haloester initiating groups are more stable than the azo-based initiators of Rühe.[17, 19] The grafted PMMA obtained may be controlled poorly due to a low concentration of initiators immobilised on the surface. However, the addition of free initiator to polymerisation solution produced free polymer which helped in controlling the polymerisation. Another advantage of the produced free polymer is that it can be characterised by conventional methods. Good agreement in the molecular weight and polydispersity (PDI) between the free and grafted polymers cleaved off silica nanoparticles has been already reported in the literature.[15, 99, 100] Patten and von Weren reported the first "grafting from" functionalisation of silica with polymer brushes using ATRP.[25] Their technique included immobilisation of the initiator (2-(4-chloromethylphenyl)ethyl) di-methylethoxysilane (CDES) on the surface of nanoparticle in the presence of ethanol, followed by a surface-initiated ATRP of styrene as shown in **Figure 1.12**. TEM micrographs and dynamic light-scattering (DLS) measurements of the CDES-modified particles showed no evidence of particle aggregation. Well-defined polymer chains were grown from the surface with high grafted density.

In later work, Patten and von Weren studied extensively the ATRP of styrene and MMA on various functionalised silica particles with diameters in the range of 75 − 300 nm under different conditions.[14] They found that the polymerisation of styrene from smaller particles with a 75 nm diameter exhibited a good molecular weight control, while polymerisations of methyl methacrylate from the same nanoparticles showed a higher degree of control only when a small amount of free initiator was added. The authors suggested that the styrene monomer could undergo thermal self-initiation while MMA did not. On the other hand, lack of control was observed in the polymerisation of both styrene and MMA from larger particles with a 300 nm diameter. However, good control was again induced by the addition of a small amount of free initiator or deactivator. Matyjaszewski *et al*.[101] conducted similar work to Patten and von Weren without added free initiator. Instead these authors added a small amount of $Cu(II)Br_2$ to

act as deactivator. In this case, no free polymer was formed, and hence no additional process was required to remove the free polymer. In that study, hybrid nanoparticles were prepared by ATRP of styrene, *n*-butyl acrylate and MMA monomers from surfaces of colloidal silica nanoparticles.

A new route for preparing ATRP initiator-grafted nanoparticles was described by Carrot *et al*. who successfully grafted styrene onto silica nanoparticles.[28] In this case, silica particles were kept in dimethylacetamide (DMAc), during the modification and the polymerisation to avoid any aggregation. Control of both the molecular weight and the density of grafted polystyrene chains were achieved. ATRP was also applied under mild conditions in aqueous media. Armes *et al*. were the first to report that ATRP of a hydrophilic monomer in aqueous media at 20 ^{o}C with various initiators.[30] In one example, the silica particles were dispersed in water and the hydrophilic methacrylate monomers were dissolved along with the ATRP catalyst in a second aqueous solution. The two solutions were mixed together and, after approximately 2 h at 20 °C, the polymerisation was terminated by exposure to air. The resulting silica-polymer hybrid particles could be dispersed in water.

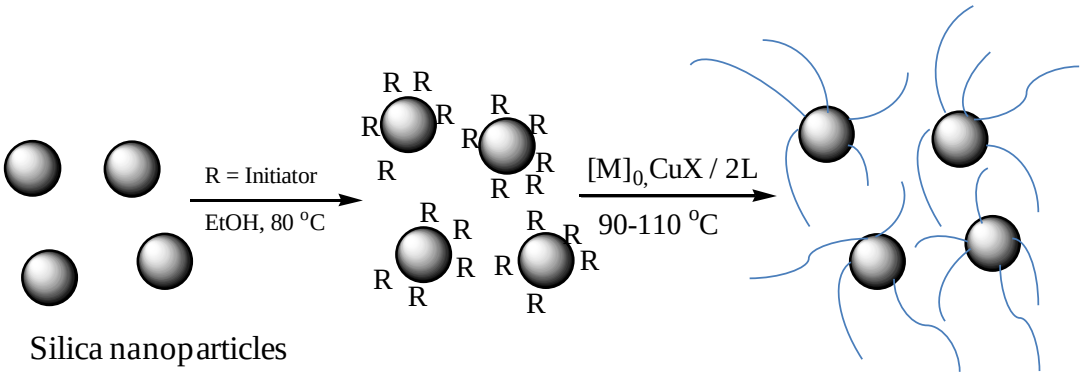

Figure 1.12: Synthetic scheme for the preparation of polymer grafted silica nanoparticles by ATRP.

A novel approach to synthesise well-defined mixed PMMA/PS brushes from an asymmetric difunctional initiator was reported by Zhao and He using a combination of surface initiated ATRP and NMP.[102] The mixed PMMA/PS brushes were successfully synthesised by sequential ATRP of MMA and NMP of styrene. ATRP of MMA was conducted first and NMP used to add the second polymer (PS) due to the activation of ATRP initiator by a metal complex is a bimolecular process, while the free radicals in NMP are generated by thermal decomposition. A similar strategy was also reported by

Zhao *et al.*[26] to synthesise poly(*tert*-butylacrylate) (P*t*BuA)/PS brushes from silica particles. Kinetic studies confirmed that the polymerisation was controlled.

More recently, Matyjaszewski and co-workers reported controlled polymerisation of PMMA brushes without added free initiator using their newly developed technique, activator generated by electron transfer (AGET) ATRP (**Figure 1.13**).[103, 104] In this technique, the catalyst is introduced in its oxidatively stable state and is subsequently activated by a non-radical-forming redox reaction with a reducing agent such as glucose[105] or ascorbic acid.[15] AGET ATRP does not require deoxygenation and can be carried out in the presence of a small amount of copper catalyst, even down to ppm levels and an excess of reducing agent.[106] Compared to normal ATRP, the AGET ATRP less stringent experimental condition required make this technique more applicable for use by scientists and in an industrial setting. Surface-initiated AGET ATRP was applied not only to methyl methacrylate (MMA) but also to monomers such as styrene,[107] styrene/acrylonitrile mixtures[108] and *n*-butyl acrylate.[109] AGET ATRP in miniemulsion was also used to graft *n*-butyl acrylate from silica particles.[109] In comparison to the bulk polymerisation, miniemulsion allowed the preparation of PBA-silica with higher monomer conversion, and a higher rate of polymerisation without the danger of macroscopic gelation. Atomic force microscopy (AFM) characterisation provided evidence for the formation of well-controlled hybrids.

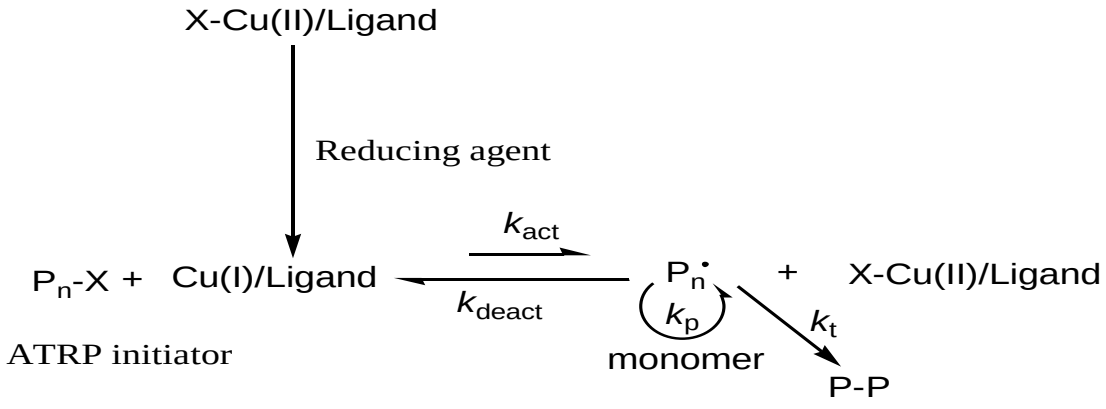

Figure 1.13: Schematic illustration of AGET ATRP mechanism.[110]

1.3.2.2 Surface Modification using RAFT

The modern RAFT polymerisation technique that is commonly used today was developed in 1998 by Moad and co-workers.[111] The RAFT technique can be used for a wide range of vinyl monomers under a variety of experimental conditions (solution, emulsion, and suspension). However, due to reactivity differences, the appropriate RAFT agent must be selected for each monomer of interest. A typical RAFT agent has a thiocarbonylthio group (S = C-S) unit with substituents R and Z (**Figure 1.14**). In general, RAFT agents such as dithioesters[112] and trithiocarbonates[113] are able to control the polymerisation of "more-activated" monomers (styrene, methyl acrylate and methyl methacrylate), meanwhile dithiocarbamates[113-115] and xanthenes[116] work well in controlling the polymerisation of "less activated" monomers, such as vinyl acetate and *N*-vinylcarbazole. The mechanism of a RAFT polymerisation involves a sequence of reversible addition-fragmentation and chain-transfer equilibrium steps as displayed in **Figure 1.15**.[53, 112] After initiation, the initiating, and later propagating radical ($P_n^{\bullet}$), adds to the RAFT agent **1.** This is followed by fragmentation of the intermediate RAFT radical **2** resulting in new RAFT agent **3** and release a new radical ($R^{\bullet}$). This radical reinitiates the reaction and forms a second propagating radical ($P_m^{\bullet}$). The final step is in equilibrium between propagation radicals ($P_n^{\bullet}$ and $P_m^{\bullet}$), and dormant polymeric RAFT agents **3.** A rapid equilibrium is necessary for all chains to grow with the same probability, leading to a desirable defined molecular weight and low polydispersity.

RAFT polymerisation has an advantage over other controlled polymerisation techniques (ATRP and NMP) due to its increased versatility. It can be used for a variety of different monomer functionalities from styrene to acrylates and dienes. It also can be used on vinyl acetates which have a disappointingly low reactivity under ATRP polymerisation,[117] and RAFT polymerisation has been used extensively in the synthesis of cyclopolymers, block copolymers and star polymers. It is also a common method of grafting polymers from the surface of nanoparticles and has been used on a variety of different monomer substrates.[118, 119]

A few research groups used the RAFT process to synthesise polymer brushes on silica nanoparticles. Baum *et al*. applied RAFT techniques to synthesise brushes of PS, PMMA, poly(*N*,*N*-dimethylacrylamide) (PDMA) and their copolymers.[120] The controlled nature of PMMA polymerisation was confirmed by the similarity between M_w values (and low PDI) of both cleaved PMMA from the surface of the particles and the free PMMA from the solution.

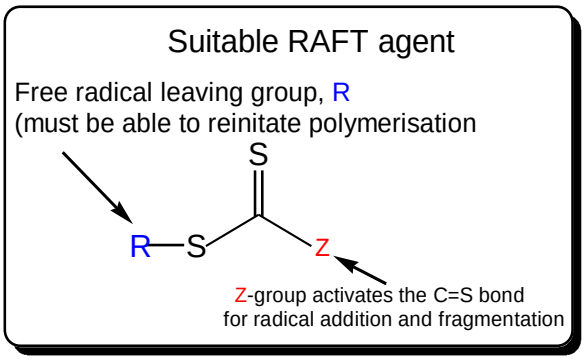

Figure 1.14: General structure of a RAFT agent.

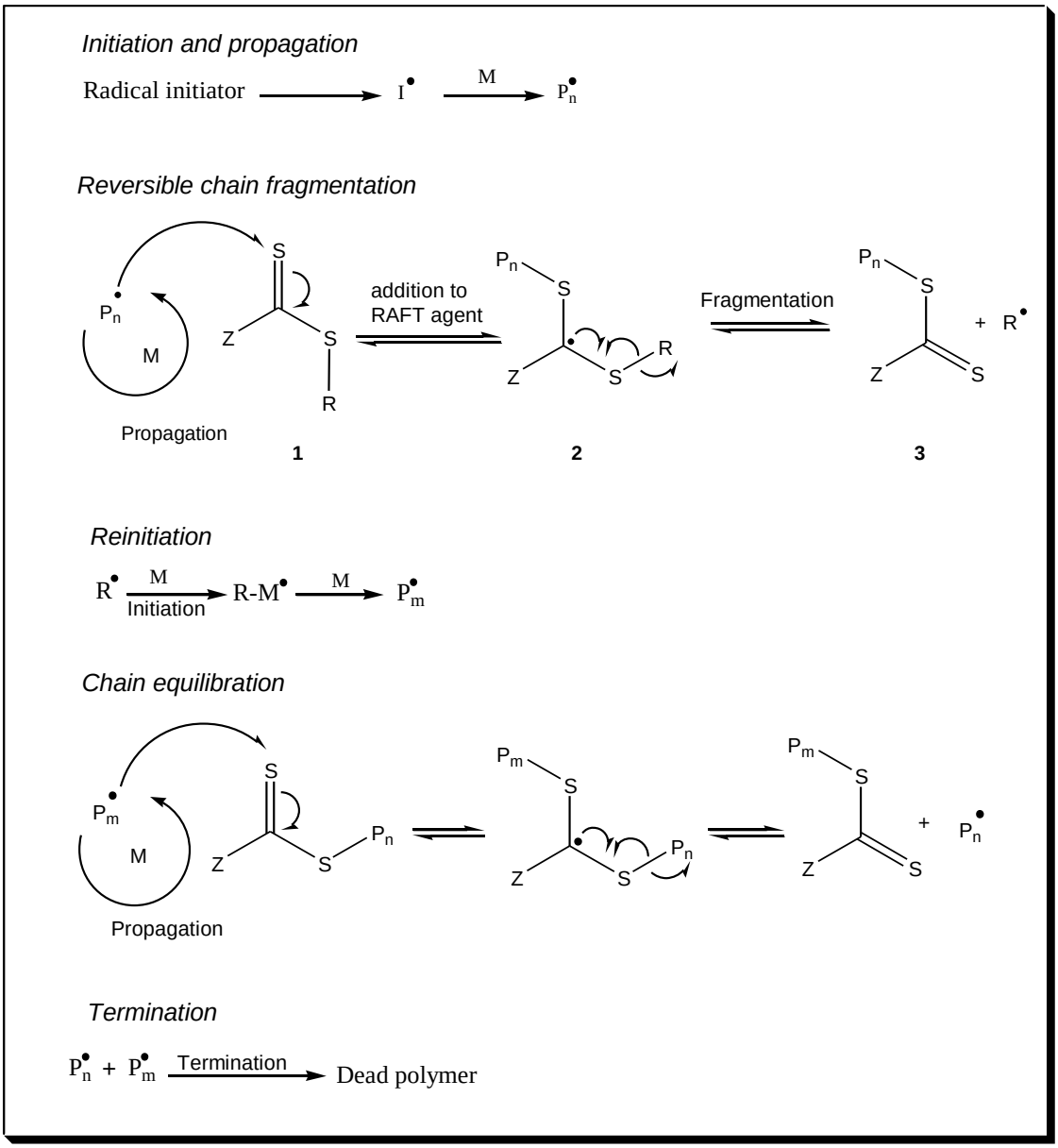

Figure 1.15: General scheme for the RAFT polymerisation mechanism.[53, 112]

1.3.2.3 Surface Modification using NMP

Like ATRP, nitroxide mediated polymerisation is also based on the concept of an activation-deactivation equilibrium between an initiator and an active species, but makes use of a stable nitroxide radical without the need of a catalyst (**Figure 1.16**). The polymerisation is thermally initiated in the absence of metal catalyst or an external radical source.

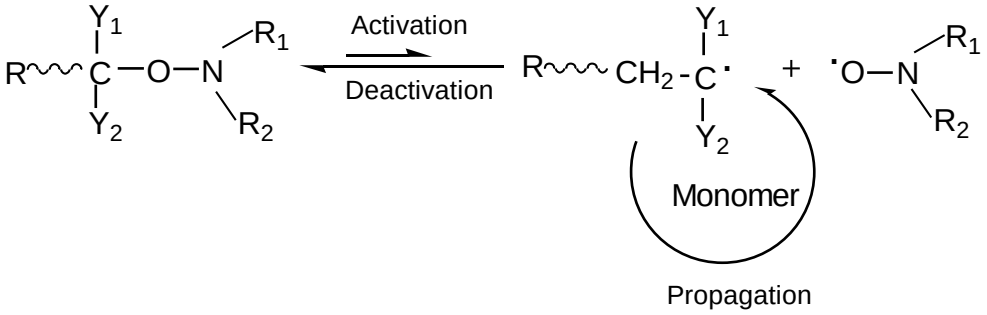

Figure 1.16: General scheme for activation-deactivation equilibrium in NMP.[121]

NMP is usually mediated by stable nitroxide radicals as outlined in literatures.[122-124] It is important that the nitroxide radicals can reversibly react with the growing chain but do not initiate polymerisations. Initiators are usually made by decomposing a conventional thermal initiator, such as *2,2`*-azobisisobutyronitrile (AIBN) or benzoyl peroxide (BPO), in the presence of monomer and a stable free nitroxide such as *2,2,6,6*-tetramethylpiperidinyl-1-oxy (TEMPO).[121] This system has certain advantages: it requires the same initiator as in a conventional radical polymerisation and only adds a free nitroxide. Georges *et al*.[122] first reported in 1993 that PS with narrow polydispersity could be synthesised by the NMP technique. Then a number of homopolymers and block copolymers were prepared by NMP using a nitroxide initiator based on TEMPO and BPO.

The first successful attempt at performing an NMP version of a surface-initiator polymerisation was carried out by Hedrick *et al* .[95] They succeeded in high density grafting PS using surface-bound alkoxyamine initiators on silicon wafers. Subsequently, Bartholome *et al*. prepared PS brush on functionalised silica nanoparticles in two steps.[125] First, an NMP initiator (triethoxysilyl-terminated alkoxyamine) based on *N*-*tert*-butyl-*N*-(1-diethylphosphono-2,2-dimethylpropyl) nitroxide (DEPN) (**Figure 1.17**), was covalently attached onto silica particles. Second, polystyrene was grown from the

DPEN functionalised nanoparticle's surface. The polymerisation was carried out in toluene and free nitroxide was added which helped in controlling the polymerisation as illustrated by **Figure 1.18**. Control of the molecular weight of both grafted polystyrene chains and free polymer can be achieved by this process.

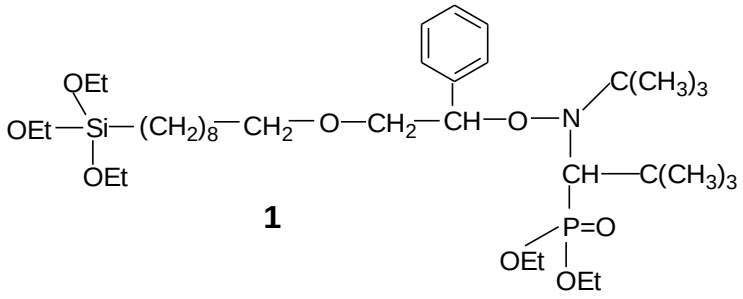

1

Figure 1.17: Chemical structure of an NMP initiator based on DEPN.[125]

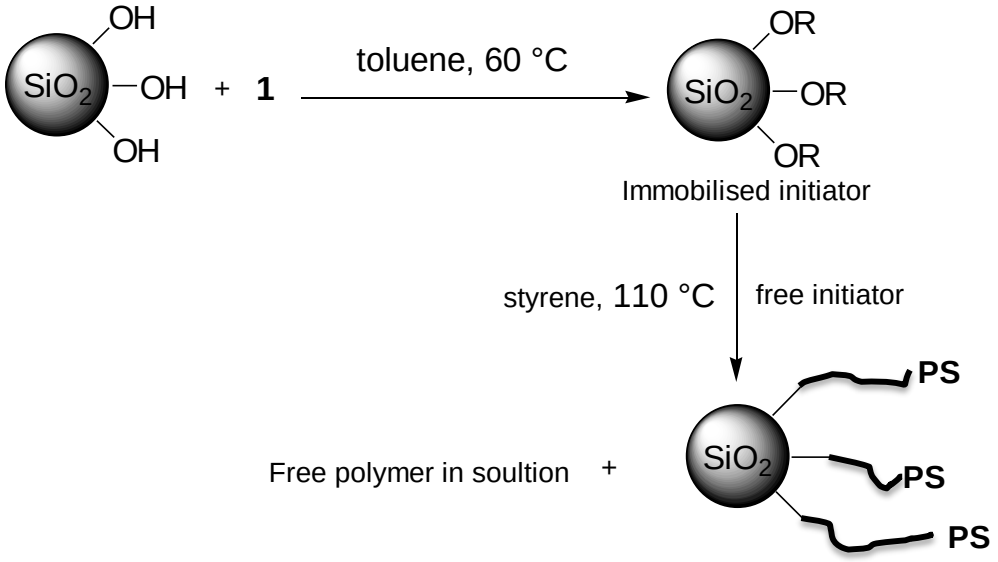

Figure 1.18: Synthetic scheme for the preparation of PS grafted silica nanoparticles by NMP.[125]

1.4 Applications of Polymer-silica Nanoparticles

Since silica is chemically inert and optically transparent, it can be used in a wide range of applications, including paints, inks, and high-quality paper coating.[29] Silica-polymer hybrids are also used to remove heavy metal ions such as cobalt and copper salts from waste water.[126] Silica nanoparticles are used as fillers in the manufacture of plastic binders and reinforced rubber products.[127] Furthermore, silica particles coated with organic modifiers are used in applications that include stationary

chromatography phases,[128] biomedical devices,[129] semiconductor devices,[130] aerospace and sensors.[63, 131] Recently, hollow polymer silica nanoparticles have been developed.[132, 133] These materials hold significant promise for many applications due to their potential for encapsulating active substances such as dyes and drugs.

1.5 Effect of Filler Materials on Thermal and Dynamic Mechanical Properties of Polymer Nanocomposites

In general, the mechanical properties of a polymer can be greatly changed by the addition of nanoparticles, and can also be affected by the properties of the nanofiller. Grafting polymers from the surface of particles is also important in this area, as more efficient bonding between the nanoparticles and the polymer can be an important factor in thermal and mechanical reinforcement. Tensile strength, impact strength, hardness, fracture toughness tests are the most widely used methods to evaluate the mechanical properties of the nanocomposite. Among these, Young's modulus (*E*), tensile strength, and impact strength are the main factors that can vary with the content of the silica.[4]

The mechanism of reinforcement is important in understanding the effects of dispersing nanofillers. However, the exact mechanism behind this reinforcement is still debated. There are three general theories that have been proposed over the years. The first theory by Payne in 1965 states that the agglomeration of the particles and the percolation of these particles through the system are responsible for an increase in mechanical reinforcement.[134] In contrast to this "particle-only" theory, other authours have suggested that both polymer chains and particles contribute to the mechanical reinforcement. Long and Sotta[135] argued that chain immobilisation occurs around nanoparticles[136] and the percolation of particles with "bound" glassy layers[11, 137] leads to mechanical reinforcement. The last proposed mechanism is that a network is formed between the particles by bridging polymer chains which strengthen the material.[138] A recent study into the mechanism was made by Kumar and co-workers[139] who prepared a well dispersed nanocomposite of polystyrene and silica using controlled radical polymerisations. By controlling the particle dispersion, the mechanical behaviour of both monodisperse and aggregated particles could be assessed, as well as the role of the polymer. By using shear experiments, the authors studied the mechanical behaviour of various nanocomposites with different polymer graft densities to determine the role of grafted chains in mechanical reinforcement. In regions of increased networking between

chains and nanoparticles, the mechanical reinforcement of the material was increased. The importance of percolation of nanoparticles for mechanical reinforcement could also be studied by varying the morphology and fraction of the nanoparticles. At high fractions of nanofiller, the nanoparticles' ability to percolate was found to be reduced. Therefore, both the grafted chains and nanoparticle percolation are significant factors in mechanical reinforcement. This reinforcement resulting from the formation of a network between particles and polymer chain entanglements effectively disproves the earliest theory, which disregards the polymer chains entirely, and supports the third theory. This mechanism also explains why grafting polymers provides better mechanical reinforcement than simply dispersing nanoparticles in a polymer matrix.

The thermal and dynamic mechanical properties of polymer nanocomposites are generally studied by techniques such as differential scanning calorimetry (DSC), thermal gravimetric analysis (TGA), dynamic mechanical thermal analysis (DMTA), and dielectric spectroscopy. TGA and DSC are the two most widely used methods to determine the thermal properties of polymer composites. TGA provides a measure of thermal stability and the degradation of the polymer as well as the percent of silica incorporated in the polymer matrix.[140, 141] DSC is used to determine any thermal transitions in the polymer nanocomposite, such as the glass transition temperature (T_g), and melting temperature (T_m).[142, 143] These properties and others are important characteristics of materials that can greatly affect the applications of polymers. By using the techniques mentioned to measure thermal and dynamic mechanical properties, the effects of nanosilica on polymer materials can be studied.

1.5.1 Effect of Filler on the Glass Transition Temperature

The glass transition temperature is the temperature at which a polymer softens from a glass to a rubbery material. This is an important parameter as mechanical strength can change significantly when the material softens. Below the T_g all amorphous polymers are stiff and glassy. However, the T_g affects the thermal and mechanical properties of the polymers. Generally, the T_g of elastomers, which need to be flexible at room temperature, is below room temperature and for thermoplastics it is above room temperature (they are rigid at room temperature).

Many researchers have studied the effect of addition of fillers on T_g and have drawn different conclusions. This is a controversial area as the T_g of polymer nanocomposites differs for a variety of reasons including filler size, filler loading, and the conditions of filler dispersion.[144] The addition of fillers has been reported to

increase, decrease or have no effect at all on the polymer's glass transition temperature, and even the disappearance of T_g has been reported in one case.[145-148] This reveals that the principles of polymer-filler interaction are still not fully understood.

Increasing filler content can seemingly have a non-linear effect on the properties of a material. Recently a study of polystyrene/silica nanocomposites showed that increasing the silica content in the composite increases the glass transition temperature up to 20% volume fraction but a slight decrease was reported as the silica content increased up to 50% by volume.[149] This result deviates from previous studies.[150] It is unclear whether the discrepancy may have arisen from non-uniform spatial distribution of the silica particles in PS matrix. Studies from Mele *et al.*[147] and Arrighi *et al.*[151] both reported a decrease in the glass transition of styrene-butadiene rubber in silica composites. Sun *et al.*[144] prepared epoxy nanocomposites and then studied the T_g of expoy/silica composites with nanometre and micrometre-sized fillers. It was observed that the micrometre filler did not have a significant effect on T_g, whereas the nanometre-size filler had a noticeable impact. With an increase in the nanofiller loading, the epoxy nanocomposites first showed an initial increase in T_g followed by a decrease with higher filler loading.[144] Their DMTA measurements revealed two peaks in the loss modulus, the first at around –50 ^oC, attributed to a sub-T_g relaxation, and the second one at 150 ^oC, which is related to the glass transition. The presence of silica in the nanocomposites did not show any change in the sub-T_g position. However, the typical glass transition of nanocomposites (T_g = 150 ^oC) decreased with increasing silica loading because of extra free volume being created at the interface of the nanocomposites which therefore assisted the large-scale segmental motion of the polymer. Similar behaviour was also observed with PS/silica nanocomposites.[71]

In some cases, the glass transition behaviour of PMMA-silica nanocomposites could not be detected by either DSC and DMTA.[148] The disappearance of the glass transition temperature was attributed to seriously restricted motion of the PMMA chains. This restriction could be also the result of cross-linking between silica particles and PMMA chains.[46]

Grafting a polymer from the surface of a nanoparticle can considerably affect the glass transition temperature. By grafting PMMA chains from the surface of ordered mesoporous silica (OMS) nanoparticles, the glass transition temperature of various hybrids was found to increase compared to the composites prepared by dispersing silica

in the polymer matrix.[152] The increase in T_g is due to the reduced mobility of the polymer chains when grafted onto the silica nanoparticles. The results of Xu and co-workers[152] also show an initial increase in the glass transition temperature with filler content and then a decrease when the silica weight fraction was in excess of 10 – 15%, supporting the trend found previously by Sun and co-workers.[144] The effect of conformational constraint on the T_g of polymer/silica nanocomposites is expected to depend on the geometry of the surface. Savin *at el.*[153] synthesised high-density PS brushes on silica nanoparticles with an average diameter of 20 nm by surface-initiated ATRP and studied them by DSC. They found the T_g of the grafted PS with M_n = 5230 g mol^{-1} was 13 K higher than the ungrafted sample of nearly the same M_w, but that the T_g difference was reduced to 2 K for a sample with an M_n of 32670 g mol^{-1}. These results suggest the effect of conformational constraint was mitigated for segments residing farther away from the immobilised surface.

1.5.2 Effect of Filler on Dynamic Mechanical Properties

Dynamic mechanical testing is often employed to study the viscoelastic behaviour of nanocomposites.[137, 144, 154, 155] Many of these studies draw conclusions based on the loss tangent (tan $\delta = E''/E'$) *vs*. temperature plot that occurs close to the T_g. The storage modulus (E') is a measure of the recoverable strain energy, the loss modulus (E'') is related to the energy dissipation, and the phase angle (δ) is defined by tan $\delta = E''/E'$. Storage modulus, loss modulus and phase angle are three important parameters of dynamic mechanical properties. Thus the stiffness and damping properties of the material can be described by any of E', E'' and tan δ. It should be mentioned that the loss tangent in the softening region (i.e. glass-to-rubber region) is influenced not only by local segmental motions, as reflected in E'', but also by filler reinforcement effects on both the loss and storage moduli at higher temperature. The T_g is often measured by DSC, but the DMTA technique where the maximum for tan δ is usually associated with the "mechanical T_g" is more sensitive and also able to resolve sub-T_g transitions, like beta, gamma, and delta transitions. Furthermore, the mechanical T_g values from the DMTA study are found to be higher than those from DSC measurements by about 5 − 12 ^{o}C.[156] In DMTA, the glass transition is evaluated based on the change in the volume of the sample while heated, whereas in DSC it is determined based on the change in heat produced by the sample in the glass to rubber transition. Numerous studies have been carried out on polymer/silica composites, but only a few selected results are described in the following paragraphs.

Early studies on filler−polymer composites have reported the presence of a second relaxation peak in the tan δ curves. There has been considerable discussion in the literature as to the origin of the high temperature secondary relaxation. Tsagaropoulos and Eisenberg[10] first suggested that the additional tan δ maximum could be associated with a second T_g. These authors proposed a three-layer polymer–filler model in which the formation of a loosely bound layer consisting of polymer chains of restricted mobility around silica filler particles accounts for the formation of the second T_g.[10] Similar behaviour has been reported for various silica−polymer composites in the literature.[157-159] Chen and co-workers[160] reported two tan δ peaks in poly(vinyl alcohol)/silica nanocomposites. They suggested that the PVA matrix exhibits the first tan δ peak and the interfacial layers around silica nanoparticles exhibit the second tan δ peak. More recently, Robertson and Rackaitis[161] commented on two tan δ peaks in polybutadiene-carbon black composites. These authors, based on their own measurements and consideration of other literature data,[138, 155, 162, 163] attributed the second peak in tan δ to the unattached chains to particles, and these unattached chains still undergo chain diffusion and flow. Some authors have also suggested that it is an artefact due to sample deformation (resulting in an incorrect calculation of the modulus by the DMTA).[164]

Size, shape and content of the silica nanoparticles affect the dynamic mechanical properties of polymer−silica composites. For example, studies by Zhang *et al.*,[165] Cho *et al.*,[166] Yong and Nelson[167] indicated that smaller nanoparticles improved the mechanical properties of the composites due to the increased interfacial area between the particle surface and the polymer matrix. However, other studies reported that an improvement in mechanical properties is mainly a function of the filler content.[156, 168-171] Yang *et al.*[172] also illustrated the influence of silica content on the mechanical properties of polyamide6 (PA6)/modified silica nanocomposites prepared by in-situ polymerisation. In that case, the mechanical behaviour such as impact and tensile strength showed an increase with increase of the silica content and have maximum values at 5% silica content, while those of PA6/ unmodified silica decrease gradually with silica loading.[172]

1.6 The Project Aims and Thesis Outline

To date, there has been no comprehensive study about the effect of grafting on the mechanical properties of polymer silica nanocomposites. Most mechanical studies have dealt with either unmodified nanosilica or commercially available surface-modified

particles. There are also various aspects which are worthy of further investigation. The main aim of this work was to study the effect of various grafted silica nanoparticles on mechanical reinforcement. An additional aim was to correlate dynamic mechanical measurements and structural properties of the resulting nanocomposites. To achieve this it was necessary to synthesise; (1) a series of grafted polymers with controlled molar mass using a both aggregated and non–aggregated silica nanoparticles, as well as (2) a series of deuterated polymers that will be used for future neutron scattering studies.

This thesis discusses the preparation and characterisation of polymer nanocomposites as well as a selection of deuterated polymers. The thermal, mechanical behaviour and morphology at various length scales of a series of nanocomposites, starting from commercial nanoparticles are also investigated.

Chapter 2 serves to provide an overview of the synthesis and analysis conducted as part of this work.

Chapter 3 describes how polymers (PMMA, PBA, PS homopolymer and PSAN copolymer) were grafted from the surface of both aggregated and non-aggregated silica nanoparticles, using an ATRP in miniemulsion system. The effects of several parameters in the ATRP process are examined, including the choice of initiator, catalyst, ligand, and reducing agent.

Chapter 4 describes a new simple method for rapid deuteration of the aromatic ring of polystyrene (PS) and poly(4-hydroxystyrene) (P4HS) using superheated C_6D_6 and D_2O as cheap deuterium sources under microwave-assisted H/D isotope exchange conditions. The synthesis of deuterated poly(4-hydroxystyrene) by a polymer-analogous reaction sequence is also included in the same chapter.

Chapters 5 and **6** investigate both the thermal and mechanical properties of grafted PMMA, PS and PSAN silica nanoparticles prepared by ATRP. These chapters will look at different factors including type and size of silica, as well as varying molecular weight of the polymer. Furthermore, the thermal and mechanical behaviour of nanocomposites (prepared by grafting chains from the surface of both silica nanoparticles) will be compared with the samples obtained by simply dispersing the same silica particles in the polymer matrices (i.e. PMMA, PS and PSAN).

Chapter 7 describes the thermal and dynamic mechanical properties of poly(butyl acrylate) grafted from both aggregated silica nanoparticles and colloidally dispersed

silica nanoparticles of different particle size prepared by an ATRP in miniemulsion process as well as polyester-resin/silica nanocomposites prepared by blending technique.

The overall conclusions and the future outlook of work in this thesis are presented in **Chapter 8**.

1.7 References

1. M. Z. Rong, M. Q. Zhang, S. L. Pan, B. Lehmann and K. Friedrich, *Polym. Int.*, 2004, **53**, 176.
2. C. M. Chan, J. S. Wu, J. X. Li and Y. K. Cheung, *Polymer*, 2002, **43**, 2981.
3. J. Lee and A. F. Yee, *Polymer*, 2002, **42**, 577.
4. H. Zou, S. Wu and J. Shen, *Chem. Rev.*, 2008, **108**, 3893.
5. D. W. Schaefer and R. S. Justice, *Macromolecules*, 2007, **40**, 8501.
6. F. Hussain, M. Hojjati, M. Okamoto and R. E. Gorga, *J. Compos. Mater.*, 2006, **40**, 1511.
7. P. M. Ajayan, L. S. Schadler, C. Giannaris and A. Rubio, *Adv. Mater.*, 2000, **12**, 750.
8. K. Pramoda, H. Hussain, H. Koh, H. Tan and C. He, *J. Polym. Sci., Part A: Polym. Chem.*, 2010, **48**, 4262.
9. S. C. Jana and S. Jain, *Polymer*, 2001, **42**, 6897.
10. G. Tsagaropoulos and A. Eisenburg, *Macromolecules*, 1995, **28**, 396.
11. G. Tsagaropoulos and A. Eisenberg, *Macromolecules*, 1995, **28**, 6067.
12. J. Evans, *Chemistry World*, November 2007, 17.
13. V. Arrighi, I. J. McEwen, H. Qian and M. B. S. Prieto, *Polymer*, 2003, **44**, 6259.
14. T. von Werne and T. E. Patten, *J. Am. Chem. Soc.*, 2001, **123**, 7497.
15. J. Pyun, S. Jia, T. Kowalewski, G. D. Patterson and K. Matyjaszewski, *Macromolecules*, 2003, **36**, 5094.
16. K. Min and K. Matyjaszewski, *Macromolecules*, 2005, **38**, 8131.
17. O. Prucker and J. Rühe, *Macromolecules*, 1998, **31**, 592.
18. O. Prucker and J. Rühe, *Macromolecules*, 1998, **31**, 602.
19. J. Rühe, *Macromol. Symp.*, 1997, **126**, 215.
20. D. Sunda, S. Curras-Medina and D. L. Green, *Macromolecules*, 2010, **43**, 4871.
21. M. A. Ver Meer, B. Narasimhan, B. H. Shanks and S. K. Mallapragada, *ACS Appl. Mater. Interfaces*, 2010, **2**, 41.
22. C.-H. Liu and C.-Y. Pan, *Polymer*, 2007, **48**, 3679.
23. C. Bartholome, E. Beyou, E. Bourgeat-Lami, P. Chaumont, F. Lefebvre and N. Zydowicz, *Macromolecules*, 2005, **38**, 1099.
24. C. Li and B. C. Benicewicz, *Macromolecules*, 2005, **38**, 5929.
25. T. von Werne and T. E. Patten, *J. Am. Chem. Soc.*, 1999, **121**, 7409.
26. D. Li, X. Sheng and B. Zhao, *J. Am. Chem. Soc.*, 2005, **127**, 6248.

27. H. Mori, D. C. Seng, M. Zhang and A. H. E. Müller, *Langmuir,* 2002, **18**, 3682.
28. A. El Harrak, G. Carrot, J. Oberdisse, C. Eychenne-Baron and F. Boué, *Macromolecules,* 2004, **37**, 6376.
29. K. Ohno, T. Morinaga, K. Koh, Y. Tsujii and T. Fukuda, *Macromolecules*, 2005, **38**, 2137.
30. C. Perruchot, M. A. Khan, A. Kamitsi, S. P. Armes, T. von Werne and T. E. Patten, *Langmuir*, 2001, **17**, 4479.
31. J. Pyun, T. Kowalewski and K. Matyjaszewski, *Macromol. Rapid Commun.*, 2003, **24**, 1043.
32. V. Goel, T. Chatterjee, L. Bombalski, K. Yurekli, K. Matyjaszewski and R. Krishnamoorti, *J. Polym. Sci., Part B: Polym. Phys.*, 2006, **44**, 2014.
33. J. Pietrasik, H. Dong, and K. Matyjaszewski, *Macromolecules*, 2006, **39**, 6384.
34. B. Radhakrishnan, R. Ranjan and W. Brittain, *Polym. Prepr.*, 2005, **46(2)**, 108.
35. R. K. Iler, *The chemistry of silica*, New York: Wiley, 1993.
36. S. M. Chang, M. Lee and W. S. Kim, *J. Colloid Interface Sci.*, 2005, **286**, 536.
37. W. Stöber, A. Fink and E. J. Bohn, *J. Colloid Interface Sci.*, 1968, **26**, 62.
38. A. K. van Helden, J. W. Jansen and A. J. Vrij, *Colloid Interface Sci.*, 1981, **8**, 354.
39. A. P. Philipse and A. J. Vrij, *J. Colloid Interface Sci.*, 1988, **128**, 121.
40. G. H. Bogush and C. F. Zukoski, *J. Colloid Interface Sci.*, 1991, **142**, 1.
41. A. van Blaaderen and A. J. Vrij, *Langmuir,* 1992, **8**, 2921.
42. A. van Blaaderen and A. Vrij, *J. Colloid Interface Sci.*, 1993, **156**, 1.
43. K. Osseoasare and F. J. Arriagada, *Colloids Surf., A*, 1990, **50**, 321.
44. A. A. Vassiliou, G. Z. Papageorgiou, D. S. Achilias and D. N. Bikiaris, *Macromol. Chem. Phys.*, 2007, **208**, 364.
45. C. L. Wu, M. Q. Zhang, M. Z. Rong and K. Friedrich, *Compos. Sci. Technol.*, 2005, **65**, 635.
46. Y. Y. Yu and W. C. Chen, *Mater. Chem. Phys.*, 2003, **82**, 388.
47. H. E. Miltner, N. Watzeels, C. Block, N. A. Gotzen, G. Van Assche, K. Borghs, K. Van Durme, B. Van Mele, B. Bogdanov and H. Rahier, *Eur. Polym. J.*, 2010, **46**, 984.
48. D. Cangialosi, V. M. Bouche, a. Alegria and J. Colmenero, *J. Chem. Phys.*, 2011, 135.
49. S. Edmondson, C. L. Osbrone and W. T. S. Huck, *Chem. Soc. Rev.*, 2004, **33**, 14.

50. K. Yoshinage, J. Shimada, H. Nishida and M. Komatsu, *J. Colloid Interface Sci.*, 1999, **214**, 180.
51. Y. Liu, C. Y. Hsu, Y. H. Su and J. Y. Lai, *Biomacromolecules*, 2005, **6**, 368.
52. S. Kang, S. I. Hong, C. R. Choe, M. Park, S. Rim and J. Kim, *Polymer*, 2001, **42**, 879.
53. C. Li, J. Han, C. Y. Ryu and B. C. Benicewicz, *Macromolecules*, 2006, **39**, 3175.
54. S. Kang, S. Hong, C. R. Choe, M. Park, S. Rim and J. Kim, *Polymer,* 2001, **42**, 879.
55. F. Yong and N. G.L, *J. Appl. Sci.*, 2004, **91**, 3847.
56. I. Mora-Barrantes, J. L. Valentìn, A. Rodrìguez, I. Quijada-Garrido and R. Paris, *J. Mater. Chem.*, 2012, **22**, 1403.
57. Y. Taniguchi, K. Shirai, H. Saitoh, T. Yamauchi and N. Tsubkawa, *Polymer*, 2005, **46**, 2541.
58. J. Ueda, H. Yamaguchi, T. Yamauchi and N. Tsubokawa, *J. Polym. Sci.; Part A: Polym. Chem.*, 2007, **45**, 1143.
59. Q. Y. Zhou, S. X. Wang, X. W. Fan, R. Advincula and J. Mays, *Langmuir*, 2002, **18**, 3324.
60. U. Eismann and S. Spange, *Macromolecules*, 1997, **30**, 3439.
61. S. Spange, *Prog. Polym. Sci.*, 2000, **25**, 781.
62. G. Carrot, D. Rutot-Houzé, A. Pottier, P. Degée, J. Hilborn and P. Dubois, *Macromolecules*, 2002, **35**, 8400.
63. R. Ranjan, *Dissertation Presented to University of Akron*, May, 2008.
64. C. M. Liauw, G. C. Lees, S. J. Hurst, R. N. Rothon and S. Ali, *Composites, Part A*, 1998, **67**, 1313.
65. S. H. Ahn, S. H. Kim and S. G. Lee, *J. Appl. Sci.*, 2004, **94**, 812.
66. A. R. Mahdavian, M. Ashjari and A. B. Makoo, *Eur. Polym. J.*, 2007, **43**, 336.
67. J. C. Tang, G. L. Lin, G. J. Yang and Y. W. Chen-Yang, *J. Appl. Sci.*, 2007, **104**, 4096.
68. S. Rafiq, Z. Man, F. Ahmad and S. Maitra, *International Ceramic Review*, 2010, **6**, 341.
69. L. Wei, N. Hu and Y. Zhang, *Materials*, 2010, **3**, 4066.
70. N. Katsikis, F. Zahradnik, A. Helmschrott, A. Münstedt and A. Vital, *Polym. Degrad. Stab.*, 2007, **92**, 1966.
71. E. Kontou and G. Anthoulis, *J. Appl. Sci.*, 2007, **105**, 1723.

72. F. Yong and G. L. Nelson, *Polym. Adv. Technol.*, 2006, **17**, 320.
73. K. Matyjaszewski and T. P. Davis, *Handbook of Radical Polymerisation*, Wiley: Hoboken, NJ, 2002.
74. R. Jordan, *Surface-Initiated Polymerisation.*, 2006, Spinger.
75. J. Ueda, S. Sato, A. Tsunokawa, T. Yamauchi and N. Tsubokawa, *Eur. Polym. J.*, 2005, **41**, 193.
76. J. Gromada and K. Matyjaszewski, *Macromolecules*, 2001, **34**, 7664.
77. G. Chakkalakal, *Dissertation Presented to Helmholtz-Zentrum Geesthacht*, 2011
78. H. Lin, C. Li and J. Lee, *J. Power Sources*, 2011, **196**, 8098.
79. C. Bartholome, E. Beyou, E. Bourgeat-Lami, P. Chaumont, F. Lefebvre and N. Zydowicz, *Macromolecules*, 2005, **38**, 1099.
80. L. Bombalski, K. Min, C. Tang and K. Matyjaszewski, *Polym. Prepr.*, 2005, **46(2)**, 359.
81. S. Habaue, O. Ikeshima, H. Ajiro and Y. Okamoto, *Polym. J*, 2001, **33**, 902.
82. A. Ramakrishnan, R. Dhamodhara and J. Rühe, *Macromol. Rapid Commun.*, 2002, **23**, 277.
83. M. Ejaz, Y. TsuJii and T. Fukuda, *Polymer*, 2001, **42**, 6811.
84. J. S. Wang and K. Matyjaszewski, *J. Am. Chem. Soc.*, 1995, **117**, 5614.
85. M. Kato, M. Kamigaito, M. Sawamoto and T. Higashimura, *Macromolecules*, 1995, **28**, 1721.
86. W. Zhang and A. H. E. Müller, *Prog. Polym. Sci.*, 2013, http://dx.doi.org/10.1016/j.progpolymsci.2013.1003.1002.
87. T. Higashihara, M. Hayashi and A. Hirao, *Prog. Polym. Sci.*, 2011, **36**, 323.
88. B. S. Shemper and L. J. Mathias, *Eur. Polym. J.*, 2004, **40**, 651.
89. Y. Wang, Y. Zhang, B. Parker and K. Matyjaszewski, *Macromolecules*, 2011, **44**, 4022.
90. C. Granel, P. Dubois, R. Jérôme and P. Teyssié, *Macromolecules*, 1996, **29**, 8576.
91. P. Lecomte, I. Drapier, P. Dubois, P. Teyssié and R. Jérôme, *Macromolecules*, 1997, **30**, 7631.
92. M. Ocuhi, T. Terashima and M. Sawamoto, *Chem. Rev.*, 2009, **109**, 4963.
93. V. Coessens, T. Pintaure and K. Matyjaszewski, *Prog. Polym. Sci.*, 2001, **26**, 337.
94. K. Matyjaszewski, J. L. Wang, T. Grimaud and D. A. Shipp, *Macromolecules*, 1998, **31**, 1527.

95. M. Husseman, E. E. Malmström, M. McNamara, M. Mate, D. Mecerreyes, G. Didier, D. G. Benoit, J. L. Hedrick, P. Mansky, E. Huang, T. P. Russell and C. G. Hawker, *Mcromolecules*, 1999, **32**, 1424.
96. V. Percec, P. Barboiu and H. J. Kim, *J. Am. Chem. Soc.*, 1998, **120**, 305.
97. J.-S. Wang and K. Matyjaszewski, *J. Am. Chem. Soc.*, 1995, **117**, 5614.
98. M. Ejaz, S. Yamamoto, K. Ohno, Y. Tsujii and T. Fukuda, *Macromolecules*, 1998, **31**, 5934.
99. F. Chen, X. Jiang, R. Liu and J. Yin, *ACS Appl. Mater. Interfaces*, 2010, **2**, 1031.
100. M. Ejaz, K. Ohno, Y. Tsujii and T. Fukuda, *Macromolecules*, 2000, **33**, 2870.
101. K. Matyjaszewski, P. J. Miller, N. Shukla, B. Immaraporn, A. Gelman, B. B. Luokala, T. M. Siclovan, G. Kickelbick, T. Vallant, H. Hoffmann and T. Pakula, *Macromolecules*, 1999, **32**, 8716.
102. B. Bin Zhao and T. He, *Macromolecules*, 2003, **36**, 8599.
103. K. Min, H. Gao and K. Matyjaszewski, *J. Am. Chem. Soc.*, 2005, **127**, 3825.
104. W. Jakubowski and K. Matyjaszewski, *Macromolecules*, 2005, **38**, 4139.
105. H. Dong, W. Tang and K. Matyjaszewski, *Macromolecules*, 2007, **40**, 2974.
106. K. Min, H. Gao and K. Matyjaszewski, *J. Am. Chem. Soc.*, 2006, **129**, 10521.
107. W. Jakubowski, K. Min and K. Matyjaszewski, *Macromolecules*, 2006, **39**, 39.
108. V. Goel, J. Pietrasik, H. Dong, J. Sharma, K. Matyjaszewski and R. Krishnamoorti, *Macromolecules*, 2011, **44**, 8129.
109. L. Bombalski, K. Min, H. C. Dong, C. B. Tang and K. Matyjaszewski, *Macromolecules*, 2007, **40**, 7429.
110. K. Min, H. F. Gao and K. Matyjaszewski, *J. Am. Chem. Soc.*, 2005, **127**, 3825.
111. J. Chiefari, Y. K. Chong, F. Ercole, J. Krstina, J. Jeffery, T. P. T. Le, R. T. A. Mayadunne, G. F. Meijs, C. L. Moad, G. Moad, E. Rizzardo and S. H. Thang, *Macromolecules*, 1998, **31**, 5559.
112. G. Moad, E. Rizzardo and S. H. Thang, *Polymer*, 2008, **49**, 1079.
113. R. T. A. Mayadunne, E. Rizzardo, J. Chiefari, Y. K. Chong, G. Moad and S. H. Thang, *Macromolecules*, 1999, **32**, 6977.
114. R. T. A. Mayadunne, E. Rizzardo, J. Chiefari, J. Krstina, G. Moad, A. Postma and S. H. Thang, *Macromolecules*, 2000, **33**, 243.
115. M. Destarac, D. Charmot, X. Franck and S. Z. Zard, *Macromol. Rapid Commun.* , 2000, **21**, 1035.
116. R. Francis and A. Ajayaghosh, *Macromolecules*, 2000, **33**, 4699.

117. C.-H. Peng, J. Kong, F. Seeliger and K. Matyjaszewski, *Macromolecules*, 2011, **44**, 7546.
118. Y. Huang, Q. Liu, X. Zhou, S. b. Perrier and Y. Zhao, *Macromolecules*, 2009, **42**, 5509.
119. V. G. Ngo, C. Bressy, C. Leroux and A. Margaillan, *Polymer*, 2009, **50**, 3095.
120. M. Baum and W. J. Brittain, *Macromolecules*, 2002, **35**, 610.
121. J. Nicolas, Y. Guillaneuf, C. Lefay, D. Bertin, D. Gigmes and B. Charleux, *Prog. Polym. Sci.*, 2013, **38**, 63.
122. M. K. Georges, R. P. N. Veregin, P. M. Kazmaier and G. K. Hamer, *Macromolecules*, 1993, **26**, 2987.
123. P. M. Kazmaier, K. A. Moffat, M. K. Georges, R. P. N. Veregin and G. K. Hamer, *Macromolecules*, 1995, **28**, 1841.
124. C. J. Hawker, E. Elce, J. Dao, W. Volksen, T. P. Russell and G. G. Barclay, *Macromolecules*, 1996, **29**, 2686.
125. C. Bartholome, E. Beyou, E. Bourgeat-Lami, P. Chaumont and N. Zydowicz, *Macromolecules*, 2003, **36**, 7946.
126. T. Meyer, S. Prause, S. Spange and M. Friedrich, *J. Colloid Interface Sci.*, 2001, **236**, 335.
127. H. Hommel, A. Touhami and A. P. Legrand, *Makromol. Chem.*, 1993, **194**, 879.
128. Y. Wei, L. M. Fan and L. R. Chen, *Chromatographia*, 1997, **46**, 637.
129. J. P. Harris, J. R. Capadona, R. H. Miller, B. C. Healy, K. Shanmuganathan, S. J. Rowan, C. Weder and D. J. Tyler, *J. Neural Eng.*, 2011, **8**.
130. S.-J. Su and N. Kuramoto, *Synth. Met.*, 2000, **114**, 147.
131. Y. Mizutani and S. Nago, *J. Appl. Polym. Sci.*, 1999, **72**, 1489.
132. S. Blomberg, S. Ostberg, E. Harth, A. W. Bosman, B. van Horn and C. J. Hawker, *Polym. Sci., Part A: Polym. Chem.*, 2002, **40**, 1309.
133. G. Zhu, S. Qiu, O. Terasaki and W. Y, *J. Am. Chem. Soc.*, 2001, **123**, 7723.
134. A. R. Payne, *J. Appl. Polym. Sci.*, 1965, **9**, 2273.
135. D. Long and P. Sotta, *Rheol. Acta*, 2007, **46**, 1029.
136. P. Vondracek and M. Schatz, *J. Appl. Polym. Sci.*, 1977, **21**, 3211.
137. R. B. Bogoslovov, C. M. Roland, A. R. Ellis, A. M. Randall and C. G. Robertson, *Macromolecules*, 2008, **41**, 1289.
138. Z. Zhu, T. Thompson, S.-Q. Wang, E. D. von Meerwall and A. Halasa, *Macromolecules*, 2005, **38**, 8816.

139. J. F. Moll, P. Akcora, A. Rungta, S. Gong, R. H. Colby, B. C. Benicewicz and S. K. Kumar, *Macromolecules*, 2011, **44**, 7473.
140. N. Katsikis, F. Zahradnik, A. Helmschrott, H. Münstedt and A. Vital, *Polym. Degrad. Stab.*, 2007, **92**, 1966.
141. D. Sunday, S. Curras-Medina and D. L. Green, *Macromolecules*, 2010, **43**, 4871.
142. B. J. Hunt and M. I. James, *Polymer Characterisation*, Blackie Academic Professional, 1993.
143. D. Campbell and J. R. White, *Polymer Characterisation, Physical techniques*, Chapman and Hall Ltd, 1989.
144. Y. Y. Sun, Z. Q. Zhang, K. S. Moon and C. P. Wong, *J. Polym. Sci., Part B: Polym. Phys.*, 2004, **42**, 3849.
145. A. Kraft, V. Arrighi, P. Adams, P.M. E. Karotsis, A. McAnaw, I. J. McEwen, L. Ragupathy and C. Waring, *Polym. Prepr.*, 2007, **48**, 203.
146. T. H. Zhou, W. H. Ruan, M. Z. Rong, M. Q. Zhang and Y. L. Mai, *Adv. Mater.*, 2007, **19**, 2667.
147. P. Mele, S. Marceau, D. Brown, Y. Depuydt and N. D. Alberola, *Polymer*, 2002, **43**, 5577.
148. Y.-L. Liu, C.-Y. Hsu and K.-Y. Hsu, *Polymer*, 2005, **46**, 1851.
149. M. Mizuno, K. Nakamura, T. Konishi and K. Fukao, *J. Non-Cryst. Solids* 2011, **357**, 594.
150. A. Bansal, H. C. Yang, C. Z. Li, K. W. Cho, B. C. Benicewicz, S. K. Kumar and L. S. Schadler, *Nat. Mater.*, 2005, **4**, 693.
151. V. Arrighi, I. J. McEwen, H. Qian and M. B. Serrano Prieto, *Polymer*, 2003, **44**, 6259.
152. L. X. Xu, F. Xu, F. Chen, J. T. Yang and M. Q. Zhong, *J. Nano Mat.*, 2012, **10**.
153. D. A. Savin, J. Pyun, G. D. Patterson, T. Kowalewski and K. Matyjaszewski, *J. Polym. Sci., Part B: Polym. Phys.*, 2002, **40**, 2667.
154. M. Pluta, J. K. Jeszka and G. Boiteux, *Eur. Polym. J.*, 2007, **43**, 2819.
155. K. W. Stöckelhuber, A. S. Svistkov, A. G. Pelevin and G. Heinrich, *Macromolecules*, 2011, **44**, 4366.
156. P. Dittanet and R. A. Pearson, *Polymer*, 2012, **53**, 1890.
157. S. Sternstein and A. Zhu, *Macromolecules*, 2002, **35**, 7262.
158. A. Yim, R. S. Chahal and L. Pierre, *J. Colloid Interface Sci.*, 1973, 583.

159. C. J. T. Landry, B. K. Coltrain, M. R. Landry, J. J. Fitzgerald and V. K. Long, *Macromolecules*, 1993, **26**, 3702.
160. L. Chen, K. Zheng, X. Tian, K. Hu, R. Wang, C. Liu, Y. Li and P. Cui, *Macromolecules*, 2010, **43**, 1076.
161. C. G. Robertson and M. Rackaitis, *Macromolecules*, 2011, **44**, 1177.
162. N. Jaouault, P. Vallat, F. Dalmas, S. Said, J. Jestin and F. Boue, *Macromolecules*, 2009, **42**, 2031.
163. C. G. Robertson, C. J. Lin, M. Rackaitis and C. M. Roland, *Macromolecules*, 2008, **41**, 2727.
164. A. Kraft, P. M. E. Adams, V. Arrighi, J. Harkins, A. McAnaw, I. J. McEwen, S. J. Mayhew, L. Ragupathy and C. Waring, *Polym. Mater. Sci. Eng.*, 2007, **96**, 43.
165. H. Zhang, Z. Zhang, K. Friedrich and C. Eger, *Acta Mater.*, 2006, **54**, 1833.
166. J. Cho, M. S. Joshi and C. T. Sun, *Compos. Sci. Technol.*, 2006, **66**, 1941.
167. F. Yong and G. L. Nelson, *J. Appl. Polym. Sci.*, 2004, **91**, 393.
168. T. Kashiwagi, A. B. Morgan, J. M. Antonucci, M. R. VanLandingham, R. H. Harris, W. H. Awad and J. R. Shields, *J. Appl. Polym. Sci.*, 2003, **89**, 2072.
169. A. C. Comer, A. L. Heilman and D. S. Kalika, *Polymer*, 2010, **51**, 5254.
170. P. Dittanet and R. A. Pearson, *Polymer*, 2012, **53**, 1890.
171. H. M. Smallwood, *J. Appl. Phys.*, 1944, **15**, 758.
172. F. Yang, Y. C. Ou and Z. Z. Yu, *J. Appl. Polym. Sci.*, 1998, **69**, 355.

Chapter 2 – Experimental

Contents

2.1 Materials

Most of the chemicals were used as received, with the exception of certain reagents such as monomers which required further purification, as detailed below. A list of chemicals used in the project and their source is shown below. Different types of silica and titanium dioxide particles were utilised as listed in **Table 2.1**.

Aldrich

Butyl acrylate (BA, +99%), methyl methacrylate (MMA, 99%), styrene (>99%), acrylonitrile (>99%), copper(II) chloride (+99%), copper(II) bromide (+99%), ascorbic acid, hexadecane, ethylenediamine tetraacetic acid disodium salt (EDTA), Brij 98, ethylalminium dichloride (1M in hexanes), 1-butyl-3-methylimidazolium chloride (>98%), *N*,*N*,*N'*,*N''*,*N''*-pentamethyldiethlenetriamine (PMDETA), *2*,*2*,*2*-trichloroethyl chloroformate (98%), ethyl 2-bromoisobutyrate (EBiB, 98%), Tin(II) 2-ethylhexanoate ($Sn(EH)_2$, ~95%), formaldehyde (37 *w/w*), formic acid (90% *w/w*), acetonitrile, dichloromethane, acetone for HPLC grade , acetyl chloride (CH_3COCl), acetic anhydride (>99.5%), hydrochloric acid (HCl, 36%), cyclohexane, aluminium chloride ($AlCl_3$, 99%), 3-aminopropyltriethoxysilane (99%), poly(styrene-*co*-acrylonitrile), anisole.

Lancaster

Tris(2-aminoethyl)amine (TREN, 97%), triethylamine (99%), acetyl chloride (98%), 2-bromoisobutyrylbromide.

Alfa Aesar

2-Picolylchloride hydrochloride (98%), 1-octylamine, tetra-n-butylammonium fluoride in THF, hydrogen peroxide (35% *w/w*).

BDH

Chloroform, hexane for HPLC grade, tetrahydrofuran (THF), sodium hydroxide, dimethylsulfoxide-d_6 (DMSO), Chloroform-d (99.8%), anhydrous magnesium sulphate, anhydrous sodium sulphate, sulphuric acid (H_2SO_4, >95%), poly(methyl methacrylate) (PMMA).

Fisher chemicals

Methanol, toluene, sodium carbonate.

Polysciences, Inc

Poly(4-hydroxystyrene) (M_w = 22,000 g/mol).

Avocado Research Chemicals Ltd

Polystyrene (M_w = 100,000 and 18,000 g/mol).

Goss scientific

Deuterium oxide (D_2O, 99.9%), benzene-d_6.

ABL (Stevens) Resin & Glass

Clear rigid epoxy resin, clear cast epoxy resin hardener, polyester resin, methyl ethyl ketone peroxide (MEKP, 33% solution in dibutyl phthalate plasticiser 67%).

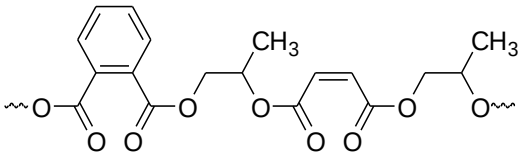

Segment of an unsaturated polyester resin

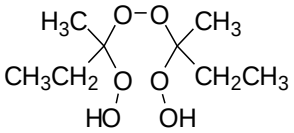

MEKP (catalyst)

Table 2.1: Types and the source of silica nanoparticles and titanium dioxide.

Materials	Information	Source
Aerosil (A300)	Specific surface area = 300±30 m^2 /g average diameter = 7 nm	Degussa-Huls
Cab-o-sil H5 (Cab H5)	Specific surface area = 300±30 m^2 /g average diameter = 7 nm	Cabot
MEK-ST	Colloidal silica, specific surface area = 217.6 m^2 /g, particle size: 10 − 15 nm, $Si0_2$ (30 – 31 wt%), H_2O (< 0.5 wt%), solvent (Methyl ethyl ketone)	Nissan Chemical
MEK-ST-L	Colloidal silica, specific surface area = 60.4 m^2 /g, particle size: 40 − 50 nm, $Si0_2$ (30 – 31 wt%), H_2O (< 0.5 wt%), solvent (Methyl ethyl ketone)	Nissan Chemical
IPA-ST-UP	Colloidal silica, specific surface area = 266.6 m^2 /g, particle size: 9 − 15 nm with a length = 40 − 100 nm, $Si0_2$ (15 – 16 wt%), H_2O (< 1.0 wt%), solvent (Isopropanol)	Nissan Chemical
Titanium dioxide (anatase)	Specific surface area = 200 − 220 m^2 /g, particle size < 25 nm, 99.7%	Sigma-Aldrich
Titanium dioxide (rutile)	Specific surface area = 14 m^2/g, particle size < 100 nm, 99.5%	Sigma-Aldrich

2.2 Purification of Monomers

(a). Methyl methacrylate (MMA)

Methyl methacrylate monomer was extracted with 0.1 M aqueous NaOH to remove the inhibitor, then washed with distilled water until neutral to litmus. After drying over anhydrous magnesium sulphate ($MgSO_4$), filtered, and degassed the purified monomer was stored in a refrigerator at 5 °C.

(b). Styrene and butyl acrylate

Styrene and butyl acrylate monomers were purified following the procedure used for methyl methacrylate

(c). Acrylonitrile

Acrylonitrile monomer was purified by distillation under atmospheric pressure, discarding the first fraction. The purified monomer was stored at 4 °C.

2.3 Characterisation Techniques

2.3.1 Nuclear Magnetic Resonance (NMR)

NMR analyses were performed with Bruker spectrometers at 200, 300 or 400 MHZ. NMR spectra were recorded for every sample prepared in order to confirm that no solvent or other impurities were present. NMR samples were prepared by dissolving 15 − 20 mg of material in 1mL of $CDCl_3$ or DMSO-d_6. Furthermore, the copolymer compositions of a number of samples were calculated from ^1H NMR spectra; in all cases, the results were comparable to those obtained by elemental analysis (see **Appendix A1**).

2.3.2 Fourier Transform Infrared Spectroscopy (FTIR)

IR measurements were performed with a Perkin Elmer RX Fourier transform infrared spectrometer and Perkin Elmer Spectrum 100 FT-IR apparatus. KBr discs made from solid powder were used to overcome solubility problems. Some samples were prepared as cast film on NaCl discss from solutions in tetrahydrofuran or acetone.

2.3.3 Elemental Analysis

Elemental analysis was carried out with an Exeter CE 440 Elemental Analyser to measure the silica content of the dispersed/grafted samples or copolymer compositions. This analysis was performed on dried samples in order to determine the percentages of

carbon, hydrogen and nitrogen. Details of the calculations are given in **Chapter 3** and **Appendix A2**.

2.3.4 Thermal Gravimetric Analysis (TGA)

TGA measurements were performed on a DuPont Instrument 951 Thermal Analyser, using a temperature ramp rate of 10 °C/ min up to 800 °C. Samples were kept under vacuum overnight prior to the measurements. TGA measurements were carried out in an inert N_2 atmosphere. The weight loss of the polymer sample was recorded as a function of temperature and this information used to determine the silica content.

2.3.5 Gel Permeation Chromatography (GPC)

The molecular weights and molecular weight distributions of the polymer samples were measured in THF at 35 °C with a flow rate of 1 mL/min using a Gilson 305 pump and Waters 410 refractometer. Polystyrene standards were used to calibrate the GPC instrument.

2.3.6 Differential Scanning Calorimetry (DSC)

Differential scanning calorimetry measurements were carried out with a TA Instruments DSC 2010. Samples were prepared by sealing 10 − 15 mg in a sealed aluminium pan. Samples were heated at a rate of 20 ^{o}C/ min under a constant nitrogen flow. Values of glass transition temperature (T_g) were taken as the midpoint of the transition. Calibration of the instrument was carried out using indium metal standard.

2.3.7 Dynamic Mechanical Thermal Analysis (DMTA)

A TA Instruments DMA 2980 dynamic mechanical analyser was used in the single cantilever mode at a frequency of 1 Hz and heating rate of 2 ^{o}C/ min. Samples were prepared in a rectangular mould using a hot press. Samples were heated to 473 K and subjected to a force of 5 tons for 30 minutes. The dimensions of the sample were typically 10.0 mm long, 12.0 mm wide and 2.5 mm thick. The major error in the results obtained from DMTA occurred in the determination of sample dimensions.

2.3.8 Scanning Electron Microscopy (SEM)

The microstructures of the prepared polymer composites were examined using a FEI Instruments Quanta 3D FEG Scanning electron microscopes (SEM). To avoid charging problems and to obtain better image definition all samples were coated by a thin film of gold.

2.3.9 Transmission Electron Microscopy (TEM)

The TEM experiments were done using a FEI Tecnai F20-G2 operated at 200 kV. The modified silica nanoparticles were dispersed in toluene (10 mg in 3 mL) for 24 hours at room temperature. The prepared samples were cast onto carbon-coated copper grids film and analysed after evaporation of the solvent.

2.4 Synthesis of Grafted Polymer Nanoparticles

2.4.1 ATRP Initiators

ATRP initiators were synthesised in two steps and attached to aggregated and non-aggregated silica nanoparticles.

Preparation of O-2,2,2-trichloroethyl N-(3-triethoxysilylpropyl)carbamate. (trichloroethyl carbamate initiator)

A mixture of 3-aminopropyltriethoxysilane (13.6 mL, 12.9 g, 58.4 mmol), *2,2,2*-trichloroethyl chloroformate (7.9 mL, 12 g, 58 mmol), and triethylamine (10.0 mL, 7.26 g, 71.7 mmol) in toluene (100 mL) was stirred at 40 °C for 4 hours. The reaction mixture was filtered to remove triethylammonium chloride. The filtrate was concentrated in vacuum to give a yellow-brown oil (20.6 g, 89%). For analysis, the crude product was further purified by vacuum distillation (Kugelrohr, 205 °C/0.4 mbar) to yield product as a colourless liquid. ^{1}H NMR (300 MHz, $CDCl_3$): δ 0.64 (t, J = 7.9 Hz, 2 H), 1.22 (t, J = 7.1 Hz, 9 H), 1.67 (tt, J = 7.9, 6.6 Hz, 2 H), 3.24 (q, J = 6.6 Hz, 2 H), 3.82 (q, J = 7.1 Hz, 6 H), 4.71 (s, 2 H), 5.38 (br. t, 1 H). ^{13}C NMR (50 MHz, $CDCl_3$): δ 7.52 (CH_2), 18.16 (CH_3), 22.88 (CH_2), 43.47 (CH_2), 58.35 (CH_2), 74.29 (CH_2), 95.62 (C), 154.47 (C=O). IR (KBr, cm^{-1}): ν 3338 (bs), 2974 (s), 1733 (s), 1538 (s), 958 (s). MS (CI, NH_3): *m/z* 417, 415, 413 (1, 3, 3%), 352, 350 (9, 10), 265 (27), 222 (100), 208 (25), 176 (33). Exact mass calcd. for $C_{12}H_{24}{}^{35}Cl_3NO_5Si + NH_4^+$ requires *m/z* 413.0828, found 413.0826 (CI, NH_3). Anal. Calcd. for $C_{12}H_{24}Cl_3NO_5Si$ (396.8): C, 36.33; H, 6.10; N, 3.53. Found: C, 35.88; H, 5.72; N, 3.53.

Preparation of 2-bromo-2methyl N-(3-triethoxysilylpropyl)propionamide. (2- bromoisobutyryl initiator)

A mixture of 3-aminopropyltriethoxysilane (6.98 mL, 6.63 g, 29.95 mmol), and triethylamine (5.48 mL, 3.94 g, 38.95 mmol) in toluene (50 mL) were placed in a round bottom flask (100 mL) with a magnetic stirrer bar. A dropping funnel fitted with a drying tube was attached to the flask and the flask was put into an ice bath. 2-bromoisobutyrylbromide (3.89 mL, 7.23 g, 31.45 mmol) was added drop-wise over

15 − 20 min. The mixture was left to cool for 10 min in an ice bath and then heated at 40 °C for 90 min. The reaction mixture was filtered under vacuum. The filtrate was concentrated in vacuum to give dark brown oil (18.0 g, 81%). For analysis, the crude product was further purified by vacuum distillation (Kugelrohr, 250°C/0.5 mbar) to yield product as a light brown liquid. ^{1}H NMR (300 MHz, $CDCl_3$): δ 0.62 (t, J = 7.7 Hz, 2 H), 1.15 (t, J = 7.0 Hz, 9 H), 1.64 (tt, J = 7.9, 6.6 Hz, 2 H), 1.90 (s, 6 H), 3.22 (q, J = 6.6 Hz, 2 H), 3.80 (q, J = 7.1 Hz, 6 H), 6.85 (br, 1H). ^{13}C NMR (50 MHz, $CDCl_3$): δ 7.52 (CH_2), 18.32 (CH_3), 22.65 (CH_2), 32.58 (CH_3), 42.55 (CH_2), 58.44 (CH_2), 63.21 (C), 171.85 (C=O). IR (NaCl, cm^{-1}): 3360 (bs, NH), 2974 (s), 1674 (s), 1526 (s), 953 (s). Anal. Calcd. for $C_{13}H_{28}BrNO_4Si$ (370.4): C, 42.15; H, 7.56; N, 3.78. Found: C, 41.78; H, 7.77; N, 3.87.

2.4.2 Synthesis of trichloroethyl carbamate-functionalised silica nanoparticles

Surface initiated polymerisations were performed to graft polymer chains onto the surface of silica nanoparticles.

Synthesis of trichloroethyl carbamate-functionalised aggregated silica nanoparticles

Silica nanoparticles were dried at 110 °C/0.03 mbar for 6 hours. A slurry of silica nanoparticles (5.1 g), trichloroethyl carbamate initiator (273 mg, 0.688 mmol), and toluene (90 mL) was heated to 110 °C for 12 hours. The solid was centrifuged (4000 rpm, 20 min) and the supernatant decanted. Centrifugation–decantation was repeated 3 times using THF as the extracting solvent. The gel layer was transferred into a pre-weighed beaker and dried in an oven at 60 °C overnight. IR and elemental analysis measurements were carried out to confirm the presence of the initiator on the particles.

Synthesis of trichloroethyl carbamate-functionalised non-aggregated silica particles

A mixture of *2,2,2*-trichloroethyl *N*-(3-triethoxy-silylpropyl) carbamate initiator (177 mg, 0.445 mmol), and silica dispersion (10 g of 30 wt% in methyl ethyl ketone) was added to a 25 mL flask equipped with magnetic stirrer bar and a reflux condenser. The flask was placed in an oil bath and gently refluxed at 70 °C for 24 hours. The functionalised particles were cooled to room temperature. IR and elemental analysis measurements were carried out to confirm the presence of the initiator on the particles.

2.4.3 Synthesis of ATRP Ligands

Synthesis of N,N-Bis(2-pyridylmethyl)octylamine (BPMOA)

BPMOA was synthesised using a procedure adapted from the literature,[1, 2] and consisting of coupling picolylchloride hydrochloride with 1-octylamin. A mixture of picolylchloride hydrochloride (5.5 g, 34 mmol) and 1-octylamine (2.8 mL, 2.19 g, 17 mmol) were dissolved in acetonitrile (50 mL) and stirred at room temperature for 10 min. Sodium carbonate (18.2 g, 170 mmol) was added and heated at 50 °C for 48 h. The obtained mixture was poured over aqueous sodium hydroxide (1 M, 100 mL), the crude product was then extracted with dichloromethane (3 × 80 mL) and the organic fractions were dried over anhydrous sodium sulphate and filtered. The solvent was evaporated under vacuum to yield the crude product as brown oil.

The product was eluted from a column of activated neutral alumina using 1:10 ethyl acetate: petroleum ether. (4.46 g, 65%). ^{1}H NMR (400 MHz, $CDCl_3$): δ 0.75 (t, 3H), 1.2 (m, 10H), 1.45 (m, 2H), 2.45 (t, 2H), 3.75 (s, 4H), 7.1 (dd, 2H), 7.45 (d, 2H), 7.6 (dd, 2H), 8.4 (d, 2H). ^{13}C NMR (50 MHz, $CDCl_3$, DEPT): δ 14.01 (CH_3), 22.65 (CH_2), 27.11 (CH_2), 27.33 (CH_2), 29.27 (CH_2), 29.44 (CH_2), 31.84 (CH_2), 54.54 (CH_2), 60.56 (CH_2), 121.81 (CH), 122.79 (CH), 136.34 (CH), 148.85 (CH), 160.10 (C). Anal. Calcd. for $C_{20}H_{29}N_3$ (311.47): C, 77.12; H, 9.38; N, 13.49. Found: C, 76.72; H, 9.35; N, 13.95.

Synthesis of Tris(2-dimethylamino)ethyl)amine(Me_6TREN)

The synthesis of Me_6TREN was carried out according to a previously reported method.[3] A mixture of 13mL formaldehyde (37 *w/w*) and 15.4 mL of formic acid (90% *w/w*) was stirred at 0 ^{o}C for 1 hour. To this mixture a solution of tris(2-aminoethyl)amine (4.22 g, 29 mmol) and 2.5 mL deionised water was added drop-wise. The mixture was gently refluxed overnight at 100 ^{o}C. After cooling to room temperature, the volatiles were removed by rotary evaporation. The residue was treated with a saturated sodium hydroxide aqueous solution (30 mL). Then the oily layer was extracted into ether.

The organic phase was dried over anhydrous sodium sulphate and the solvent was removed by rotary evaporation to produce a slightly brown oil product. Yield (65%). For analysis, the crude product was further purified by vacuum distillation (Kugelrohr, 230 °C/0.4 mbar). ^{1}H NMR (300 MHz, $CDCl_3$): δ 2.21(s, 18H), 2.32 (dd, 12H), 2.55

(dd, 12H). Anal. Calcd. For $C_{12}H_{30}N_4$ (230.39): C, 62.56; H, 13.12; N, 24.32. Found: C, 62.64; H, 13.32; N, 24.21.

2.4.4 ATRP on Surface Initiated Polymerisation

Synthesis of Grafted PMMA-silica Composites by ATRP in Miniemulsion using PMDETA as the Ligand

Copper(II) chloride (5.1 mg, 38 μmol), PMDETA (38 μL, 6.5 mg, 38 μmol), methyl methacrylate (4.0 mL, 3.8 g, 38 mmol) and deionised water (3 mL) were continuously stirred in a Schlenk flask at 50 °C for 15 minutes until the solution had turned blue due to the presence of a copper(II) amine complex. The solution was then cooled in an ice bath. A solution of Brij 98 (115 mg, 100 μmol) in deionised water (17 mL), hexadecane (0.23 mL) and trichloroethyl carbamate-initiator functionalised silica nanoparticles (0.61 g) were added to the Schlenk flask. The solution was then sonicated for 7 minutes. The homogenised miniemulsion was then deoxygenated with nitrogen for 30 minutes before being heated to 70 °C in a poly(ethylene glycol) bath. An aqueous solution of ascorbic acid (4.0 mg, 23 μmol, dissolved in 0.5 mL of deionised water) was added to initiate the polymerisation. After 90 min, the polymerisation was stopped by opening the flask and exposing the catalyst to air.

An aqueous solution of EDTA (15.5 mg, dissolved in 3 mL of deionised water) was then added. The solid was collected by suction filtration and washed with methanol (20 mL). After suspension of the solid in deionised water (50 mL), the treatment with EDTA and subsequent filtration was repeated once. The crude product was further purified by Soxhlet extraction with THF (100 mL, 12 hours at 90 °C). The residual solid was dried for 24 hours in an oven at 160 °C. Yield: 2.90 g. The silica composite was characterised by GPC, IR, ^{1}H NMR. TGA and elemental analysis.

Synthesis of Grafted PMMA-silica Composites by ATRP in Miniemulsion using BPMOA as the Ligand

Copper(II) chloride (9.4 mg, 70 μmol), BPMOA (70 μL, 21.8 mg, 70 μmol), methyl methacrylate (3.7 mL, 3.4 g, 35 mmol) and deionised water (3 mL) were continuously stirred in a Schlenk flask at 50 °C for 15 minutes until the solution had turned blue. The solution was then cooled in an ice bath. A solution of Brij 98 (115 mg, 100 μmol) in deionised water (17 mL), hexadecane (0.23 mL) and trichloroethyl

carbamate-initiator functionalised silica nanoparticles (0.61 g) were added to the Schlenk flask. The solution was then sonicated for 7 minutes. The homogenised miniemulsion was then deoxygenated with nitrogen for 30 minutes before being heated to 70 °C in a poly(ethylene glycol) bath. An aqueous solution of ascorbic acid (10 mg, 57.7 μmol, dissolved in 1 mL of deionised water) was added to initiate the polymerisation. The polymerisation was stopped by opening the flask and exposing the catalyst to air after 120 min. An aqueous solution of EDTA (15.5 mg, dissolved in 3 mL of deionised water) was then added in order to extract the copper complex. The mixture was added into methanol drop-wise and allowed to precipitate for 30 min. The supernatant was removed by filtration. The crude product was further purified by Soxhlet extraction with THF (100 mL, 12 hours at 90 °C). The residual solid was dried in a vacuum oven at 160 °C. Yield: 2.60 g. The polymer–silica composite was characterised by GPC, IR, ^{1}H NMR, TGA, SEM, TEM and elemental analysis.

The % silica content was determined from the elemental analysis results for the dried silica–PMMA hybrid particles and by comparison with the expected values for pure PMMA [Anal. Calcd. for $(C_5H_8O_2)_n$: C, 59.98; H, 8.05]. Elemental analysis data have an error of *±0.3*%. This could be affecting the results of % silica or % PMMA values for the composites. Results are summarised in **Table 2.2.**

Table 2.2. Elemental analysis results of various grafted PMMA-silica nanoparicles

Sample	%C[(c)]	%H[(c)]	%PMMA (C)	%PMMA (H)	%PMMA (avg.)	% SiO_2
PMMA-silica [(a)]	48.00	6.28	80.0	78.0	79.0	20.0
PMMA-silica [(b)]	50.31	6.46	83.9	80.2	82.1	16.1
PMMA-silica [(b)]	48.82	6.69	81.4	83.1	82.2	18.6
PMMA-silica [(b)]	46.90	6.20	78.2	77.0	77.7	21.8
PMMA-silica [(b)]	54.64	7.45	91.1	92.5	91.8	8.90
Error	*±0.3*	*±0.3*	*± 0.5*	*±3.7*	*±2.1*	

[(a)]PMMA-Cab H5. [(b)]PMMA-MEK-ST. [(c)] Calculated by elemental analysis

Synthesis of Grafted PBA-silica Composites by ATRP in Miniemulsion

Copper(II) chloride (5.1 mg, 38 μmol), PMDETA (38 μL, 6.5 mg, 38 μmol), butyl acrylate (5.4 mL, 4.8 g, 38 mmol) and deionised water (3 mL) were continuously stirred in a Schlenk flask at 50 °C for 15 minutes. The solution became blue due to the

presence of the copper (II) amine complex. The solution was then cooled in an ice bath. A solution of Brij 98 (115 mg, 100 μmol) in deionised water (17 mL), hexadecane (0.23 mL), and trichloroethyl carbamate initiator-functionalized silica nanoparticles (0.61 g) were added to the Schlenk flask. The mixture was sonicated with a Sonozap ultrasonic probe for 8 – 10 min whilst being stirred. Nitrogen gas was then bubbled through the homogenised miniemulsion for 30 minutes before heating the solution to 70 °C in a poly(ethylene glycol) bath. An aqueous solution of ascorbic acid (8.0 mg, 46 μmol dissolved in 0.5 mL of deionised water) was added to initiate the polymerisation. The polymerisation was stopped after 6 hours by opening the flask and exposing the catalyst to air. An aqueous solution of EDTA (15.5 mg, dissolved in 3 mL of deionised water) was then added. The miniemulsion was added to methanol to precipitate the solid, and filtered. The collected product was further purified by Soxhlet extraction with THF (100 mL) for 12 hours and dried for 24 hours in an oven at 160 °C. Yield: 3.13 g. Modified silica nanoparticles were characterised by FT-IR, ^{1}H NMR, GPC, SEM, TEM and elemental analysis.

Synthesis of Grafted PS-silica Composites by ATRP in Miniemulsion

Copper(II) chloride (10.2 mg, 75 μmol), BPMOA (75 μL, 23.4 mg, 75 μmol), styrene (4.34 mL, 3.95 g, 38 mmol) and deionised water (3 mL) were continuously stirred in a Schlenk flask at 50 °C for 15 min. The solution became blue due to the presence of a copper(II) amine complex. The solution was then cooled in an ice bath. A solution of Brij (124 mg, 108 μmol) in deionised water (17 mL), hexadecane (0.3 mL) and trichloroethyl carbamate-initiator functionlised silica nanoparticles (0.61 g) were added to the Schlenk flask. The mixture was then sonicated for 7 minutes to get a uniform suspension. The homogenised miniemulsion was then deoxygenated with nitrogen for 30 minutes before being heated at 95°C in a poly(ethylene glycol) bath. An aqueous solution of ascorbic acid (20 mg, 115 μmol, dissolved in 1.5 mL of deionised water) was added to initiate the polymerisation. The polymerisation was stopped after 48 hours by opening the flask and exposing the catalyst to air. An aqueous solution of EDTA (15.5 mg, dissolved in 3 mL of deionised water) was then added to the mixture. The mixture was added into methanol drop-wise and allowed to precipitate for 30 min. The supernatant was removed by filtration. The collected product further purified by Soxhlet extraction with THF (100 mL, 12 hours at 90 °C). The residual solid was dried in a vacuum oven at 160 °C. Yield: 3.50 g of colourless solid. ^{1}H NMR spectroscopy

FT-IR, TGA and elemental analysis were used to confirm the presence of attached PS on the particles. The PS nanocomposites was characterised by GPC, SEM and TEM.

Synthesis of Grafted Styrene/Acrylonitrile Copolymer-silica Composites by ATRP

The synthesis of grafted-PSAN-silica nanoparticles, was carried out according to a previously reported method.[4] 2-Bromoisobutyryl-initiator modified silica nanoparticles (0.20 g) were dispersed in anisole (6 mL) with stirring for 12 hours in a Schlenk flask. Styrene (2.44 mL, 2.21 g, 21.3 mmol) and acrylonitrile (0.82 mL, 0.66 g, 12.5 mmol) were added, and then a solution of $CuBr_2$ (0.21 mg, 0.94 μmol) and Me_6TREN (0.395 μL, 0.22 mg, 0.94 μmol) complex in anisole (0.75 mL) was added. The mixture was degassed by three freeze-pump thaw cycles. A solution of $Sn(EH)_2$ (0.61 μL, 0.76 mg, 1.88 μmol) and Me_6TREN (0.79 μL, 0.44 mg, 1.88 μmol) in anisole (0.5 mL) was added before heating the mixture at 95°C in a poly(ethylene glycol) bath. The reaction was stopped after 48 hours by exposing the catalyst to air. The product was precipitated into methanol (350 mL) over 30 minutes then the supernatant was removed by filtration. The precipitate was dried in a vacuum oven at 60 ^{o}C. The collected product was further purified by Soxhlet extraction with THF and dried in a vacuum oven at 160 ^{o}C. Yield: 1.9 g of colourless solid. The SAN nanocomposites was characterised by ^{1}H NMR, FT-IR spectroscopy, TGA, GPC, SEM and TEM.

Synthesis of Styrene/Acrylonitrile Copolymer by ATRP

The SAN copolymer was synthesised according to a literature procedure.[4] A mixture of styrene (4.88 mL, 4.42 g, 42.6 mmol), acrylonitrile (1.64 mL, 1.32 g, 25 mmol), and anisole (5.15 mL) were stirred in a dry Schlenk flask for 10 min. Then, ethyl 2-bromoisobutyrate (EBiB) (10 μL, 0.066 mmol) and a solution of $CuCl_2$ complex (0.223 mg, 1.66 μmol) and Me_6TREN (0.38 μL, 0.39 mg, 1.66 μmol) in anisole (0.8 mL) were added. The resulting mixture was degassed by three freeze-pump thaw cycles. A solution of $Sn(EH)_2$ (8.95μL, 11.34mg, 0.028 mmol) and Me_6TREN (6.36 μL, 6.53 mg, 0.028 mmol) in anisole (0.5 mL) was added. The sealed flask was placed in a poly(ethylene glycol) bath at 80 °C. The polymerisation was stopped after 48 hours by exposing the catalyst to air. The product was precipitated into methanol over 30 minutes then the supernatant removed by filtration. The precipitate was dried in a vacuum oven

at 60 ^{o}C. Yield: 3.66 g of colourless solid. The copolymer was characterised by GPC, FT-IR and ^{1}H NMR spectroscopy.

2.4.5 General Procedure for the Cleavage of Polymers from Silica

A procedure similar to that described by Antoni *et al*.[5] was used for cleaving polymer chains from functionalised silica nanoparticles. Polymer silica hybrid nanoparticles (0.3 g) were suspended in THF (15 mL) and a 1 M solution of tetrabutylammonium fluoride in THF (1.5 mL) was added. The mixture was then stirred for 3 days. After centrifugation (4000 rpm, 20 min), the supernatant was decanted and poured into hexane. The precipitate was collected by suction filtration and dried in an oven at 75 °C.

2.4.6 Preparation of Silica-filled Polymers by Solution Dispersion

A 5% solution of pure polymer in THF along with the required amount of dried silica particles (Cab-o-sil H5, A300), or colloidal silica dispersed in organic solvents (MEK-ST, MEK, ST-L and IPA-ST-UP), or titanium dioxide (anatase, rutile) was added to a flask. The flask was sealed to prevent evaporation and stirred for 48 hours or sonicated for 30 min. The solvent was then allowed to evaporate at room temperature. Samples were dried in an oven at 160 °C for 24 hours. The absence of residual solvent was confirmed by ^{1}H NMR spectroscopy.

2.4.7 General Procedure for the Preparation of Polyester Resin/non-aggregated Silica Nanocomposites

The compatibility of the polyester resin with the required amount of colloidal silica dispersed in an organic solvent such as methyl ethyl ketone (MEK-ST or MEK-ST-L) was first examined by mixing the polyester resin together with silica nanoparticles in a disposable plastic container to obtain a clear and transparent solution. Methyl ethyl ketone was removed by distillation at 80 °C. Methyl ethyl ketone peroxide (MEKP, 33% solution in dibutyl phthalate plasticiser 67%) was added and mixed well into the polymer resin using a plastic or wooden spoon. The catalyst and polyester resin-silica nanoparticles were slowly and carefully poured into the mould to avoid air bubbles. The polyester resin-silica mixture was then allowed to cure at 40 °C for 2 hours. The final product was characterised by SEM.

2.4.8 General Procedure for the Preparation of Polyester Resin/aggregated Silica Nanocomposites

The procedure of solvent-aided dispersion was carried out according to a previously reported method.[6] To suppress aggregation of silica nanoparticles, methanol was used as a solvent to lower the viscosity of the polyester resin and to aid mixing. The required amount of dried Cab-o-sil H5 (2 g) was mixed first with methanol (40 mL) followed by sonication for 40 min. The mixture was placed in a flask and the polyester resin (20 g) was added. The mixture was stirred mechanically at 360 rpm for 30 min. Methanol was removed by distillation at 65 °C. The catalyst MEKP (0.3 g) was added and mixed manually, then the dispersion was poured into the mould and the polyester resin-silica nanoparticles mixture was allowed to cure at 40 °C for 2 hours.

2.4.9 General Procedure for the Preparation of Epoxy Resin/silica Nanoparticles

Epoxy resin (100 g) was mixed with (10 g) of colloidal silica dispersed (MEK-ST) to obtain a clear and transparent solution. Methyl ethyl ketone was removed by distillation at 80 °C. To this mixture 45 g of hardener was added and mixed mechanically at 360 rpm for 25 min. The mixture was poured into the mould and allowed to cure at 60 °C for 15 hours. The nanocomposites was characterised by SEM, DSC and DMTA. In the case of aggregation silica nanoparticles (Cab H5), ethanol was used as a solvent. A required amount of dried Cab-o-sil H5 (2 g) was mixed with ethanol (50 mL), followed by sonication at 25 °C for 40 min. The mixture was placed in a flask and epoxy resin was added. The mixture was stirred mechanically at 360 rpm for 30 min. The ethanol was evaporated in a vacuum oven at 100 °C for 5 hours. Clear-cast epoxy hardener was added to the mixture and mixed at 500 rpm for 10 min. The epoxy resin-silica nanoparticle was left to cure at 60 °C for 15 hours. The product was characterised by SEM, DSC and DMTA.

2.5 Synthesis of Deuterated Polymers

2.5.1 Deuteration of Polystyrene under Microwave Conditions

Polystyrene (280 mg, 2.69 mmol) was dissolved in 2.4 mL of benzene-d_6. A 1 M ethylaluminum dichloride solution in hexane (800 μL, 0.53 mg, 6.30 μmol) was added until the mixture turned dark orange followed by 1-butyl-3-methylimidazolium chloride (0.40 g, 2.29 mmol). The mixture was irradiated at 150 W to 150 °C for 10 min.

Following irradiation the mixture was precipitated into methanol. The polymer was dissolved in THF and reprecipitated in methanol to remove all the ionic liquid and dried in vacuum oven overnight at 70 °C. Yield: 240 mg. ^{1}H NMR (300 MHZ, $CDCl_3$, δ, pmm): δ 1.3 (br, s, CH_2), 1.8 (br, s, CH-Ar). IR spectrum υ (cm^{-1}): 2923, 2845 alkyl (C−H), 2270 (C−D aromatic), and 1575 (Ar−C=C).

2.5.2 Deuteration of Poly(4-hydroxystyrene) under Microwave Conditions

A solution poly(4-hydroxystyrene) (200 mg, 1.66 mmol) in THF (2mL) was added to a 10 mL microwave reaction vial. To this D_2O (1 mL) was added drop-wise. This was followed by addition of 10M HCl (0.1 mL). The vial was sealed with a cap and the mixture was irradiated for 2 x 30 minutes at 165 °C. After irradiation the mixture was placed on a pre-weighted Teflon plate and the solvent left to evaporate. The sample was dried in a vacuum oven overnight at 120 °C. Yield: 190 mg. IR spectrum υ (cm^{-1}): 3015(C-H aromatic) 2923, 2845 alkyl (C-H), 2270 (C-D aromatic), and 1585 (Ar-C=C)

2.5.3 Synthesis of Deuterated Poly(4-hydroxystyrene) from Deuterated Polystyrene

The synthesis was adapted from procedures reported in literature[7, 8] for the synthesis of hydrogenated poly(4-hydroxystyrene). Preparation of several other deuterated polymers starting from deuterated PS following a "conventional" sequence of polymer-analogous reactions: poly(4-acetylstyrene-d_4), poly(4-acetoxystyrene-d_4) and poly(4-hydroxystyrene-d_4).

Synthesis of Deuterated Poly(4-acetylstyrene) (ACPS-d_4)

Polystyrene-*d5* (2.60 g, 24.04 mmol) was dissolved in 25 mL cyclohexane. A three-necked round–bottom flask equipped with a condenser, dropping funnel, and magnetic bar for stirring was placed in hot bath at 55 °C. $AlCl_3$ (6.7 g, 0.05 mol) and 25 mL cyclohexane were added and the mixture was stirred vigorously. To this solution (3.5 mL, 3.86 g, 0.05 mol) acetyl chloride (CH_3COCl) was added dropwise. The reaction mixture turned yellow, with the evolution of hydrogen chloride (HCl) gas during the addition. The reaction was continued for 7 hours until the evolution of hydrogen chloride ceased. The reaction was stopped, and cyclohexane was removed by rotary evaporation. The residue obtained had a light yellow colour; air dried overnight and transferred into a beaker containing 100 g crushed ice and 5 mL of concentrated hydrochloric acid. The precipitate was filtered, dried in vacuum oven at 80 °C for 2h (aluminium chloride decomposed and polymer was obtained as a yellow precipitate) and then dissolved in 6.5 mL acetone, and precipitated in water. The suspension was dissolved in 5.5 mL THF and then precipitated in methanol. Yield: 2.80 g (77.7%).

^{1}H NMR (300 MHZ, $CDCl_3$): δ 1.3 − 1.6 (m, CH_2 and CH-Ar), 2.50 (s, CH_3-CO), 6.2 − 7.5 (m, Ar-C-H). IR spectrum υ (cm^{-1}): 2923, 2845 alkyl (C−H), 2272 (C−D aromatic), 1670 (C=O) and 1576 (Ar−C=C).

Synthesis of Deuterated Poly(4-acetoxystyrene) (APS-d_4)

Poly(4-acetylstyrene)-d_4 (1.0 g, 6.66 mmol) was dissolved in 25mL of $CHCl_3$. This was added to an oxidizing solution consisting of 5 mL of acetic anhydride, 5 mL of 30% H_2O_2, and trace amounts of concentrated H_2SO_4 (as the catalyst) and refluxed for 142 h at 85°C . At the end of every 12 h, 2.5 mL of acetic anhydride and 2.5 mL of H_2O_2 were added. After 142 hours the reaction was stopped, the organic layer was separated with a separating funnel and precipitated into 20 times methanol. The precipitated polymer was filtered and dried under vacuum. Yield : 1.3 g (63%). ^{1}H NMR (300 MHZ, $CDCl_3$): δ 1.3 (br, s, CH_2) 1.7 (br, s, CH-Ar), 2.25 (s, CH_3-COO), 6.3 − 6.8 (m, Ar−C−H). IR spectrum υ (cm^{-1}): 3024(Ar−C−H), 2923, 2845 alkyl (C−H), 1750 (O−C=O), 2272 (C−D aromatic).

Synthesis of Deuterated Poly(4-hydroxystyrene) (P4HS-d_4)

Poly(4-acetoxystyrene)-d_4 (50 mg, 0.30 mmol) was dissolved in 2 mL of acetone. To this mixture 0.3 mL of concentrated HCl was added. The mixture was starried at 50 °C for overnight under reflex. Followed by cooling slowdown to room temperature. The mixture was poured into hexane to precipitate the polymer. The precipitated polymer was filtered and re-dissolved in hexane and the filtered left in fume-cupboard overnight to evaporate most of the solvent and dried in vacuum oven for 4 hours at 85°C. Yield 25 mg (67%). ^{1}H NMR (300 MHZ, $CDCl_3$): δ 1.1 − 1.8 (br, m, CH_2 and CH−Ar), 6.5 (br, s, Ar−C−H)), 9.0 (br, OH). IR spectrum υ (cm^{-1}): 3024 (Ar−C−H), 2923, 2845 alkyl (C−H), 3300−3500 (OH).

2.6 References

1. J. C. Mareque Rivas, R. Torres Martin de Rosales and S. Parsons, *Dalton Trans.*, 2003, 2156.
2. J. Xia and K. Matyjaszewski, *Macromolecules*, 1999, **32**, 2434.
3. J. Queffelec, S. G. Gaynor and K. Matyjaszewski, *Macromolecules*, 2000, **33**, 8629.
4. J. Pietrasik, H. Dong and K. Matyjaszewski, *Macromolecules*, 2006, **39**, 6384.
5. P. Antoni, D. Nyström, E. Malmström, M. Johansson and A. Hult, *Polym. Prepr.* , 2005, **46(1)**, 477.
6. G. Lekakou, I. Kontodimopouls, A. K. Murugesh, Y. L. Chen, D. A. Jesson, J. F. Watts and P. A. Smith, *Polym. Eng. Sci.*, 2008, **48**, 216.
7. S. Deokar, R. Ghadage, C. Rajan and S. Ponrathnam, *J. Appl. Polym. Sci.*, 2004, **91**, 3192.
8. J. M. Nasrullah, S. Raja, K. Vijayakumaran and R. Dhamodharan, *J. Polym. Sci., Part A: Polym. Chem.*, 2000, **38**, 453.

Chapter 3 - Synthesis of Grafted Polymers-silica Nanoparticles

Contents

3.1 Introduction

The preparation of polymer nanocomposites using micrometer fillers with high surface–to–volume ratios is currently studied intensively in both industry and academia. Silica nanosize is of particular interest since a range of types are now commercially available and their high surface-to-volume ratio promises excellent compatibility with many polymer matrices.[1, 2] Growing polymer chains to or from the surface of silica nanoparticles is very important as the polymer coating alters the thermal and mechanical properties. The reinforcement effect is not only due to interaction between the polymer matrix and the silica nanoparticle but also a consequence of particle-particle interaction and aggregation.

Rühe first reported the attachment of polymers to silica nanoparticles using a surface-grafted azo initiator and a conventional radical polymerisation.[3, 4] More recently, controlled radical polymerisations have been used to generate surface-grafted polymer chains. The general strategy involves the covalent linking of a suitable initiator onto the silica surface, followed by controlled radical polymerisation of a vinyl monomer. Contributions from termination reactions that are typical for conventional radical processes become, if not negligible, at least minimised in controlled radical polymerisations as the concentration of active radical species is considerably reduced. This allows well-defined polymers to be synthesised with narrow molar mass distributions (M_w/M_n < 1.3) and predetermined degrees of polymerization (DP = [monomer]/[initiator]). Atom-transfer radical polymerisation (ATRP) has been successful in controlling molecular weight and polydispersity of various surface-grafted polymers, such as polystyrene (PS), poly(methyl methacrylate) (PMMA), poly(butyl acrylate) (PBA) and poly(styrene-co-acrylonitrile) (PSAN),[5-14] and even block copolymers.[14, 15] In contrast, nitroxide-mediated polymerisation and reversible addition fragmentation chain transfer (RAFT) polymerisation seem to be more restricted with regard to the choice of monomer and require a more elaborate synthesis for the surface initiating group.[16, 17]

In this thesis, the AGET (activators generated by electron transfer) version of an ATRP polymerisation was used to graft polymers from the surface of both aggregated and non-aggregated silica nanoparticles, in which crosslinking and macroscopic gelation are minimised by using a miniemulsion system. Surface initiated ATRP polymerisations were performed to synthesise PMMA, PBA, PS homopoymer and PSAN copolymer

brushes. The effects of several parameters in ATRP process were examined, including the effect of initiator, catalyst, ligand, and reducing agent.

3.2 Silica Nanoparticles

In this study, commercially available aggregated silica nanoparticles Aerosil 300 from Degussa-Hüls and Cab-o-sil H5 from Cabot and various non-aggregated silica nanoparticles [Organosilicasol^{TM}, MEK-ST, MEK-ST-L and IPA-ST-UP from Nissan Chemical America Corporation] were used. Most other groups have either chosen one or the other, but never compared the effect the type of silica has on surface-grafted filler particles on the mechanical and thermal properties of these nanocomposites. Aerosil 300 and Cab-o-sil H5 have been chosen as they both have similar specifications according to the manufacturer's specification (specific surface area equal to 300 ± 30 m^2 g^{-1} and an average particle size of 7 nm), and would therefore be expected to behave similarly, although a slightly larger mean particle diameter in A300 has been found by dynamic light scattering (22 nm).[18] Different types of commercial aggregated silica particles (Aerosil 300 and Cab-o-sil H5) were chosen to study the effect of aggregation on the mechanical and thermal properties of nanocomposites. **Figure 3.1** shows the TEM images of aggregated silica nanoparticles (Cab-o-sil H5). The TEM image of Cab-o-sil H5 shows nanometer-size domains of stringy-shapes aggregated particles.

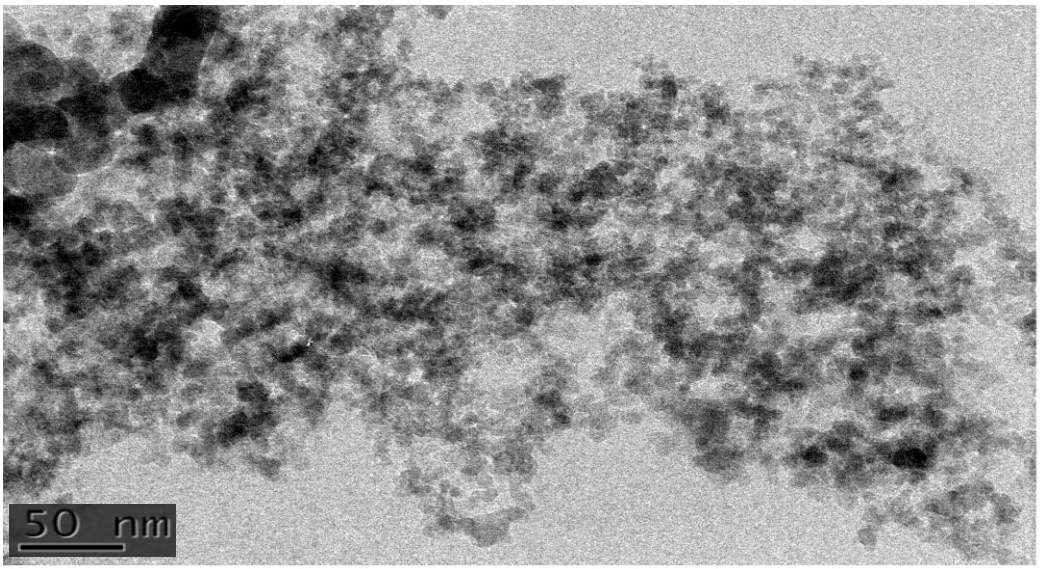

Figure 3.1: TEM image of unmodified aggregated silica nanoparticles (Cab-o-sil H5).

Aggregated particles such as Aerosil are known to aggregate strongly,[18] which promises a greater impact on modulus and mechanical properties than if the silica nanoparticles were uniformly dispersed in the polymer matrix (**Figure 3.2**). Furthermore, aggregated silica nanoparticles possess an additional dimensional network that further strengthens the composites.[19-21] Various types of silica nanoparticles that are available and of interest for this project were discussed in detail in **Chapter 1**.

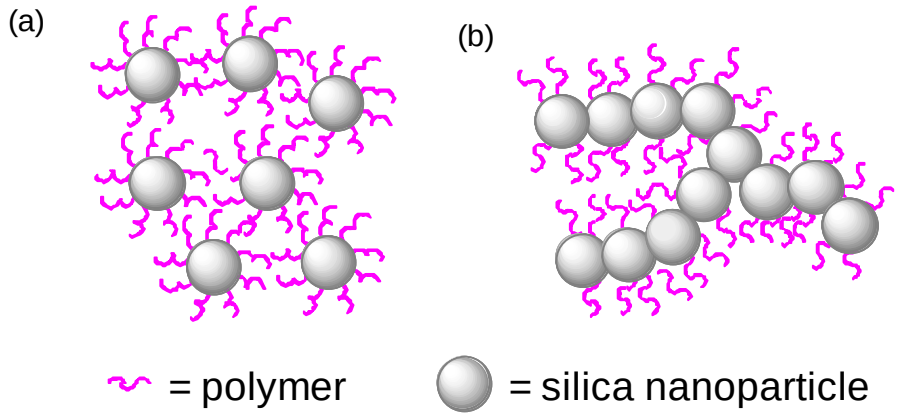

Figure 3.2: Schematic drawing of a polymer-silica nanocomposite where the polymer has been grafted from the surface of (a) non-aggregated silica nanoparticles. (b) aggregated silica nanoparticles.

3.2.1 Surface Modification of Silica Nanoparticles by Surface-initiated Atom Transfer Radical Polymerisation

The synthesis of polymer brushes on silica nanoparticles using surface-initiated polymerisation techniques is being increasingly reported in the literature. Polymer brushes by surface-initiated polymerisation on silica can be prepared using conventional free radical,[3, 4] Nitroxide Mediated Polymerisation,[22-24] Atom Transfer Radical Polymerisation,[5, 11, 25] and Reversible Addition Fragmentation Transfer polymerisation.[17, 26] Among these various methods, controlled ATRP has emerged as a popular technique to covalently bond polymers to a surface due to its versatility and simplicity, whereas NMP and RAFT polymerisation requires a more elaborate initiator synthesis. The strategy involves pre-treating inorganic nanoparticles with compounds having initiating groups. In the present study the surfaces of silica were modified with polymer and copolymer brushes. It is proposed that the particles in different media can be made more compatible by grafting polymer chains from the surface of silica nanoparticles. The facile polymerisation of ATRP and less stringent experimental

conditions promoted the application to grow polymer chains from glass surfaces and nanoparticles, especially silica. Various reported methods regarding surface-initiated atom transfer radical polymerisation from the surface of silica nanopartices were discussed in detail in **Chapter 1**.

3.2.2 Surface-bound ATRP Initiator

Although there are many literature procedures for making an ATRP initiator suitable for attaching to the surface of silica,[27-30] the majority of these are multi-step processes and often time-consuming. Thus, following a report on the suitability of trichloromethyl groups as ATRP initiators,[31] a new ATRP initiator **1** was synthesised in a one-step process from commercially available and inexpensive compounds 3-aminopropyltriethoxysilane and trichloroethyl chloroformate (**Figure 3.3**). Although the trichloroethyl group is primarily considered in Organic Chemistry to be a protecting group for amines, thiols and alcohols, abstraction of a single chlorine by a suitable copper catalyst is possible and will initiate the controlled radical polymerisation. The use of a triethoxysilane group provides up to three sites for the attachment to silica. In addition, the reaction between the triethoxysilane and the silica surface forms a stable Si−O−Si bond via a condensation reaction.[30] It should be mentioned that, unlike bromoisobutanoate initiators, this initiator requires a C−Cl bond to be broken. The C−Cl bond is less reactive, which makes the polymerisation more controlled.

In this study, a trichloroethyl carbamate initiator **1** was used for immobilisation onto the silica surface. This initiator was selected for surface-initiated polymerisation as it had a simple structure and contained both a functional group suitable for surface attachment to silica and an ATRP initiating unit. The initiator was purified by vacuum distillation (Kugelrohr, 205 °C/0.4 mbar). The overall yield exceeded 80%, and its high purity was confirmed by ^{1}H NMR, ^{13}C NMR spectroscopy (**Figure 3.4 and 3.5)** and elemental analysis. Another ATRP initiator **2** was synthesised by reacting 2-bromoisobutyryl bromide with 3-aminopropyltriethoxysilane adapting a reported procedure (**Figure 3.6**).[27, 32] One advantage of using initiator **2** is its higher reactivity since the abstraction of bromine atom to produce the active radical form is faster than the abstraction of a chlorine atom from initiator **1**. The reaction again was easy to carry out, and the product could be purified by Kugelrohr distillation. The initiator was characterised by elemental analysis, ^{1}H NMR and ^{13}C NMR spectroscopy (**Figures 3.7** and **3.8**).

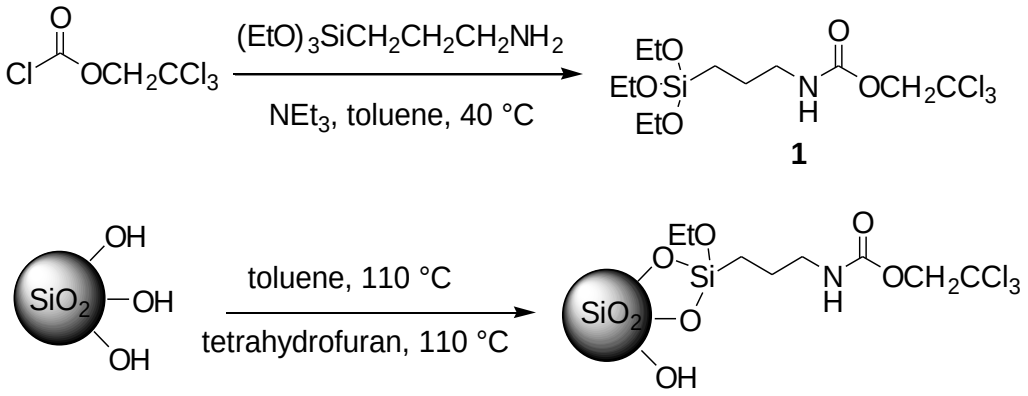

Figure 3.3: Synthesis of trichloroethyl carbamate ATRP initiator **1**.

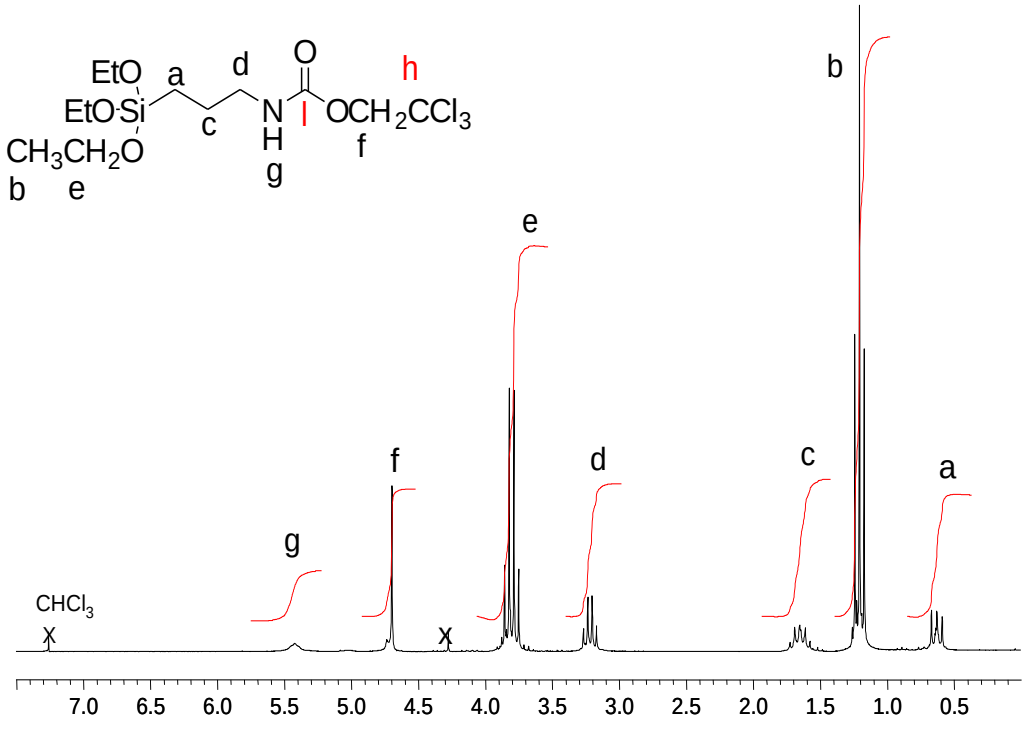

Figure 3.4: ^{1}H NMR spectrum (200 MHz, $CDCl_3$) of trichloroethyl carbamate ATRP initiator

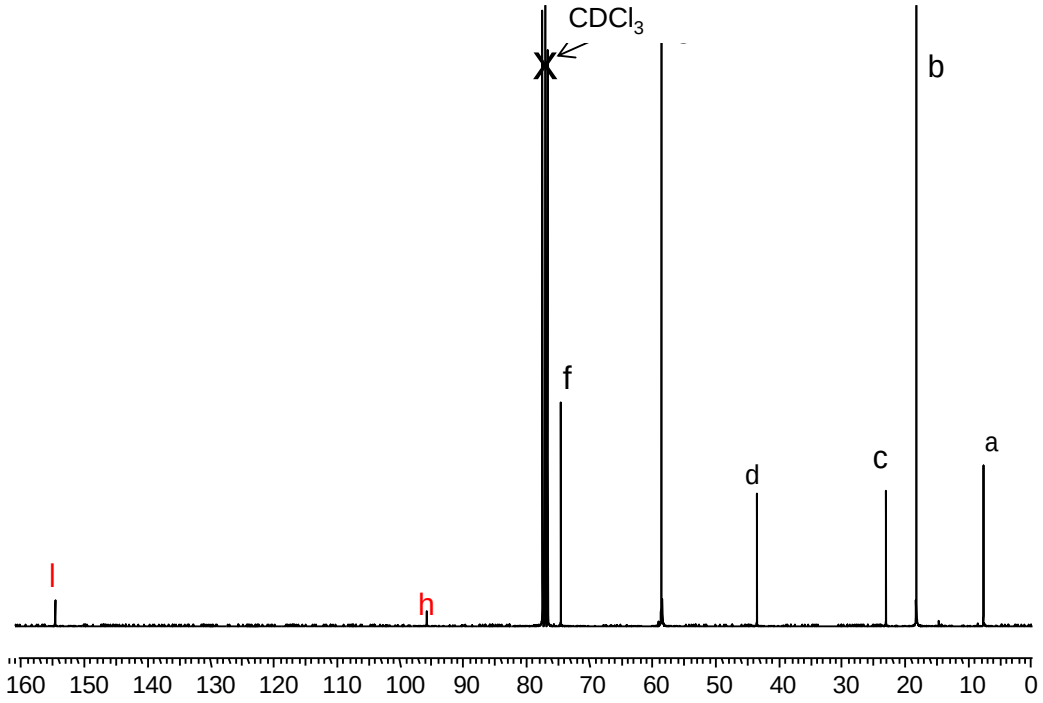

Figure 3.5:^{13}C NMR spectrum (300 MHz, $CDCl_3$) of trichloroethyl carbamate ATRP initiator

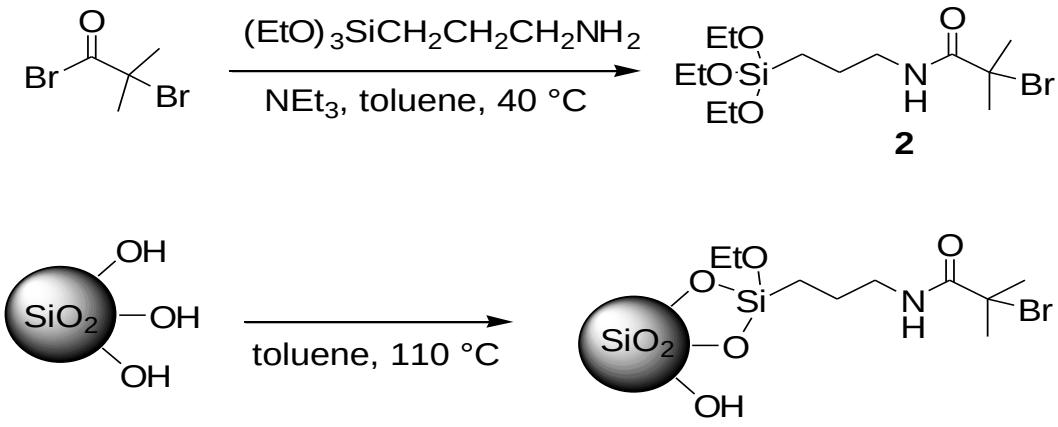

Figure 3.6: Synthesis of 2-bromoisobutyryl ATRP initiator

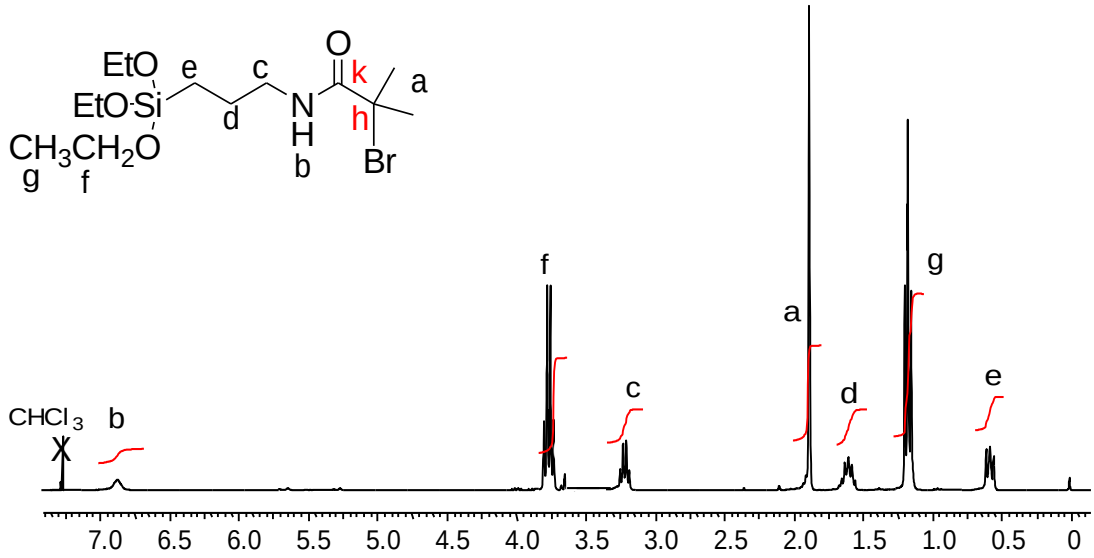

Figure 3.7: ^{1}H NMR spectrum (300 MHz, $CDCl_3$) of 2-bromoisobutyryl ATRP initiator.

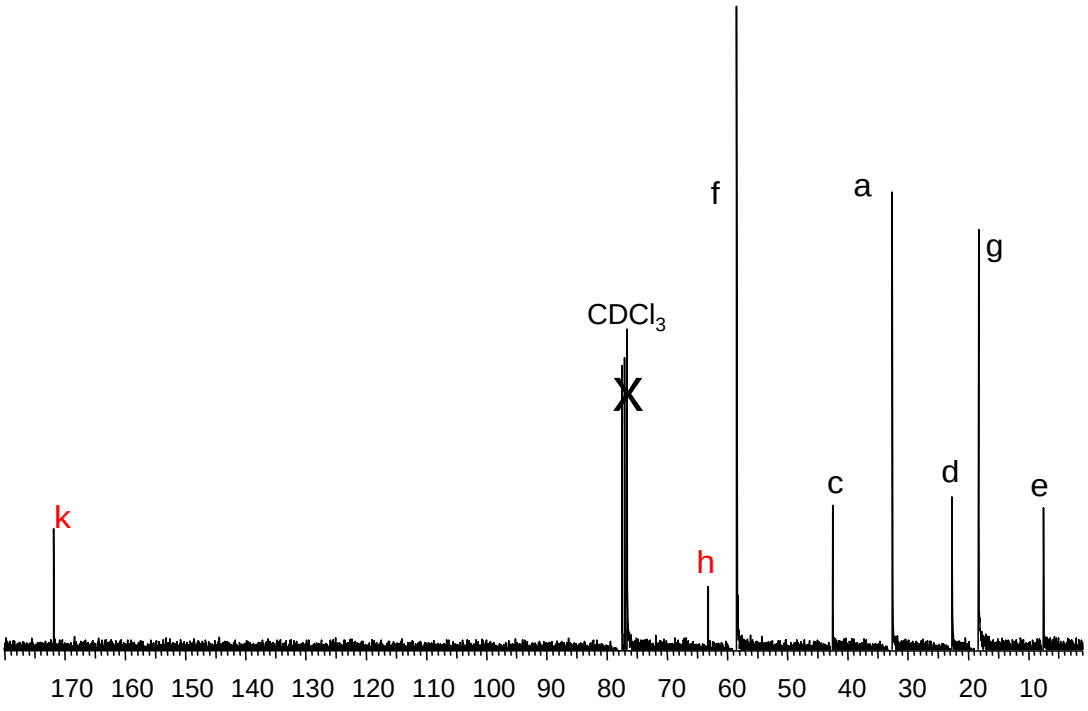

Figure 3.8: ^{13}C NMR spectrum (300 MHz, $CDCl_3$) of 2-bromoisobutyryl ATRP initiator.

3.2.3 Immobilisation of Initiator on the Surface of Silica Nanoparticles

The initiator **1** or **2** was reacted with silica at 110 °C in anhydrous toluene or tetrahydrofuran (**Figure 3.3** and **3.6**). Under these conditions its triethoxysilane group condenses with surface of OH groups of dried silica nanoparticles.[33] Unreacted initiator was washed from the nanoparticles by repeated suspension, centrifugation and decanting of the supernatant. FT-IR spectroscopy was performed to observe the characteristic peaks for the initiator-modified silica and unmodified silica (Cab-o-sil H5). For example, in the FT-IR spectrum a weak but noticeable urethane C=O stretch was observed at 1730 cm^{-1} in addition to the broad Si–O–Si vibration of the bulk silica at 1100 cm^{-1} (**Figure 3.9)**.

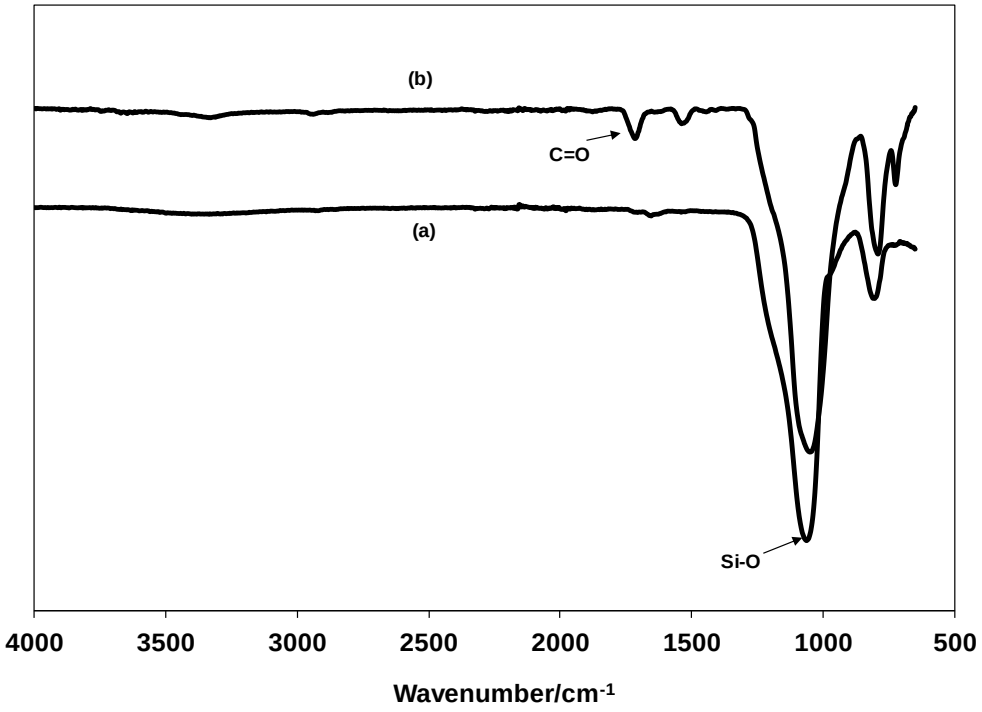

Figure 3.9: FT-IR spectra of (a) unmodified Cab-o-sil H5 silica nanoparticles, (b) silica–trichloroethyl carbamate initiator particles. The spectrum is presented in transmittance units.

3.3 Synthesis of ATRP Ligands

The reactivity of ATRP initiators depends crucially on the choice of ligand for the ATRP catalyst. The activity of metal catalyst complex in ATRP increases in the following order: bidentate ligands < tetradentate (linear) < tridentate < tetradentate (cyclic) < tetradentate (branched) < tetradentate (cyclic-bridged).[34] In general, the activity of the Cu complex strongly depends on the ligand's structure, and even small changes in the ligand's structure may lead to large difference in its activity (**Figure 3.10**).[35] *N,N,N′,N′*-tetramethylethylenediamine (TMEDA) , *2,2′*-bipyridine (bpy) and *4,4'*-di-5-nonyl-*2,2'*-bipyridine (dNbpy) are bidentate ligands. Compared with bpy, dNbpy complexes are ~6 times more active. The high reactivity of the dNbpy complex is due to the additional alkyl chains which increases the solubility of the complex in less polar solvents.[35] The reactivity of *N,N,N,N′,N″*–pentamethyldiethylenetriamine (PMDETA) is 300 times more than the related N[2,3]. Both ligands have a quite similar structure except that N[2,3] has one –CH2- spacer more than PMDETA.[36]

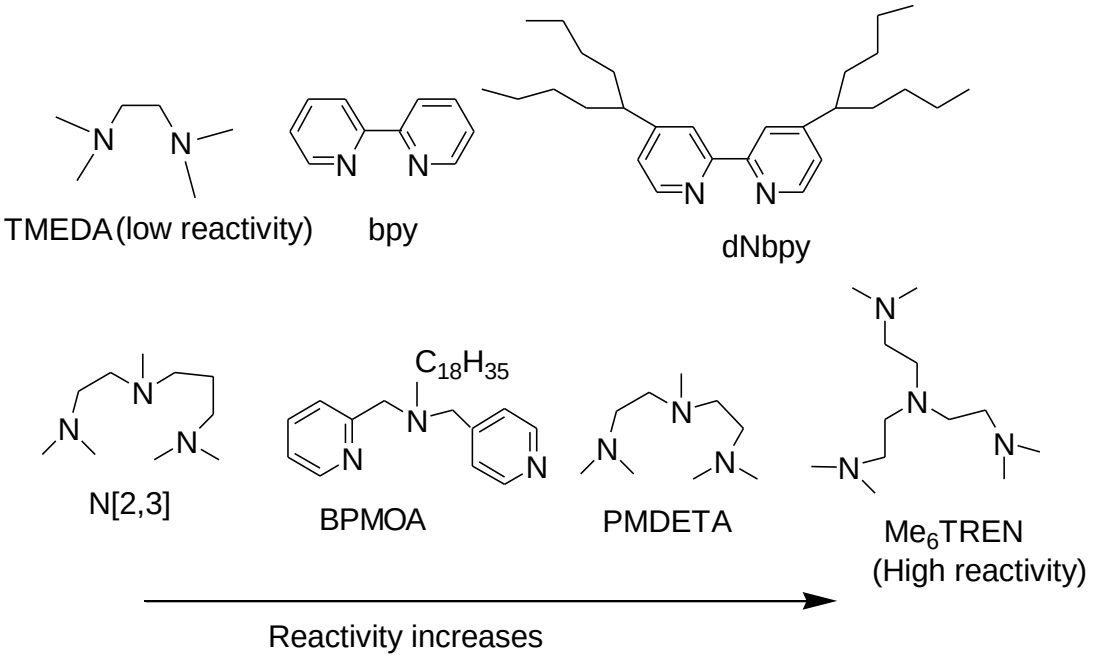

Figure 3.10: Structures of the most common ATRP amine ligands.

3.3.1 Synthesis of N,N-Bis(2-pyridylmethyl)octylamine (BPMOA)

In ATRP process the main role of the ligand is to solubilise the copper salts and tune their activity. Therefore, the effectiveness of the catalyst is greatly influenced by the choice of the ligand. Initially the commercially available tridentate ligand PMDETA was considered for use as the ligand in the ATRP catalyst due to its low cost and common use in ATRP. However, the resulting Cu complex was suspected to have a low solubility in organic solvents which resulted in a gradual decrease in polymerisation rate. Previous literature procedures[35-37] have replaced PMDETA with BPMOA, a tridentate ligand containing an octyl chain, which led a Cu complex that is soluble in nonpolar monomers, although its activity is only 2 times less than that of Cu-PMDETA. The use of Cu-BPMOA led to lower radical concentrations and prevented excessive terminations. In this study BPMOA was used in an AGET ATRP in miniemulsion polymerisation of methyl methacrylate and styrene from the surface of both aggregated and non-aggregated silica nanoparticles, whereas Cu-PMDETA had already previously been used successfully for grafting PS, PMA, and PMMA homopolymer from silica.[36]

The synthesis of BPMOA was adapted from a literature procedure[36, 38] by coupling of picolyl chloride hydrochloride with 1-octylamine, both of which are commercially available (**Figure 3.11)**. The primary amine with its long octyl chain improved the solubility of the copper-ligand complex in the organic phase (i.e. the monomer). The resulting BPMOA was purified by column chromatography on activated neutral alumina using ethyl acetate:petroleum ether (1:9). The ligand was characterised by ^{1}H NMR, ^{13}C NMR spectroscopy and elemental analysis (**Figure 3.12** and **3.13**).

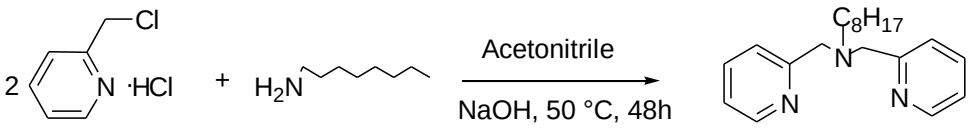

Figure 3.11: Synthesis of *N*,*N*-Bis(2-pyridylmethyl)octylamine (BPMOA).

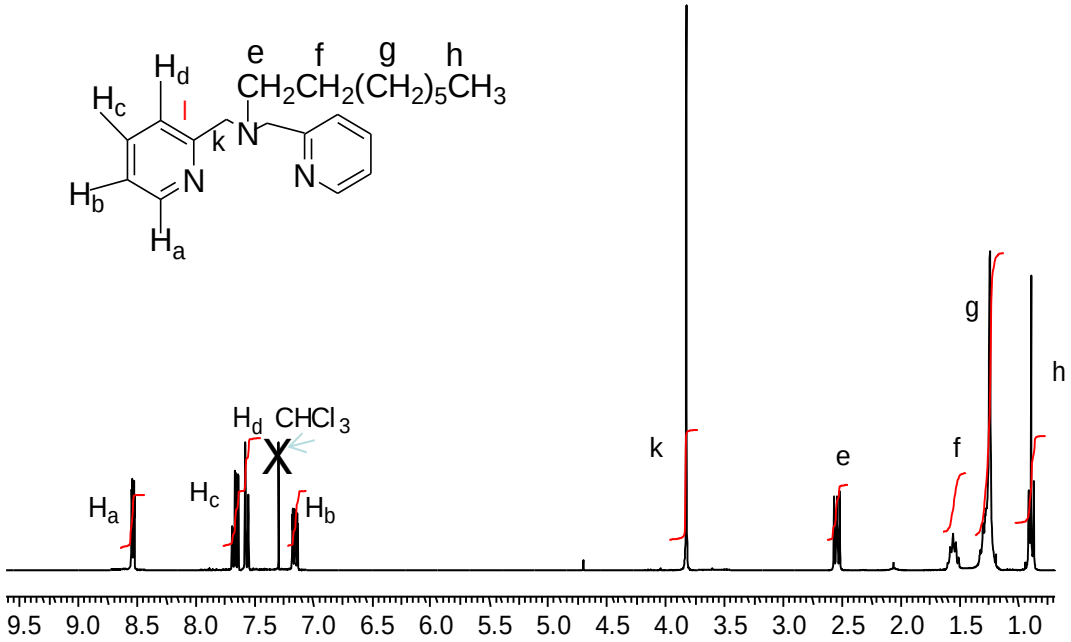

Figure 3.12: ^{1}H NMR spectrum (300 MHz, $CDCl_3$) of BPMOA

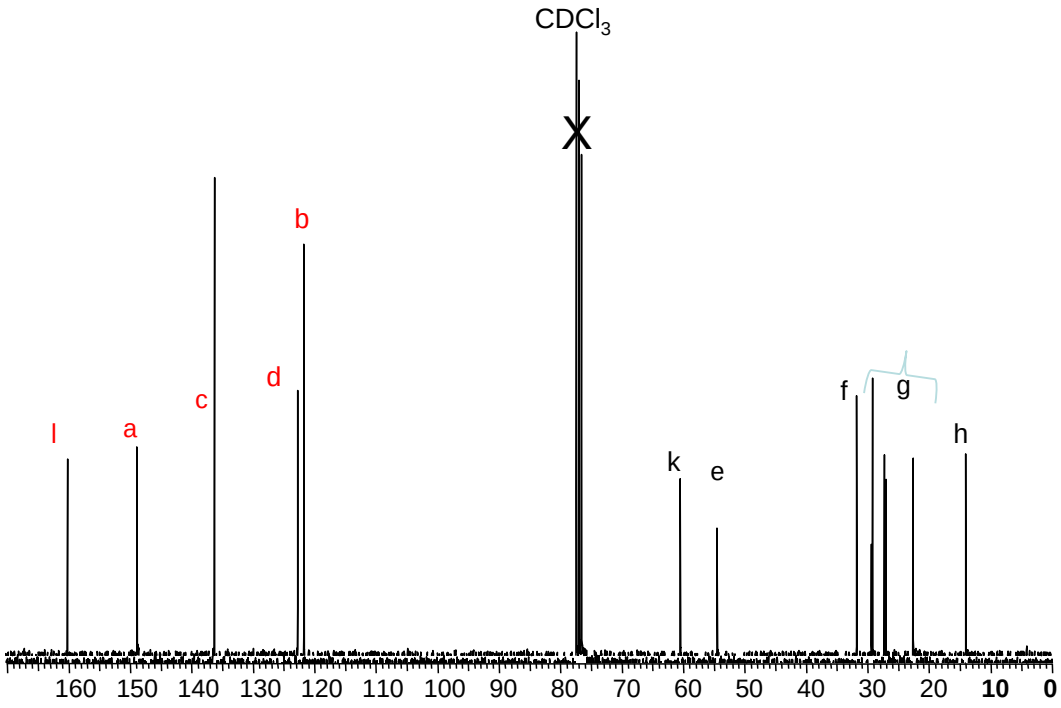

Figure 3.13: ^{13}C NMR spectrum (300 MHz, $CDCl_3$) of BPMOA.

3.3.2 Synthesis of Tris(2-dimethylamino)ethyl)amine(Me_6TREN)

The synthesis of Tris(2-dimethylamino)ethyl)amine was carried out according to a previously reported method in the literature.[39] Me_6TREN can be readily synthesised in one step from commercially available tris(2-aminoethyl)amine and a mixture of formaldehyde and formic acid.

3.4 Surface-initiated Polymerisation of Methyl methacrylate, Butyl acrylate, Styrene and Styrene/Acrylonitrile using ATRP

A series of surface-initiated ATRP polymerisations were performed to synthesise PMMA, PBA, PS homopolymer and PSAN copolymer brushes. Despite their potential wide-ranging engineering applications, very little is known about the effect of surface-grafted filler particles on the properties of the resulting nanocomposites. Therefore, a part of this thesis is devoted to investigate the thermal and mechanical properties of selected polymer-modified silica nanoparticles prepared by ATRP on the basis of different factors including type and size of silica, as well as varying molecular weight and graft density of the polymer.

PMMA has been extensively used in industry because of its good optical clarity, good resistance to weathering and high tensile modulus.[40] However, the variety of applications of PMMA is limited due to the polymer's brittleness. PBA is a component of many commercial paints owing to PBA's good water resistance, low temperature flexibility (T_g ca. -45 ^oC) and excellent weather resistance.[41] Paints with grafted PBA nanofiller are expected to exhibit improved properties such as high temperature resistances and impacts.

The glass transition temperature T_g of PSAN (~ 120 ^oC for a 25 wt% AN) which is slightly higher than the T_g of PS (T_g ~ 100^oC). PSAN has also a better impact strength than PS.[42] In addition, PSAN is compatible with a range of thermoplastics polymers, such as nylon[43] or polypropylene,[44] and is also used as toughening additive for those polymers.[42] Therefore, further improving the properties of PSAN by grafting the polymer to nanoparticles could have great influence in the applications.

3.4.1 Synthesis of Grafted PMMA-silica Composites by ATRP in Miniemulsion using PMDETA as the Ligand

The synthetic strategy in order to preparate grafted PMMA-silica nanoparticles is outlined in **Figure 3.14**. In this study a recently developed technique, AGET-ATRP in miniemulsion was used to graft polymers from the surface of silica nanoparticles since this process was straightforward and had already been demonstrated to work successfully for grafting poly(butyl acrylate) from the surface of colloidally dispersed silica nanoparticles.[14] In this technique, the ATRP catalyst is introduced in its higher oxidation state (in the form of Cu(II)) and then reduced by the addition of ascorbic acid to its activated Cu(I) form by a non-radical forming redox reaction. Since the copper catalyst was added in its oxidatively stable state, it can be added together with the macroinitiators. The reducing agent, ascorbic acid, has the advantage that it is water-soluble and environmentally benign.[45] Moreover, it dissolves completely in the aqueous phase and reduces the Cu(II) complexes, either at the surface of monomer droplets or in the aqueous phase. In addition, a poly(oxyethylene oleylether) surfactant (Brij 98) was added to generate a stable miniemulsion.[46] In order to ensure that the polymerisation continued smoothly, the amount of the ascorbic acid should be higher than the copper catalyst. However, too much ascorbic acid tends to lead to the reduced level of control, whereas too little causes a very slow polymerisation and a carefully optimised intermediate amount is essential. The best ratio of ascorbic acid to Cu(II) complex is ~0.4:1.[45] Matyjaszewski's procedure for polymerisation in miniemulsion proved more convenient, as the surfactant-stabilised dispersion was easily stirred even at high conversion, unlike polymerisations in bulk monomer which solidified quickly.[45, 47, 48] Polymerisations took typically between 90 and 120 minutes. Upon work-up, care was taken to remove any unattached polymer chains (ca. 1 − 4%) through extensive Soxhlet extraction of the crude product with tetrahydrofuran. The presence of unattached polymer chains is usually the result from small amounts of residual free initiator remaining after the functionalisation of the silica nanoparticles.[49]

Elemental analysis of the as-purified PMMA-silica hybrid materials revealed that the amount of PMMA was in the range of 78.2 to 90.2 wt%, corresponding to a silica content of 9.8 to 21.8 wt % as shows in **Table 3.1.** Elemental analyses data were found to be in agreement with thermal gravimetric analysis (TGA) measurements, as shown in **Figure 3.15** for one of the silica–PMMA hybrid systems. However, for practical (and cost) reasons most composites were analysed by elemental analysis.

The morphology of the grafted PMMA-silica nanoparticles was analysed by using TEM (transmission electron microscopy). Dilute suspension of PMMA grafted silica nanoparticles in toluene were cast onto carbon-coated copper grids and analysed after evaporation of the solvent. **Figure 3.16** shows the TEM images of PMMA-Cab-o-sil H5 (10.0 wt%) and PMMA-MEK-ST (16.1 wt%). The aggregated silica in the grafted PMMA-Cab-o-sil H5 are mostly destroyed after polymerisation, and the silica particles appears regularly distributed within the PMMA film as shown in **Figure 3.16 (a)**. **Figure 3.16 (b)** shows a typical TEM image of a cast film of colloidally dispersed silica grafted with PMMA chains. It can be seen that each particle is individually dispersed without any evidence of aggregate formation.

TEM measurements of more than one hundred nanoparticles showed an estimated particle core of 20 nm and 18 nm for PMMA-Cab-o-sil H5 (10.0 wt%) and MEK-ST (16.1 wt%), respectively. Using the procedure described by Li, Sheng and Zhao,[6] it was possible to estimate the average diameter of the aggregated silica–PMMA hybrid particles (PMMA-Cab-o-sil H5). The calculation requires the average diameter for a single nanoparticle (7 nm). The ratio of polymer to silica was obtained from elemental analysis. Together with the known densities of PMMA and silica, a diameter of 13 – 15 nm could be calculated. Both measurements indicate that the dimensions of the particles are greater than those expected from the average particle dimensions of Cab-o-sil H5 (7 nm) advertised by the manufacturer.

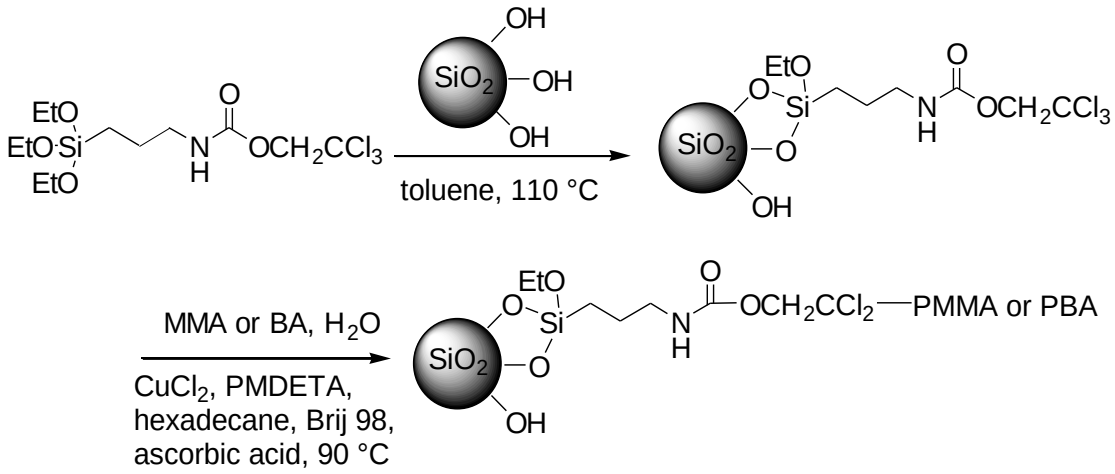

Figure 3.14: Surface-initiated polymerisation of methyl methacrylate (MMA) or butyl acryl ate (BA) from silica nanoparticles.

Table 3.1: Composition and estimated grafting density for grafted PMMA-silica nanocomposites.

Silica	*% SiO_2*	M_n [a)] [g mol^{-1}]	M_w/M_n	Grafting density by TGA (chains/nm^2)	Grafting density by elemental analysis (chains/nm^2)
Cab-o-sil H5	10	250000	1.50	----	0.07
Cab-o-sil H5	21.8	345000	1.37	----	0.01
MEK-ST	9.8	252000	1.54	0.10	0.09
MEK-ST	19.5	294000	1.98	----	0.03
MEK-ST	20.0	373000	1.33	----	0.02
MEK-ST-L	16.1	260000	1.52	----	0.17
MEK-ST-L	19.8	290000	1.85	----	0.11
IPA-ST-UP	20.0	252000	1.54	----	0.03

a) Calculated by GPC.

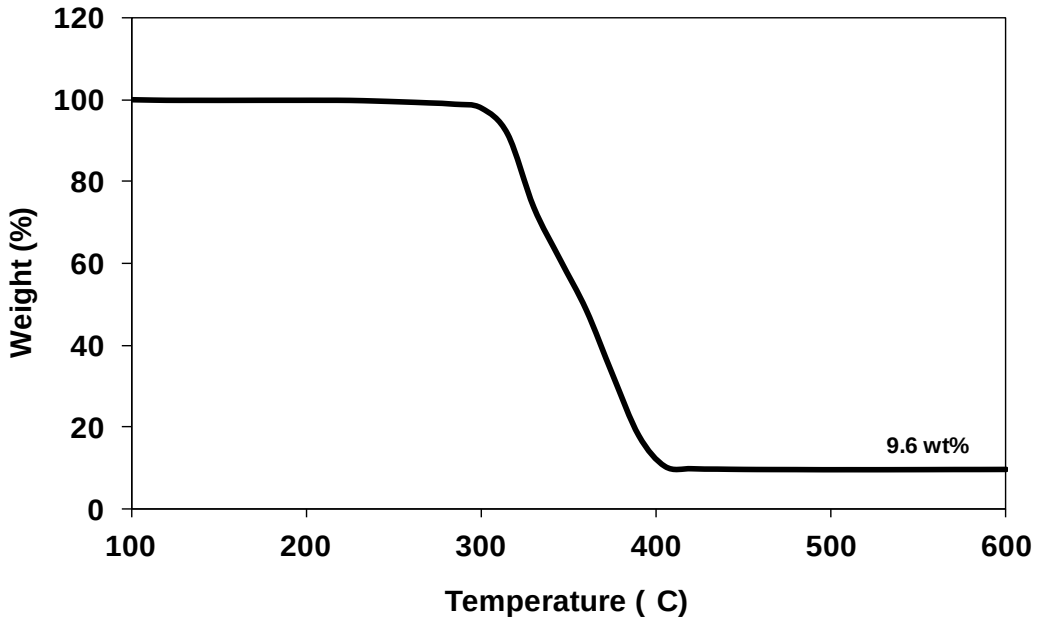

Figure 3.15: TGA analysis of a grafted-PMMA/MEK-ST (M_n 252,000 g mol^{-1}).

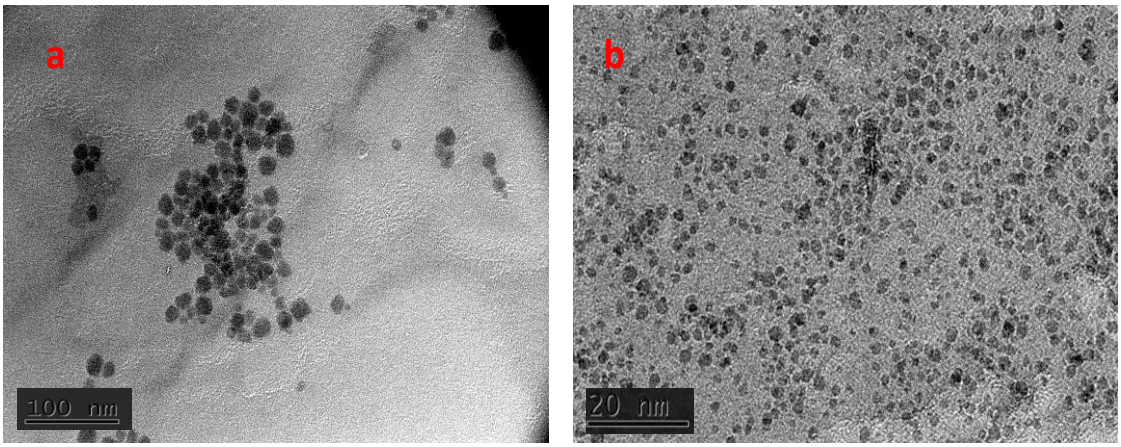

Figure 3.16: TEM images of (a) PMMA-Cab-o-sil H5 (10.0 wt%) and (b) PMMA-MEK-ST (16.1 wt%).

It was possible to record ^{1}H NMR spectra of grafted PMMA suspended in chloroform. These ^{1}H NMR spectra showed the typical signal pattern of radically polymerised PMMA (**Figure 3.17**). **Figure 3.18** illustrates the infrared spectrum of grafted polymer, with the characteristic alkyl C−H stretch at 2984 and 2949 cm^{-1}, a C=O stretch at 1728 cm^{-1}, an O–CH_3 stretching band at 1436 cm^{-1} and an Si−O−Si stretch at 1139 cm^{-1}. These results are in good agreement with previous studies describing PMMA nanocomposites.[50, 51]

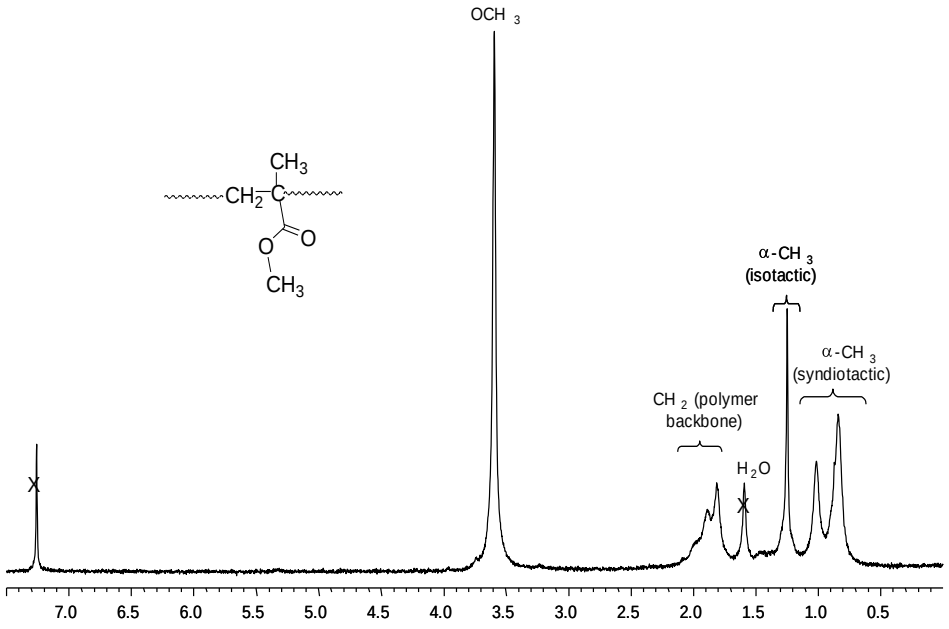

Figure 3.17: ^{1}H NMR spectrum (300 MHz, $CDCl_3$) of grafted PMMA–silica nanoparticles.

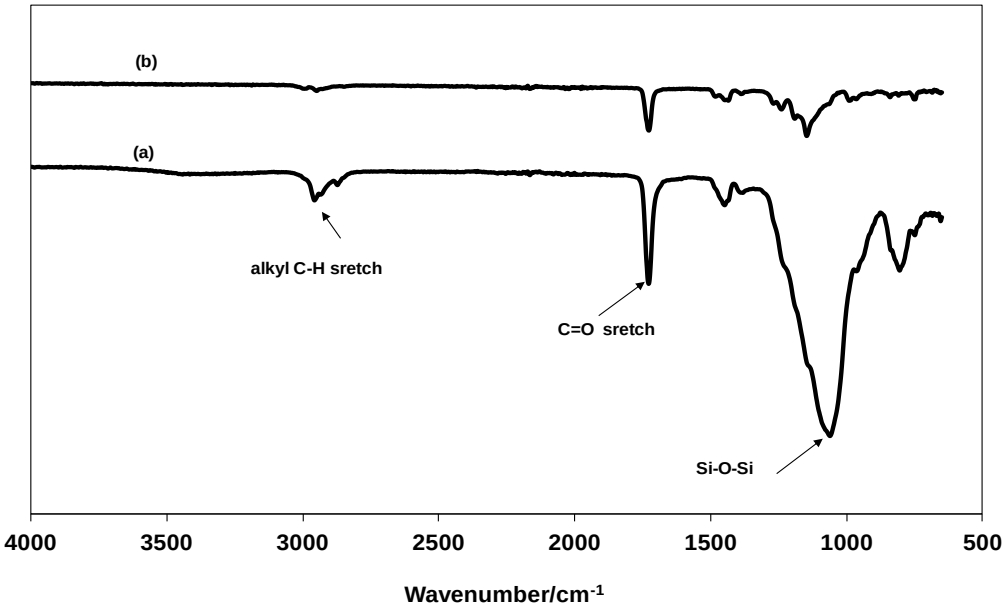

Figure 3.18: FT-IR spectrum of (a) a grafted PMMA-MEK-ST nanoparticles (9.8 wt%) and (b) PMMA cleaved from MEK-ST (9.8 wt%).

Average molar mass values for the grafted polymers were obtained by gel-permeation chromatography (GPC), after cleaving the polymer chains from the silica surface using tetrabutylammonium fluoride, and are reported in **Table 3.**1.

The molar masses were surprisingly high (**Table 3.1**) and molar mass distributions were found to be rather broad, with polydispersities of 1.33 – 1.98, which indicated an uncontrolled radical polymerisation process. It is generally easier to achieve high-molecular-weight polymers for rapidly propagating methacrylate monomers.[34] One reason for the poor control could be the use of a water-soluble chelating amine ligand (PMDETA) instead of the more hydrophobic ligands for the ATRP catalyst recommended in the literature. The polymerisations were initially carried out with PMDETA for reasons of convenience since this ligand was commercially available. However, the resulting active copper complex had a low concentration in the organic monomer phase which decreased the rate of the polymerisation.[52] Although the more polar catalyst predominantly resided in the aqueous rather than the organic phase of the miniemulsion, it still initiated polymerisation and allowed polymer chains to be grafted from the silica surface, which was the main objective with regard to this investigation. On the basis of GPC, TGA, and elemental analysis, the grafting density δ or (number chains/nm^2) was then calculated according to **equation (3.1)**.[53]

$$\delta = \frac{\frac{W_1}{W_2} \times 100 - W_2}{M \times S \times 100} \times N_A \times 10^{-18} \qquad (\mathbf{3.1})$$

where W_1 and W_2 is the amount of the polymer brush and silica nanoparticle respectively, M is the number average molecular weight of the polymer brush determined by GPC, S is the specific surface area in $m^2\ g^{-1}$ of the silica nanoparticle before grafting and N_A is Avogadro's number. The distance D (in nm) between the grafting sites also can be calculated using the follow **equation** (**3.2**).[54]

$$D = 4\ \delta\pi^{\frac{1}{2}} \qquad (\mathbf{3.2})$$

where δ is the grafting density (number chains/nm^2).

Figure 3.19. shows the GPC trace of PMMA-Cab-o-sil H5 (21.8 wt%), PMMA-MEK-ST (20.0 wt%), and PMMA-MEK-ST (19.5 wt%), where the samples had molar masses of 345,000, 373,000 and 294,000 g/mol, resp., and the polydispersity index was 1.37, 1.33 and 1.98, respectively. The surface grafting density was calculated to be 0.016, 0.02 and 0.03 chains/nm^2, respectively. This corresponded to a distance of 8.9 nm between the grafting sites for PMMA-Cab-o-sil H5 (21.8 wt %), 8.1 nm for PMMA-MEK-ST (20.0 wt %) and 6.7 nm for PMMA-MEK-ST (19.5 wt %). The grafting densities were smaller than those observed earlier for grafted PMMA-silica nanoparticles (0.12 chains/nm^2) reported in literature.[19] The apparent decrease in the grafting density for the highest molecular weight composites could be attributed to the fact that, at later stage of grafting process, the deactivator cannot readily diffuse to the dormant species because the surface of the silica are nearly completely occupied by the chains.[55] Ohno et al.[26] similarly found low grafted densities of PS brushes on silica nanoparticles in a RAFT polymerisation. According to their findings the decrease in graft density was attributed to the enhanced recombination of polymer radicals on the surface, which could be observed in the GPC traces as shoulder peak. However, in the present samples, almost no such shoulder peak, assignable to dead chains, is detectable in the GPC traces of both samples as seen in **Figure 3.19**.

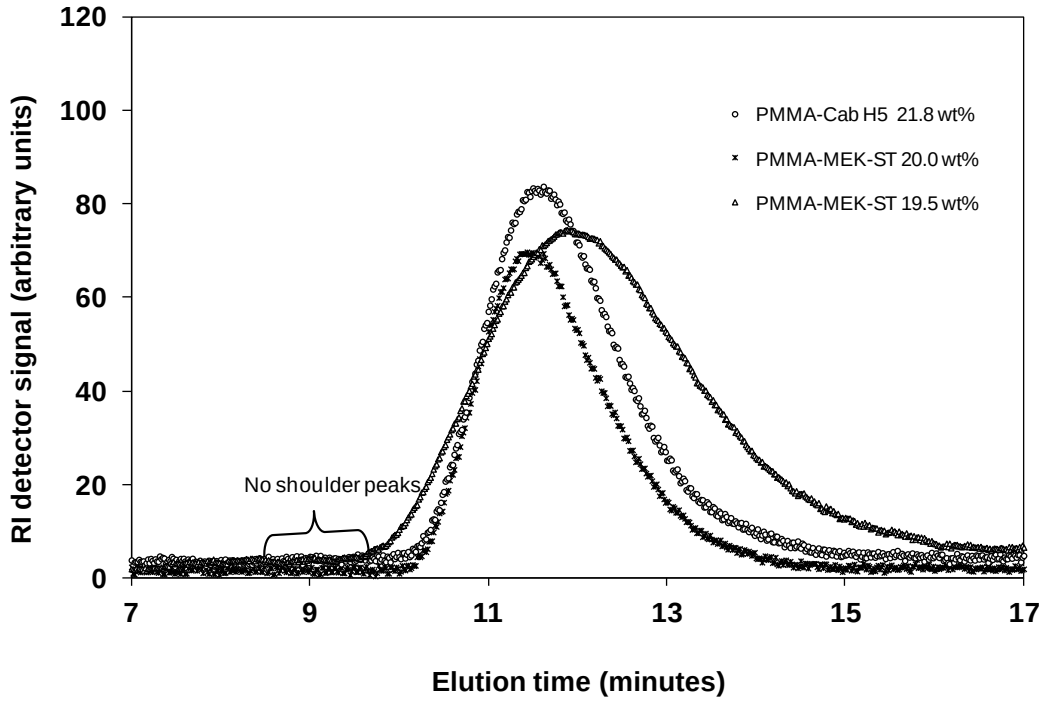

Figure 3.19: GPC traces of various grafted PMMA cleaved from silica–PMMA.

3.4.2 Synthesis of Grafted PMMA-silica Composites by ATRP in Miniemulsion using BPMOA as the Ligand

Copper-mediated ATRP in miniemulsion of methyl methacrylate was carried out under the same conditions using another amine ligand, namely *N*,*N*-bis(2-pyridylmethyl)octylamine (BPMOA) **Figure 3.14**. PMMA was successfully grafted from the surface of both aggregated and colloidally dispersed silica nanoparticles. Whereas a pale green colour was observed in the reaction mixture when PMDETA was used as the ligand, the polymerisation reaction mixtures employing BPMOA were yellow and more homogenous at room temperature. With BPMOA as the ligand, the copper complex was more soluble. A reduction in the polymerisation rate was observed which could be attributed to a lower radical concentration and, consequently, a better-controlled radical polymerisation producing a polymer with a narrower molar mass distribution.[52] This prevented excessive termination and depletion of the active copper(I) species. The molar mass of both free polymer and cleaved polymer were determined using GPC, and the results are summarised in **Table 3.2**. It was possible to make PMMA with medium molecular weights of the order of 20,000 – 30,000 g/mol. The polydispersities (1.05 − 1.14) were very narrow indicating that polymerisation occurred in a controlled manner. The molar mass and polydispersity of PMMA grafted

from silica (and subsequently cleaved) was similar to that of free PMMA formed in solution (**Figure 3.20**). A similar behaviour has been reported in the literature.[56-58] Since the chains grown from the surface have molecular weights similar to those grown in solution, they provide information about the composition and size of their counterpart chains grown from the surface.

The grafted PMMA-Cab-o-sil H5 has a significantly lower grafted density compared to non-aggregated silica composites (**Table 3.2).** This could be due to the aggregation of the particles, which reduces the accessible surface area for grafting. The distance between grafting sites also tends to increase with increasing the molecular weight of the grafted polymer. For example, in the case of PMMA-MEK-ST (~20%) where the polymer had molar mass of 27,000 and 373,000 g/mol the distances between grafting were 1.97 and 8.16 nm, resp. (**Table 3.1 and 3.2**). These data demonstrate that it is possible to control the spacing of grafting sites in a polymer by controlling the molecular weight of the grafted polymer. The grafting density of PMMA brushes was in range of 0.30 − 0.70 chains/nm^2, which were similar to those achieved for PMMA grafted from silica nanoparticles using conventional ATRP.[9] In contrast, the grafting density of PMMA-silica obtained with RAFT polymerisation was 0.30 − 0.38 chains/nm^2.[26] Compared to the grafting density of the RAFT polymerisation, the grafting density of PMMA-silica nanocomposites were higher for the ATRP polymerisation.

Table 3.2: Composition and estimated grafting density for both free and grafted PMMA-silica nanocomposites.

PMMA-silica nanopraticles	SiO_2 %	*Free polymer in solution*		*Grafted polymer*		Grafting density (chains/nm^2)
		M_n(g/mol)	M_w/M_n	M_n(g/mol)	M_w/M_n	
Cab-o-sil H5	16.0	------	------	28000	1.14	0.30
MEK-ST	20.0	------	-------	31000	1.11	0.29
MEK-ST	8.9	-------	-------	36000	1.05	0.70
IPA-ST-UP	21.1	27285	1.15	27000	1.10	0.31

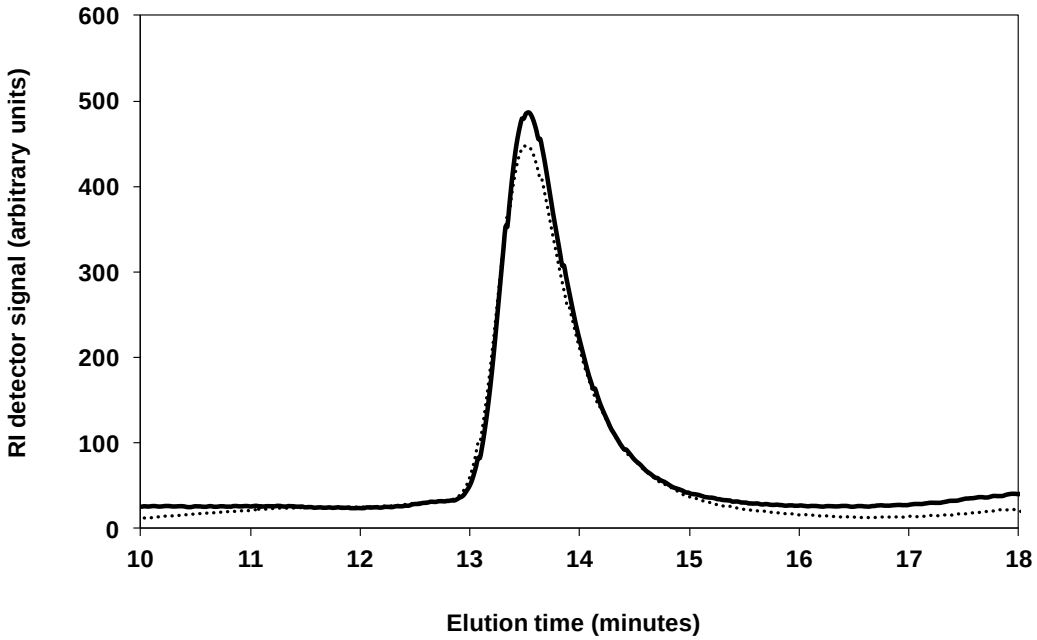

Figure 3.20: GPC traces of PMMA cleaved from silica–PMMA (IPA-ST-UP 21.1 wt%) hybrid nanoparticles (solid line) and free polymer produced during the polymerisation (dotted line)

3.4.3 Synthesis of Grafted PBA-silica Composites by ATRP in Miniemulsion using PMDETA as the Ligand

Grafted PBA-silica nanoparticles were prepared following Matyjaszewski's procedure as described in **Figure 3.14**. After the polymerisation had been terminated by exposure to air, the resulting Cu(II) complexes were easily removed by extraction with an aqueous solution of EDTA. It was observed that the blue color, which is indicative of Cu(II), almost completely disappeared.

The amount of covalently attached PBA calculated from elemental analysis data was in the range of 79.4 to 95.2 wt%, corresponding to a silica content of 20.6 to 4.8 wt%. **Table 3.3** shows the elemental analysis results and GPC measurements of the various silica-PBA composites made. Although these grafted particles did not dissolve in any solvent, the samples could still be dispersed in $CDCl_3$ and a ^1H NMR spectrum of this dispersion confirmed the absence of any soluble impurities such as unreacted monomer or traces of solvents (**Figure 3.21**).

Comparison of the IR spectra also indicated that PBA has been grafted from particle's surface. The spectrum shows the expected peaks for PBA: an alkyl C−H stretch at 2984 and 2949 cm^{-1}, a C=O stretch at 1728 cm^{-1} and an Si−O−Si stretch at 1139 cm^{-1}(**Figure 3.22**). Elemental analysis for the PBA-silica nanoparticles was carried out to estimate the amount of PBA grafted on the surface of the silica, with which the graft density was calculated using equation **3.1**. The graft density was estimated to be about 0.03 − 0.30 chains/nm^2 which is somewhat lower than that of poly(butyl acrylate) grafted from the surface of silica nanoparticles reported in literature.[26] Nonetheless, the graft density is high enough to support the production of polymer brush. **Figure 3.23** exhibits the GPC traces of ATRP of PBA synthesised at 85 and 65 ^oC. The PDI of the polymers prepared at 65 ^oC (1.40) were lower than those prepared at higher temperature (2.30), indicating that the side reactions were effectively reduced at lower temperature, although the polymerisation occurred over a longer time. Similar behavior has been reported by Matyjaszewski *et al*., using a less reactive initiator, ethyl 2-bromoisbutyrate functionalised silica for ATRP of acrylonitrile (AN).[59]

Table 3.3: Composition and estimated grafting density of grafted PBA-silica.

PBA/Silica type	%SiO_2	M_n [c)] (g/mol)	M_w/M_n	Grafting density (chains/nm^2)
MEK-ST[a)]	20.6	193,000	2.20	0.05
MEK-ST [a)]	12.6	117, 000	2.30	0.14
MEK-ST [a)]	4.8	174,000	2.20	0.30
Cab-o-sil H5[b)]	13.0	374000	1.40	0.03

[a)] Temp. = 85 °C. Time = 6 h, Ligand: PMDETA
[b)] Temp. = 65 °C. Time = 10h, Ligand: PMDETA
[c)] Calculated by GPC

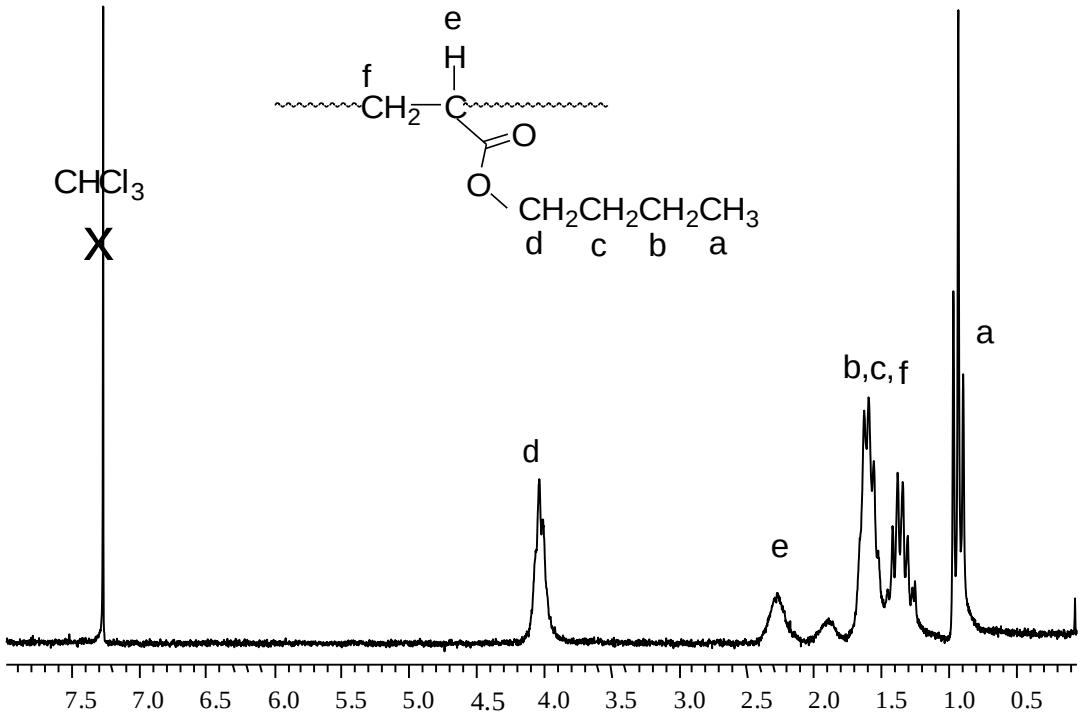

Figure 3.21: ^1H NMR spectrum (300 MHz, $CDCl_3$) of a grafted PBA-MEK-ST nanocomposite (4.8 wt %)

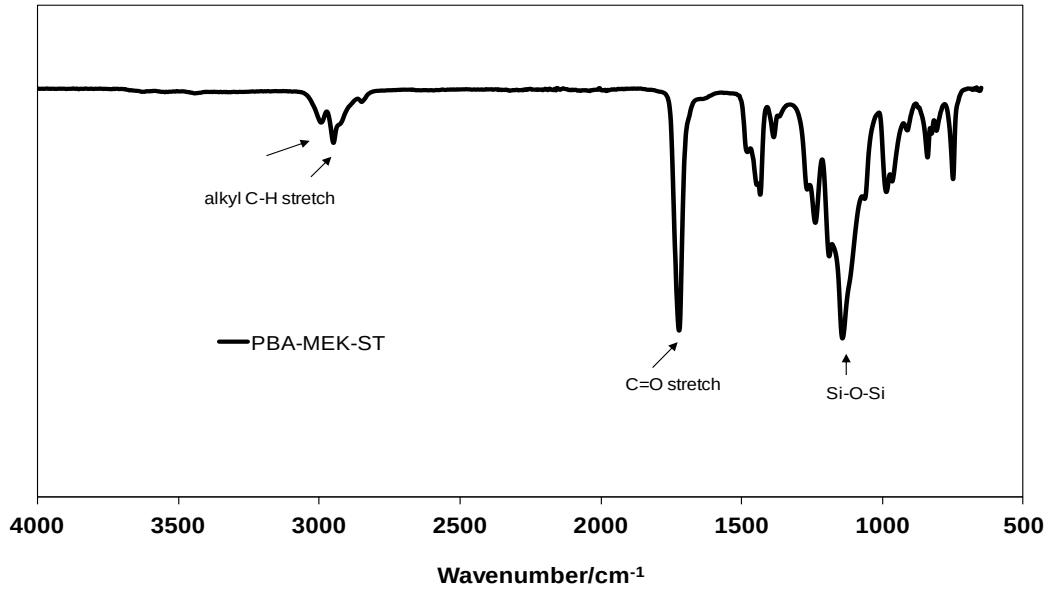

Figure 3.22: FT-IR spectrum of a grafted PBA-MEK-ST nanoparticles (12.6 wt%). The spectrum is presented in transmittance units.

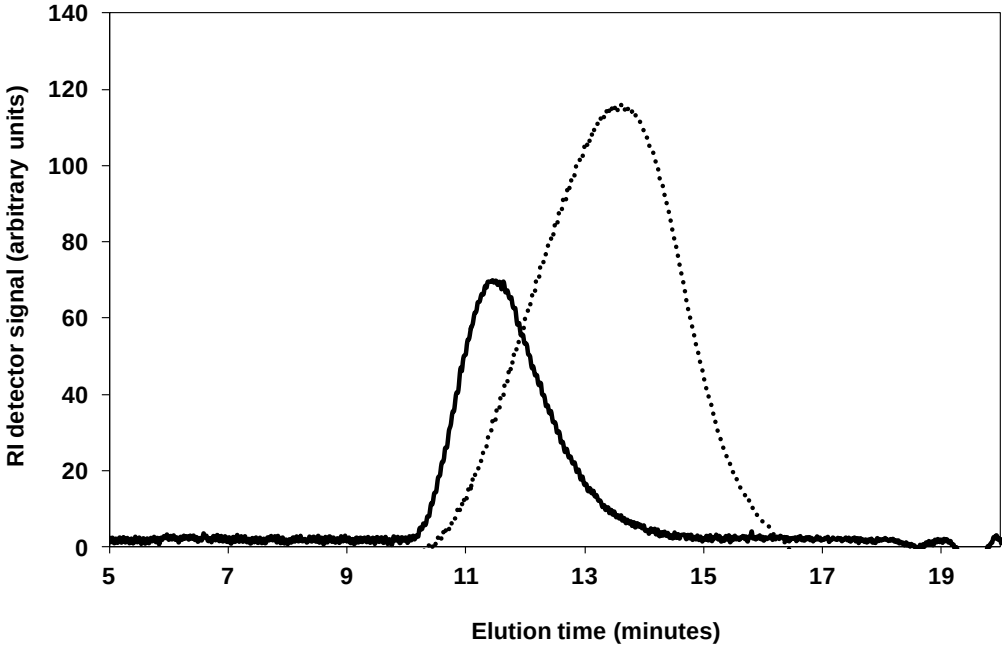

Figure 3.23: GPC traces of PBA cleaved from Cab-o-sil-PBA (13.0 wt%) hybrid nanoparticles (solid line) and MEK-ST-PBA (12.6 wt%) hybrid nanoparticles (dotted line).

3.4.4 Synthesis of Grafted PS-silica Composites by ATRP in Miniemulsion

The technique of ATRP in miniemulsion was applied to styrene monomer as well **Figure 3.24**. Styrene was successfully polymerised from the surface of both aggregated and colloidally dispersed silica nanoparticles using different ATRP initiators. However, the reaction time for the polymerisation of styrene was much longer than that observed for both methyl methacrylate and butyl acrylate. The reason for the increased reaction time is not clear. The choice of halogen atom in the ATRP initiator has an impact on the rate of polymerisation. ATRP of styrene with a Br-based initiator (e.g. a 2-bromoisobutyryl ester or amide initiator) is much faster and provides more control than ATRP polymerisations with a Cl-based initiator system.[60, 61] The polymerisation of styrene using a trichloroethyl-carbamate initiator functionalised silica resulted in a low initiation efficiency, suggesting that the trichloroethyl carbamate initiator might not be suitable for polymerising styrene. However, 2-bromoisobutyryl amide ATRP initiator was an efficient initiator for polymerisation of styrene. Matyjaszewski *et al*. studied the activation rate constants in the ATRP of PS using 1-phenylethyl bromide (PEBr) and 1-phenylethyl chloride (PECl) as ATRP initiators. In that report, the activation rate constant of bromide-based initiator (PEBr) was about 1000 times greater than that of PECl and deactivation rate is again 6 times higher than that of the chloride-based initiator. Thus higher rate of polymerisation for Br-based initiator since the overall equilibrium is dominated by the difference in the activation rate constants.[61] In addition, the slower deactivation rate leads to higher PDI.[62] Even with the more reactive Br-based initiator the polymerisation took typically 48 hours (2 days). After the polymerisation had gone to completion, care was taken to remove any unattached polymer through extensive Soxhlet extraction of the crude product with THF. The presence of some unattached polystyrene chains could be due to either the formation of new chains in solution, such as thermal self-initiation of styrene or, more likely, from traces of residual free initiator remaining after the functionalisation of the silica.[26, 49, 61, 63] The amount of unattached polystyrene could be significantly reduced by both decreasing the reaction temperature from 90 to 70 ^{o}C and using a more active ATRP complex for faster polymerisation. May *et al.* suggested that reducing the amount of free PS could be attributed to a slower rate of self-initation of styrene at low temperature.[64]

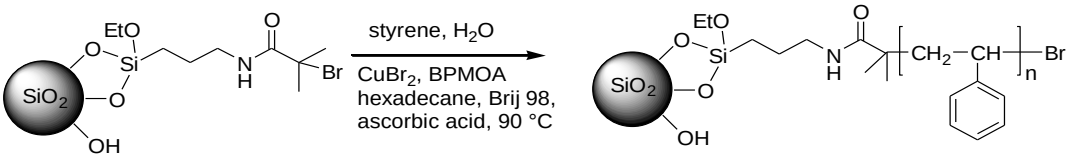

Figure 3.24: Synthetic scheme for the surface-initiated polymerisation of styrene from silica nanoparticles.

The resulting polymer–silica hybrid particles possessed a silica content of 8.3 – 23.7 wt% according to elemental analysis (**Table 3.4)**. In order to gain further proof that PS chains were covalently linked at silica surfaces, FTIR and ^{1}H NMR spectroscopy were employed to study the PS/silica hybrid nanoparticles. **Figure 3.25** shows the FT-IR spectra for the unmodified Cab-o-sil H5 silica nanoparticles, silica-initiator particles, silica-PS hybrids particles and PS cleaved from silica nanoparticles. The FTIR spectrum of PS/silica indicated aromatic ring vibrations at 1455 cm^{-1} and an aromatic C−H stretch at 3030 cm^{-1}, and a deformation mode characteristic for a monosubstituted benzene peak at 700 cm^{-1} (**Figure 3.25(c)**). Furthermore, it can be seen that there is a very pronounced peak appearing at 1102 cm^{-1} corresponding to the vibration absorption of Si–O–Si groups. This peak is disappeared when PS was cleaved from silica nanoparticles as shown in **Figure 3.25 (d)**. These results confirmed that PS had been successfully immobilised on the silica. A ^{1}H NMR spectrum is displayed in **Figure 3.26**. The signals of the aromatic protons from the side chains are found in the range from 6.5 to 7.4 ppm, and whereas the signals belonging to the polymer backbone (−CH−CH$_2$−) were found at δ_H 1.8 and 1.4, respectively. In order to determine the molecular weight of the graft polymer a small sample of the hybrid particles was treated with tetrabutylammonium fluoride to detach the polymer from the silica particles.[65] The grafting of styrene from the 2-bromoisobutyryl amide ATRP initiator functionalised silica particles, that a bromide-based initiator, proceeded in a controlled manner resulting in polymers having molecular weights and polydispersity index values between 26000 and 32000 g/mol and 1.12 and 1.14, resp., as determined by GPC (**Table 3.4**) which are in agreement with the results reported by other research groups.[64, 66] In general, the polymerisation control in ATRP in miniemulsion was slightly better with the bromide-based initiator instead of chloride-based initiator (**Table 3.4.)**. Furthermore, selective TEM images of grafted PS silica particles are shown in **Figure 3.27 (a** and **b)**. The TEM image clearly demonstrates that a good dispersion of particles in the polymer matrix was observed.

Table 3.4: Composition and estimated grafting density of grafted PS-silica nanoparticles.

Sample	%SiO_2	M_n [c)] (g/mol)	M_w/M_n	δ (chains/nm^2)
PS-A 300 [a)]	14.4	18000	1.10	0.57
PS-Cab H5[a)]	10.0	26000	1.12	0.62
PS-MEK-ST[a)]	10.0	32000	1.14	0.70
PS-MEK-ST[b)]	23.7	68000	1.36	0.10
PS-MEK-ST[b)]	14.0	83000	1.40	0.17

[a)] ATRP used a 2-bromoisobutyryl initiator (attached onto silica) and $CuBr_2$/BPMOA as catalyst.
[b)] ATRP used a trichloroethyl carbamate initiator (attached onto silica) and $CuCl_2$/ BPMOA as catalyst.
[c)] Calculated by GPC.

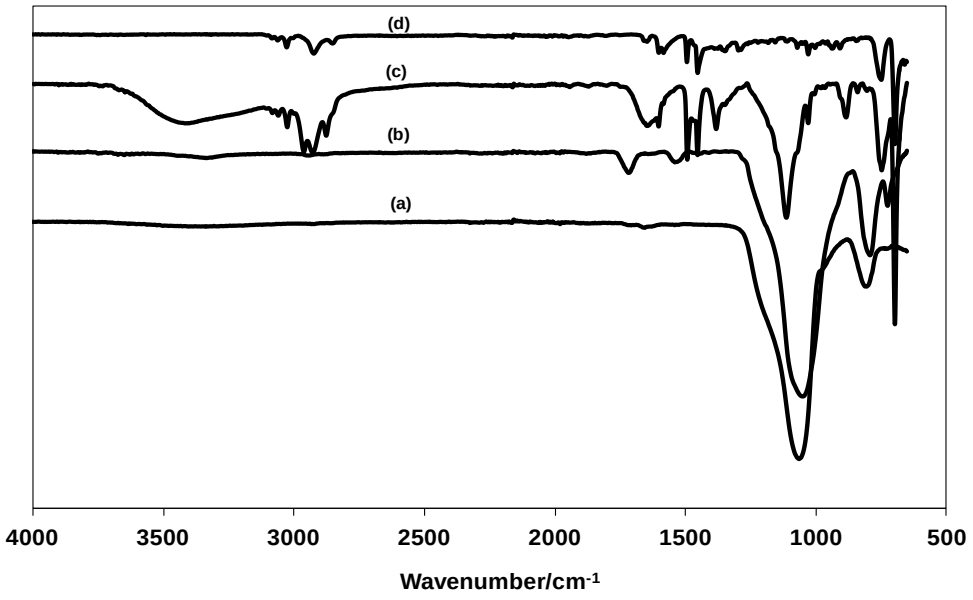

Figure 3.25: FT-IR spectra of (a) unmodified Cab-o-sil H5 silica nanoparticles, (b) silica–initiator particles, (c) silica–PS hybrid particles, and (d) PS cleaved from silica nanoparticles. The spectra presented in transmittance and it has been shifted vertically for clarity.

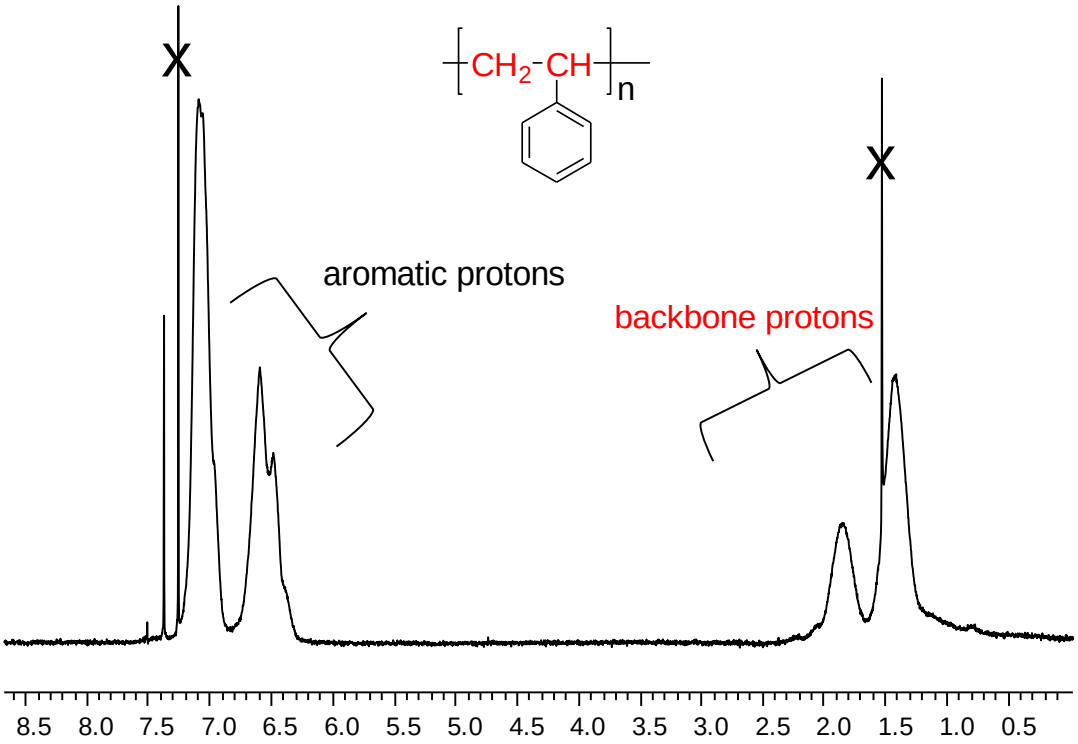

Figure 3.26: ^{1}H NMR spectrum (300 MHz, $CDCl_3$) of silica–PS hybrid particles. Solvent and water signals are marked by X.

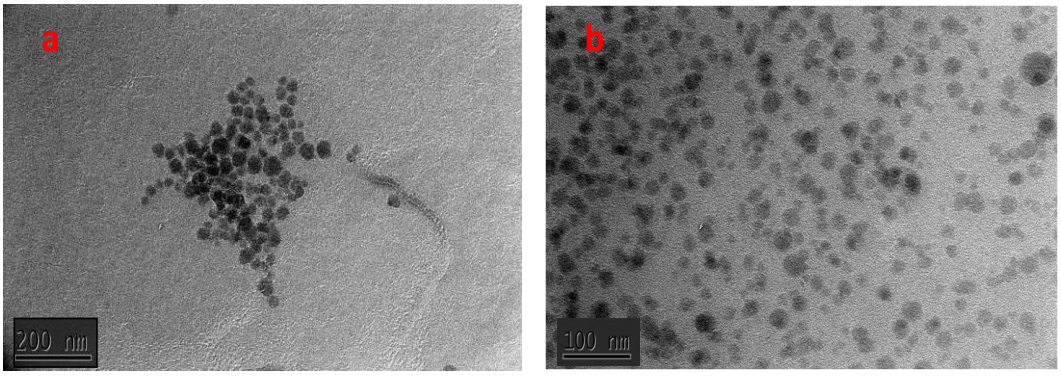

Figure 3.27: TEM images of (a) PS-Cab-o-sil H5 (10.0 wt%) and (b) PS-MEK-ST (14 wt%). The average diameter of the silica particles is 22 nm for Cab-o-sil H5 and 18 nm for MEK-ST.

Figure 3.28 shows the GPC curves of the cleaved polystyrene, as well as the polystyrene formed in solution and extracted after the polymerisation. It can be seen that the molar mass of free polymer (3300 g mol^{-1}) clearly differs from that of the grafted polymer (18000 g mol^{-1}). In addition, the molar mass distribution of free polymer was slightly broader (PDI=1.24) than that of the surface of silica (1.10). A possible reason for these phenomena is that all the chains in grafted PS which are attached to the particles started to grow at the early stages of the polymerisation due to the surface-bound initiator; whereas, chains formed by self-initiation in solution are continuously

formed during the reaction. This result is consistent with those reported in the literature.[26, 67] Nonetheless, PS brushes can be obtained with a quite high graft density of around 0.70 chains/nm^2 which was calculated according to equation **3.1**. The distance between the grafting sites is 1.4 nm which also can be calculated from equation **3.2**. It is evident from these results that steric constraints around silica particles have little influence on the control of the free radical process. The grafting density of PS obtained by the "grafting from" method in this study was higher than the grafting densities obtained by the "grafting to" approaches reported in the literature.[54] In the "grafting from" method, only low-molecular-weight monomer diffuses to the silica surface, while in the "grafting to" approach, polymer chains must diffuse to and react with the silica particles, which is less likely to happen.

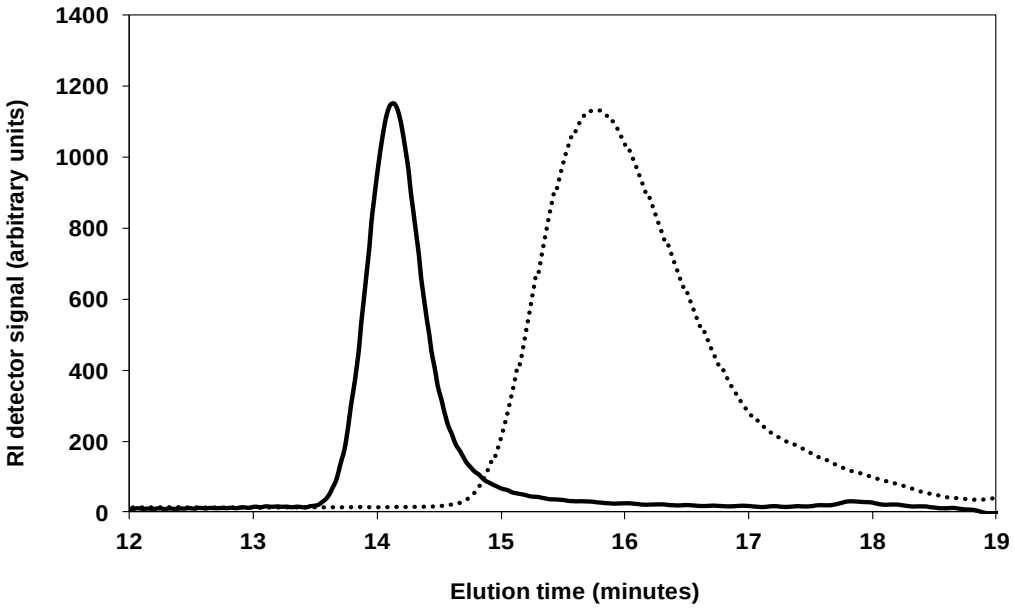

Figure 3.28. GPC traces of PS cleaved from silica–PS hybrid nanoparticles (solid line) and free polymer produced during the polymerisation (dotted line).

3.4.5 Synthesis of Poly(styrene-co-acrylonitrile) Grafted onto Silica Nanoparticles by ATRP

The grafting of SAN from the surface of silica nanoparticles was achieved first by attaching an ATRP initiator to the surface of the silica nanoparticles and then growing the chain from the modified silica surface. Initially, ATRP in miniemulsion was attempted with a mixture of styrene and acrylonitrile, following the same synthesis route as described in **Figure 3.14**. However, mini-emulsion is carried out in water, and acrylonitrile is relatively soluble in water.[68] Thus, the attempted copolymerisation of styrene and acrylonitrile using the ATRP in mini-emulsion method resulted only in the synthesis of polystyrene. Therefore, the SAN copolymer was synthesised by AGET ATRP from the surface of functionalised aggregated silica (Cab-o-sil H5 and A 300), as well as of colloidally dispersed silica nanoparticles (MEK-ST) using procedure similar to those reported previously for PSAN copolymer.[13] The monomer feed was close to the azeotropic composition (ca. 63 mol% styrene and 37 mol% acrylonitrile), and copolymerisation was conducted in the presence of catalyst system in anisole as shown in **Figure 3.29**. ATRP was conducted with 2-bromoisobutyryl amide or trichloroethyl-carbamate functionalised silica as initiators, Me_6TREN/Cu(II) as the catalyst, and an organic-soluble tin salt for reducing Cu(II) to Cu(I) instead of ascorbic acid in anisole at 90 ^{o}C. The reason for using tin(II) 2-ethylhexanoate ($Sn(EH)_2$) is because ascorbic acid is not soluble in anisole. Tin(II) 2-ethylhexanoate can reduce copper(II) to copper(I) as displayed in **Figure 3.30**. $Sn(EH)_2$ was successfully used as the reducing agent in ATRP polymerisation, with different monomers such as butyl acrylate, styrene, methyl methacrylate and acrylonitrile.[13, 59, 69]

The amounts of catalyst were varied to define the optimum conditions for control of SAN polymerisations. Three different amounts of Cu(II) were used 0.50, 1.00, and 2.00 equiv *vs.* $Sn(EH)_2$. An organic reducing agent, glucose, was also examined for the ATRP of SAN to reduce the absolute amount of any metals in an ATRP process. Glucose has the advantage that it is soluble in polar solvents and environmentally benign.[59] However, using glucose as reducing agent no polymerisation of SAN was observed. This result could be due to the added amount of glucose not being enough to initiate the polymerisation. The polymerisation was finished by opening the flask and exposing the catalyst to air after 50 h. The product was further purified by extensive Soxhlet extraction with THF to remove free, unattached polymer. The nanocomposite was obtained in a yield of typically 65%, corresponding to about 2 g of nanocomposites. To obtain a consistent copolymer composition and different silica content, the synthesis

was repeated several times using the same amounts of reagents with different amount of initiator-modified silica nanoparticles. In all cases, azeotropic feed ratio of acrylonitrile and styrene (37:63 molar ratios) was used. A reliable copolymer composition is important as it affects properties such as thermal and mechanical properties of the copolymer.

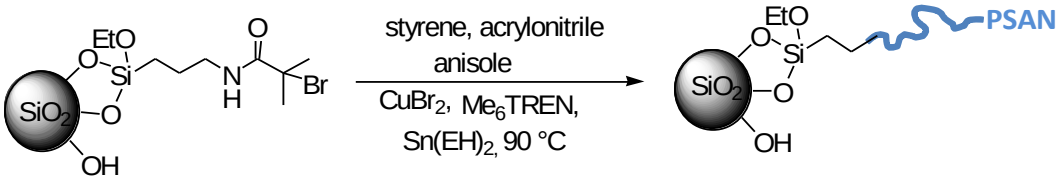

Figure 3.29: Synthetic scheme for the surface-initiated polymerisation of styrene/acrylonitrile from silica nanoparticles.

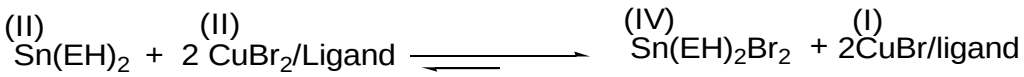

Figure 3.30: Reduction of Cu(II) to Cu(I) by tin(II) 2-ethylhexanoate ($Sn(EH)_2$).[69]

Molar mass and molar mass distribution of SAN copolymers were measured by gel permeation chromatography (**Table 3.5**). The molar mass was slightly higher and molar mass distribution relatively broader than expected for AGET ATRP polymersiation, with polydispersites of 1.7 − 2.3. The high PDI can be attributed to very small amount of Cu(II) and relatively slow the deactivation.[13] The best result was achieved when 1.0 equiv. of Cu(II) *vs*. $Sn(EH)_2$ was used (**Table 3.5**). Nonetheless, the polymerisations were quite controlled as evidenced by the GPC traces (**Figure 3.31**).

Table 3.5: Composition and estimated grafting density of grafted PSAN-silica nanoparticles.

Sample PSAN/silica type	$\%SiO_2$	M_w [c)] (g/mol)	M_n [c)] (g/mol)	M_w/M_n	δ (chains/nm^2)
PSAN-Cab H5[a)]	18.3	140000	63000	2.22	0.12
PSAN-Cab H5[b)]	12.7	184000	110000	1.67	0.11
PSAN-MEK-ST[a)]	12.7	139000	60000	2.31	0.28
PSAN-MEK-ST[b)]	13.0	181000	98000	1.84	0.16
PSAN-MEK-ST[b)]	09.5	190000	106000	1.80	0.23

ATRP of SAN: [a)] with 0.50 equiv Cu(II) *vs.* $Sn(EH)_2$. [b)] with 1.00 equiv of Cu(II) *vs.* $Sn(EH)_2$

[c)] Calculated by GPC

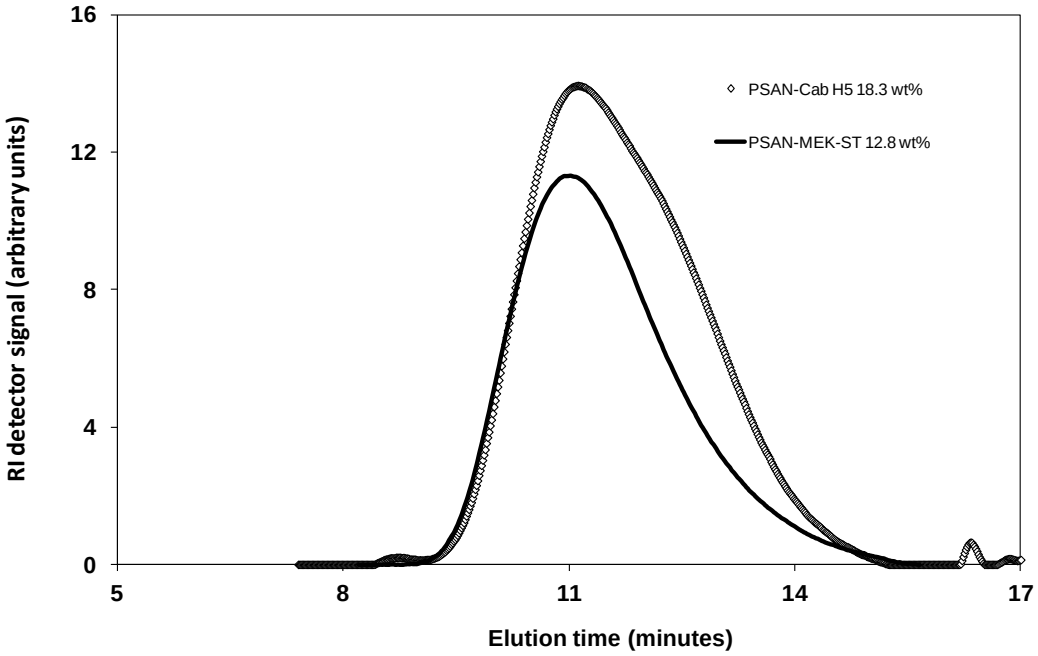

Figure 3.31: GPC traces of PSAN cleaved from Cab-o-sil-PSAN (18.3 wt%) hybrid nanoparticles and MEK-ST-PSAN (12.8 wt%) hybrid nanoparticles.

Elemental analysis was performed on all the grafted samples prepared to quantify both the composition of the copolymer and the percentage of silica present in the samples from the same measurement. The styrene/acrylonitrile copolymer composition was calculated from the nitrogen content. The calculation of the mole fraction of acrylonitrile (37 mol%) in PSAN-MEK-ST (12.8 wt%) from the elemental analysis is ~0.38. Details of the calculations are given in **Appendix A2**.

^{1}H NMR measurements were also carried out to check the copolymer composition, as well to provide support that the PSAN chains were covalently linked to the surface of the silica nanoparticles (**Figure 3.32).** The copolymer composition was calculated from the ^{1}H NMR integrals of the aromatic proton signals at 6.66 – 7.05 ppm and the signal of the protons of the polymer backbone (styrene and acrylonitrile) at 1.15 – 2.5 ppm. However, low solubility of the modified silica nanoparticles affected the quality of the spectra, by reducing the signal-to-noise ratio and broadening the signals. Copolymer compositions calculated by elemental analyses were found to be in good agreement with the values obtained from ^{1}H NMR spectroscopy measurements, as shown in **Table 3.6** of most the silica–PSAN hybrid systems. The calculation of the mole fraction of acrylonitrile (37 mol%) in PSAN-MEK-ST (12.8 wt%) from ^{1}H NMR spectroscopy measurements is ~0.36. Details of the calculations are given in **Appendix A1**.

FTIR was also used to identify the incorporation of both co-monomers into the polymeric chains. The FTIR spectrum of the grafted SAN copolymer clearly showed the presence of a nitrile (CN triple bond) stretch at around 2200 cm^{-1}. The absorption band at 1600 cm^{-1} is representative of the aromatic ring of the styrene comonomer, and a large peak at around 695 cm^{-1} is due to the aromatic out-of-plane bending mode (**Figure 3.33**).

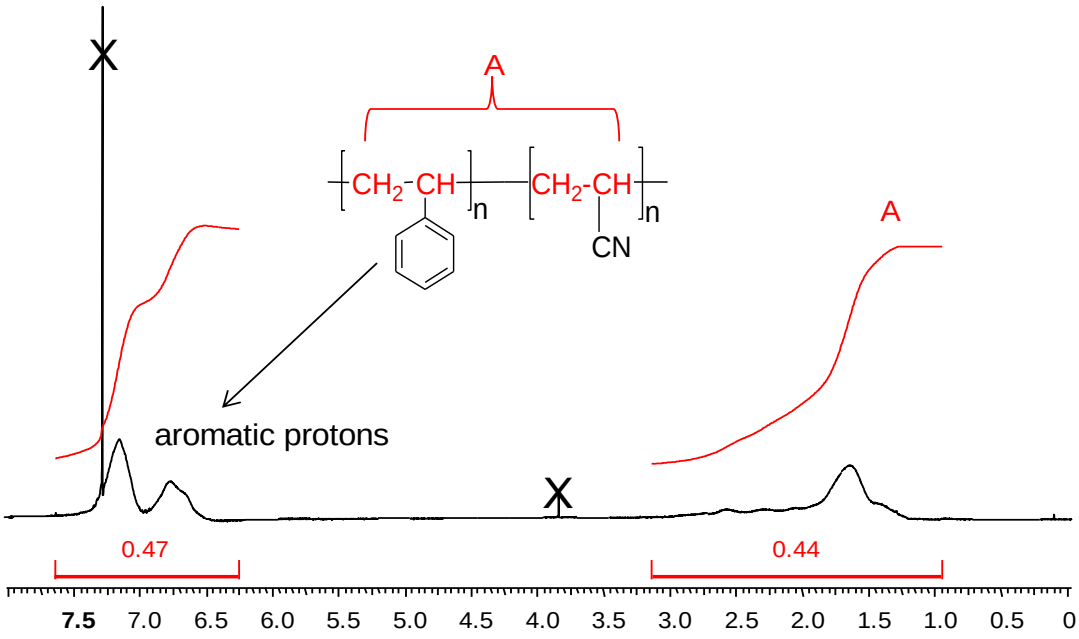

Figure 3.32: ^{1}H NMR spectrum (300 MHz, $CDCl_3$) of PSAN-MEK-ST (18.3 wt%.) Solvent and impurities signals are marked by X.

Table 3.6: Details of SAN copolymerisation.

Polymer	Silica type	Wt% of silica	F_{AN})a	F_S)a	F_{AN})b	F_S)b
PSAN	None	0.00	0.380	0.610	0.365	0.635
PSAN	Cab H5	18.3	0.381	0.619	-----	-----
PSAN	Cab H5	17.4	0.383	0.617	0.375	0.625
PSAN	MEK-ST	18.3	0.38	0.620	-----	-----
PSAN	MEK-ST	12.8	0.382	0.618	0.360	0.640
PSAN	MEK-ST	12.7	0.385	0.615	0.391	0.628
PSAN	MEK-ST	09.5	0.387	0.613	0.370	0.630

The mole fraction of acrylonitrile (F_{AN}) and styrene (F_S) in copolymer composition are calculated:)a by elemental analysis and)b by ^{1}H NMR (Appendix A2 and A1 resp.)

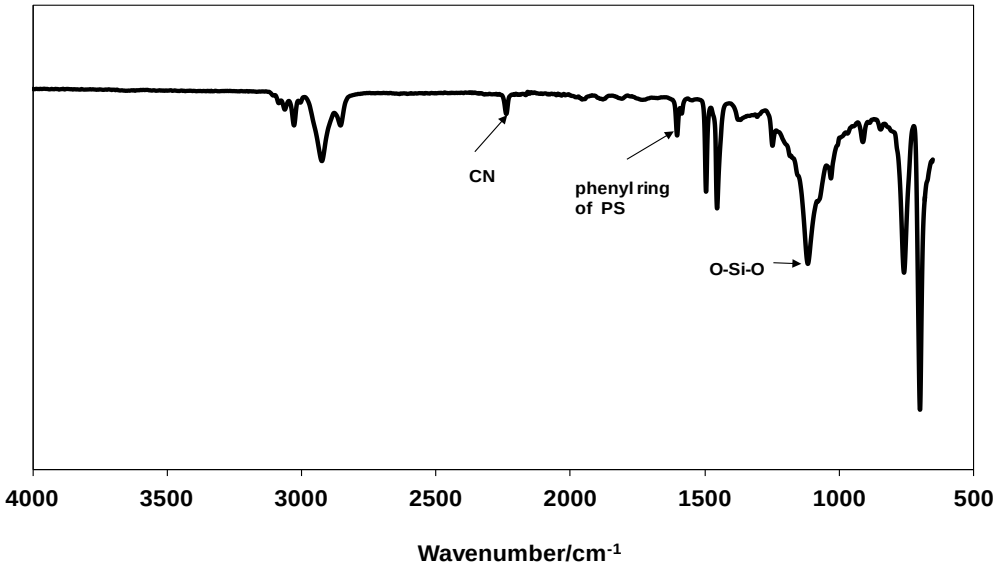

Figure 3.33: IR spectrum of grafted PSAN-MEK-ST (09.50 wt%). The spectrum is presented in transmittance units.

3.5 Conclusion

In summary, well-defined polymer nanocomposites were successfully prepared by AGET ATRP in miniemulsion. The monomers that were successfully polymerised include methyl methacrylate, butyl acrylate, and styrene. AGET ATRP allowed a significantly reduced amount of a copper catalyst to be employed and effectively suppressed side reactions, in particular termination, thus making the polymerisation better controlled.

New ATRP initiators **1** and **2** was synthesised in a one-step process from commercially available and inexpensive compounds. They were then immobilised onto the surface of both aggregated and non-aggregated silica nanoparticles. Both PMDETA and BPMOA served as ligands in ATRP of those monomers. When BPMOA was used the polymer chains exhibited quite low polydispersity (1.05 − 1.40), while a higher polydispersity (1.37 − 2.24) was observed for PMDETA. The difference in control the polymerisation was attributed to the solubility difference of the catalyst. Grafting densities of polymer chains grown from the surface of aggregated silica was lower than for chains grown from the surface of non-aggregated silica.

The choice of halogen atom in the ATRP initiator has an impact on the rate of polymerisation. A Br-based initiator was a more efficient initiator for polymerisation of styrene than a Cl-based initiator. The molecular weight and polydispersity of PMMA grafted from silica (and subsequently cleaved) was similar to that of free PMMA formed in solution. However, molecular weight and polydispersity of free PS clearly differed from those of grafted polymer.

SAN copolymers were synthesised by AGET ATRP from the surface of functionalised aggregated silica as well as of colloidally dispersed silica nanoparticles using Me_6TREN/Cu(II) as the catalyst, and an organic-soluble tin salt as reducing agent. The monomer feed was close to the azeotropic composition (ca. 63 mol% styrene and 37 mol% acrylonitrile), and reproducible, but molar mass distribution slightly broader than for PS.

3.6 References

1. A. Tregub, J. Karger-Kocsis, K. Koennecke and H. J. Zimmermann, *Macromolecules*, 1995, **28**, 3890.
2. H. Zou, S. Wu and J. Shen, *Chem. Rev.*, 2008, **108**, 3893.
3. O. Prucker and J. Rühe, *Macromolecules*, 1998, **31**, 602.
4. O. Prucker and J. Rühe, *Macromolecules*, 1998, **31**, 592.
5. T. von Werne, T. E. Patten and *J. Am. Chem. Soc.*, 1999, **121**, 7409.
6. D. Li, X. Sheng and B. Zhao, *J. Am. Chem. Soc.*, 2005, **127**, 6248.
7. H. Mori, D. C. Seng, M. Zhang and A. H. E. Müller, *Langmuir*, 2002, **18**, 3628.
8. A. El Harrak, G. Carrot, J. Oberdisse, C. Eychenne-Baron and F. Boué, *Macromolecules*, 2004, **37**, 6376.
9. K. Ohno, T. Morinaga, K. Koh, Y. Tsujii and T. Fukuda, *Macromolecules*, 2005, **38**, 2137.
10. C. Perruchot, M. A. Khan, A. Kamitsi, S. P. Armes, T. von Werne and T. E. Patten, *Langmuir*, 2001, **17**, 4479.
11. J. Pyun, T. Kowalewski and K. Matyjaszewski, *Macromol. Rapid Commun.*, 2003, **24**, 1043.
12. V. Goel, T. Chatterjee, L. Bombalski, K. Yurekli, K. Matyjaszewski and R. Krishnamoorti, *J. Polym. Sci., Part B: Polym. Phys.*, 2006, **44**, 2014.
13. J. Pietrasik, H. Dong, and K. Matyjaszewski, *Macromolecules*, 2006, **39**, 6384.
14. J. Pyun, S. Jia, T. Kowalewski, G. D. Patterson and K. Matyjaszewski, *Macromolecules*, 2003, **36**, 5094.
15. B. Radhakrishnan, R. Ranjan and W. Brittain, *Polym. Prepr.*, 2005, **46(2)**, 108.
16. C.-H. Liu and C.-Y. Pan, *Polymer*, 2007, **48**, 3679.
17. C. Li and B. C. Benicewicz, *Macromolecules*, 2005, **38**, 5929.
18. M. M. Demir, P. Castignolles, Ü. Akbey and G. Wegner, *Macromolecules*, 2007, **40**, 4190.
19. P. Akcora, S. K. Kumar, V. García Sakai, Y. Li, B. C. Benicewicz and L. S. Schadler, *Macromolecules*, 2010, **43**, 8275.
20. S. S. Sternstein and A.-J. Zhu, *Macromolecules*, 2002, **35**, 7262.
21. Z. Zhu, T. Thompson, S.-Q. Wang, E. D. von Meerwall and A. Halasa, *Macromolecules*, 2005, **38**, 8816.
22. C. Bartholome, E. Beyou, E. Bourgeat-Lami, P. Chaumont, F. Lefebvre and N. Zydowicz, *Macromolecules*, 2005, **38**, 1099.

23. J. Parvole and L. B. Montfort, *Macromol. Chem. Phys.*, 2004, **205**, 1369.

24. G. Moad, E. Rizzardo and S. H. Thang, *Material Matters.*, 2010, **5**, 2.

25. K. Matyjaszewski, H. Dong, W. Jakubowski, J. Pietrasik and A. Kusumo, *Langmuir*, 2007, **23**, 4528.

26. K. Ohno, Y. Ma, Y. Huang, C. Mori, Y. Yahata, Y. Tsujii, T. Maschmeyer, J. Moraes and S. Perrier, *Macromolecules*, 2011, **44**, 8944.

27. P. J. Miller and K. Matyjaszewski, *Macromolecules*, 1999, **32**, 8760.

28. D. Sunda, S. Curras-Medina and D. L. Green, *Macromolecules*, 2010, **43**, 4871.

29. H. Bottcher, M. L. Hallensleben, S. Nuss and H. Wurm, *Polym. Bull.*, 2000, **44**, 223.

30. K. Ohno, T. Morinaga, K. Koh, Y. Tsujii and T. Fukuda, *Macromolecules*, 2005, **38**, 2137.

31. A. Malinowska, P. K. Vlček, J. , L. Toman, P. Látalová, M. Janata and B. Masař, *Polymer*, 2005, **46**, 5.

32. M. A. Ver Meer, B. Narasimhan, B. H. Shanks and S. K. Mallapragada, *ACS App. Mater. Interfaces*, 2010, **2**, 41.

33. T. von Werne and T. E. Patten, *J. Am. Chem. Soc.*, 2001, **123**, 7497.

34. K. Matyjaszewski, *Macromolecules*, 2012, **45**, 4015.

35. W. Tang and K. Matyjaszewski, *Macromolecules*, 2006, **39**, 4953.

36. J. Xia and K. Matyjaszewski, *Macromolecules*, 1997, **30**, 7697.

37. K. Min, H. Gao and K. Matyjaszewski, *J. Am. Chem. Soc.*, 2006, **129**, 10521.

38. J. C. Mareque Rivas, R. Torres Martín de Rosales and S. Parsons, *Dalton. Trans.*, 2003, 2156.

39. J. Queffelec, S. G. Gaynor and K. Matyjaszewski, *Macromolecules*, 2000, **33**, 8629.

40. X. Huang and W. J. Brittain, *Macromolecules*, 2001, **34**, 3255.

41. K. Matyjaszewski, Y. Nakagawa and C. B. Jasieczek, *Macromolecules*, 1998, **31**, 1535.

42. I. Hwang, J.; and B. K. Kim, *J. Appl. Polym. Sci.*, 1998, **67**, 27.

43. S. V. Nair, A. Subramaniam and L. A. Goettler, *J. Mater. Sci.*, 1998, **33**, 3455.

44. Y. T. Sung, M. S. Han, J. C. Hyun, W. N. Kim and H. S. Lee, *Polymer*, 2003, **44**, 1681.

45. K. Min, H. F. Gao and K. Matyjaszewski, *J. Am. Chem. Soc.*, 2005, **127**, 3825.

46. S. G. Gaynor, J. Qiu and K. Matyjaszewski, *Macromolecules*, 1998, **31**, 5951.

47. L. Bombalski, K. Min, C. Tang and K. Matyjaszewski, *Polym. Prepr.*, 2005, **46(2)**, 359.
48. M. Li, K. Min and K. Matyjaszewski, *Macromolecules*, 2004, **37**, 2106.
49. L. Bombalski, K. Min, H. C. Dong, C. B. Tang and K. Matyjaszewski, *Macromolecules*, 2007, **40**, 7429.
50. K. Moller, T. Bein and R. X. Fischer, *Chem. Mater.*, 1998, **10**, 1841.
51. F. A. Zhang, D. K. Lee and T. J. Pinnavaia, *Polymer*, 2009, **50**, 4768.
52. J. Xia and K. Matyjaszewski, *Macromolecules*, 1999, **32**, 2434.
53. H. Lin, C. Li and J. Lee, *J. Power Sources*, 2011, **196**, 8098.
54. A. Voronov and O. Shafranska, *Langmuir*, 2002, **18**, 4471.
55. M. Kruk, B. Dufour, E. B. Celer, K. T. M. Jaroniec and K. Matyjaszewski, *Polym. Mater. Sci. Eng. Preprints*, 2007, **97**, 274.
56. F. Chen, X. Jiang, R. Liu and J. Yin, *ACS App. Mater. Interfaces*, 2010, **2**, 1031.
57. C. Bartholome, E. Beyou, E. Bourgeat-Lami, P. Chaumont and N. Zydowicz, *Macromolecules*, 2003, **36**, 7946.
58. M. Ejaz, K. Ohno, Y. Tsujii and T. Fukuda, *Macromolecules*, 2000, **33**, 2870.
59. H. Dong, W. Tang and K. Matyjaszewski, *Macromolecules*, 2007, **40**, 2974.
60. J. S. Wang and K. Matyjaszewski, *J. Am. Chem. Soc.*, 1995, **117**, 5614.
61. K. Matyjaszewski, H. j. Paik, P. Zhou and S. J. Diamanti, *Macromolecules*, 2001, **34**, 5125.
62. K. Matyjaszewski, T. E. Patten and J. Xia, *J. Am. Chem. Soc.*, 1997, **119**, 674.
63. M. N. Tchoul, M. Dalton, L. S. Tan, H. Dong, C. M. Hui, K. Matyjaszewski and R. A. Vaia, *Polymer*, 2012, **53**, 79.
64. F. R. Mayo, *J. Am. Chem. Soc.*, 1953, **75**, 6133.
65. P. Antoni, D. Nyström, E. Malmström, M. Johansson and A. Hult, *Polym. Prepr.* , 2005, **46(1)**, 477.
66. N. V. Tsarevsky, T. Pintauer and K. Matyjaszewski, *Macromolecules*, 2004, **37**, 9768.
67. M. N. Tchoul, M. Dalton, L.-S. Tan, H. Dong, C. M. Hui, K. Matyjaszewski and R. A. Vaia, *Polymer*, 2012, **53**, 79.
68. Q. Lu, Z. X. Weng, G. R. Shan, G. Q. Lai and Z. R. Pan, *J. Appl. Polym. Sci.*, 2006, **101**, 4270.
69. W. Jakubowski and K. Matyjaszewski, *Macromolecules*, 2005, **38**, 41

Chapter 4 - Synthesis of Deuterated Polymers

Contents

4.1 Introduction

Recently, deuterated polymers have aroused interest not only for use in neutron scattering studies but also as materials for applications in optical communication due to their transparency in the infrared, particularly the region between 500 and 800 cm^{-1}.[1, 2] Although a wide variety of deuterated polymers are commercially available, they can be quite expensive and viable synthetic routes to such polymers are desirable.

The synthesis of deuterated polymers is accomplished by the polymerisation of a deuterated monomer or by H/D isotope exchange of a non-deuterated polymer. For example, the N-H protons in polyamides are readily exchangeable with deuterium oxide,[3] whereas partial H-D exchange on the aromatic ring of polystyrene is usually performed under hydrothermal conditions in the presence of a deuterium source and with the assistance of a Lewis acid catalyst.[2] A number of synthetic methods for the H/D exchange in polycyclic aromatic hydrocarbons have been reported in literature.[4-7]

The preparation of deuterium-labelled compounds has been aided recently by the development of microwave-assisted techniques.[8-12] The main advantage of using microwave heating over traditional batch reactions is that faster, often cleaner and more selective reactions are possible. Microwave reactors use microwave radiation (300 – 300,000 MHz)[13] to generate heat within the reaction mixture through two ways: dipole rotations and ionic conduction. This allows the reaction to be heated very rapidly; at the same time, the mixture retains a homogeneous temperature throughout. As heating depends on dipole rotation and ionic conduction, substrates or solvents with no dipole moment reduce the efficiency of microwave heating. In such cases, addition of a co-solvent to the reaction mixture can enhance the effectiveness of microwave heating. Ionic liquids are particularly strong microwave absorbers and are potentially recoverable from the reaction mixture on completion of the reaction.[10] Although microwave reactions can be carried out in open or closed vessels, the closed vessel approach allows for reactions to be carried out safely in superheated solvents (= at temperatures above the boiling point of the solvent). This avoids the need to use high-boiling solvents which are not easy to remove after the reaction and often are also more expensive. The use of high temperatures enhances the rate of the reaction (Arrhenius law). The very rapid heating noticeable in microwave reaction make it apparent that, based on applying the Arrhenius law [$k = A \exp(^{-}E_a/RT)$], conversions that need long time when carried out in a solvent at conventional heating may reach completion in a short time using superheated solvents in a microwave reactor.

This Chapter describes a new simple method for rapid deuteration of the aromatic ring of polystyrene (PS) and poly(4-hydroxystyrene) (P4HS). The present work focuses on a time and cost-efficient synthesis of deuterated polystyrene and simple derivatives using microwave heating, which makes the deuteration more specific and faster than the literature-known methods. To the best of my knowledge, no attempts have been made, so far, for the synthesis of deuterated polymers using microwave-assisted H/D isotope exchange reactions. The starting materials for this synthesis were non-deuterated PS and P4HS, as well as benzene-d_6 or D_2O which are both readily available and much cheaper than deuterated monomers. This Chapter also describes a successful preparation of several other deuterated polymers starting from deuterated PS following a "conventional" sequence of polymer-analogous reactions: poly(4-acetylstyrene-d_4), poly(4-acetoxystyrene-d_4) and poly(4-hydroxystyrene-d_4).

4.2 Synthesis of 2,3,4,5,6–Pentadeuteropolystyrene (PS-d_5)

The synthesis of this deuterated polymer was adapted from a literature procedure by Willenberg.[14] The author used a Lewis acid, ethyl aluminium dichloride, as a catalyst to aid proton/deuterium exchange of the aromatic protons and benzene-d_6 as deuterium source. In Willenberg's procedure the reaction had taken 4 hours at 25°C to complete and the reaction had to be repeated several times to achieve full deuteration. Microwave heating to 150 °C allowed the reaction time to be reduced to 10 min (**Figure 4.1**). In addition, more than 90% deuteration was obtained in the first run. A higher enrichment could be achieved by repeating the procedure a second time. This approach had advantages other than time benefits. Reducing the reaction time also reduces the risk of lowering the molecular weight and broadening the molecular weight distribution.[14]

Using benzene-d_6 as the only reaction solvent, the reaction temperature did not exceed 78 °C even at the maximum microwave power setting (300 W) due to the non-polar nature of the solvent. In order to further increase the temperature, a microwave-absorbing co-solvent was required. Ionic liquids have previously been used for proton/deuterium exchange in polyphenols.[10] Ionic liquids are highly efficient in absorbing microwave energy and in transferring the heat to the reaction mixture. After adding a small amount of a strongly microwave absorbing ionic liquid,[10] 1-butyl-3-methylimidazolium chloride, [BMIM]Cl, to the reaction mixture the rate of the heating in the microwave increased considerably. Using 150 W of microwave energy allowed the reaction to be heated to 150 °C in less than 2 min. This temperature is well above

the boiling point of benzene-d_6 (79 °C). After only 10 minutes of microwave irradiation the deuterated polymer was isolated by precipitating the polymer into methanol.

Non-polar solvents are a very weakly microwave absorbing as compared to polar solvents. In general, the ability of a solvent to convert microwave energy into heat is determined by tan delta or loss tangent (tan δ), and the reaction medium with a high tan δ is required for strong microwave absorption and, therefore, for efficient heating. **Table 4.1** lists the values of tan δ values for non-polar solvents such as toluene and polar solvents such as methanol at standard operating frequency of microwave reactor (2.45 GHz).[15]

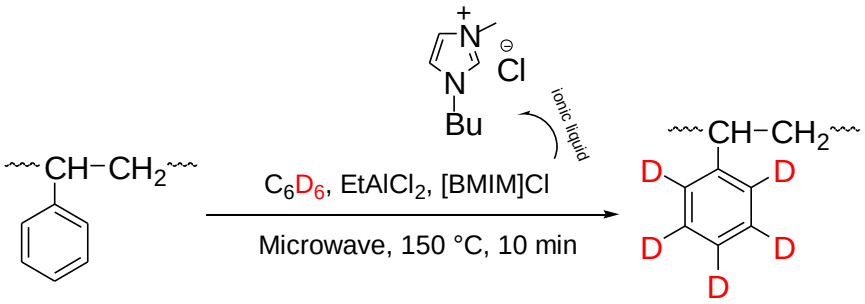

Figure 4.1: Deuteration of polystyrene under microwave/ ionic liquid conditions.

Table 4.1: tan δ values of selected solvents (2.45 GHz, 20 °C).[15]

Solvent	tan δ	Solvent	tan δ
Toluene	0.040	Methanol	0.692
Hexane	0.020	Ethanol	0.941
Tetrahydrofuran	0.047	Water	0.123
DMF	0.161	DMSO	0.825
Acetonitrile	0.062	Acetic acid	0.174

The polystyrene was characterised before and after the H/D exchange by FT-IR (**Figure 4.2**) and ^{1}H NMR (**Figure 4.3**). The FT-IR spectrum showed a small but noticeable C−D stretch at around 2270 cm^{-1} together with a considerable reduction in the intensity of the C−H stretch peaks. Furthermore, the bending mode at 700 cm^{-1} in non-deuterated polystyrene, which is characteristic of monosubstituted benzene in the non-deuterated polystyrene, was absent and had shifted to 540 cm^{-1}, thus making the deuterated polymers virtually transparent in the infrared area of 550 – 800 cm^{-1}. It is worth bearing in mind that, it was possible to calculate the aromatic C−D stretching frequency for PS-d_5 using **equation** (**4.1**).[16]

$$v = \frac{1}{2\pi c}\frac{\overline{k}}{\mu} \qquad (\mathbf{4.1})$$

where c is the speed of light and μ the reduced mass. If it is assumed that the force constant k is the same for both bonds, then the ratio of the reduced masses needs only be calculated.

$$\mathrm{C-H\ stretch:}\ \mu = \frac{m1m2}{m1+m2} = \frac{12 \times 1}{12 + 1} = 0.92$$

$$\mathrm{C-D\ stretch:}\ \mu = \frac{m1m2}{m1+m2} = \frac{12 \times 12}{12 + 2} = 1.71$$

The vibrational frequency of a C−D stretch can be estimated from the square root of the ratio of the two reduced masses:

$$\frac{v_H}{v_D} = \frac{\overline{\mu_H}}{\mu_D} = \frac{\overline{0.92}}{1.72} = 0.73$$

So, while a C−H stretch for PS occurs at 3060 cm^{-1}, the C−D stretching is expected at 0.73×3060 cm^{-1} = 2233 cm^{-1}. The differences to the experimental value are due to the fact the force constant does change a bit.

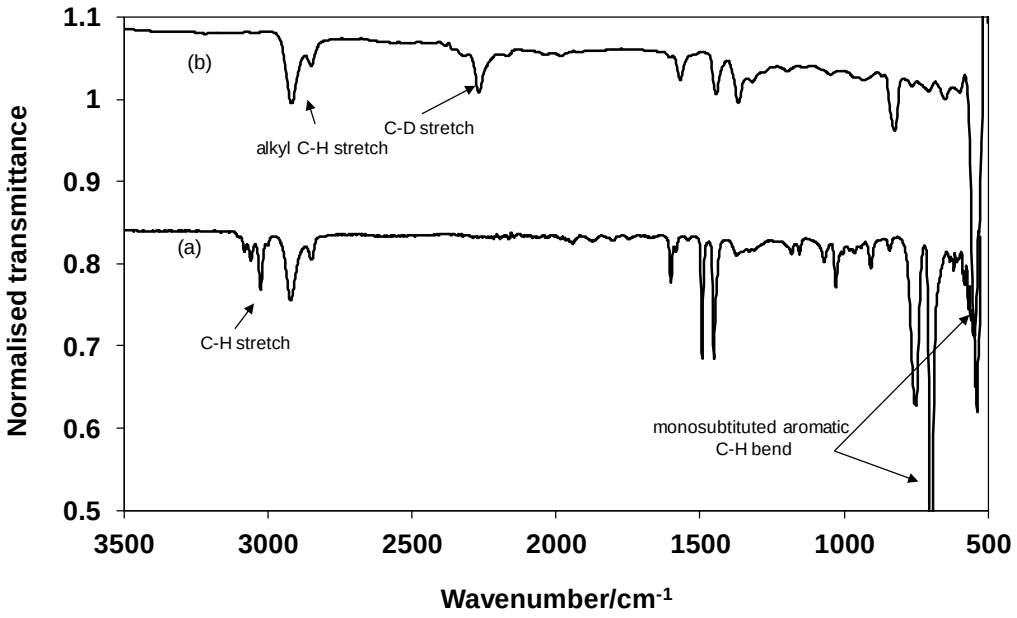

Figure 4.2: FT-IR spectra of polystyrene (a) before and (b) after deuteration. (Spectra are normalised for comparison).

^{1}H NMR analysis also confirmed the successful deuteration of the aromatic ring as evidenced by the absence of aromatic proton NMR signals between 6.5 and 7.4 ppm **[Figure 4.3 (c)]**. The degree of deuteration was determined by integration of the ^{1}H NMR signals in the aliphatic region and the aromatic region; a comparison of the integrals revealed more than 90% H/D exchange had occurred after a single run **[Figure 4.3 (b)]**. The H/D exchange on aromatic ring was nearly completed after the procedure had been repeated once **[Figure 4.3 (c)]**. In the absence of an ionic liquid, H/D exchange occurred at a level of only about 40%, showing that the presence of ionic co-solvent was crucial. The result of H/D exchange reaction of polystyrene under microwave and thermal conditions are summarised in **Table 4.2** and **4.3**.

The molecular weight (M_w) and polydispersity (PDI) of PS samples before and after the exchange were measured by GPC (**Figure 4.4**). No significant change was found in the M_w and polydispersity of the polystyrene before and after the deuteration. These results differ from the findings of Willenberg who observed that H/D exchange under conventional conditions led to a noticeable decrease of the M_w accompanied by a broadening of the PDI **(Table 4.3)**, whereas microwave-assisted deuteration showed no such decrease. It can be expected that the influence of the exchange on molecular weight and molecular weight distribution can be reduced by changing the conditions of the exchange to a shorter reaction time using microwave heating.

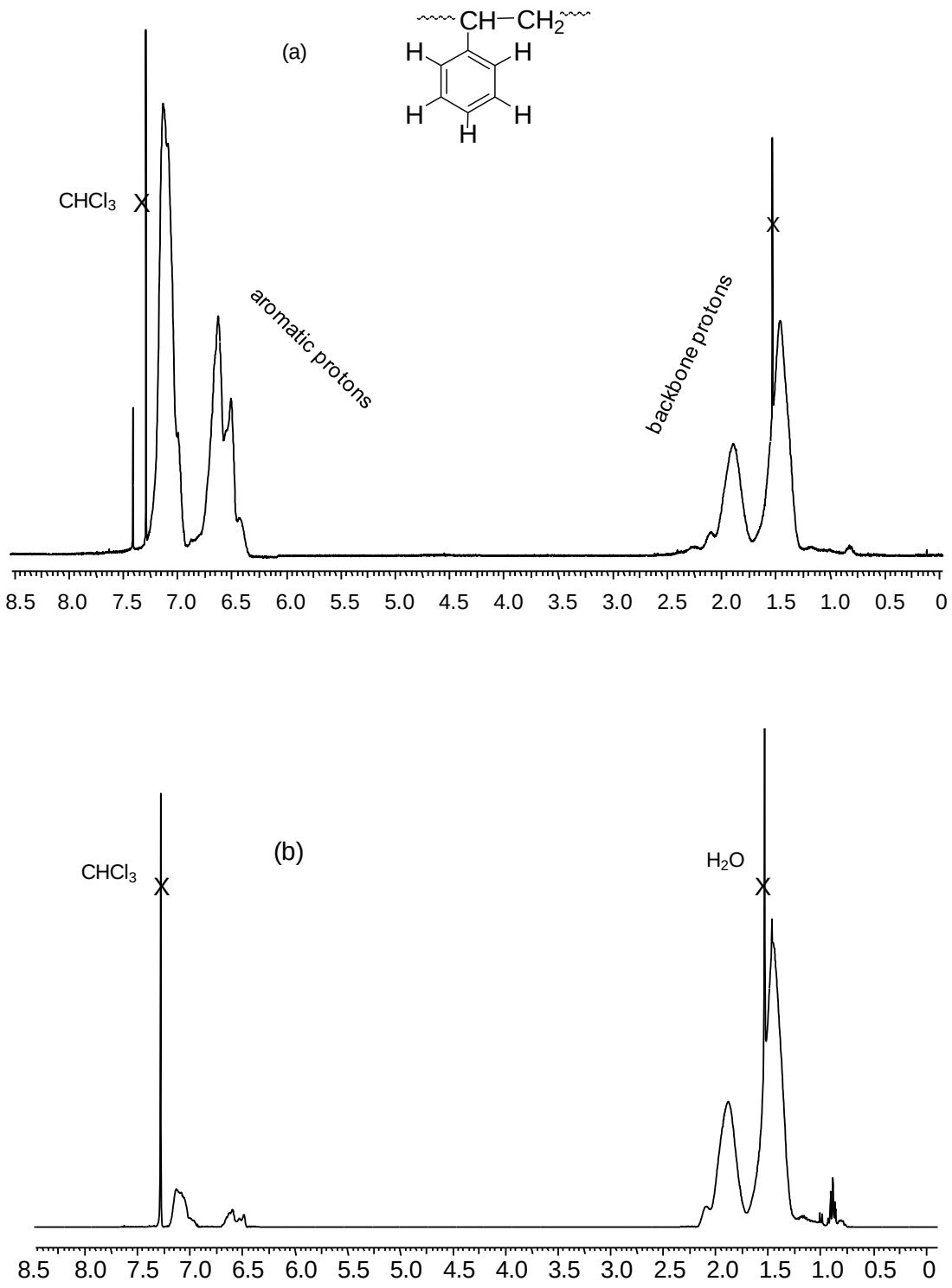

Figure 4.3: ^{1}H NMR spectra of polystyrene (300 MHz, $CDCl_3$) (a) before deuteration, (b) after deuteration (first run) and (c) after deuteration (second run). Solvent and water signals are marked by X.

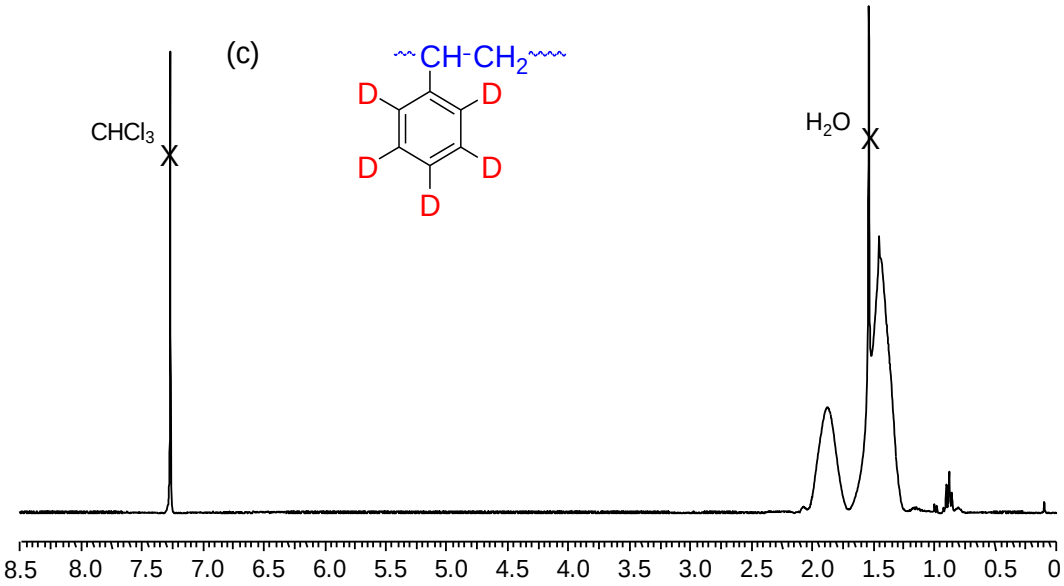

Table 4.2: Deuteration of polystyrene under different conditions.

Method	Reaction time (min)	%D (on Ph)	Ref.
C_6D_6, $EtAlCl_2$, 25 °C	240	80	14
C_6D_6, $EtAlCl_2$, 25 °C	3 × 240	>90	14
D_2O, PtO_2, 250 °C	840	61	2
C_6D_6, $EtAlCl_2$, MW, 150 °C	**10**	**90**	**This work**
C_6D_6, $EtAlCl_2$, MW, 150 °C	**2 × 10**	**>98**	**This work**

Table 4.3: Effect of H/D exchange on M_w and PDI of polystyrene under thermal and microwave conditions.

Method	M_w (g mol^{-1})[a]	PDI[a]	M_w (g mol^{-1})[b]	PDI[b]	Ref.
C_6D_6, $EtAlCl_2$, 25 ^oC	470,000	1.95	400,000	2.18	14
C_6D_6, $EtAlCl_2$, MW, 150 ^oC	100,000	1.05	95,800	1.06	**This work**
C_6D_6, $EtAlCl_2$, MW, 150 ^oC	18,000	1.02	18,000	1.03	**This work**

[a] Before and [b] after deuteration.

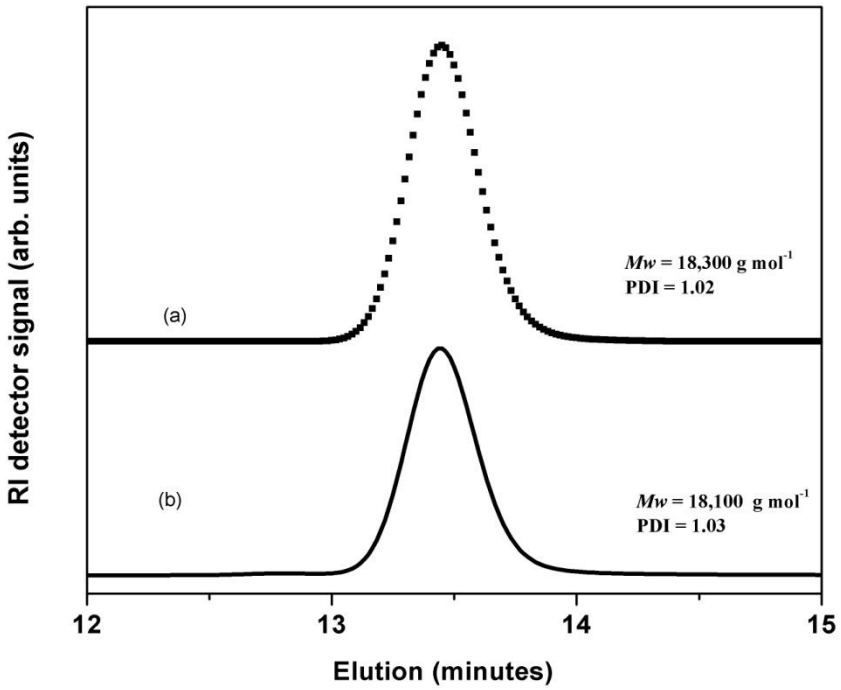

Figure 4.4: GPC results of polystyrene (a) before and (b) after deuteration.

4.3 Synthesis of Deuterated Poly(4-hydroxystyrene) (P4HS-d_4)

The synthesis of deuterated poly(4-hydroxystyrene) was adapted from the procedure reported by Lautens and Martins for the deuteration of anilines (**Figure 4.5**).[17] In this procedure the authors found that the best results of deuterated 2-methyl-3-nitroaniline (97% D), under microwave conditions were obtained from using 1 equiv of conc. HCl in D_2O, and heating to 180°C for 30 min. However, poly(4-hydroxystyrene) was found to be insoluble in D_2O and HCl. To overcome this problem, solubility tests were carried out which revealed that P4HS dissolved in tetrahydrofuran (THF), dimethylsulfoxide (DMSO), dimethylformamide (DMF) and methyl ethyl ketone (MEK).[18] These solvents are all miscible with water, thus allowing for a single-phase reaction. Then, the microwave absorption properties of these solvents when mixed with water were also determined. Whereas the reaction in DMF–D_2O caused the polymer to decompose, reactions in DMSO–D_2O and THF–D_2O both yielded a deuterated product. Even though THF is known to be a poor microwave absorber compared to DMSO, there was still enough water present in the mixed solvent to make sure that high temperatures could be reached and in a reasonable time. We decided to carry out the reaction with THF as the co-solvent of choice since THF is more volatile and therefore easier to remove than DMSO (**Figure 4.6**). After the reaction was completed the product was placed on a Polytetrafluoroethylene (PTFE) plate and the solvent was allowed to evaporate at room temperature. The product was dried in a vacuum oven to aid removal of the remaining solvent and FTIR and ^{1}H NMR spectrum were recorded.

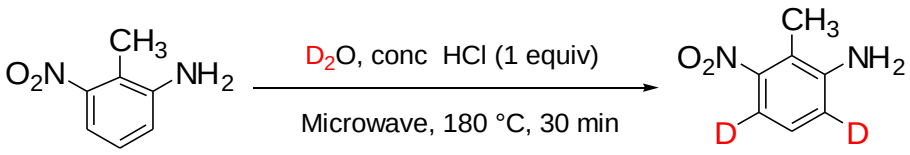

Figure 4.5: Deuteration of 2-methyl-3-nitroaniline under microwave conditions.[17]

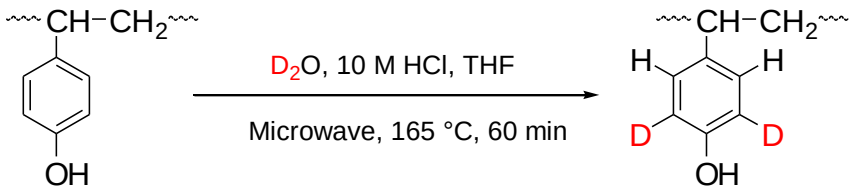

Figure 4.6: Deuteration of poly(4-hydroxystyrene) under microwave conditions.

A ^{1}H NMR spectrum was recorded to determine the degree of deuteration by comparing the integrals of the hydroxyl signal, the polymer backbone signals and the aromatic region. It was found that exchange had reduced the integral of the aromatic region to ~50% after 2 × 30 minutes at 165 °C. The protons *ortho* to the hydroxyl group are most activated towards electrophilic aromatic substitution and had exchanged exclusively (**Figure 4.7**). The reaction also was carried out again for 2 × 40 minutes to increase the degree of deuteration but that caused some of the polymers to begin decompose. Deuteration was also confirmed by FTIR spectrum of the polymer formed. FT-IR analysis showed a new C−D stretch at 2270 cm^{-1} (**Figure 4.8**). When a test reaction was conducted using conventional heating (in an oil bath) at 150 °C for 30, 60 and 120 min, no H/D exchange was observed since the reaction temperature under these conditions will be the boiling point of the lowest boiling component (THF, boiling point 66 °C).

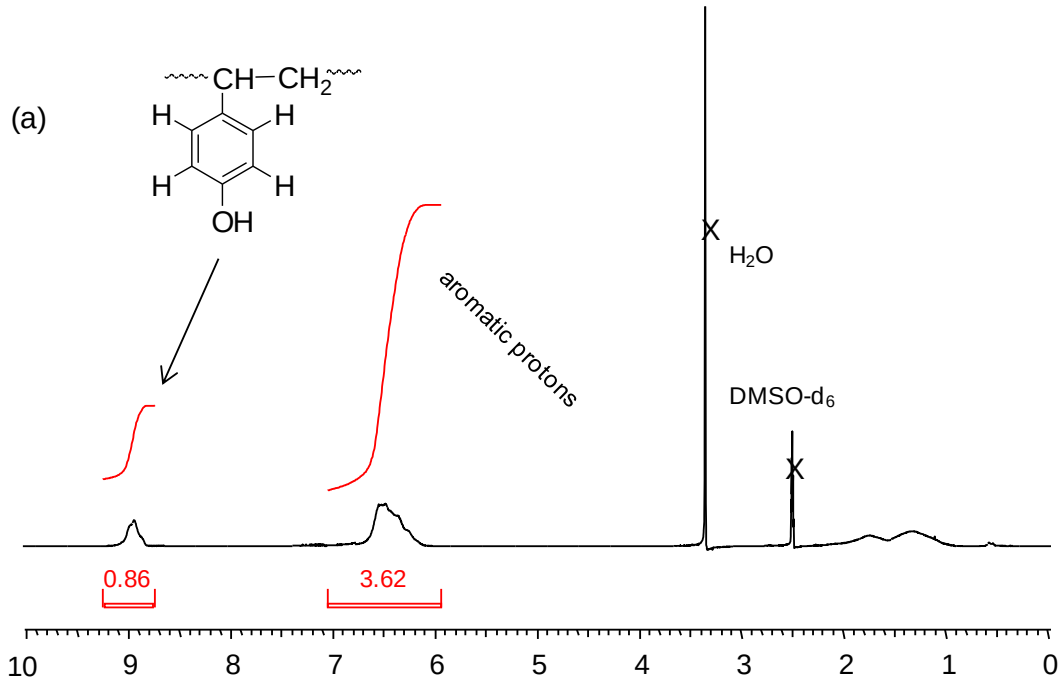

Figure 4.7: ^{1}H NMR spectrum of P4SH (300 MHz, DMSO-d_6) (a) before deuteration and (b) after deuteration. Solvent and water signals are marked by X.

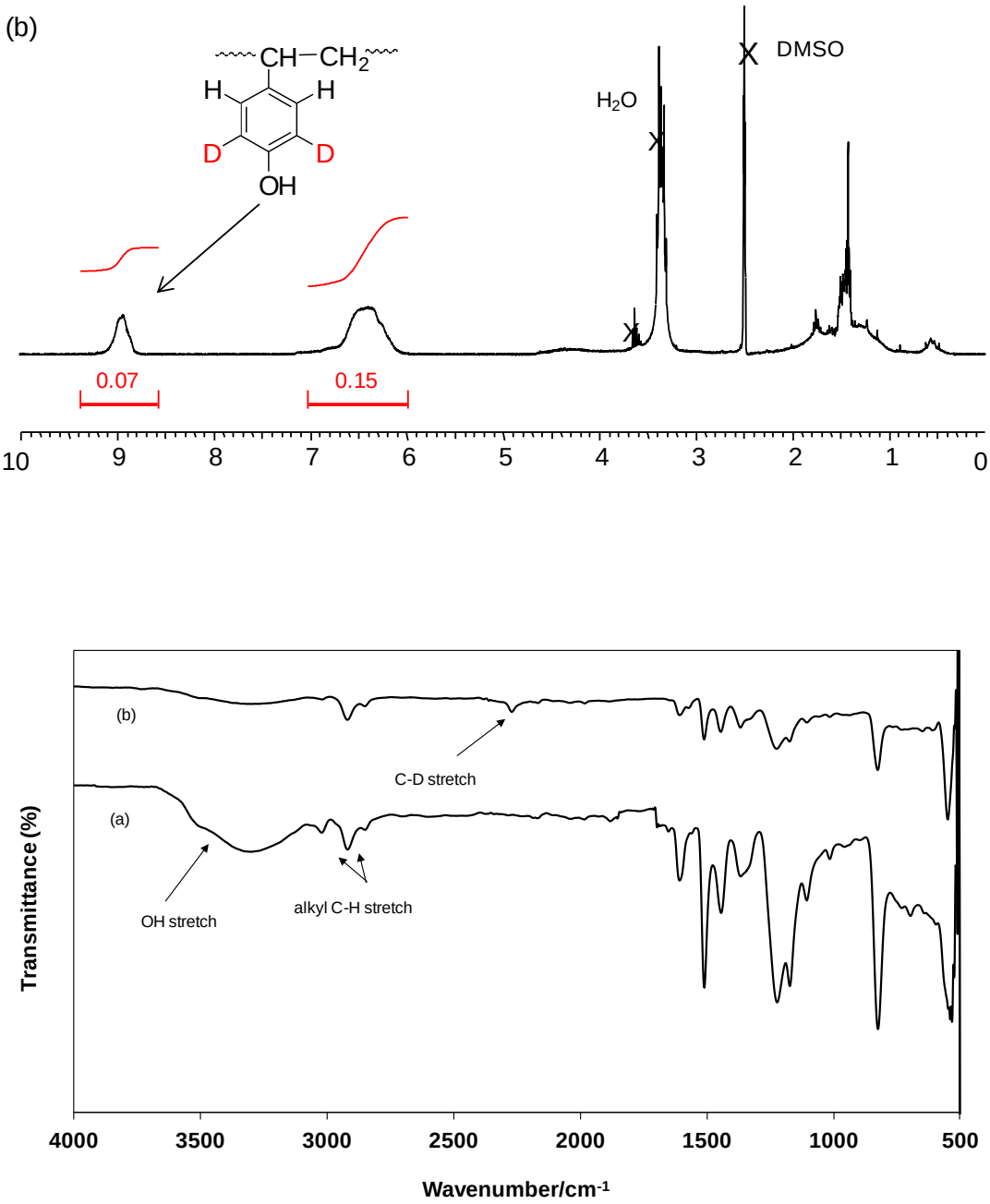

Figure 4.8: FT-IR spectra of poly(4-hydroxystyrene), (a) before and (b) after deuteration.

4.4 Synthesis of Deuterated Poly(4-hydroxystyrene) by a Polymer-analogous Reaction Sequence Starting from Deuterated Polystyrene

The synthesis was adapted from procedures reported in literature,[19, 20] for the synthesis of non-deuterated poly(4-hydroxystyrene) as shown in **Figure 4.9**. The starting compound for this synthesis was PS-d_5, which was prepared under microwave conditions described in **Section 4.2**. Thus, PS-d_5 was acetylated to deuterated poly(4-acetylstyrene) and subsequently oxidised to deuterated poly(4-acetoxystyrene). The deuterated poly(4-hydroxystyrene) was obtained after hydrolysis of deuterated poly(4-acetoxystyrene).

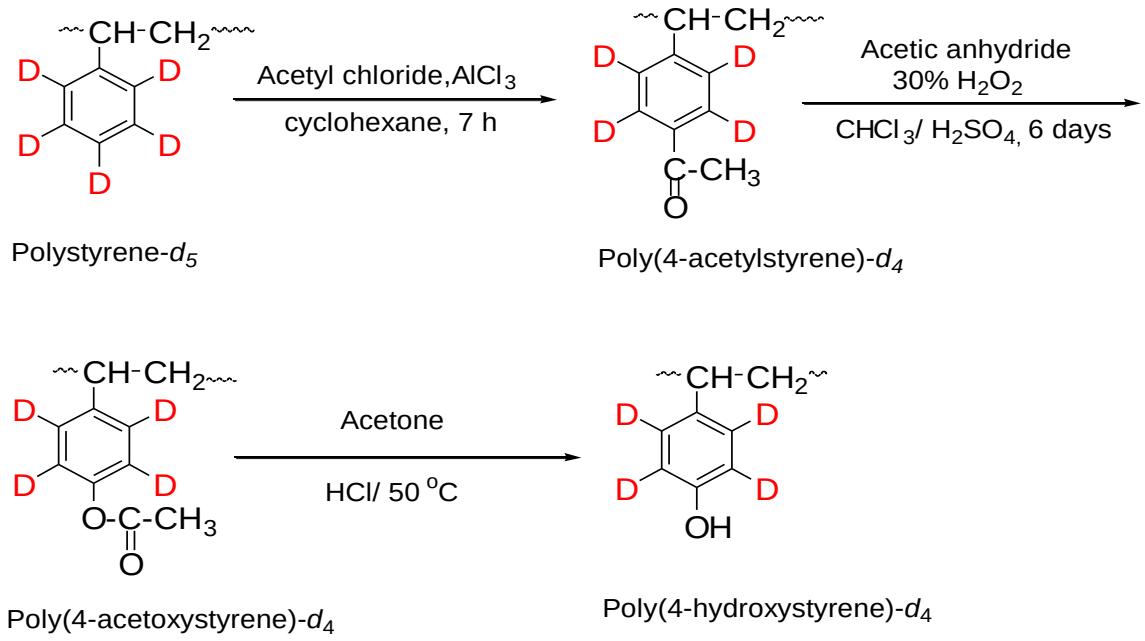

Figure 4.9: Reaction scheme for synthesis of deuterated P4HS form PS-d_5.

4.4.1 Synthesis of Deuterated Poly(4-acetylstyrene) (ACPS-d_4)

The acetylation of PS-d_5 (degree of deuteration ~85%) was conducted using cyclohexane (instead of the toxic and flammable carbon disulfide proposed in the literature)[20] as the solvent and acetyl chloride as the acylation agent (**Figure 4.9**). The mono-substituted aromatic rings in the polymer side chain were acylated at the *para* position because of the large steric requirement of the attacking reagent. It should be noted that acylation reactions conducted in non-polar solvent such as cyclohexane are faster than acylation reactions in halogenated solvents.[20]

The mechanism of the reaction can be described by Friedel-Crafts acylation reaction of benzene which occurs in three steps. The mechanism is illustrated in **Figure 4.10**.[21] In the first step, an acyl halide reacts with the Lewis acid to form an acyl cation. In the second step, the benzene reacts with the acyl cation electrophile and forms a Wheland intermediate. In last step, removal of the proton from the intermediate restores the aromatic system and regenerating the active catalyst. The extent of the acylation of long chain molecules, such as polystyrene-d_5 presents difficulty in the accessibility of a particular reaction site due to conformational complexity. For this reason, the acetylation of polystyrene, like so many polymer-analogous reactions, was not quantitative. The progress of acetylation in benzene and other lower mass analogs such as toluene and so on depends on catalyst, acyl component, solvent, and the ratio of the catalyst to acyl component.[20]

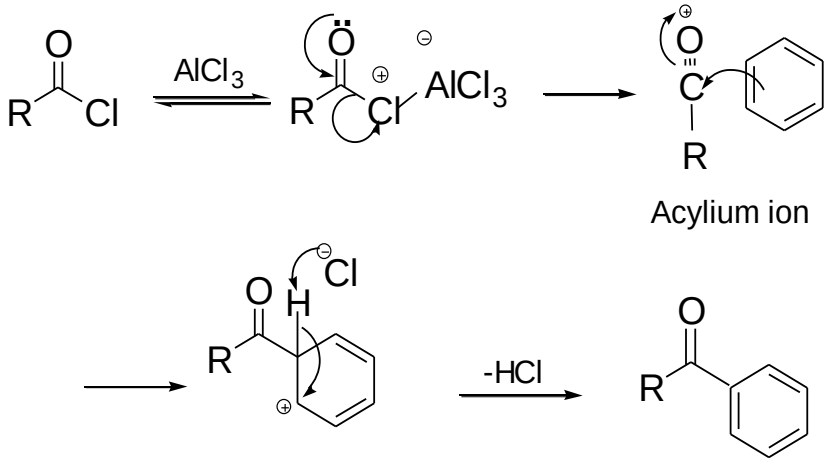

Figure 4.10: The mechanism of Friedel-Crafts acylation reaction of benzene.

In general, the dependence of the extent of acetylation of non-deuterated polystyrene could be easily monitored by the reduction in FT-IR peak at 700 cm^{-1} which is characteristic of monosubstituted benzene. However, this peak was absent in the deuterated polystyrene. Furthermore, the reaction was monitored by the reduction in ^1H NMR signal at 7.15 ppm; there was also a new signal at 7.55 ppm which is characteristic of the protons *ortho* to the acetyl group. The structure of the product was confirmed by ^1H NMR and FT-IR spectroscopy. The ^1H NMR spectra of PS-d_5 and ACPS-d_4 are shown in **[Figure 4.11** (**a** and **b**)**]**. The ^1H NMR spectrum of ACPS-d_4, when compared to PS-d_5 shows a new signal at 2.50 ppm which is due to the methyl

(CH_3) protons of acetyl moiety and a new signal due to the protons *ortho* to the acetyl group appears around 7.55 ppm whereas, in the aromatic region, the intensity of the broad signal at 7.15 ppm is reduced.

The FTIR spectrum of ACPS-d_4 is displayed in **Figure 4.12**. The presence of a C=O stretching at 1670 cm^{-1} and C-O stretch at 1240 cm^{-1} along with ^1H NMR results confirms that the acetylation had indeed occurred. The molecular weight and molecular weight distribution of ACPS-d_4 was also determined by GPC. The M_w of ACPS-d_4 was 95,000 g mol^{-1} and PDI was 1.1. When the starting material PS-d_5 had an M_w of 100,000 g mol^{-1} and a polydispersity of 1.05. The decrease in the M_w of ACPS-d_4 could be attributed to long reaction time (7 h) which caused degradation of the polymer.[14, 22]

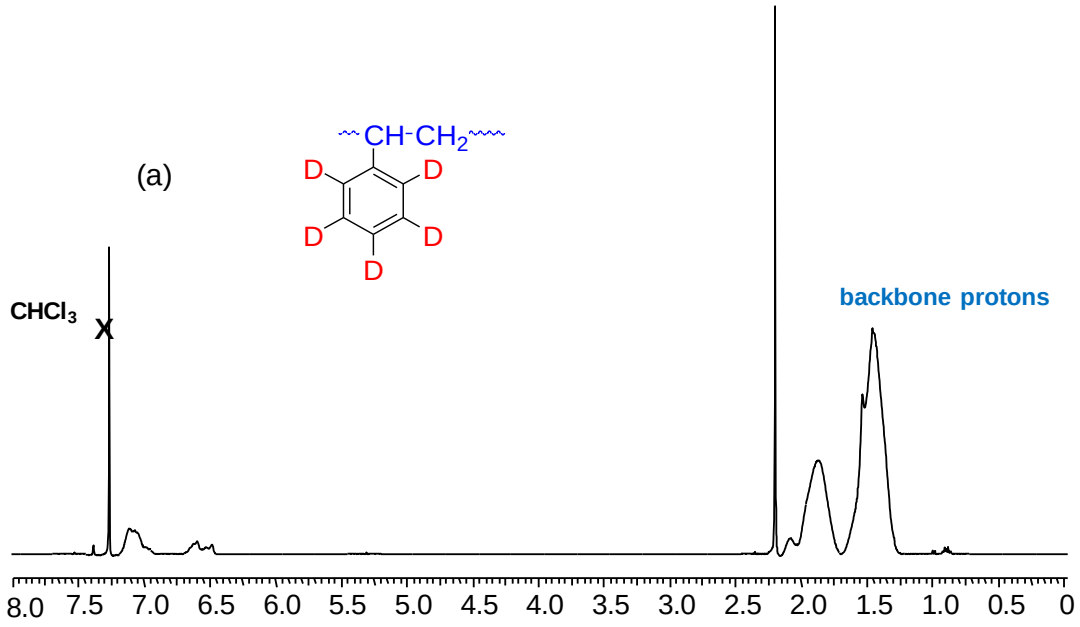

Figure 4.11: ^1H NMR spectra (300 MHz, $CDCl_3$) of (a) PS-d_5 (80% deuteration), (b) ACPS-d_4 and (c) PAS-d_4. Solvent and water signals are marked by X.

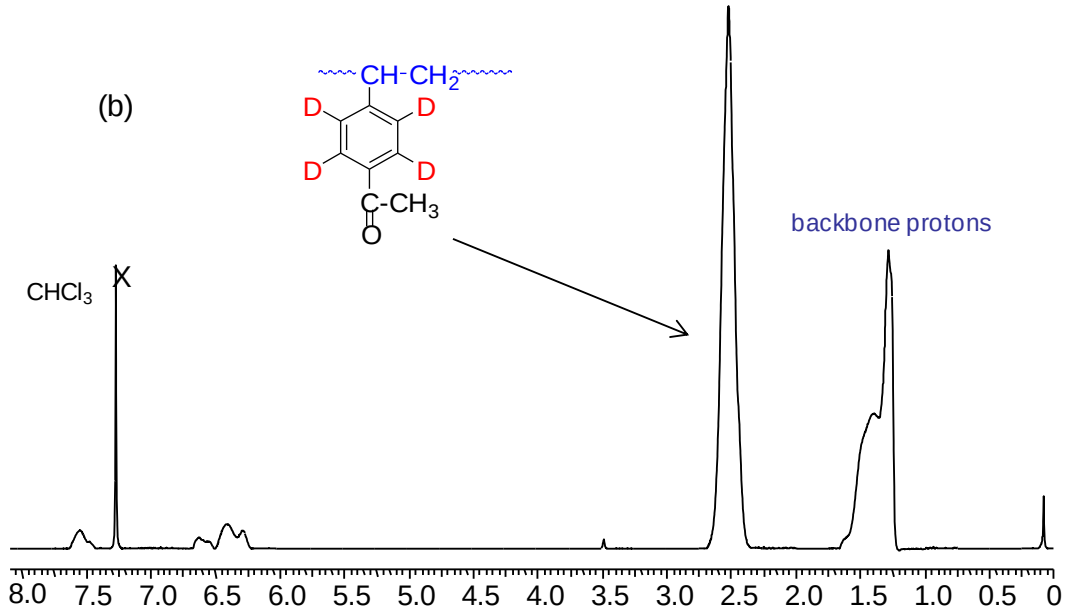
(b)
CH-CH2
D
D
D
D
C-CH3
O
backbone protons
CHCl3
8.0 7.5 7.0 6.5 6.0 5.5 5.0 4.5 4.0 3.5 3.0 2.5 2.0 1.5 1.0 0.5 0

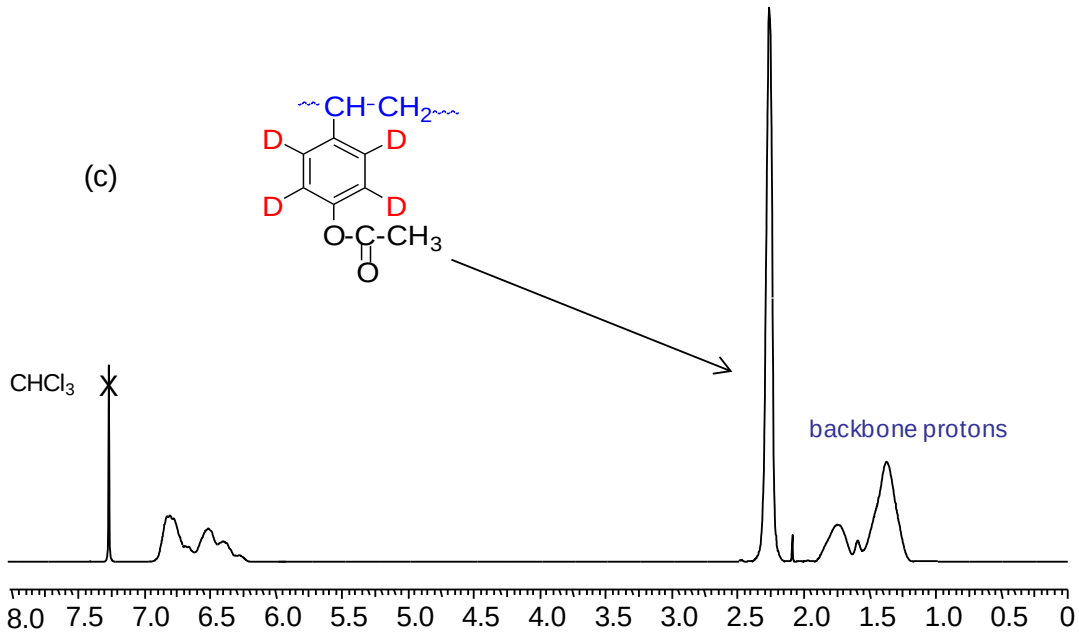
(c)
CH-CH2
D
D
D
D
O-C-CH3
O
backbone protons
CHCl3
8.0 7.5 7.0 6.5 6.0 5.5 5.0 4.5 4.0 3.5 3.0 2.5 2.0 1.5 1.0 0.5 0

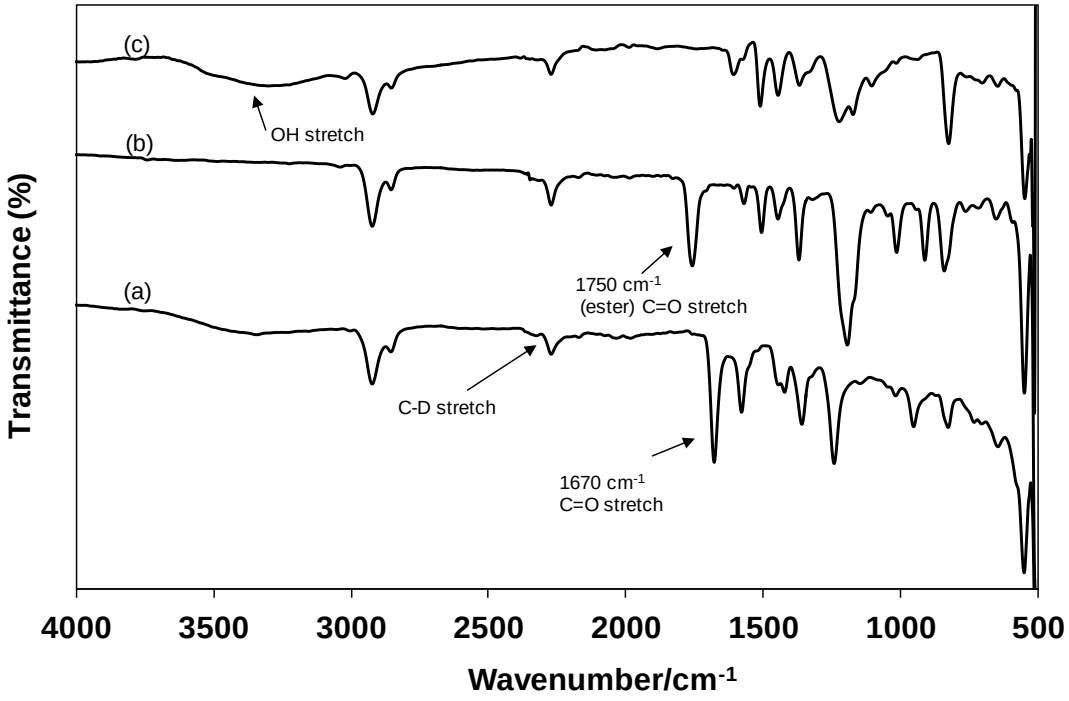

Figure 4.12: FT-IR spectra of (a) ACPS-d_4 and (b) PAS-d_4 and (c) P4HS-d_4. The spectra have been shifted vertically for clarity.

4.4.2 Synthesis of Deuterated Poly(4-acetoxystyrene) (APS-d_4)

Poly(4-acetoxy styrene) can be prepared from poly(4-acetylstyrene) by Baeyer-Villiger oxidation. Several oxidation agents have been reported in the literature to facilitate Baeyer-Villiger oxidations of aromatic ketones to esters. The mechanism of the Baeyer-Villiger reaction may be demonstrated in four steps, with persulfuric acid used as the oxidant in this example as shown in **Figure 4.13**.[23] In this reaction, the reactivity of the carbonyl group is increased by protonation at the carbonyl group; addition of the peroxide to the carbonyl carbon yields a hydroxyperoxide to afford the Criegee intermediate. The subsequent migration of R_2 or R_1 onto the neighbouring carbon is accompanied by cleavage of the peroxo O−O bond and loss of a proton in the last step to afford the ester in the usual way.

In this study, several peroxy acids were tested as reagents to convert ACPS-d_4 to APS-d_4 in a Baeyer-Villiger oxidation: potassium persulfate,[24] sodium perborate in acetic acid,[20] and peracetic acid[19] with chloroform as the solvent. The results for the oxidation of acetyl polystyrene-d_4 to acetoxy polystyrene-d_4 are summarised in **Table 4.4**. Potassium persulfate gave no reaction at all. Sodium perborate in acetic acid resulted in partial hydrolysis so that the final product was mixture of poly(4-hyroxystyrene-*co*-acetoxystyrene). The best result was obtained when the

Baeyer-Villiger oxidation was conducted in the presence of peracetic acid after 142 h (**Figure 4.9**). The oxidation kinetics with peracetic acid was followed by FT-IR and ^{1}H NMR spectroscopy. The transformation of acetyl group to acetoxy was complete after 142 h.

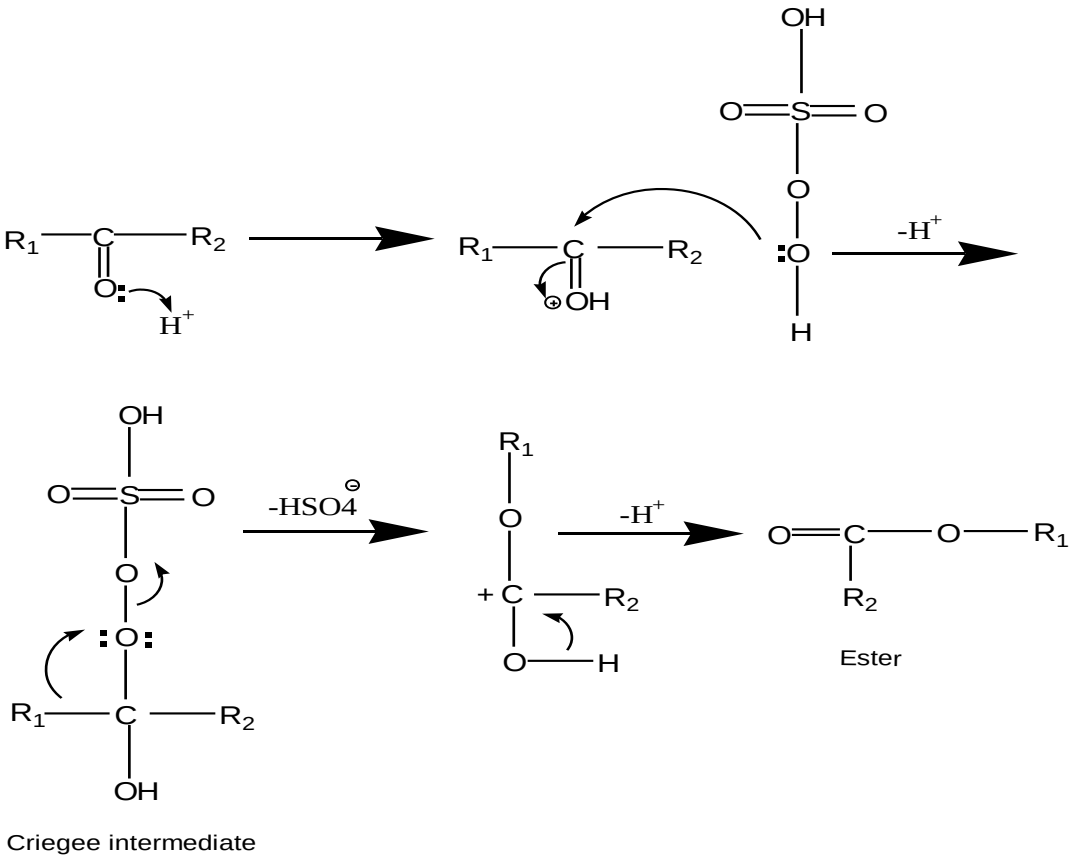

Figure 4.13: The mechanism scheme of Baeyer-Villiger reaction.

Table 4.4: Oxidation of Acetylated PS-d_4 to PAS-d_4 under various conditions.

System	Results
Potassium persulfate	No reaction at all.
Sodium perborate in acetic acid	Acetylation with partial hydrolysis
Peracetic acid	Works well with high extent of acetylation

The FTIR spectrum showed the appearance of a new peak at 1750 cm^{-1} due the new ester C=O stretch (for the acetoxy group), whereas the aromatic ketone C=O stretch of the acetyl group at 1670 cm^{-1} disappeared (**Figure 4.12)**. The ^{1}H NMR spectrum supported the FT-IR findings (**Figure 4.11)**. The acetyl signal at 2.50 ppm was replaced gradually with time by an acetoxy methyl at 2.25 ppm . In addition, the residual aromatic signal at 7.5 ppm also gradually shifted upfield to 6.80 ppm as a result of the oxidation [**Figure 4.11** (**b** and **c**)**]**. After 142 h the oxidation was complete as evident from the appearance of signals at 2.25 and 6.80 ppm and the disappearance of the signals at 2.50 and 7.50 ppm.

The M_w as well as PDI of ACPS-d_4 and PAS-d_4 was determined by GPC (**Figure 4.14**). The M_w of the PAS-d_4 (15,000 g mol^{-1}) was decreased compared to the M_w of deuterated poly(4-acetylstyrene) (95,500 g mol^{-1}) and the PDI increased from 1.1 to 1.8. This suggests that the decrease in M_w could be due to degradation of the ACPS-d_4 during Baeyer-Villiger oxidation of the acetyl group.

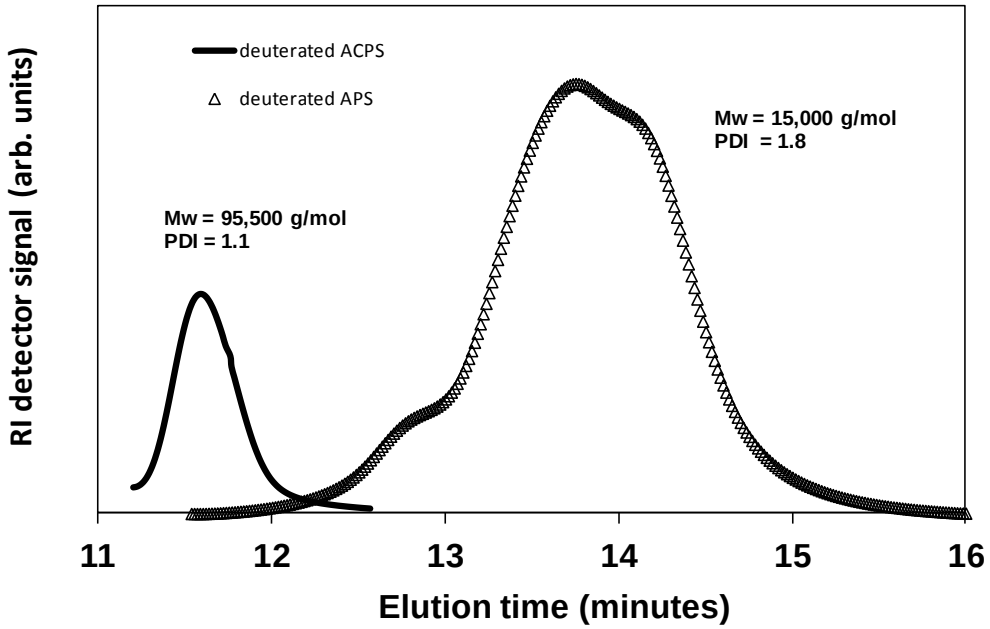

Figure 4.14: GPC traces of deuterated ACPS and deuterated APS.

4.4.3 Synthesis of Deuterated Poly(4-hydroxystyrene) (P4HS-d_4)

A number of methods have been used to convert poly(4-acetoxystyrene) to poly(4-hydroxystyrene).[19, 20, 25, 26] Some authors mentioned that phenolic oxidation[26] and gelation reactions[27] might occur during conversion of the acetyl groups to hydroxyl groups. In the present study a number of experiments were carried out to investigate the suitability of the different hydrolysis methods for deuterated poly(4-acetoxystyrene). First, deuterated poly(4-acetoxy styrene) was readily hydrolysed using THF by the addition of sodium hydroxide solution at 50 ^{o}C.[28] However, ^{1}H NMR spectrum result indicated that low-molecular weight impurities were present in the final product. Although previous literature reports had suggested that a drying temperature of 110 °C was adequate to remove all the residual THF present,[29] this proved not to be the case for P4HS-d_4 , and residual THF could be detected in the ^{1}H NMR spectrum of the final product even after drying the product at 160 °C. A low-molecular-weight impurity such as THF was found to act as a plasticizer and, even in small amounts, noticeably lowered the T_g of the final polymer product. Another process was used to obtain pure product by substitution of 1,4-dioxane for tetrahydrofuran at room temperature, the resulting polymer gelled after 12 hours. It seems that tetrahydrofuran is better than 1,4-dioxane as dispersion medium. Dhamodharan *et al.*[19] reported better result by carrying out the hydrolysis of hydrogenated PAS with hydrazine hydrate. To avoid the need to use a highly toxic reagent (hydrazine hydrate), an alternative method was tried in which deuterated poly(4-acetoxystyrene) was dissolved in acetone, a small amount of concentrated HCl was added and the reaction was heated to 50 $^{\circ}$C. The reaction was allowed to proceed overnight with stirring. The hydrolysed product dissolved easily in DMSO-d_6 and ^{1}H NMR spectroscopy indicated the absence of any impurities (**Figure 4.15**). A ^{1}H NMR spectrum of P4HS-d_4 confirms that the intense signal at 2.25 ppm representing the acetoxy methyl group of PAS had disappeared. Furthermore, a new signal at 9 ppm could be assigned to the hydroxyl group. This is also confirmed by the FT-IR spectrum where the strong carbonyl absorption peak at 1750 cm^{-1} has disappeared **Figure 4.12**.

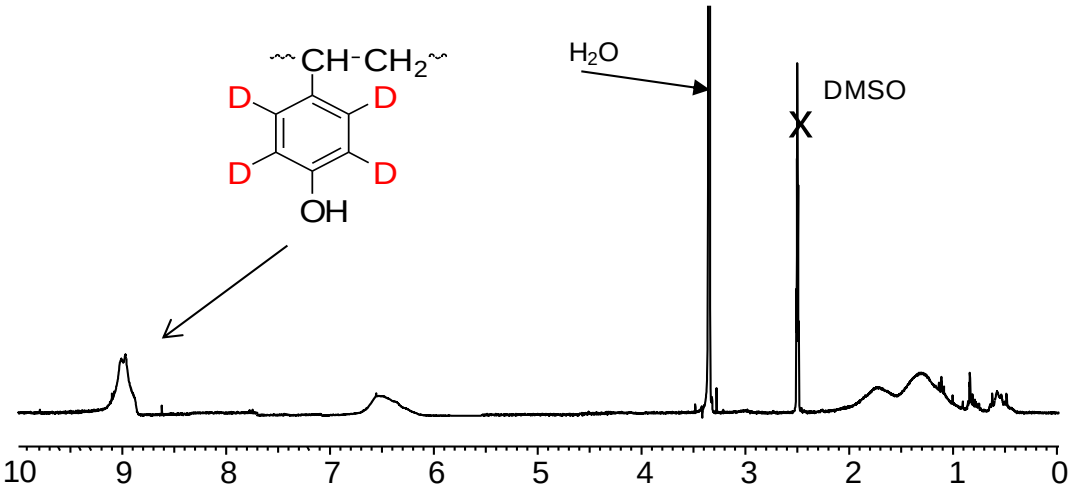

Figure 4.15: ^{1}H NMR spectrum (300 MHz, DMSO-d_6) of P4HS-d_4. Solvent is marked by X.

4.4 Conclusions

In conclusion, a fast, high-yielding method for the deuteration of polystyrene under microwave irradiation using superheated C_6D_6 in the presence of ethylaluminum dichloride and an ionic liquid was developed. This method was simple to carry out and shortened reaction times from several hours to 10 minutes. Partial H/D exchange on the aromatic hydrogens of poly(4-hydroxystyrene) was achieved using superheated D_2O as a cheap deuterium source under microwave irradiation in the presence of a small amount of an acid catalyst.

ACPS-d_4, APS-d_4 and P4HS-d_4 can be obtained by a simple chemical transformation of PS-d_5 under thermal conditions. The PS-d_5 was acetylated using cyclohexane as solvent instead of carbon disulfide (a highly toxic and flammable solvent) and acetyl chloride as the acetylating agent. The acetyl group was converted to an acetoxy group by Baeyer-Villiger oxidation. Hydrolysis of deuterated poly(4-acetoxystyrene) then proceeded smoothly in acetone/HCl at 50 ^{o}C. This method offers cost-effective and alternative route to preparing deuterated polymers that otherwise have to be prepared from the deuterated monomers.

4.5 References

1. T. Kaino, K. Jinguji and S. Nara, *Appl. Phys. Lett.*, 1983, **42**, 567.
2. M. Yamamoto, Y. Yokota, K. Oshima and S. Matsubara, *Chem. Commun.*, 2004, 1714.
3. N. H. Werstiuk and T. Kadai, *Can. J. Chem.*, 1985, **63**, 530.
4. G. J. Ellames, J. S. Gibson, J. M. Herbert, W. J. Kerr and A. H. McNeill, *Tetrahedron Lett.*, 2001, **42**, 6413.
5. A. V. Santoro, E. J. Barrett and H. W. Hoyer, *J. Am. Chem. Soc.*, 1967, **89**, 4545.
6. S. R. Klei, J. T. Golden, T. D. Tilley and R. G. Bergman, *J. Am. Chem. Soc.*, 2002, **124**, 2092.
7. C. B. Castellani, A. Perotti, M. Scrivanti and G. Vidari, *Tetrahedron*, 2000, **56**, 8161.
8. K. Fodor-Csorba, G. Galli, S. Holly and E. Gács-Baitz, *Tetrahedron Lett.*, 2002, **43**, 3789.
9. J. R. Jones, W. J. S. Lockley, S.-Y. Lu and S. P. Thompson, *Tetrahedron Lett.*, 2001, **42**, 331.
10. U. Hakala and K. Wähälä, *J. Org. Chem.*, 2007, **72**, 5817.
11. A. K. Greene and L. T. Scott, *J. Org. Chem.*, 2012.
12. S. Anto, G. S. Getvoldsen, J. R. Harding, J. R. Jones, S. Y. Lu and J. C. Russel, *J. Chem. Soc., Perkin Trans.*, 2000, **2**, 2208.
13. R. Martinze-Palou, *J. Mex. Chem. Soc.*, 2007, **51**, 252.
14. B. Willenberg, *Makromol. Chem.*, 1976, **177**, 3625.
15. C. Oliver Kappe, *Chem. Soc. Rev.*, 2008, **37**, 1127.
16. B. H. Stuart, *Infrared spectroscopy: fundamentals and application*, John Wiley, 2004.
17. A. Martins and M. Lautens, *Org. Lett.*, 2008, **10**, 4351.
18. E. Malone, *MChem Dissertation*, Heriot Watt University, 2010.
19. J. M. Nasrullah, S. Raja, K. Vijayakumaran and R. Dhamodharan, *J. Polym. Sci., Part A: Polym. Chem.*, 2000, **38**, 453.
20. S. Deokar, R. S. Ghadage, C. R. Rajan and S. Panrathnam, *J. Appl. Polym. Sci.*, 2004, **91**, 3192.
21. P. Wathers, N. Greeves, S. Warren and J. Claden, *Organic Chemistry*, Oxford University Press, 2001.

22. J. L. Garnett, M. A. Long, R. F. W. Vining and T. Mole, *Tetrahedron Lett.*, 1973, 4075.
23. T. Laue and A. Plagens, *Named Organic Reactions*, John Wiley and Sons, New York, 1981.
24. N. C. Deno, W. E. Billups, K. E. Kramer and R. R. Lastomirsky, *J. Org. Chem.*, 1970, **35**, 3080.
25. R. Arshady, G. W. Kenner and A. J. Ledwith, *J. Polym. Sci., Polym. Chem. Ed.*, 1974, **12**, 2017.
26. M. Kato, *J. Polym. Sci.*, 1969, **23**, 150.
27. S. Arichi, N. Sakamoto, M. Yoshida and S. Himuro, *Polymer*, 1986, **30**, 461.
28. C. A. Khatri, V. Vaidya, K. Levon, S. K. Jha and M. M. Green, *Macromolecules*, 1995, **28**, 4719.
29. J. Keddie, R. Jones and R. Cory, *Europhys. Lett.*, 2007, **27**, 59.

Chapter 5 - Thermal and Mechanical Properties of PMMA-Filler Nanoparticles Composites

Contents

5.1 Introduction

To improve the dispersion of the nanoparticles and endow the compatibility between PMMA matrix and nanosilica, PMMA was grafted from the surface of the silica as described in Chapters **2** and **3**. Despite their potential wide-ranging engineering applications, very little is known about the effect of surface-grafted filler particles on the mechanical and thermal properties of the resulting nanocomposites. Most mechanical studies have dealt with either unmodified nanosilica or commercially available surface-modified particles.[1,2]

Reactive silica particles have already been converted into PMMA composites.[3, 4] These studies were carried out by dispersing non-aggregating spherical silica nanoparticles, which were either untreated or surface-modified, in methyl methacrylate monomer, followed by polymerisation using a free radical initiator. Although chemical bonds between organic and inorganic phase are likely to exist in such cases, the free radical polymerisation process also produces free polymer chains, unattached to the silica surface. This is therefore different from the grafting process described in this chapter.

This chapter describes the thermal and dynamic mechanical properties of the surface-grafted poly(methyl methacrylate) chains from both aggregated silica nanoparticles (Degussa Aerosil 300 and Cab-o-sil H5) or colloidally dispersed silica (Nissan MEK-ST, MEK-ST-L or IPA-ST-UP). To be able to compare the properties of PMMA-grafted particles to those of more conventional PMMA/nanosilica composites, we prepared also a series of samples by dispersing silica nanoparticles (both aggregated and non-aggregated) in a tetrahydrofuran (THF) solution of PMMA and investigated their thermal and mechanical behavior using differential scanning calorimetry (DSC) and dynamic mechanical thermal analysis (DMTA). DMTA results were expected to provide useful information about the structure and viscoelastic properties of the composite, especially when these results are extended to a wide frequency range. For this purpose, master curves for storage modulus E' for all materials examined, were generated applying the time-temperature superposition principle.

5.2 DSC Analysis of Dispersed PMMA/filler Nanocomposites

A series of solution-dispersed PMMA-silica and PMMA-titanium dioxide nanoparticles with different filler types and contents (10, 20, 30 wt%) were analysed by differential scanning calorimetry. According to the DSC measurements, the T_g values of

the PMMA-Cab-o-sil H5 composites seem to be slightly higher than the T_g of pure PMMA as can be seen from **Figure 5.1** and **Table 5.1** although there is little or no change in the T_g between the various composites containing 10 wt%, 20 wt% or 30 wt% of silica which all have the same T_g values.

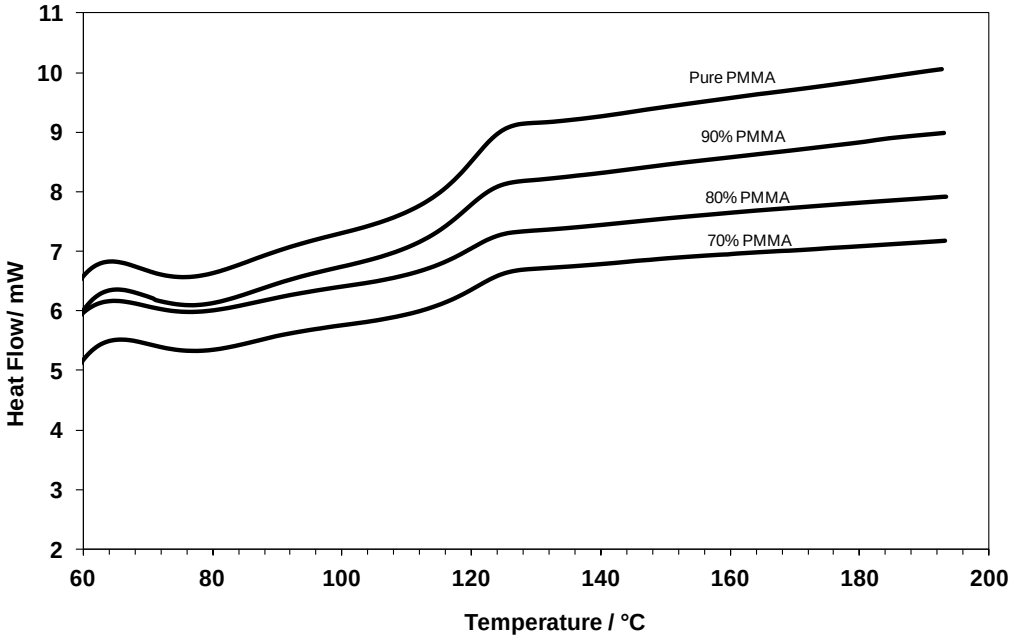

Figure 5.1. DSC traces of dispersed PMMA–Cab-o-sil H5 composites. The traces have been shifted vertically for clarity.

This result was found with all PMMA-silica composites (A300, MEK-ST, MEK-ST-L and IPA-ST-UP). The A300 composites appear to show a slightly lower T_g than other silica samples (i.e. Cab-o-sil H5, MEK-ST, MEK-ST-L or IPA-ST-UP) of similar composition (**Table 5.1**). The difference is, however, small and may be due to small amount of residual solvent or moisture present acting as a plasticiser. Moreover there is no change in the T_g value when the samples were prepared with or without ultrasonication (**Figure 5.2**). Therefore, one might conclude that the T_g did not vary either with the presence of silica or with increasing silica concentration in PMMA. These results are in good agreement with the results by Kraft *et al.*[5] The lack of changes in T_g could be attributed to the polymer not being adsorbed onto the surface of the particles. Yim *et al.*[6] investigated polydimethylsiloxane-silica composites and found that the increase in T_g was directly proportional to filler concentration. According to their finding the increase in T_g was as a result of the adsorption of the polymer onto the

surface of the filler which restricted molecular motion of the polymer. Grima *et al.*[7] suggested that unaffected T_g values of PBA-silica composites could be attributed to the low concentration of silica in the composites. It is worth saying that the influence of silica nanoparticles should be limited to those polymer chains that are close to the particles' surface. This means that, at low concentration, silica nanoparticles will be more dispersed among the polymer chains and they would affect only a small fraction of the whole sample.

The glass transition temperature, T_g, is the temperature when the polymer softens on heating. Above T_g, the thermal energy enables the segmental motion of polymer chains. Restricting the mobility of the polymer chains requires more thermal energy, and a higher T_g might be expected with an increasing concentration of filler nanoparticles.[1] However, none of the DSC traces showed any evidence for such a change in T_g, and the composites were therefore studied by DMTA where the maximum of the tan δ peak is usually associated with the "mechanical T_g" and provides a more sensitive sensor for revealing a change in the glass temperature.

In addition to the glass transition temperature, the DSC measurements also reveal changes in heat capacity, ΔC_p. It should be mentioned that the ΔC_p value of PMMA might be expected to decrease in proportion to the amount of filler added. However, this is not the case and ΔC_p varies not only with the amount of filler but also with the type of filler. The ΔC_p value of PMMA-A300 silica nanoparticles is consistently lower than for other samples (**Table 5.1)**. The reason for that is not clear and is subject to further investigation. **Figure 5.3** shows ΔC_p *vs.* silica content (*wt*%) for various PMMA silica composites. As the silica content increase, ΔC_p decrease, as expected since the glass transition only involves the pure polymer. In fact, the entire reduction in changes in heat capacity, ΔC_p can be calculated by consideration of the amount of polymer from **equation 5.1**.[8]

$$\Delta Cp \text{ wt} = \Delta Cp\ 0 \times \text{wt. fraction polymer} \qquad (\mathbf{5.1})$$

where $\Delta Cp\ 0$ is the change in heat capacity of pure PMMA.

The decrease of the ΔC_p is attributed to a decrease in the number of degrees of freedom for the polymer chain segments resulting from silica nanoparticles/matrix interaction.[9] Therefore, measuring the change of heat capacity of the polymer

nanocomposites could be useful to detect a change in polymer chain mobility in the nanocomposites directly. This approach has already been successfully applied to hyper-branched polymers/silica nanocomposites.[10] Thomas *et al*. proposed a simple model to interpret similar changes in the ΔC_p values of PS/calcium phosphate nanocomposites. (**Figure 5.4**).[11] The model proposed that a rigid amorphous fraction is formed when the nanoparticles strongly interact with the amorphous region of the polymer. The authors then suggested that the decrease in ΔC_p could be attributed to the formation of rigid amorphous fraction.

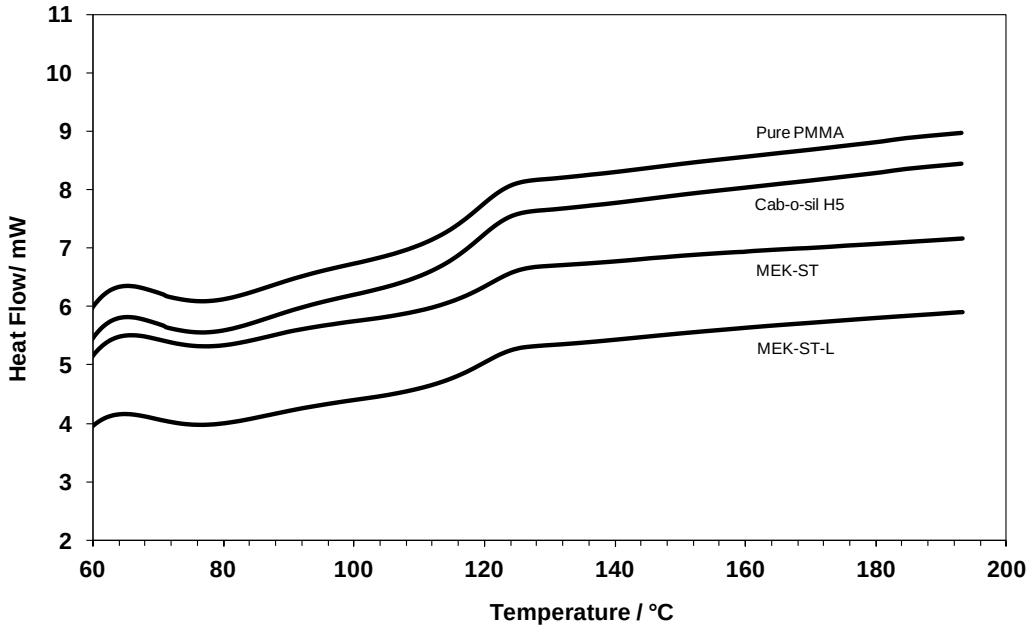

Figure 5.2. DSC traces of PMMA and silica-PMMA composites (30 wt% silica, using ultrasonication). The traces have been shifted vertically for clarity.

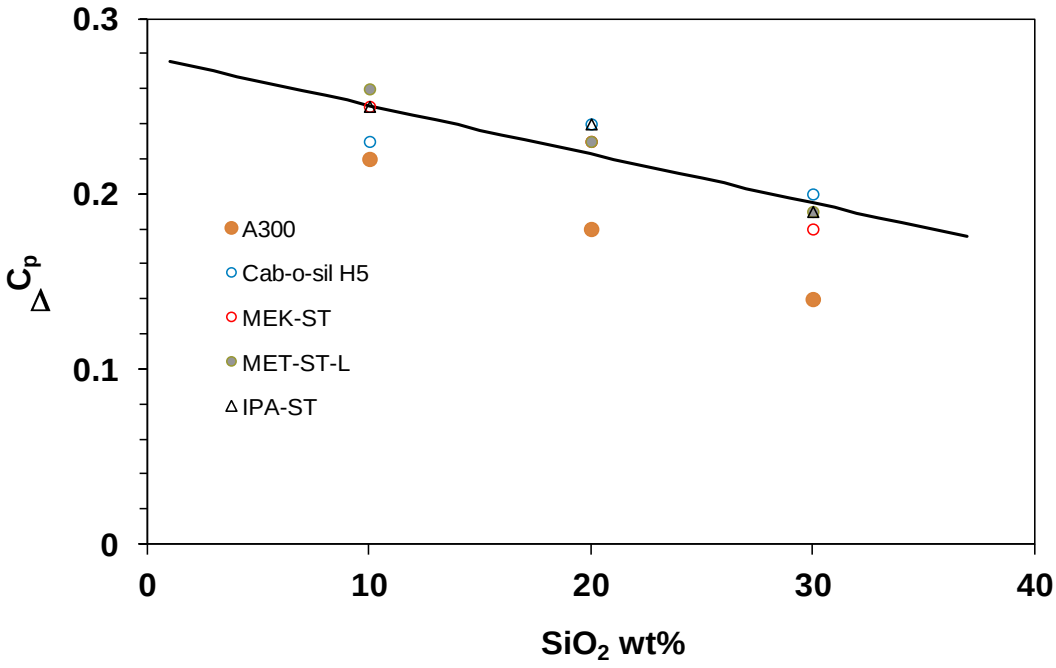

Figure 5.3: Difference in heat capacity for various dispersed PMMA-silica composites, along with the ΔC_p calculated assuming no contribution from the silica (solid line).

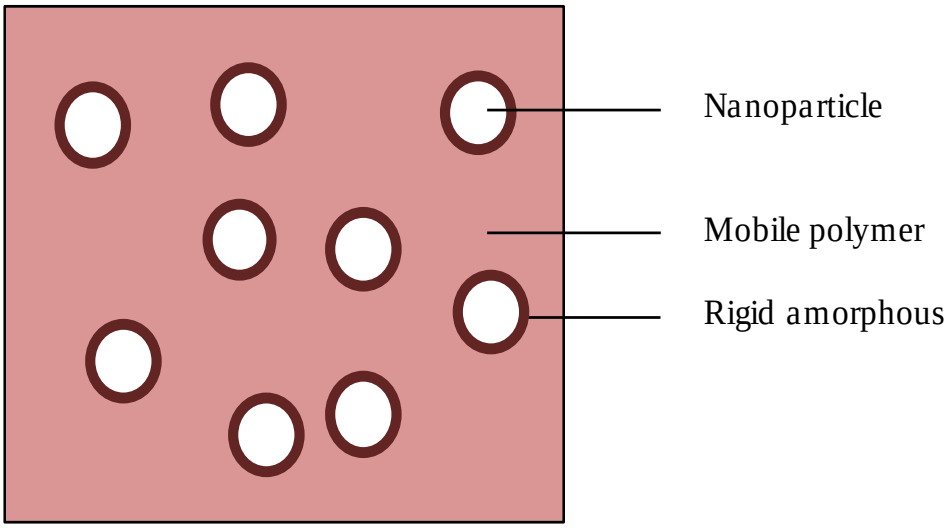

Figure 5.4: Simple model indicating the rigid amorphous fraction in nanocomposites.[11]

Table 5.1: Glass transition temperatures and heat capacity changes for various PMMA filler composites.

Filler wt%	T_g / °C	ΔC_p / J g^{-1} °C^{-1}	ΔC_p / J g^{-1} °C^{-1} "a"
Pure PMMA	120	0.31	----
Cab-o-sil H5 10%	120	0.22	0.25
Cab-o-sil H5 20%	120	0.24	0.22
Cab-o-sil H5 30%	121	0.20	0.19
A300 10%	119	0.22	0.25
A300 20%	118	0.18	0.22
A300 30%	120	0.14	0.19
MEK-ST 10%	119	0.25	0.25
MEK-ST 20%	120	0.23	0.22
MEK-ST 30%	121	0.18	0.19
MEK-ST-L 10%	120	0.26	0.25
MEK-ST-L 20%	119	0.23	0.22
MEK-ST-L 30%	121	0.19	0.25
IPA-ST-UP 10%	121	0.25	0.25
IPA-ST-UP 20%	120	0.24	0.22
IPA-ST-UP 30%	120	0.19	0.19
Error	±1	±0.01	±0.01

"a" Calculated by **eq. (5.1)**.

Similar composites could be prepared with titanium dioxide, although the maximum concentrations of filler were more limited, making the preparation of composites with >10 wt% TiO_2 very difficult. This was attributed to the different surface of the filler which made the filler less compatible with the polymer matrix and has strong tendency to aggregate.[12, 13] While the smaller anatase filler particles showed a noticeable increase in the T_g by up to 3 °C with increasing concentration of anatase, the larger rutile filler particles gave rise to only minor changes in T_g as shown in **Figure 5.5** and **Table 5.2**. These results confirm those obtained by Luyt *et al*.[12]

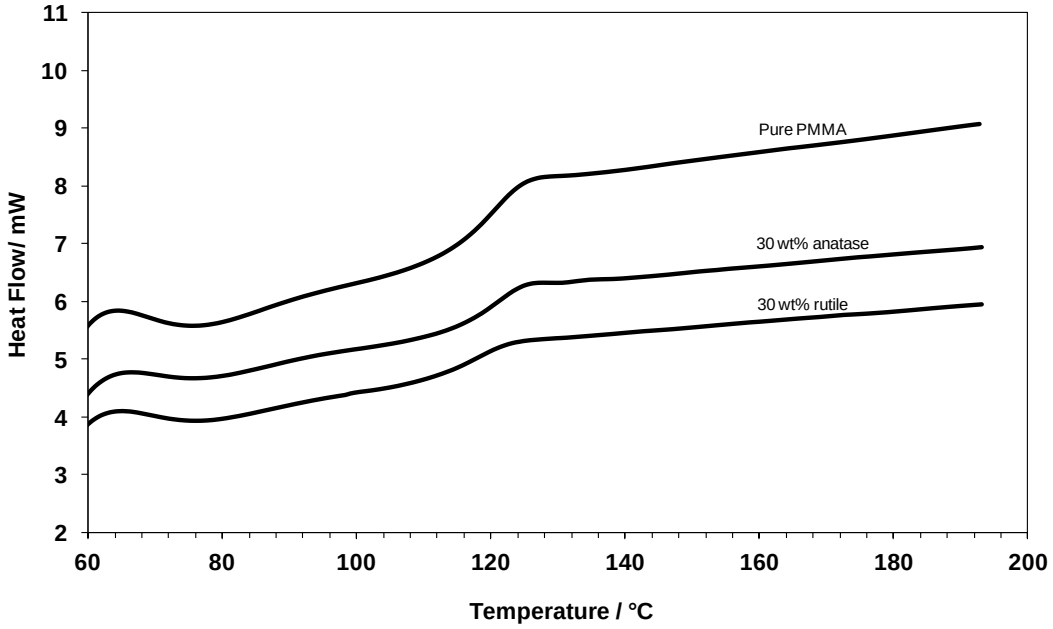

Figure 5.5: DSC traces of PMMA-TiO_2 (30 wt% TiO_2). The traces have been shifted vertically for clarity.

Table 5.2: Glass transition temperatures and heat capacity changes for PMMA-TiO_2 composites.

Filler wt%	T_g / ºC	ΔC_p / J g^{-1} °C^{-1}	ΔC_p / J g^{-1} °C^{-1} "a"
Pure PMMA	120	0.31	….
TiO_2 (Anatase) 10 wt%	121	0.23	0.25
TiO_2 (Anatase) 20wt%	121	0.21	0.22
TiO_2 (Anatase) 30wt%	123	0.18	0.19
TiO_2 (Rutile) 10wt%	117	0.22	0.25
TiO_2 (Rutile) 30wt%	120	0.15	0.19
Error	±1	±0.01	±0.01

"a" Calculated by **eq. (5.1)**.

5.3 DMTA Analysis of Dispersed PMMA/filler Nanocomposites

Figures 5.6 (a) shows the non-normalised storage modulus (E') *vs*. temperature curves for PMMA and a series of PMMA–Cab-o-sil H5 silica composites that were prepared by dispersing silica nanoparticles in PMMA (details of the preparation are described in the Experimental Section). The difficulty of preparing homogenous samples of all composites led to small variations in the sample dimensions. Since the DMTA instrument used the dimensions to calculate the modulus, this resulted in variations of the modulus, which is particularly noticeable at low temperatures. Therefore, the curves were normalised to facilitate comparison of the modulus of all composites above T_g **[Figures 5.6 (b)]**. At room temperature and slightly above, the modulus of the polymer composites levelled at approximately 1 GPa before dropping abruptly at the T_g of the polymer. Owing to the onset of flow at higher temperature, the pure PMMA sample and the sample with 10 wt% filler lost their dimensional stability above 150 °C. From this point onwards, the dimensions of the sample change leading to an artificial increase in modulus recorded by the DMTA instrument. Addition of >10 wt% silica yielded very small changes in the low temperature E' modulus, as reported previously for PMMA/nanosilica composites.[3, 5] However, these samples show a considerable increase in E' values above T_g and retain dimensional stability to much higher temperature, i.e. up to ca. 200 °C. As expected, the increase in storage modulus above T_g is a function of silica content, reinforcement being more pronounced at higher filler concentration. This is likely to be a result of the formation of a 3-dimensional network structure involving polymer and filler, aided by the aggregation of the silica particles.

The loss modulus of pure PMMA **[Figure 5.6 (c)]** shows a peak at 115 °C which is associated with the polymer glass transition. Only small changes in peak position are observed with increasing filler content, and this is in agreement with the DSC measurements which indicated only minor variations between the glass transition temperature of PMMA and the T_g of the composites. Reinforcement effects increase the storage as well as loss moduli above the polymer glass transition.

The loss factor, $\tan\delta$, is defined as the ratio of the loss modulus to storage modulus. It provides a good measure of whether a sample behaves as an elastic material ($\tan\delta < 0.1$) or efficiently dissipates mechanical energy into heat ($\tan\delta > 0.5$). The plot of $\tan\delta$ as a function of temperature displays large variations with filler content **[Figure 5.6 (d)]**. The main α-relaxation associated with the T_g of PMMA gives rise to a maximum in the $\tan\delta$ *vs*. temperature plot which is located at almost the same

temperature regardless of filler concentration. This confirms the previously discussed DSC data. In contrast, the size of tan δ decreases with increasing amount of filler and this is a consequence of the increasing storage modulus values with filler content, particularly at high temperature.[14] The breadth of the tan δ peak relates to the relaxation of the polymer chains.[15] However, considerable broadening of the α-relaxation is observed for the composites, suggesting that the segmental motion of the PMMA chains is altered to some extent. Furthermore, the broadening of the tan δ peak is consistent with the E'' changes discussed before. Most importantly, only samples with higher filler content (40 wt% silica) showed not only better thermal stability, but also their loss factor indicated the onset of an apparent second relaxation process. This is consistent with the results of Kalika *et al*.,[16] who observed two peaks in the tan δ curve for PMMA filled only at high particle loading. According to their finding the failure to observe the second tan δ peak at lower loading as a result of the lower degree of compatibility between the polymer and silica particles.

There are several possible explanations for such a second relaxation. Deformation of DMTA sample and the resulting changes in geometry occasionally give rise to what appears to be a second maximum in the tan δ *vs*. temperature plot. Sample deformation was indeed observed for PMMA and its composites with ≤ 30 wt% of silica. In those samples no second tan δ peak was observed at higher temperature because the samples broke during the DMTA measurement as a result of huge deformation. There has been considerable discussion in the literature as to the origin of the second relaxation in polymer–filler composites. Tsagaropoulos and Eisenberg [1] proposed a model to interpret similar second relaxation peaks recorded for several polymer–filler composites **(Figure 5.7)**.[17] The authors suggested a three-layer model in which the formation of a loosely bound layer consisting of polymer chains of restricted mobility around silica particles accounts for the formation of the second T_g.[1, 18] However, such a claim has never been confirmed by the measurement of a second, high-temperature glass transition using DSC.

Recently, the existence of a second T_g in polymer filler systems has been questioned.[11] By noting that the additional relaxation takes place in the region of the spectrum where the unfilled polymer exhibits terminal flow,[15, 18-20] a different interpretation was brought forward **(Figure 5.8)**. It was argued that formation of a 3-dimensional polymer–filler network suppresses chain diffusion. Therefore, only chains

that are unaffected by the presence of the filler particles would undergo relaxation, leading to the lower temperature at the "normal T_g".

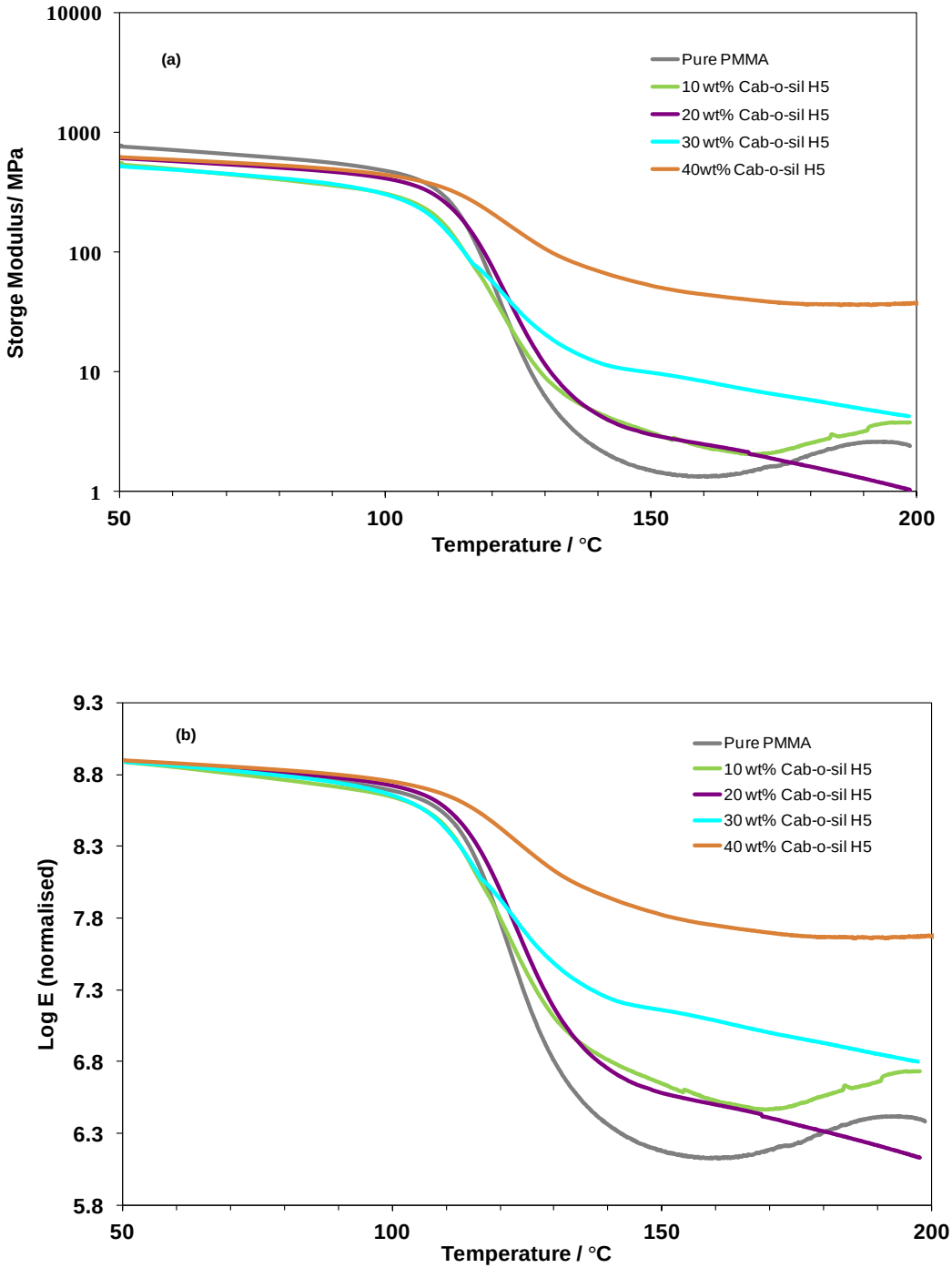

Figure 5.6: (a) Plot of storage modulus as a function of temperature for PMMA-Cab-o-sil H5 composites, and **(b)** Plot of normalised storage modulus as a function of temperature for PMMA-Cab-o-sil H5 composites.

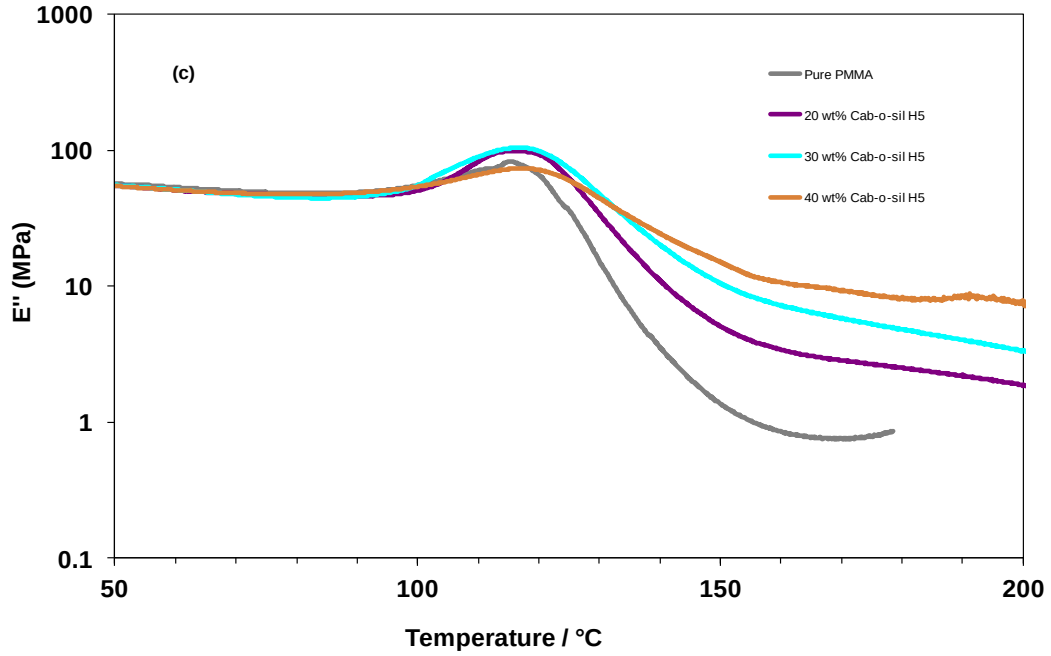

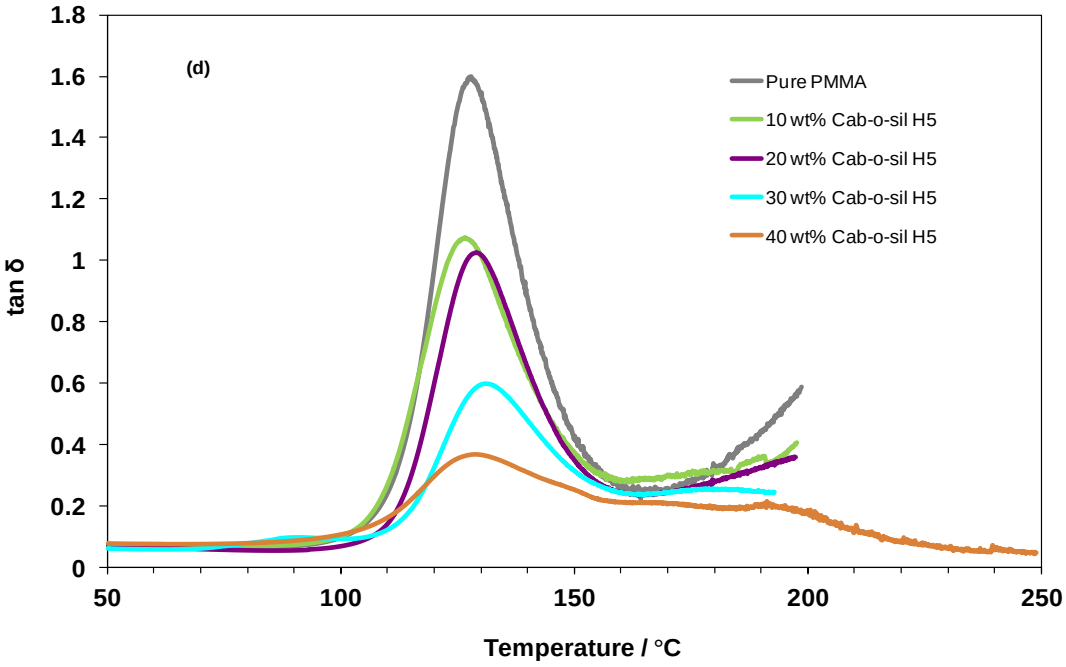

Figure 5.6: (c) Plot of loss modulus as a function of temperature for PMMA-Cab-o-sil H5 composites, and **(d)** Plot of tan δ as a function of temperature for PMMA-Cab-o-sil H5 composites.

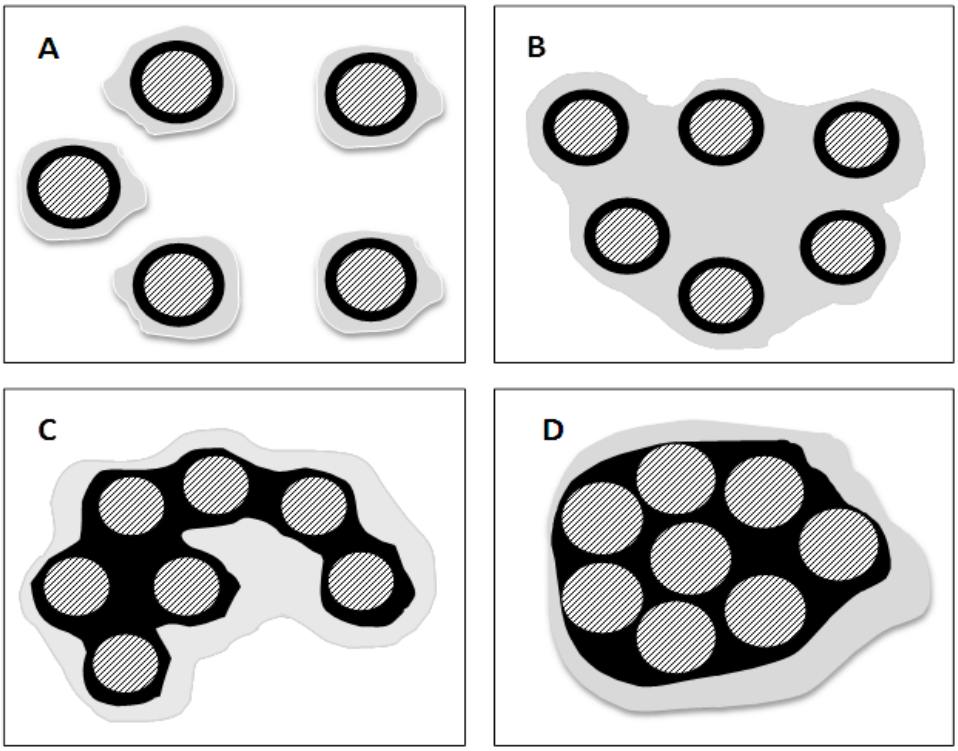

Figure 5.7: Schematic diagram illustrating the Tsagaropoulos–Eisenberg model as a function of silica content from (a) 10 wt%, (b) 20 wt%, (C) 30 wt% to (d) 40 wt%. The line-shaded areas correspond to the silica particles, the black areas to the tightly bound polymer and the grey areas to loosely bound polymer.[17]

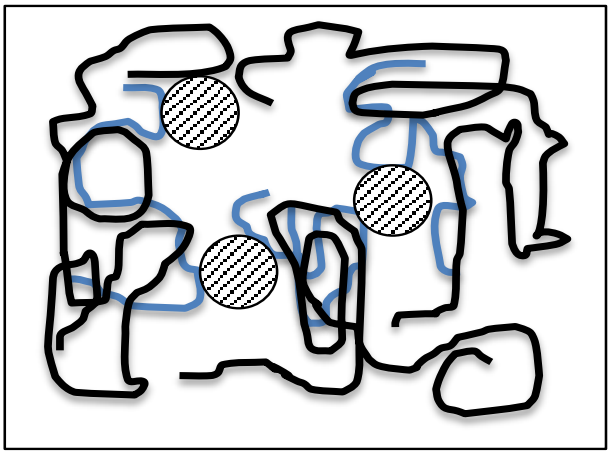

Figure 5.8: The Robertson-Rackaitis model of polymer flow restriction due to particles. The solid blue chains are strongly adsorbed onto the filler which restrict the overall motion. The solid black chains are polymer chains that are not affected by the presence of the filler and are free to flow.[18]

A comparison between the DMTA data (E' and tan δ) for a series of nanocomposites with different silica nanoparticles prepared by dispersing various silica nanoparticles into PMMA at fixed silica content is made in **Figure 5.9**. The storage modulus *vs*. temperature curves for PMMA and a series of PMMA-silica composite containing 30 wt% silica is displayed in **Figure 5.9 (a)**. At room temperature, the modulus of the polymer composite was in all cases approximately 1 GPa. The PMMA-aggregated silica (Cab-o-sil H5 and A300) nanocomposites clearly show a large rubbery plateau which is typical of a cross-linked network. However, all of the non-aggregated silica (MEK-ST and MEK-ST-L) samples display properties that are similar to those of pure PMMA **[Figure 5.9 (a)]**. The wide working temperature range (as evident from the large rubbery plateau) can be attributed to the formation of a network structure involving polymer and filler.

Size, shape and extent of aggregation of the silica nanoparticles have a significant impact on the dynamic properties of PMMA-silica composites. The tan δ *vs*. temperature plots of samples made with various silica, but keeping the same composition, illustrate that the most noticeable difference amongst the curves is a broadening of α-relaxation [**Figure 5.9 (b)**]. The maximum of the tan δ plot **(Table 5.3)** is typically about 10 °C higher than the T_g determined by DSC **(Table 5.1** and **5.2)** and close to the maximum of the tan δ plot for unfilled PMMA (127.6 °C). MEK-ST and MEK-ST-L differ in surface area (220 and 60 m^2/g, resp.) as well as nanoparticle size (12.5 and 45 nm). The PMMA-MEK-ST-L composites containing the larger silica particles show the onset of deformation already at 160 ^oC, indicating that larger silica nanoparticles are less effective at reinforcement of the PMMA-silica composites. In contrast, composites made with Cab-o-sil H5 or A300, both highly aggregated silica nanoparticles with a surface area of 300 ± 30 m^2/g and a 7 nm particle size, showed little signs of deformation even after heating to temperatures of over 50 ^oC above the T_g of the neat polymer. These results are in good agreement with earlier work reported by Yang and Nelson, who observed significant improvements in the mechanical properties of PMMA-silica nanocomposites when the nanoparticles size decreased.[21]

Similar composites could be prepared with titanium dioxide as filler. The modulus–temperature curves for the TiO_2 composites are shown in **Figure 5.10 (a)**. Data have been normalised to the max E' value obtained among all samples. It is evident that there is an increase in the modulus above the glass transition with increasing TiO_2 concentration. Comparison between the anatase (small particles size) and rutile (large

particles size) modulus–temperature curves reveals that the increase in modulus value above T_g is higher with anatase than rutile TiO_2. This is consistent with the different surface area of these fillers; the interaction between polymer chains and the filler is higher with an increasing surface area.[1] In addition, the composites exhibited little mechanical damping at high temperature, especially in a PMMA-anatase 30 wt% composite as seen in **Figure 5.10(b)**.

Table 5.3: Peak maximum values from the tan δ plot for various PMMA-filler composites.

Filler	**Maximum of tan δ peak / °C**		
	10 wt%	20 wt%	30 wt%
A300	127	127	124
Cab-o-sil H5	127	129	130
MEK-ST	128	130	131
MEK-ST-L	129	131	130
IPA-ST-UP	129	129	129
TiO_2, anatase	129	130	132
TiO_2, rutile	128	129	127
Error	±1	±1	±1

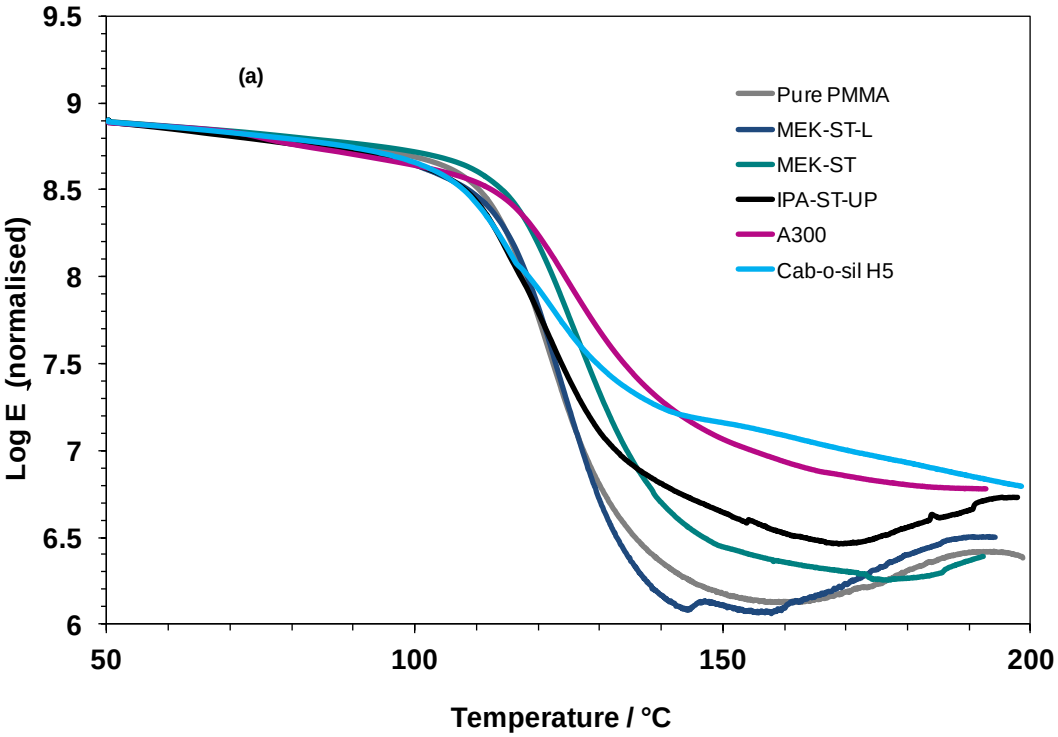

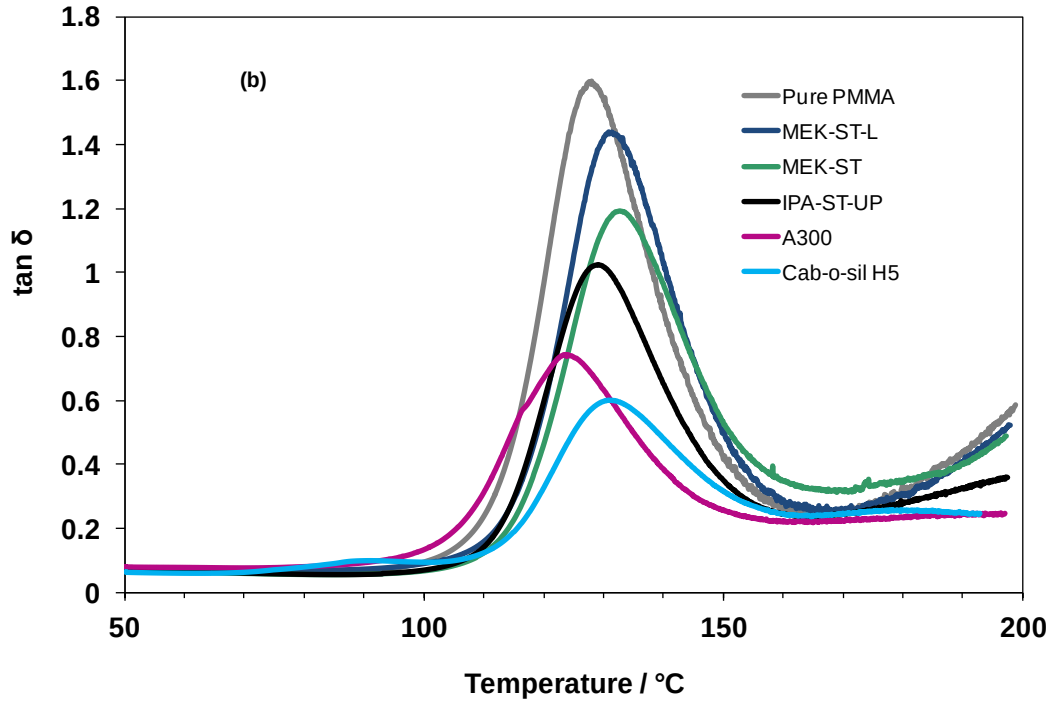

Figure 5.9: (a) Plot of normalised storage modulus as a function of temperature for PMMA-silica (30 wt%) composites. **(b)** Plot of tan δ as a function of temperature for PMMA-silica (30 wt%) composites.

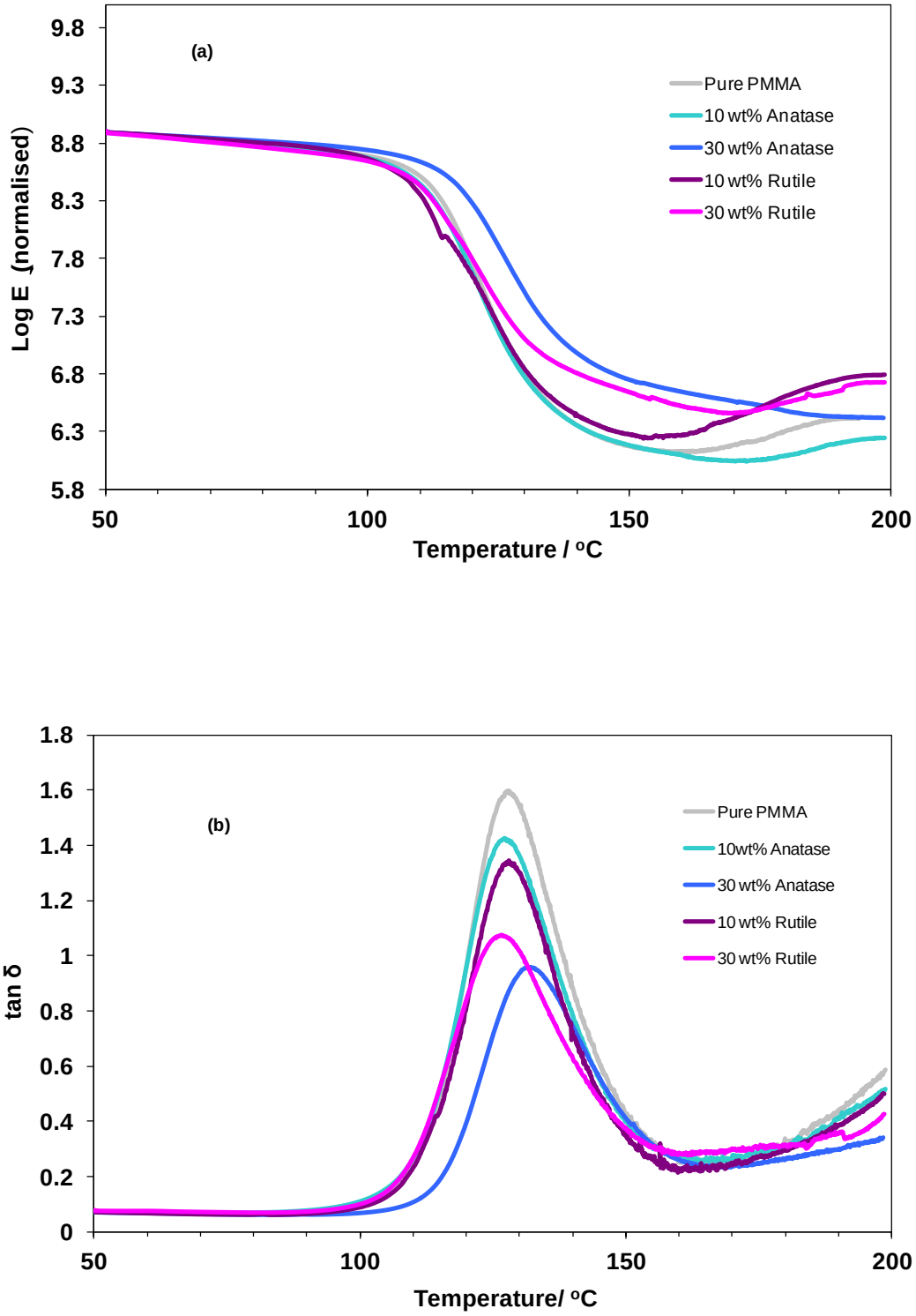

Figure 5.10: (a) Plot of normalised storage modulus as a function of temperature for PMMA-TiO_2 composites (10 and 30 wt%). **(b)** Plot of tan δ as a function of temperature for PMMA-TiO_2 composites (10 and 30 wt%).

5.4 Thermal and Dynamic Mechanical Properties of Grafted PMMA-silica Nanocomposites

All samples were thoroughly dried at 160 °C since the T_g of PMMA was sensitive to the presence of plasticising solvents. The absence of residual solvent was confirmed by running a ^{1}H NMR spectrum of the as-prepared silica–PMMA hybrid particles as shown in Chapter **3**. As illustrated in **Figure 5.11** and **Table 5.4**, the glass transition temperatures measured by DSC are usually higher for the hybrid material compared to pure PMMA. This could be due to the strong adhesion between PMMA and silica when linked together by a covalent bond,[22] which restricts the mobility of the PMMA chains. Similar conclusions can be drawn by considering the temperatures corresponding to the loss peak and tan δ maximum (**Table 5.4**). The glass transitions obtained by DSC (mid-point T_g) are located a few degrees above the E'' maxima and, as expected, the tan δ maxima occur 8 − 10 °C above the loss peak maxima. The higher T_g values obtained by DMTA relative to the DSC are due to differences in the measuring frequency.

The T_g increase observed for the grafted systems compared to PMMA (at most 10 °C for **G31-20Si**) seems to be dependent on the molecular weight of the grafted chains as well as nanosilica content. For example, for the sample with lowest M_w, **G12-24Si**, the T_g is close to that of pure PMMA. In this case, the expected decrease due to the low molecular weight is probably offset by the relatively high silica content, leading to a T_g close to that of pure PMMA. Furthermore, the sample with lower silica content and close M_w to neat PMMA, **G29-4.5Si**, also has T_g similar to pure PMMA (**Table 5.4**). **Figure 5.12** shows the relationship between the T_g of differently grafted PMMA/silica nanocomposites and the silica content. All the T_g values of grafted PMMA samples increased with the silica content. The glass transition temperature of both grafted PMMA-silica (i.e. Cab-o-sil H5 and MEK-ST) composites increases from 119 °C to 130 °C as the silica loading increases to ~ 20 wt%. The adhesion between the particles and PMMA molecules is strong when the PMMA is grafted to silica nanoparticles, so the T_g of these composites increases. The trends of how T_g varies with the tan delta maximum are consistent with the DSC results.

Figure 5.13 shows DSC curves of the **G30-21.8Si (Cab-o-sil H5)** and **G31-20Si (MEK-ST)** samples after the silica has been removed using tetrabutylammonium fluoride. In these samples the T_g values were around 120 − 122 °C. Therefore, after removal of the silica, all samples show a noticeable decrease in T_g values from 131 to 122 °C, although these were still slightly higher than for the pure PMMA (119.6 °C).

Grafting a polymer onto a filler makes the bonding interaction between them stronger compared to simply dispersing particles in a polymer matrix.[20] Most researchers report an increase in the T_g as a function of filler content.[3, 6, 22]

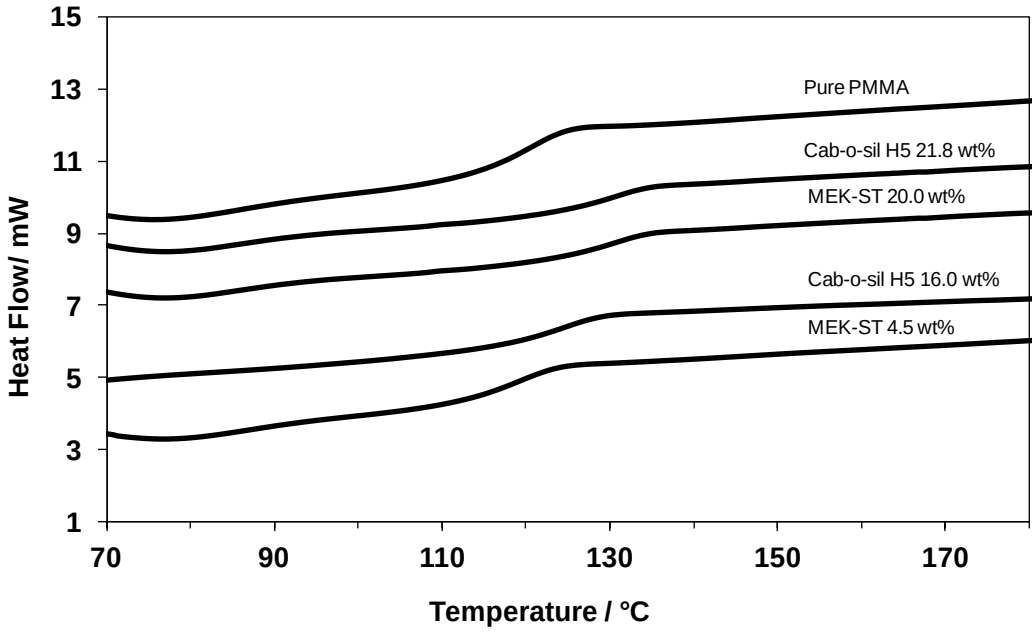

Figure 5.11: DSC traces of pure PMMA and grafted PMMA-silica nanoparticles. The traces have been shifted vertically for clarity.

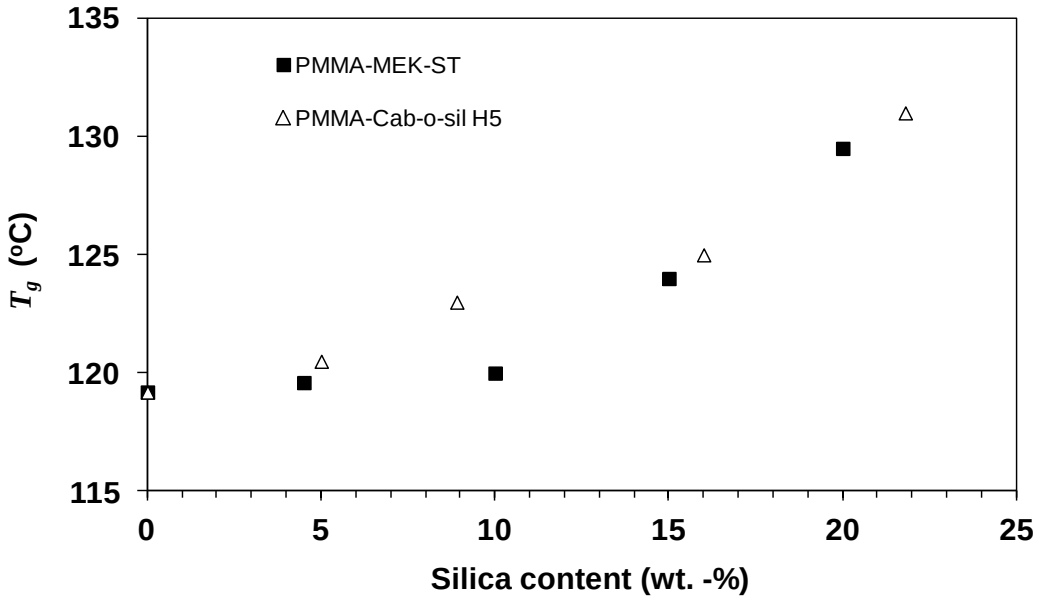

Figure 5.12. Comparison of T_g values for different grafted PMMA-silica nanocomposites as a function of silica content.

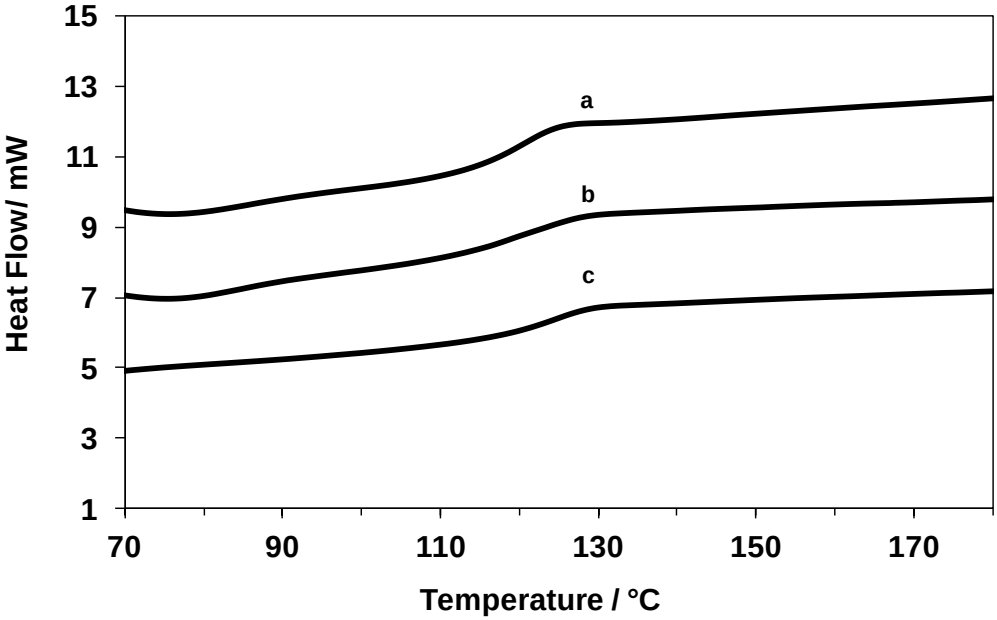

Figure 5.13: DSC traces of (a) pure PMMA, (b) G30-21.8Si, and G31-20Si (after silica cleavage). The traces have been shifted vertically for clarity.

Table 5.4: Loss and tan δ values corresponding to peak maximum and comparison to DSC glass transitions.

Sample	*% SiO_2*	M_w [g mol^{-1}]	$T_{max}(E'')$ °C	$T_{max}(\tan\delta)$ °C	T_g °C
PMMA	-------	32000	115	127	119
G29-4.5Si [a)]	4.5	29000	115	128	120
G28-10Si [a)]	10.0	28000	117	128	121
G36-15Si [a)]	15.1	36000	122	129	124
G31-20Si [a)]	20.0	31000	125	138	130
G27-5Si [b)]	5.0	27000	115	129	121
G36-9Si [b)]	8.9	28000	116	132	124
G28-16Si [b)]	16.0	28000	119	131	125
G30-22Si [b)]	21.8	30000	126	139	131
G12-24Si [b)]	24.0	12000	115	129	120
Error	--	-----	±1	±1	±1

[a)] PMMA-MEK-ST. "G31" refers to a number-average molecular weight of 31 kg mol^{-1} for the grafted PMMA, "4.5Si" stands for a silica content of 4.5 wt%. [b)] PMMA-Cab-o-sil H5.

A comparison between the DMTA data (E', and tan δ) for the grafted PMMA samples prepared in this project is made in **Figure 5.14** and **5.15.** The normalised E' versus temperature curves once again reveal a pronounced reinforcement effect at temperatures above the glass transition. Similar to the polymer–silica mixtures studied before, the modulus of the hybrid materials containing 8 and 22% of silica remained almost plateau-like above T_g, until up to 240 °C and did not show the irreversible deformation that unfilled PMMA exhibits above 160 °C **[Figure 5.14 (a)** and **5.15 (a)]**. Such a plateau is observed for solution-dispersed filler-PMMA composites only at much higher filler content.[5, 7] It is interesting to note that the PMMA grafted from aggregated Cab-o-sil H5 silica nanoparticles led to an even higher rubbery plateau modulus

compared to grafted PMMA from colloidally dispersed silica. Such a substantial increase of storage modulus can be attributed to the formation of a 3-dimensional network of silica nanoparticles (with Cab-o-sil H5), which is absent when the polymer was grafted from the surface of non-aggregated silica nanoparticles.[23] The reinforcing effect on the modulus is not unusual and comparable to composites of single-walled carbon nanotubes in styrene–isoprene copolymers,[24] which also possessed a rubbery plateau that extended to over 250 °C.

As shown in Figures **5.14 (b)** and **5.15 (b)**, grafting PMMA to the surface of silica nanoparticles shifts the tan δ peak values of these composites to a high temperature region, implying a strong interaction between PMMA molecules and the silica. Increasing the silica content also broaders the tan δ peak, and lowers its intensity from 1.6 to 0.6. The breadth of the tan δ peak relates to the relaxation of the polymer chain.[15] Unlike non-aggregated silica, the aggregated Cab-o-sil H5 exhibited little mechanical damping at high temperature as evidenced by a low tan δ (< 0.1) throughout the plateau region of the modulus **[Figure 5.14 (b)** and **5.15 (b)]**. Furthermore, the hybrid material exhibited little signs of degradation or irreversible deformation. The low tan δ values measured for the grafted-PMMA/silica nanocomposites suggest that the mechanical response above the glass transition is elastic. The tan δ curves provide clear evidence for the suppression of the terminal flow region, a result that is similar to that expected for single-phase, cross-linked amorphous materials.[25]

We note that the tan δ *vs.* temperature profiles of the hybrid material show no evidence of a second relaxation above T_g. The absence of a second maximum in the tan δ *vs.* temperature curves supports the idea that this is indirectly related to the suppression of chain diffusion. If only chains that are not interacting with the filler take part in this high-temperature process, then its absence in the grafted sample is a manifestation of chain diffusion being fully suppressed when chains are grafted to the nanoparticles.

One reason for missing the second relaxation above T_g in grafted PMMA could be due to the absence of any matrix free polymer. The amount of free polymer is likely to be low because no free initiator was added during the polymerisation and further purification of the grafted PMMA involved extensive Soxhlet extraction to remove free, unattached polymer. It may be concluded that the reason for missing the second peak in the grafted polymers requires more investigation.

Representative dynamic mechanical results for PMMA and grafted PMMA-silica nanoparticles at various measurement frequencies are shown in **Figures 5.16** and **5.17**. The range of frequencies is 0.1 − 100 Hz. Generally the dynamic mechanical properties of a polymer are dependent on frequency (time) and temperature. These mechanical measurements are done over a temperature range at constant frequency or over a frequency range at constant temperature. When a material is subjected to constant stress, its elastic modulus will decrease over a period of time. The reason for this is due to the fact that the material undergoes molecular rearrangement in an attempt to minimise the localised stresses.[8] Modulus measurements performed at a high frequency (short time) produce higher values whereas lower frequency (long time) results in lower values. This can be noticeably seen in **Figures 5.16** and **5.17**, which show the variation of storage modulus and tan δ of PMMA and grafted PMMA-silica nanoparticles with temperature at various frequencies. In these cases, the storage modulus increases and tan δ shifts to higher values with increasing frequency, consistent with their origin as motional relaxation processes.[16] Similar behavior has been observed for PEI and PS nanocomposites.[11, 16]

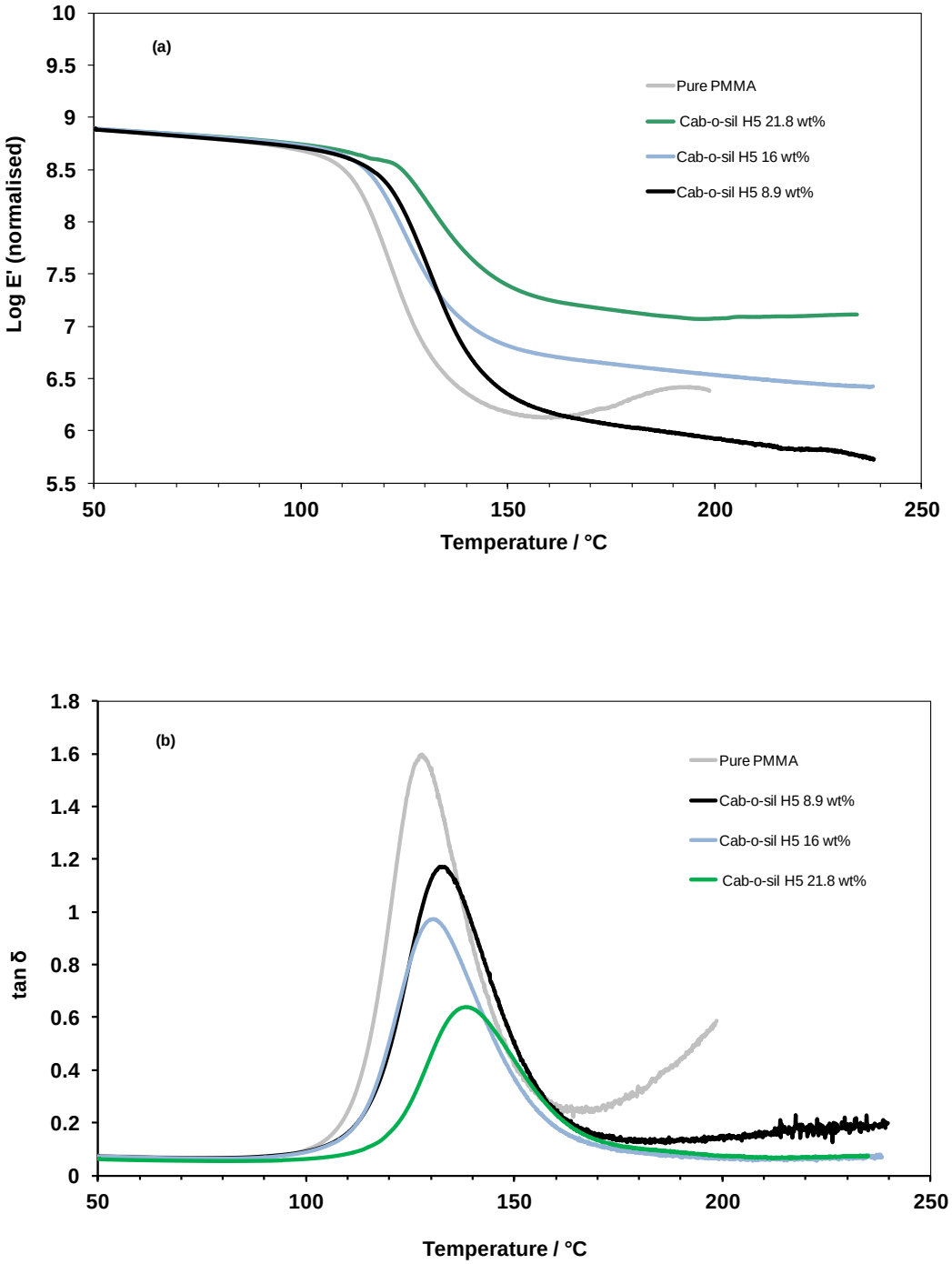

Figure 5.14: (a) Plot of storage modulus (normalised) as a function of temperature for PMMA and various grafted-PMMA/Cab-o-sil H5 silica nanocomposites. **(b)** Plot of tan δ as a function of temperature for PMMA and various grafted-PMMA/Cab-o-sil H5 silica nanocomposites.

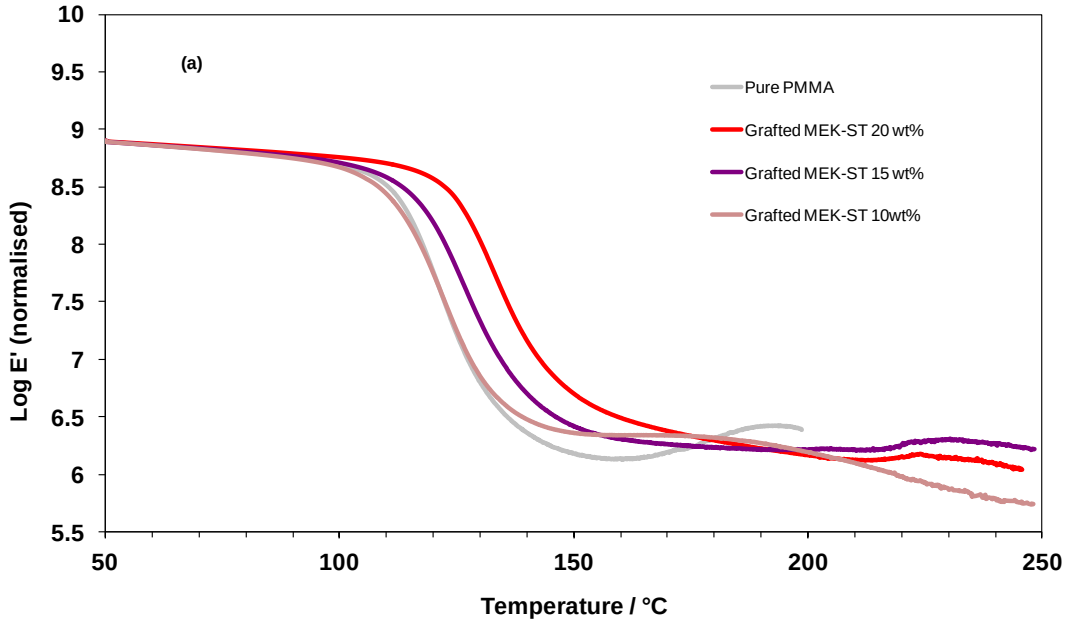

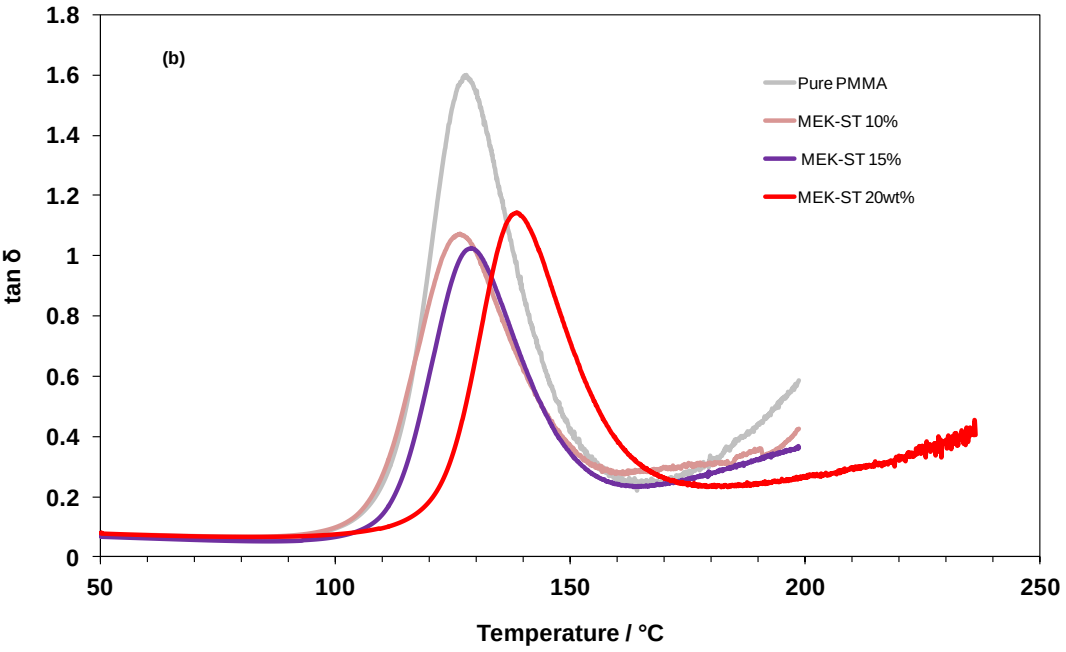

Figure 5.15: (a) Plot of storage modulus (normalised) as a function of temperature for PMMA and various grafted-PMMA/MEK-ST silica nanocomposites. **(b)** Plot of tan δ as a function of temperature for PMMA and various grafted-PMMA/MEK-ST silica nanocomposites.

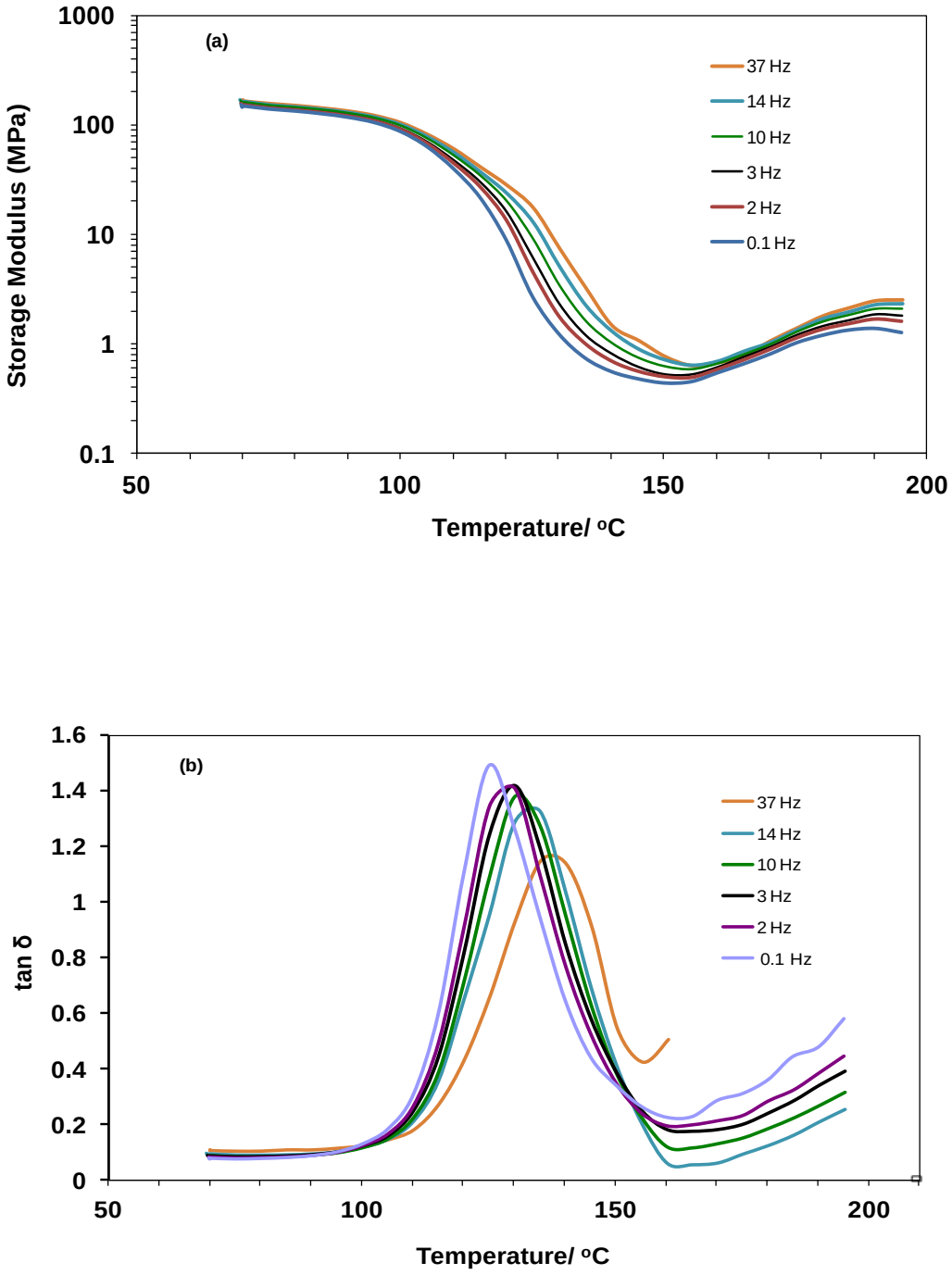

Figure 5.16: Effect of frequency on dynamic mechanical properties as a function of temperature for pure PMMA. **(a)** Storage modulus; **(b)** tan δ.

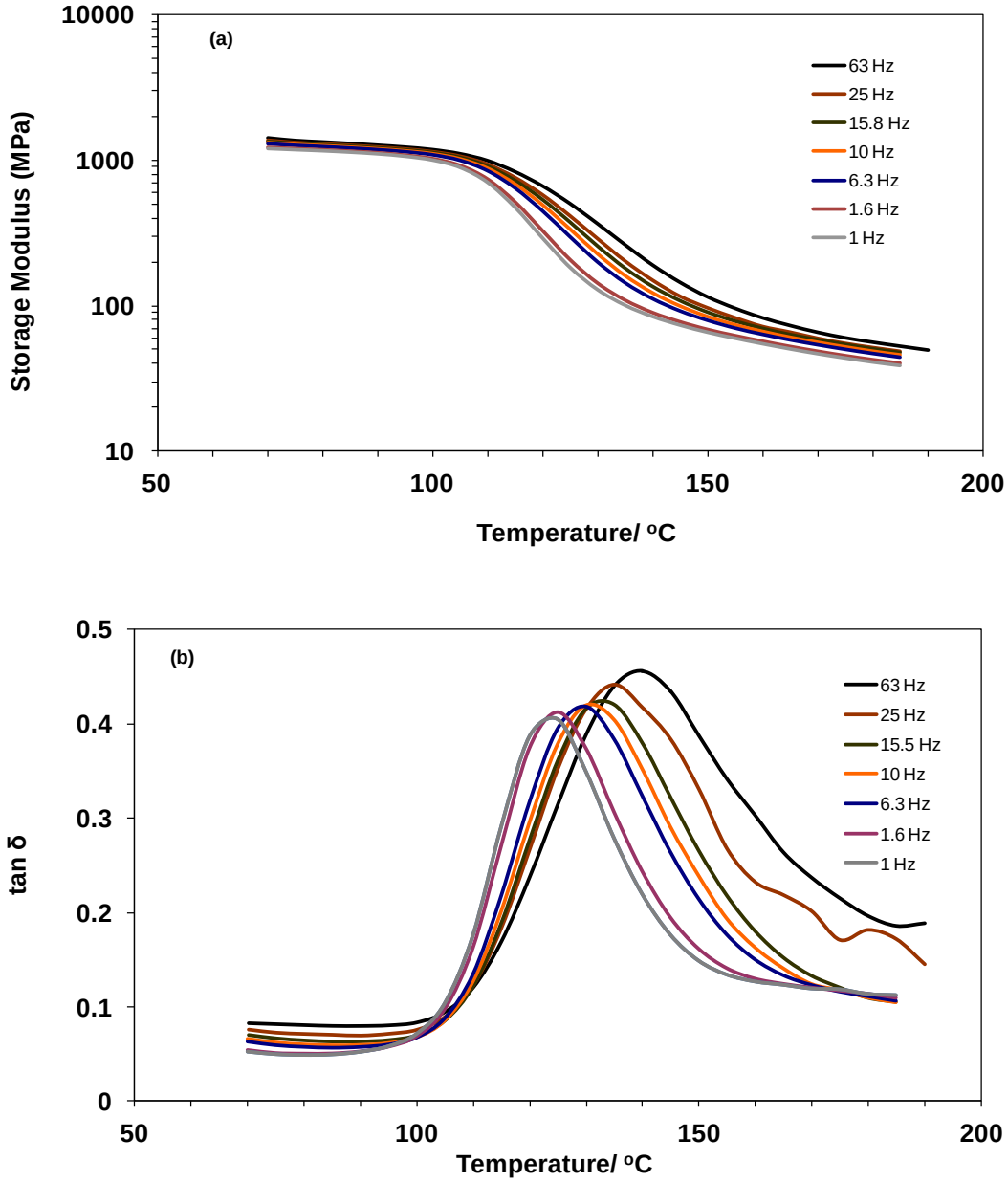

Figure 5.17: Effect of frequency on dynamic mechanical properties as a function of temperature for grafted PMMA-Cab-o-sil H5 (16 wt%). **(a)** Storage modulus; **(b)** tan δ.

5.5 Comparison between Dispersed and Grafted PMMA/silica Nanocomposites

A direct comparison of the E' *vs.* temperature curves of dispersed and grafted samples with comparable silica content (**Figure 5.18**) shows that there are clear differences in the glass transition region (in terms of its location, and width of the relaxation process). The T_g values of the dispersed composites are similar to that of pure PMMA (120 °C), while the T_g of the grafted composites has risen to 121 − 131 °C (**Table 5.1** and **5.4**). This result may be explained by the fact that, in dispersed samples, the interaction occurring between the polymer and the surface of the filler is not strong (van der Waals forces and dipole-dipole interactions) in comparison to grafted samples

where the polymer is covalently attached to the filler. It is apparent from **Figure 5.18** that the grafted composites have a higher storage modulus above the glass transition and suppressed sample deformation compared to pure PMMA or dispersed samples. Furthermore, the DMTA data of grafted composites could be collected up to 250 °C, more than 130 °C above the T_g of pure PMMA. Storage modulus values at high temperature are close for Cab-o-sil H5 samples having similar wt% silica. This leads us to conclude that the reinforcement effect is largely determined by the 3-dimensional network structure of polymer and filler, and therefore related to the silica content.

Colloidally dispersed silica nanoparticles (MEK-ST) gave rise to only a marginal improvement in modulus compared to grafted Cab-o-sil H5. Thus, for this system grafting has little impact on the extent of reinforcement but, in suppressing chain diffusion and flow, it appears to extend the region over which rubbery behavior is observed, without a need for cross-linking. In composite systems, high values of storage modulus have been attributed to strong effective interfacial interaction between the polymer matrix and the fillers.[26, 27] Therefore, from the improvement in the storage modulus of grafted PMMA-silica nanoparticle composites in comparison with that of dispersed composites at the same filling content, it could be concluded that there is better interface when the PMMA is grafted to the nanosilica.

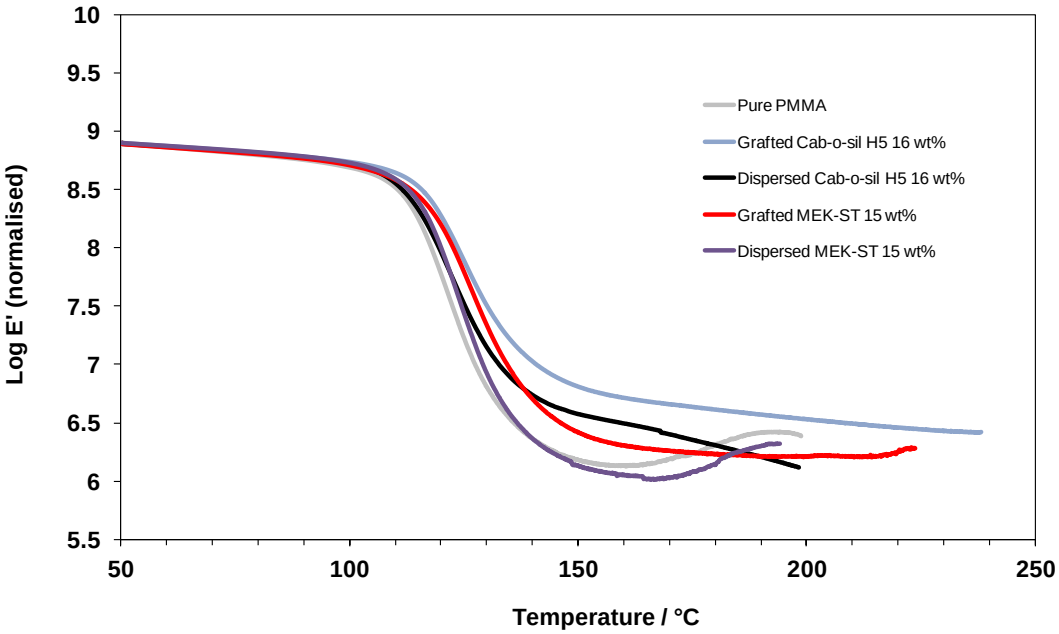

Figure 5.18: Plot of normalised storage modulus for PMMA, two dispersed PMMA/silica nanocomposites containing 15 and 16 wt% silica, and two grafted-PMMA/silica nanocomposites of similar composition.

5.6 Time Temperature Superposition

The dynamic properties of polymers are affected by temperature and the frequency of the dynamic loading. Superposition principles for the dynamic moduli can be used to obtain master curves that cover a wide range of viscoelastic properties. The superposition principle states that a function of the dynamic moduli (such as E') at a specific temperature is similar to the shape of the same function at an adjacent temperature.[28] This procedure relies on the assumption that the relaxation times describing a given relaxation process have the same temperature dependence. Thus, the curves of E' against the logarithm of frequency produced by frequency sweep measurements can be horizontally shifted until they overlap with each other; producing a master curve. This master curve can then be analysed using a suitable model, such as the William-Landel-Ferry (WLF) equation **(eq. 5.2)**.[29, 30] The WLF equation is used to describe the time-temperature behaviour of polymers within the glass transition temperature (T_g) region:

$$\log \alpha_T = \log \frac{\lambda_T}{\lambda_{T_o}} = -\frac{C_1\ T - T_0}{C_2 + T - T_0} \qquad (5.2)$$

The time-scale shift factor α_T is defined as the ratio of the relaxation time, λ_T, at a

given temperature, T, and the relaxation time, λ_{T_o}, at reference temperature, T_0, C_1 and C_2 are temperature independent constants.

The WLF equation can also be related to the free volume by the following equations:[28, 29]

$$C_1 = \frac{B}{2.303 f_0} \qquad (\mathbf{5.3})$$

$$C_2 = \frac{f_0}{a_f} \qquad (\mathbf{5.4})$$

where f_0 is the fractional free volume, a_f is the degree of thermal expansion and B is a constant (often simplified to unity).

Figure 5.19 shows the master curves for the storage modulus as a function of reduced frequency for pure PMMA and grafted PMMA nanocomposites at a reference temperature equal to the glass transition temperature of the samples (**Table 5.4**). In the preparing the master curve, the measured frequency curves were horizontally shifted according the WLF theory. A vertical shifting procedure[31] that is often needed in highly filled polymer composites was not necessary. At a very low frequency (or long times), the samples have a low modulus and behave like rubber, whereas at high frequencies (or short times) the samples are elastic and have a high modulus. A substantial increase in the modulus was observed for PMMA-silica nanocomposites throughout the frequency range. The effect is at its most significant when the polymer is grafted onto aggregated silica. The master curves also show the same mechanical reinforcement evident in the DMTA measurements: the frequency range for the polymer is greatly increased when the polymer is grafted to the surface of silica nanoparticles and there is an increase in storage modulus. This can be interpreted as change in the mobility of the polymer chains, where the mobility of the chains is constrained by the strong effective interfacial interaction between the PMMA and silica nanoparticles when the PMMA is grafted onto the surface of the filler.[32]

Grafting PMMA from aggregated silica nanoparticles led to a large rubbery plateau and absence of any terminal flow region up to 10^{-4} Hz. However, the use of colloidally dispersed silica (MEK-ST) nanoparticles led to a shorter rubbery plateau region (**Figure 5.19**). The existence of a plateau in the low frequency region is clearly related

to the formation of a 3-dimensional network of aggregated silica, which is not possible when the polymer is grafted from the surface of colloidally dispersed silica (MEK-ST). Such behaviour also has been observed for other polymers such as styrene butadiene rubber copolymers and PS silica composites.[33-35]

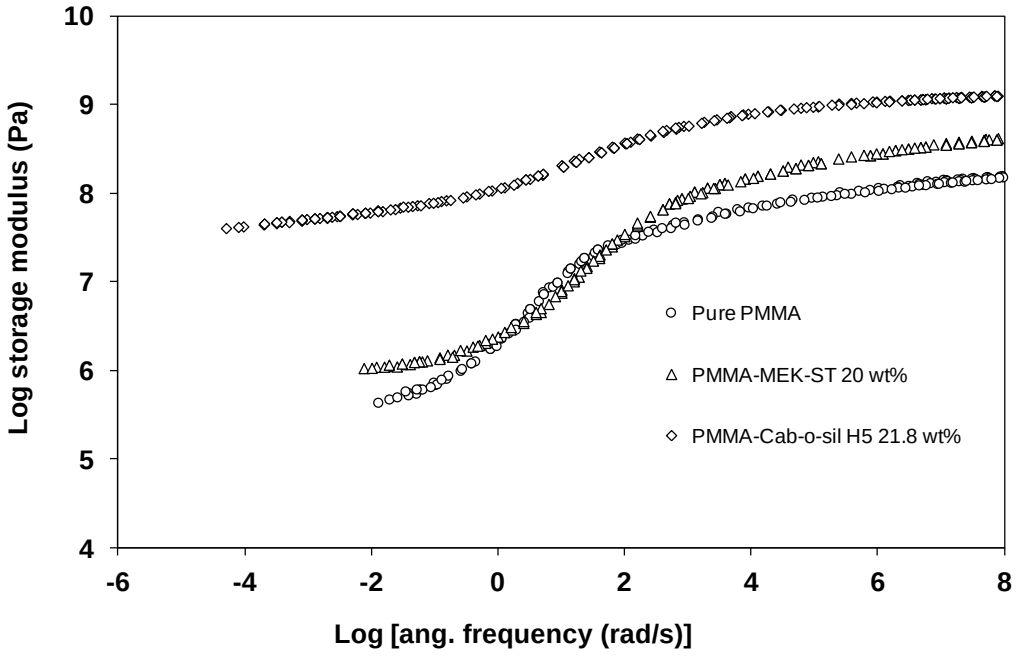

Figure 5.19: Master curves of storage modulus *vs*. frequency for pure PMMA and various grafted PMMA/ silica nanocomposites.

After generating these master curves and obtaining the shift factors for all temperatures, **equation 5.2** is adopted to provide the values of the WLF fitting parameters C_1 and C_2 by plotting the manually determined shift factors as a function of temperature. **Figure 5.20** displays a plot of the experimentally determined shift factors of pure PMMA and grafted PMMA silica nanocomposites as a function of temperature. The data are fitted according to the WLF model: the shift factor plot of PMMA and grafted PMMA composites is slightly curved, reflecting WLF-type behaviour. An excellent fit for pure PMMA is obtained when C_1 = 8.34 and C_2 = 72.24 K. These values compare favourably with data in the literature **(Table 5.5)**. The values of C_1 and C_2 for grafted PMMA-nanocomposite are within the typical range of the majority of amorphous polymers.[36] Further details of the WLF fit are presented in **Table 5.5**.

These WLF parameters can then be used to approximate the fractional free volume, f_0, and the thermal expansion coefficient of the free volume, a_f, as expressed by **equations 5.3** and **5.4**. Furthermore, the fractional free volume at the glass transition temperature, f_g, can be calculated using equation **5.5**, which can then be substituted back into **equations 5.3** and **5.4** to calculate C_1 and C_2 at the glass transition temperature.[31] As we have chosen the reference temperature to be equal to the glass transition temperature, so $f_0 = f_g$.

$$f_0 = f_g + a_f\ T - T_o \qquad (\mathbf{5.5})$$

The values for C_1 and C_2 of PMMA are relatively close to literature values. The values of C_1 and C_2 for pure PMMA and PMMA grafted to MEK-ST (**G36-15Si**) are very similar; however PMMA grafted to Cab-o-Sil H5 (**G28-16Si)** shows a higher C_1 and C_2 value and thus a lower fractional free volume and expansion coefficient. This could be due to the change in molecular motion in the glass transition region because of the formation of a three-dimensional network between the polymer and the aggregated silica that is not present in the colloidally dispersed silica sample. However, the effect of molecular weight on the fractional volume should also be considered, as a low molecular weight can decrease f_0.[37]

The WLF parameters can also be used to calculate the apparent activation energy at the glass transition region, E_a, with the help of the following relationship based on the WLF equation.[31]

$$E_a = R\frac{d\ ln\ a_T}{d\ \frac{1}{T}} = 2.303\frac{C_1 C_2 R T^2}{(C_2 + T - T_0)^2} \qquad (\mathbf{5.6})$$

The apparent activation energies at the glass transition for PMMA and grafted PMMA nanocomposites obtained from **eq. 5.6** are displayed in **Figure 5.21**. We would expect the activation energy to be affected by the surface properties of the filler materials and the degree of interaction between the polymer and the filler. This can be seen clearly in **Figure 5.21** as whilst PMMA grafted to colloidal silica (**G36-15Si)** shows very similar values to the activation energy of pure PMMA, PMMA grafted to aggregated silica (**G28-16Si)** shows considerably higher activation energy values across

a range of temperatures. The results are consistent with the literature: there are additional interactions in grafted polymer nanocomposites that raise the activation energy significantly compared to pure matrix.[35] The increased E_a values indicate that grafting to aggregated silica leads to a more stable material than either pure PMMA or PMMA grafted to colloidal silica.

Table 5.5: WLF fitting parameters of pure PMMA and grafted PMMA nanocomposites.

Sample	C_1	C_2	Ref. Temp./K	T_g/K	f_0/K^{-1}	a_f	Ref.
PMMA	12.21	70.10	393.1	390	0.036	5.1 x 10^{-4}	37, 38
PMMA	08.34	72.24	393.0	393	0.052	7.2 x 10^{-4}	
G36-15Si [a)]	08.45	71.87	400.0	400	0.051	7.1 x 10^{-4}	
G28-16Si [b)]	14.42	110.2	398.0	398	0.030	2.7 x 10^{-4}	

[a)] PMMA-MEK-ST. "G36" refers to a number-average molecular weight of 36 kg mol^{-1} for the grafted PMMA, "15" stands for a silica content of 15 wt%. [b)] PMMA-Cab-o-sil H5.

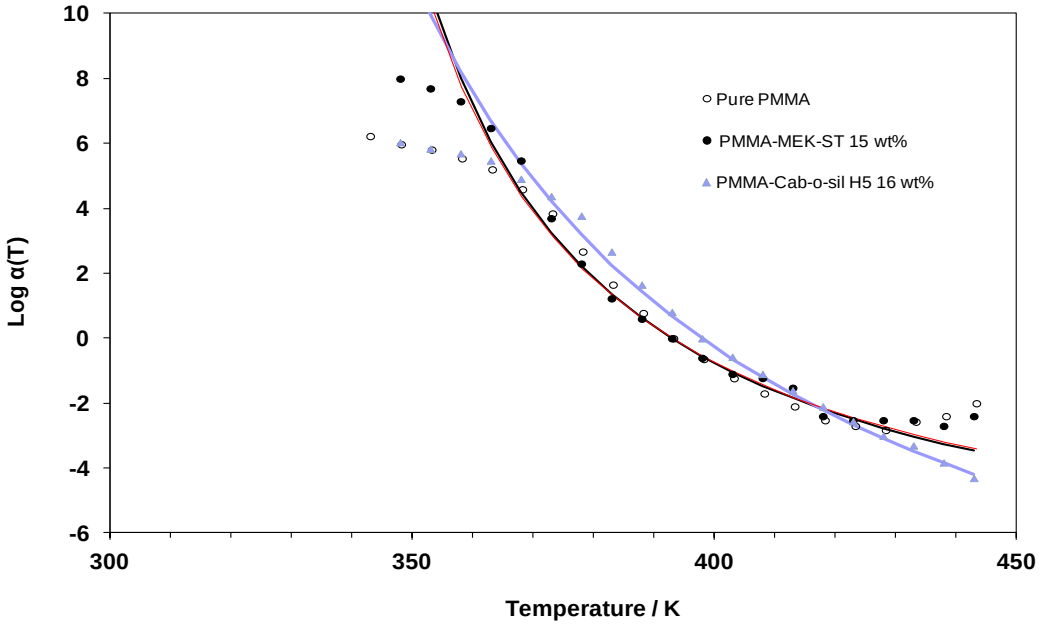

Figure 5.20: Plot of shift factors as a function of temperature for PMMA and PMMA nanofiller composites. Solid line curves represent the fits to the WLF equation.

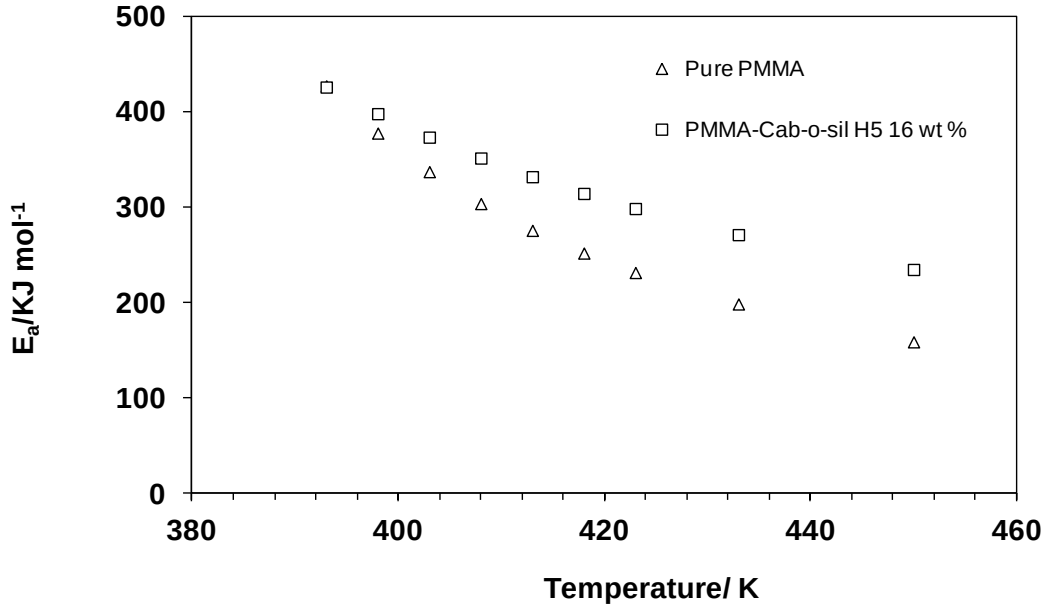

Figure 5.21: Apparent activation energy vs. temperature of pure PMMA and grafted PMMA silica nanocomposites.

5.7 Conclusions

Both DSC and DMTA measurements have indicated relatively little change in the glass transition temperature of dispersed PMMA-silica nanoparticles and PMMA-titanium dioxide nanocomposites. However, the heat capacity change $\Delta C_{p,}$ in the transition region was found to decrease with silica content. On the other hand, a T_g shift was detected between the various grafted PMMA samples. Silica content, particle size and the molecular weight all affect the T_g of the grafted polymer. As the silica content increases, and/or the silica nanoparticle size decreases, the final composites exhibit higher T_g compared to pure PMMA.

Silica nanoparticles were found to significantly lower the high-temperature damping in PMMA–silica nanocomposites, at temperatures well (in some cases more than 100 °C) above the T_g of PMMA. The increase in the rubbery modulus was accompanied by the formation of a temperature-independent plateau between 140 and 240 °C. While neat PMMA started to flow and deform irreversibly above about 150 °C, the new silica–polymer hybrid materials maintain their dimensional stability up to 240 °C. For these materials, the improvement in dynamic mechanical properties is similar to that of crosslinked polymers and provides clear evidence for suppression of polymer flow. The mechanical damping properties at high temperature were also noticeably improved. Colloidally dispersed silica nanoparticles exerted a much less pronounced effect than aggregated silica particles. Apart from this, the relative position

of the master curves for the storage modulus of grafted PMMA nanocomposites, on a logarithmic frequency scale, provided further evidence of the improved dynamical mechanical properties of grafted PMMA aggregated silica nanoparticles. The study has emphasised that aggregation of the filler nanoparticles plays a significant role in the reinforcement of the nanocomposites.

5.8 References

1. G. Tsagaropoulos and A. Eisenberg, *Macromolecules*, 1995, **28**, 396.
2. V. Arrighi, I. J. McEwen, H. Qian and M. B. Serrano Prieto, *Polymer*, 2003, **44**, 6259.
3. T. Kashiwagi, A. B. Morgan, J. M. Antonucci, M.R. Van Landingham, R. H. Harris, W. H. Awad and J. R. Shields, *J. Appl. Polym. Sci*., 2003, **89**, 2072.
4. R. Kostilkova, D. Fragiadakis and P. Pissis, *J. Appl. Polym. Sci., Part B: Polym. Phys.*, 2005, **43**, 522.
5. A. Kraft, P. M. E. Adams, V. Arrighi, J. Harkins, A. McAnaw, I. J. McEwen, S. J. Mayhew, L. Ragupathy and C. Waring, *Polym. Mater. Sci. Eng*., 2007, **96**, 43.
6. A. Yim, R. S. Chahal and L. Pierre, *J. Colloid Interface Sci*., 1973, **43**, 583.
7. A. Kraft, V. Arrighi and N. Grima, *Polym. Mater. Sci. Eng.*, 2008, **98**, 6875.
8. R. B. Bogoslovov, C. M. Roland, A. R. Ellis, A. M. Randall and C. G. Robertson, *Macromolecules*, 2008, **41**, 1289.
9. S. Vyazovkin and I. Dranca, *J. Phys. Chem. B*, 2004, **108**, 11981.
10. R. Ruggerone, V. Geiser, S. D. Vacche, Y. Leterrier, and J. A. E. Månson, *Macromolecules*, 2010, **43**, 10490.
11. P. S. Thomas, S. Thomas, S. Bandyopadhyay, A. Wurm and C. Schick, *Compos. Sci. Technol.*, 2008, **68**, 3220.
12. T. E. Motaung, A. S. Luyt, F. Bondioli, M. Messori, M. L. Saladino, A. Spinella, G. Nasillo and E. Caponetti, *Polym. Degrad. Stab.*, 2012, **97**, 1325.
13. E. Džunuzović, M. Marinović-Cincović, J. Vuković, K. Jeremić and J. M. Nedeljković, *Polym. Compos.*, 2009, **30**, 73.
14. C. G. Robertson, C. J. Lin, M. Rackaitis and C. M. Roland, *Macromolecules*, 2008, **41**, 2727.
15. Y. H. Hu, C. Y. Chen and C. H. Wang, *Polym. Degrad. Stab*., 2004, **84**, 545.
16. A. C. Comer, A. L. Heilman and D. S. Kalika, *Polymer*, 2010, **51**, 5254.
17. G. Tsagaropoulos and A. Eisenberg, *Macromolecules*, 1995, **28**, 6067.
18. C. G. Robertson and M. Rackaitis, *Macromolecules*, 2011, **44**, 1177.
19. Z. Zhu, T. Thompson, S. Q. Wang, E. D. von Meerwall and A. Halasa, *Macromolecules*, 2005, **38**, 8816.
20. N. Jaouault, P. Vallat, F. Dalmas, S. Said, J. Jestin and F. Boue, *Macromolecules*, 2009, **42**, 2031.
21. F. Yong and G. L. Nelson *J. Appl. Polym. Sci*., 2004, **91**, 393.

22. R. Y. Hong, H. P. Fu, Y. J. Zhang, L. Liu, J. Wang, H. Z. Li and Y. Zheng, *J. Appl. Polym. Sci.*, 2007, 105, 2176.
23. J. Fitzgerald, J. L. Christine and J. M. Mochan, *Macromolecules*, 1992, **25**, 3715.
24. M. L. P. Ha, B. P. Grady, G. Lolli, D. E. Resasco and W. T. Ford, *Macromol. Chem. Phys.*, 2007, **208**, 446.
25. H. Sugimoto, K. Daimatsu, E. Nakanishi, Y. Ogasawara, T. Yasumura and K. Inomata, *Polymer*, 2006, **47**, 3754.
26. J. Jancar, *J. Mater. Sci.*, 1989, **24**, 3947.
27. A. Zhu, A. Cai, J. Zhang, H. Jia, and J. Wang, *J. Appl. Polym. Sci.*, 2008, **108**, 2189.
28. R. Z. Li, *Mater. Sci. Eng.*, A. 2000, **278**, 36.
29. F. A. Zhang, D. K. Lee and T. Pinnavaia, *J. Polym, Chem*., 2010, **1**, 107.
30. M. L. William, R. F. Landel and J. D. Ferry, *J. Am. Chem. Soc*., 1955, **77**, 3701.
31. M. F. Lai, J. Li and J. J. Liu, *J. Therm. Anal. Calorim*., 2005, **82**, 293
32. H. Y. Chen, E. V. Stepanov, S. P. Chum, A. Hiltner and E. Baer, *J. Plym. Sci., Polym. Phys.*, 1999, **37**, 2373.
33. M. Klüpple, *J. Phys. Condens. Matter*., 2009, **21**, 035104.
34. K. W. Stöckelhuber, A. S. Svistkov, A. G. Pelvin and G. Heinrich, *Macromolecules*, 2011, **44**, 4366.
35. C. Bartholome, E. B. Bourgeat-Lami, P. Cassagnau. P. Chaumont. L. David and N. Zydowicz, *Polymer*, 2005, **46**, 9965.
36. P. Cassagnau, *Polymer*, 2003, **44**, 2455.
37. J. E. Mark, *Physical Properties of Polymers Handbook*, Woodbury, New York, 1996.
38. A. V. Tobolsky, *Properties and Structure of Polymers*, Wiley, New York, 1967.

Chapter 6 - Thermal and Dynamic Mechanical Properties of PS and PSAN-silica Nanoparticle Composites

Contents

6.1 Introduction

The overall aim of this work was to correlate thermal, dynamic mechanical and structural properties of various polymer-silica nanoparticles composites (using both aggregated or colloidally dispersed silica). Polystyrene and styrene–acrylonitrile copolymers were investigated as representative examples of amorphous polymers, all with a glass transition temperature, T_g, well above room temerature. The composites were synthesised according to the method described in Chapters 2 and 3.

PS has been extensively used as a hard segment in copolymers for nanocomposite applications due to its low cost compared to other polymers such as polycarbonate and PMMA.[1] Although few studies have been carried out on the dynamic mechanical properties of PS-silica nanoparticles, there has been no comprehensive study about the effect of surface-grafted silica particles on mechanical properties of the resulting nanocomposites. Most mechanical studies have concentrated on either unmodified nanosilica or commercially available surface-modified particles' incorporation in PS.[2-6] Furthermore, most other groups have either chosen aggregated[7] or non-aggregated[8] silica nanoparticles, but never compared the effect of surface-grafted filler particles on the thermal and mechanical properties of nanocomposites made using both types of silica. Since the type of silica particles is known to significantly influence the properties of the polymer composites[7] it is instructive to carry out comparative studies.

This Chapter also describes the thermal and dynamic mechanical properties of surface-grafted PSAN chains from aggregated and non- aggregated silica nanoparticles. To the best of my knowledge, no studies have been reported, so far, on how silica fillers with surface-grafted PSAN chains will affect the mechanical properties of PSAN-filler composites. To be able to compare the properties of PS or PSAN–grafted particles to those of more conventional PS or PSAN/nanosilica composites, a series of samples were prepared by dispersing silica nanoparticles (both aggregated and non-aggregated) in a tetrahydrofuran (THF) solution of PS or PSAN and their thermal and mechanical behavior was investigated using DSC and DMTA.

6.2 Thermal and Dynamic Mechanical Properties of PS-silica Nanocomposites

6.2.1 DSC and DMTA Analysis of Dispersed PS/silica Nanoparticles

A series of PS-silica samples with different filler types and contents (10, 20, 30 wt%) was prepared by the dispersion of silica nanoparticles in a THF solution of the PS, followed by evaporation of the solvent and extensive drying up to 160 °C in an oven. Ground dried samples were then investigated by DSC and DMTA.

The DSC results of the PS-Aerosil 300 composites are shown in **Figure 6.1** and **Table 6.1**. DSC results indicated only small changes in the glass transition temperature between neat polystyrene and PS-Aerosil 300 composites: T_g values of composites containing 10 wt%, 20 wt%, or 30 wt% of Aerosil 300 are very close. This result was found with all PS-silica composites (i.e. aggregated such as Cab-o-sil H5 and non-aggregated silica such as MEK-ST, MEK-ST-UP) as can be seen from **Table 6.1**. Kontou *et al.*[4] in their study also reported that the T_g of PS is not affected by addition of silica nanoparticles. Meanwhile, Bansal *et al*. observed that the T_g of PS-nanosilica samples decreases with increasing the silica contents.[9] They also reported that the change in behaviour of the T_g of PS-silica nanofiller depends on the distribution of the filler particles in the polymer matrix. The present results are different from those of Bansal *et al.* This divergence between the present results and previous studies could be attributed to the difference in the distributions of the nanofiller in the PS matrix. Also studies from Mele *et al.*[10] and Arrighi *et al.*[11] both reported a decrease in the glass transition of styrene-butadiene rubber in silica composites.

A wide variety of polymer-silica composites have shown interesting changes in the bulk T_g values.[12] Many researchers have studied the effect of the filler materials on T_g and have drawn different conclusions. Most of the researches reported an increase in the glass transition temperature as a function of filler content,[13, 14] however, decreases or no effect on the glass transition of the polymer composites also have been found.[11, 15, 16] Furthermore, the DSC measurements also reveal changes in heat capacity, ΔC_p. It should be mentioned that the ΔC_p value of PS decreases with increasing the amount of filler added. The decrease in ΔC_p could be attributed to the formation of rigid amorphous fraction in these composites,[17] (see **Figure 5.4** in Chapter 5).

More significant differences were observed in the DMTA data. **Figure 6.2** shows an example of a series of storage modulus *vs.* temperature curves for PS-Aerosil 300 composites. While neat PS samples deformed already at a temperature of 135 ºC (roughly 35 ºC above the T_g of the polymer) and the DMTA run stopped at 155 ºC as a result of sample disintegration, the addition of only 10 wt% silica nanoparticles delayed sample deformation significantly and made it possible to extend the DMTA measurement to up 200 ºC. In addition, there is an increase in the modulus above the glass transition with increasing filler concentration. A similar result was also observed for PMMA/silica composites (Chapter 5). The tan δ peak at the main α-relaxation, which is generally associated with the T_g, showed a decrease with increasing silica content as shown in **Figure 6.3.** It should be mentioned that, no second tan δ peak (second maximum) was observed at higher temperature. In many previous studies on filler-polymer composites, the existence of a second relaxation peak, or β relaxation, in the tan δ curves has been reported. This peak appears as a shoulder at a temperature above α relaxation peak. For example, Tsagaropoulos and Eisenberg[14] reported that there are two peaks in the tan δ curve for PVAc-silica nanoparticles. The second peak was located at 100 ^{o}C above the main α relaxation peak (T_g). They attributed the second peak to the glass transition temperature of immobilised chains near the particles.

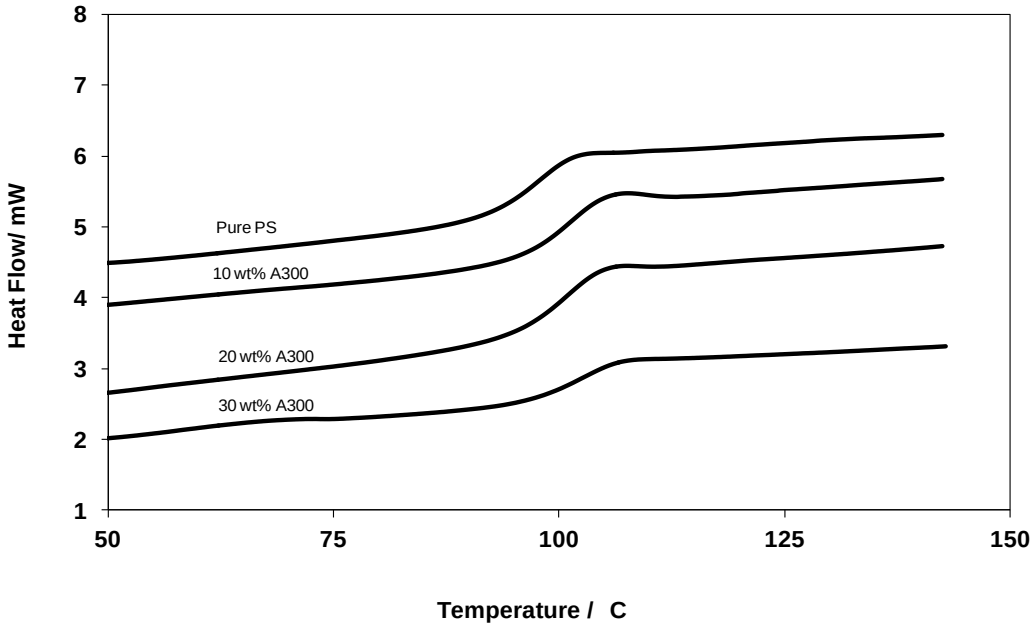

Figure 6.1: DSC traces of pure PS and various PS/Aerosil 300 nanocomposites. The traces have been shifted vertically for clarity.

Table 6.1: Glass transition temperatures and heat capacity changes for various dispersed PS-silica composites.

Filler wt%	T_g / °C	ΔC_p / J g^{-1} °C^{-1}	ΔC_p / J g^{-1} °C^{-1}"a"
Pure PS	100	0.31	----
Cab-o-sil H5 10%	101	0.30	0.27
Cab-o-sil H5 20%	100	0.28	0.24
Cab-o-sil H5 30%	101	0.18	0.20
A300 10%	100	0.28	0.27
A300 20%	101	0.27	0.24
A300 30%	100	0.20	0.20
MEK-ST 10%	102	0.28	0.27
MEK-ST 20%	100	0.23	0.23
MEK-ST 30%	102	0.18	0.20
Error	±1	±0.01	±0.01

"a" Calculated by **eq. (5.1)**.

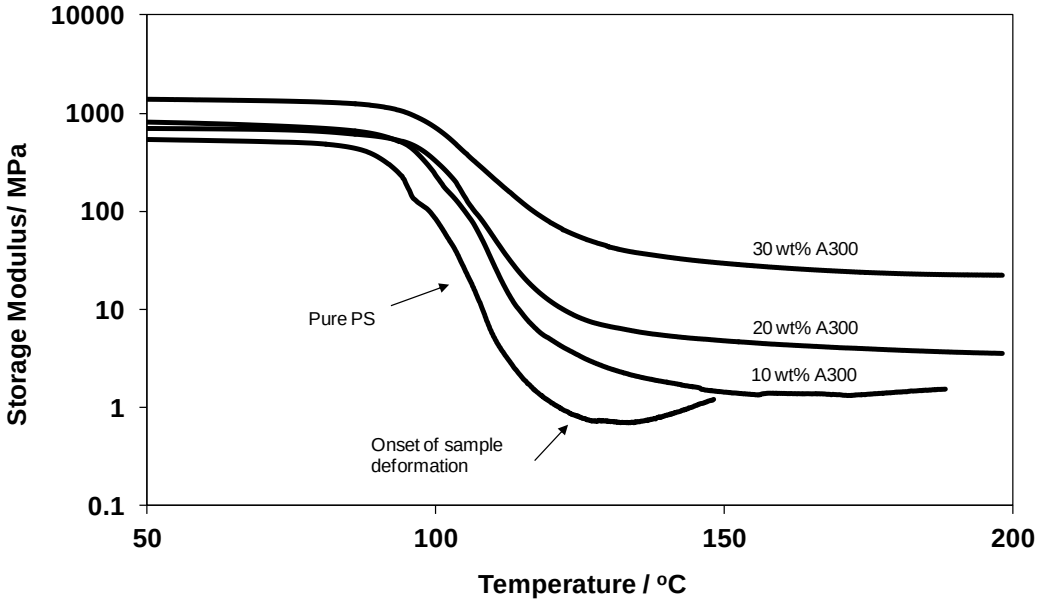

Figure 6.2: Plot of storage modulus as a function of temperature for pure PS and various PS/Aerosil 300 nanocomposites prepared by dispersion technique.

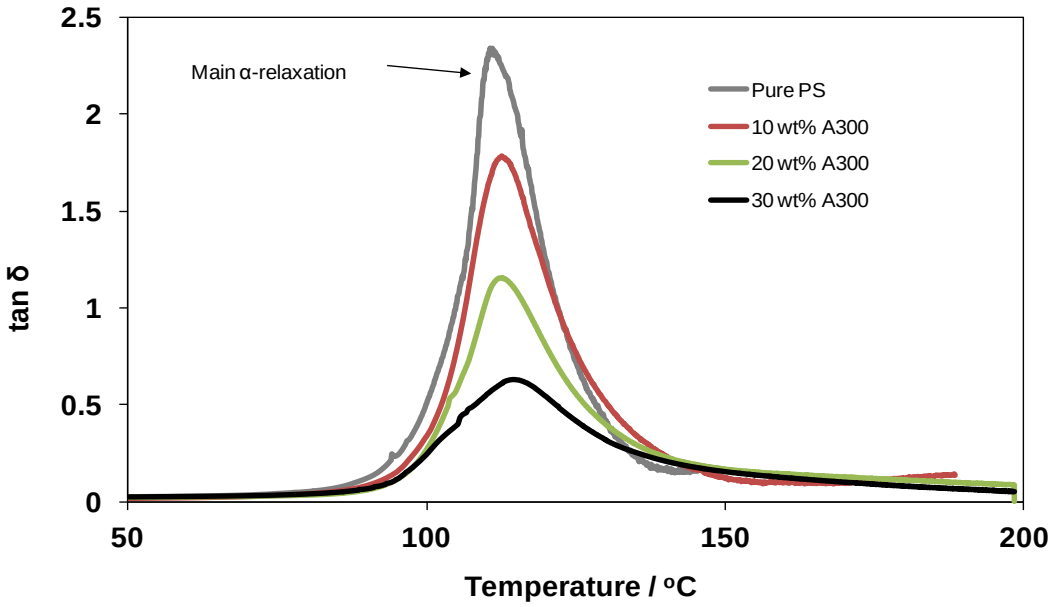

Figure 6.3: Plot of tan δ as a function of temperature for pure PS and various dispersed PS/Aerosil 300 nanocomposites.

6.2.2 DSC and DMTA Analysis of Grafted PS/silica Nanoparticles

PS-silica composites with various molecular weights and silica content were studied by DSC. As illustrated in **Figure 6.4** and **Table 6.2**, the glass transition temperatures of the hybrid material are usually higher compared to neat PS, which indicates a strong interaction between PS and silica nanofiller when linked together by a covalent bond.[18] Theses strong interactions restrict the movement of the PS chain segments.[19]

The T_g increase observed for the grafted systems compared to pure PS seems to be dependent on the molecular weight of the grafted chains as well as nanosilica content and type. For example, for the grafted PS-MEK-ST with lowest M_n, **G32-10Si**, the T_g is close to that of neat PS. In this case, the expected decrease due to the low molecular weight is probably offset by the relatively high silica content, leading to a T_g close to that of pure PS. It is interesting to find that the grafted PS-Cab-o-sil H5 composite (**G26-10Si)** has a higher T_g than the grafted PS-MEK-ST (**G32-10Si)** with similar silica content and closer molecular weight. This fact indicates that the glass transition of the composites are also strongly dependent on the nature of the silica (i.e. aggregated or non-aggregated). This could be due to the decrease in the segmental mobility of grafted chains with aggregation of nanoparticles.[20] Overall these observations indicate that the T_g values of the grafted PS samples increase with the silica content. The trend observed

for the tan δ maxima is consistent with the DSC results. A similar trend was also observed for the grafted PMMA/silica composites as discussed in Chapter 5.

The enhancement of the glass transition temperature of the grafted composites was also observed relative to the cleaved polymer as shown in **Figure 6.5** and **Table 6.2**. The T_g for the lowest molecular weights (26 and 32 kg/mol) of the hybrid polymer composites (**G26-10Si** and **G32-10Si)**, was elevated by 10 and 5 ºC respectively in comparison with that of cleaved PS. These differences in glass transition are decreased to ~2 and 3 ºC for (**G83-14Si** and **G68-23Si)**, respectively. The largest difference in the glass transition between the grafted polymer and cleaved polymer was noticed in lower molecular weight samples (**G26-10Si** and **G32-10Si)**. This was attributed to the steric constraint affecting polymer chains that are near to the surface of the filler.[21] As the grafted chains increase in length (**G83-14Si** and **G68-23Si)**, the part of the chains that is far away from the surface of the particles increases, and the glass transition approaches to bulk polymer's value.

It is known that the addition of silica nanoparticles to a polymer matrix increases the glass transition temperature if strong adhesion forces between the particles and polymer are present. In the grafted samples the covalent attachment of the chains to the surface of the filler decreases the mobility of the polymer chains, thereby increasing the T_g from 102 to 120 ^oC. Grafted polymers have a much stronger bonding interaction with the filler than simply dispersing the silica nanoparticles which could account for the increase in T_g (**Tables 6.1** and **6.2**). This effect is seen less in lower concentrations of silica as a lower surface area means that less polymer chains are affected.

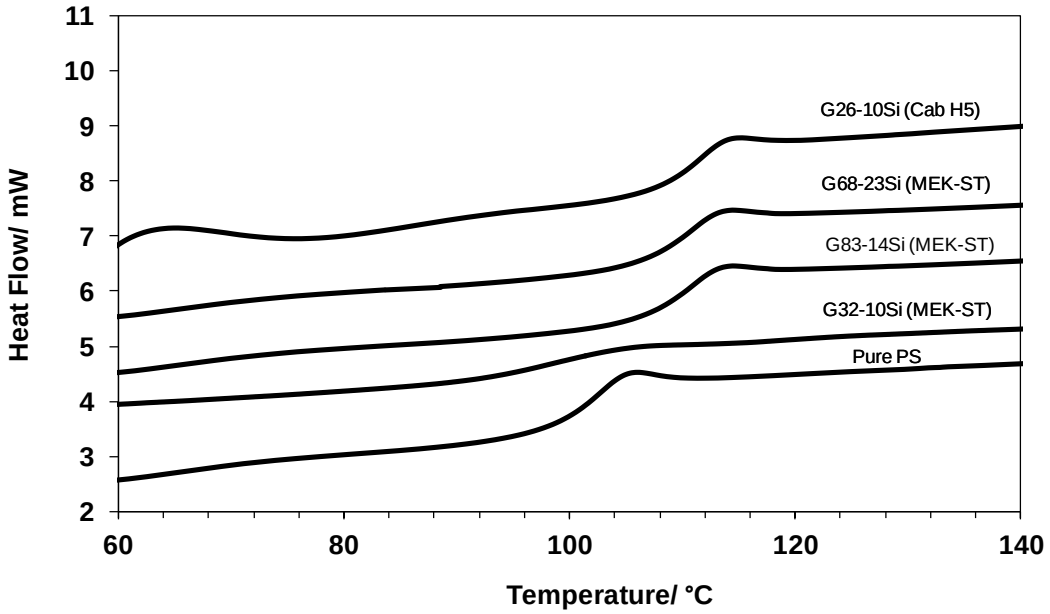

Figure 6.4: DSC traces of pure PS and grafted PS-silica nanoparticles. The traces have been shifted vertically for clarity.

Table 6.2: DSC results for various PS-silica composites and comparison to tan δ values corresponding to peak maximum.

Sample code	*% SiO_2*	M_n [g mol^{-1}]	T_{max} (tan δ) °C	T_g "c" °C	T_g "d" °C
PS	0.0	100000	113	102	…..
G32-10Si [a)]	10.0	32000	113	102	97
G83-14Si [a)]	14.0	83000	117	110	108
G68-23Si [a)]	23.7	68000	117	110	107
G26-10Si [b)]	10.0	26000	120	112	102
Error	-----	--------	±1	±1	±1

[a)] PS-MEK-ST. "G32" refers to a number-average molecular weight of 32 kg mol^{-1} for the grafted PS, "10Si" stands for a silica content of 10 wt%. [b)] PS-Cab-o-sil H5. "c" T_g of grafted PS-silica composites by DSC. "d" T_g of grafted PS-silica composites (after silica cleavage).

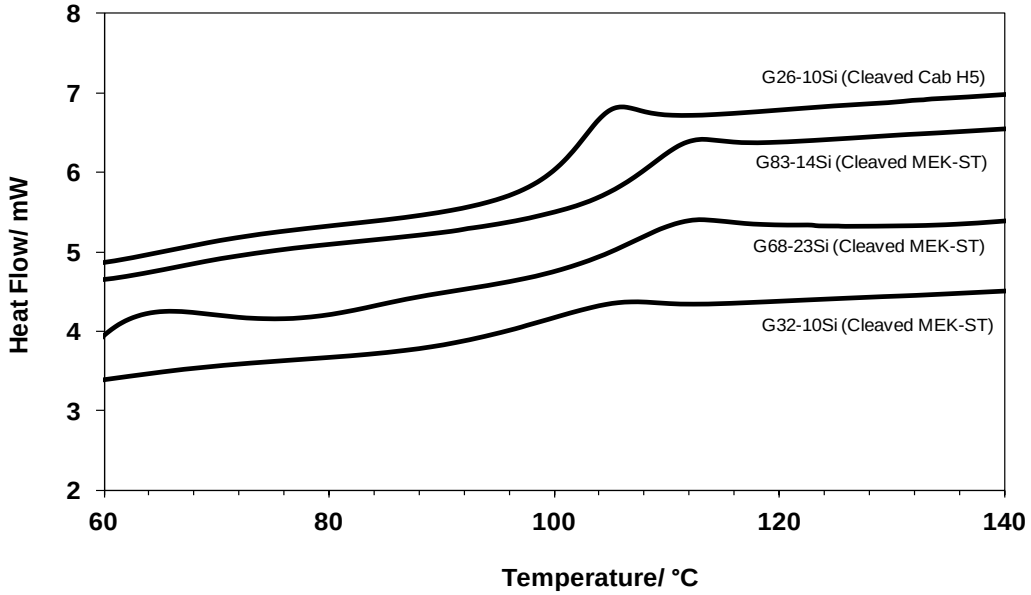

Figure 6.5: DSC traces of grafted PS-silica nanoparticles (after silica cleavage). The traces have been shifted vertically for clarity.

DMTA was used to measure the temperature dependence of the storage modulus (E'), and tan δ (E''/E'), varying both the chemical interaction between the polymer and the filler as well as the surface morphology of the filler particles. **Figure 6.6** shows the change in storage modulus as a function of temperature for a pure polystyrene sample and for polystyrene grafted from silica nanoparticles. A substantial increase in the modulus was observed for all polystyrene-silica nanoparticles at temperatures above T_g, and this reinforcement was more pronounced with larger amount of colloidally dispersed silica content (MEK-ST) and, even more so, when aggregated silica nanoparticles were used (Cab-o-sil H5). The modulus *vs*. temperature plot for unfilled polystyrene shows an onset of deformation at about 130 − 140 ºC, which is no longer seen in the grafted PS-silica nanocomposites. At silica content ≥ 10 wt% the DMTA test could be extended to 200 ºC, in some cases even up to a temperature of 250 ºC ─ more than 130 ºC above the glass temperature of PS. No second transition at ~ 65 ºC below T_g was evident from the modulus *vs*. temperature curves which had been noted by others and attributed to chain mobility in polymer-silica composites.[8] Grafting PS from aggregated Cab-o-sil H5 silica nanoparticles (**G26-10Si**) led to an even higher storage modulus than grafting PS from colloidally dispersed silica (**G32-10Si**, **G83-14Si** and **G68-23Si)**. Such a substantial increase of storage modulus can be attributed to the formation of a 3-dimensional network of silica nanoparticles (with Cab-o-sil), which is not possible when the polymer was grafted from the surface of the collodially dispersed silica. This is consistent with the TEM and SEM results in **Figure 6.7**, which show that

the silica particles in PS-Cab-o-sil H5 nanocomposites (**G26-10Si**) are aggregated. The mean aggregates' diameter is found to be around 25 − 35 nm [**Figure 6.7 (a** and **c)**].

Aggregated silica nanoparticles possess an additional dimensional network that further strengthens the composites.[22-24] However, TEM and SEM showed no evidence of aggregation for colloidally dispersed silica nanoparticles (**G83-14Si)** as shown in **Figure 6.7 (b** and **d)**. Whether or not the polymer itself is part of a 3-dimensional network (due to combination of growing polymer chain radicals originating from different silica particles) cannot be ruled out and is subject to further investigation. This result strongly supports previous arguments of Wang,[24] Strenstein[23] and Kumar[20] on the effect of grafting on the dynamic mechanical properties of a polymer.

For PS-silica composites there is a question as to whether the difference in mechanical behaviour may be attributed to differences in molar mass of the chains and/or filler content. Here we point to the results of grafted PS from the surface of non-aggregated silica (MEK-ST), where **G68-23Si** showed higher storage modulus compared to **G83-14Si (Figure 6.7)**. These results indicate that the filler content has a significant role in the reinforcement of the grafted nanocomposites.

Smallwood[25] studied the effect of non-aggregated filler on the mechanical properties of rubber based composites. A simple equation was proposed to calculate the modulus enhancement, E_δ :

$$E_\delta = \frac{E_c}{E_m} = 1 + 2.5\,\phi, \qquad \phi \ll 1 \tag{6.1}$$

where ϕ is the volume fraction of filler, E_c is the Young's modulus of the composites and E_m is the Young's modulus of the matrix. This equation is relevant only at low filler content and it also assumes strong interaction between filler and matrix. The study of Smallwood also assumes that there is no alteration of the elastic properties of the polymer matrix due to the filler. From these calculations it is found that the increase in modulus, is independent of the particle size of the filler and it is directly proportional to the loading.

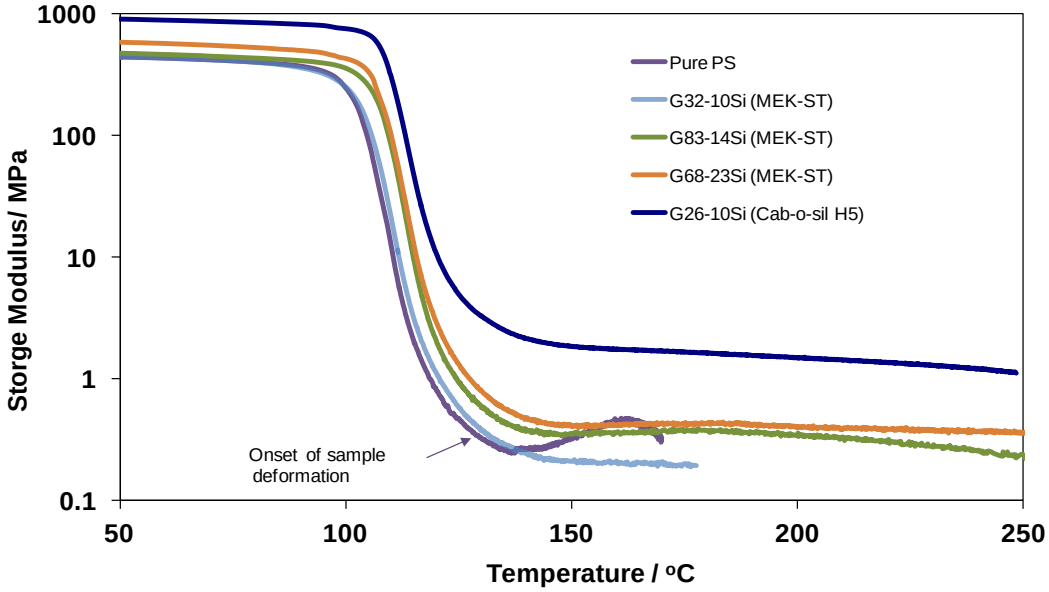

Figure 6.6: Plot of storage modulus as a function of temperature for pure PS and grafted PS-silica samples prepared from MEK-ST or Cab-o-sil H5 (percentage of silica, as indicated).

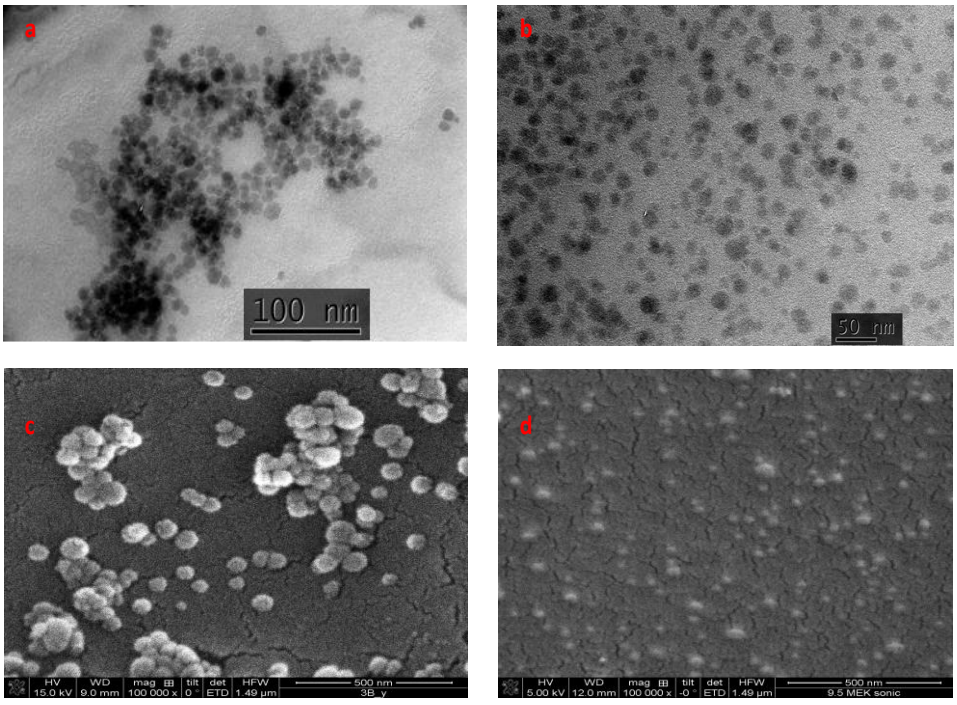

Figure 6.7. a) TEM of G26-10Si; b) TEM of G83-14Si; c) SEM of G26-10Si and d) SEM of G83-14Si

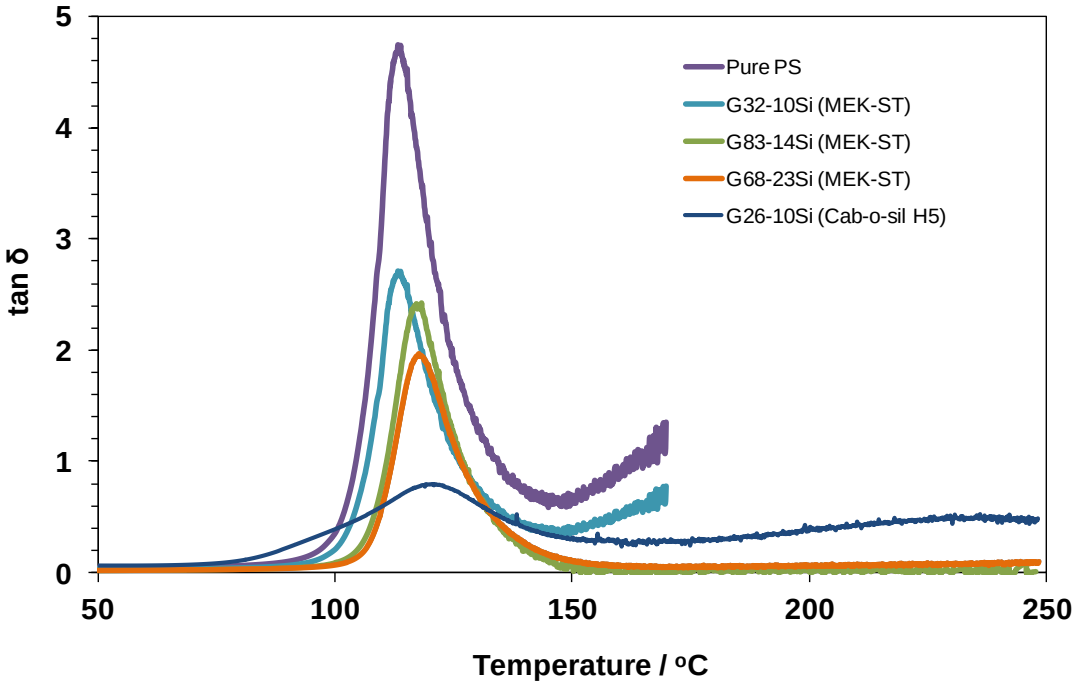

Figure 6.8: Plot of tan δ as a function of temperature for pure PS and grafted PS-silica samples prepared from MEK-ST or Cab-o-sil H5(percentage of silica, as indicated).

Figure 6.8 displays plots of tan δ as a function of temperature for various PS-silica composites. The main tan δ peak is generally associated with the glass transition and found at a temperature roughly 8 − 10 ºC above the T_g determined by DSC (**Table 6.2**). Only the T_g of the grafted aggregated silica (**G26-10Si)** was slightly higher by about 4 ºC. The size of the tan δ peak decreases with increasing filler content, which suggests that the mobility of the polymer was, reduced in the hybrid materials that make up the composites. At elevated temperature well above T_g, a high silica content lowered tan δ to small values close to zero, indicating that the composites softened but remained elastic and were able to recover from small deformation.

As observed for PMMA in Chapter 5, the results presented above show that grafting improves not only the modulus but also the high-temperature properties of the composites. While that attachment of the polymer chains to the nanoparticles makes the composites less susceptible to breaking at high temperature, the additional improvement in Cab-o-sil H5 samples is attributed to the presence of a 3-dimensional network of silica nanoparticles. These results offer a basis for designing composite materials based on PS with controlled thermal and dynamic mechanical properties for precise application.

The effect of frequency on the dynamic mechanical properties of a grafted PS nanocomposite (**G68-23Si)** is given in **Figure 6.9**. The storage modulus increases and tan δ shifts to higher values with increasing frequency, consistent with their origin as motional relaxation processes.[26] In general the frequency has a direct impact on storage modulus and tan δ especially at high temperature.[27] **Figure 6.9 (b)** shows tan δ values that were measured at various frequencies (1, 3, 14 and 37 Hz) for **G68-23Si**. As the frequency increase from 1 − 37 Hz the tan δ peak shifts to higher temperature. The damping peak is related with the partial loosening of composites' structure which leads to movement of some polymer chain segments.[27] A similar observation was made by Thomas *et al*.[17] in their study of polystyrene nanocomposites. It should be mentioned that a similar behaviour was also observed in PMMA nanocomposites as discussed in Chapter 5.

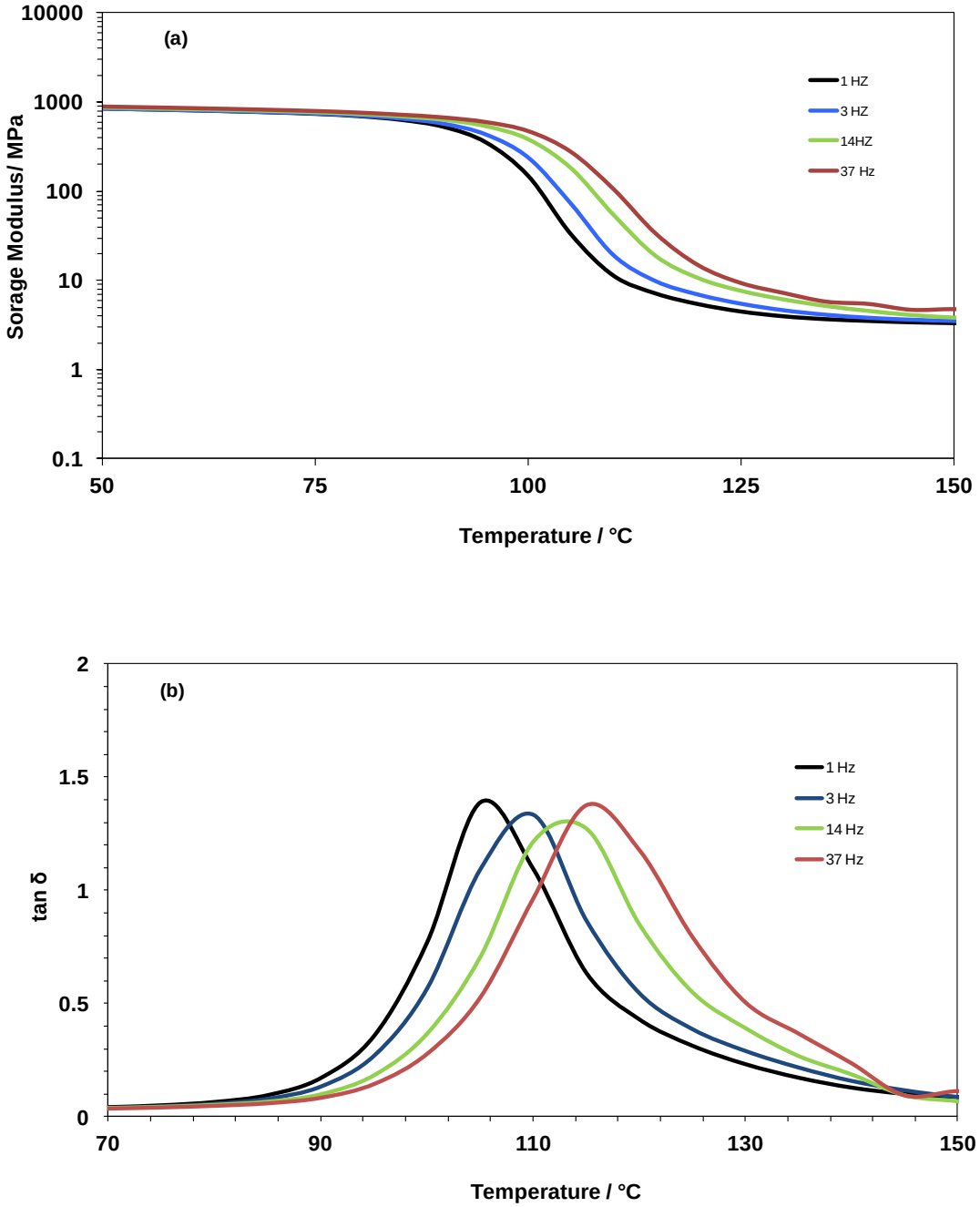

Figure 6.9: Effect of frequency on dynamic mechanical properties as a function of temperature for PS-MEK-ST (**G68-23Si)**. (a) Storage modulus; (b) tan δ.

The time-temperature superposed data for the storage modulus as a function of reduced frequency for both pure PS and grafted PS nanocomposites at a reference temperature of 115 °C are plotted in **Figure 6.10.** The master curves were generated using only horizontal (frequency) shift factors according the WLF theory.[28] Values of shift factors needed to generate the master curves are given in **Table 6.3**. As can seen in **Figure 6.10** the value of the storage modulus at the low/intermediated frequencies is higher for the PS-Cab-o-sil H5 10 wt% (**G26-10Si)** compared to PS-MEK-ST 14 wt%

(**G83-14Si)** and pure PS. The behaviour of PS nanocomposites at high frequencies is very close to the one of pure PS. This observation is clearly a confirmation that in the glassy state region below T_g there is almost no segmental movement of the chains.[29] However, local molecular motion can cause slow changes in physical properties such as volume and enthalpy.[30] A much more differentiated behaviour is observed at intermediate and low frequencies and this suggests that grafting greatly increases terminal relaxation time. It should be mentioned that, when frequency is reduced further, full terminal relaxation is prevented in the grafted PS nanocomposites and overall flow is arrested. Similar behavior were also reported by Stöckelhuber *et al.*[31] for styrene butadiene/silica rubber composites and by Zhu *et al.*[24] for polybutadiene silica composites

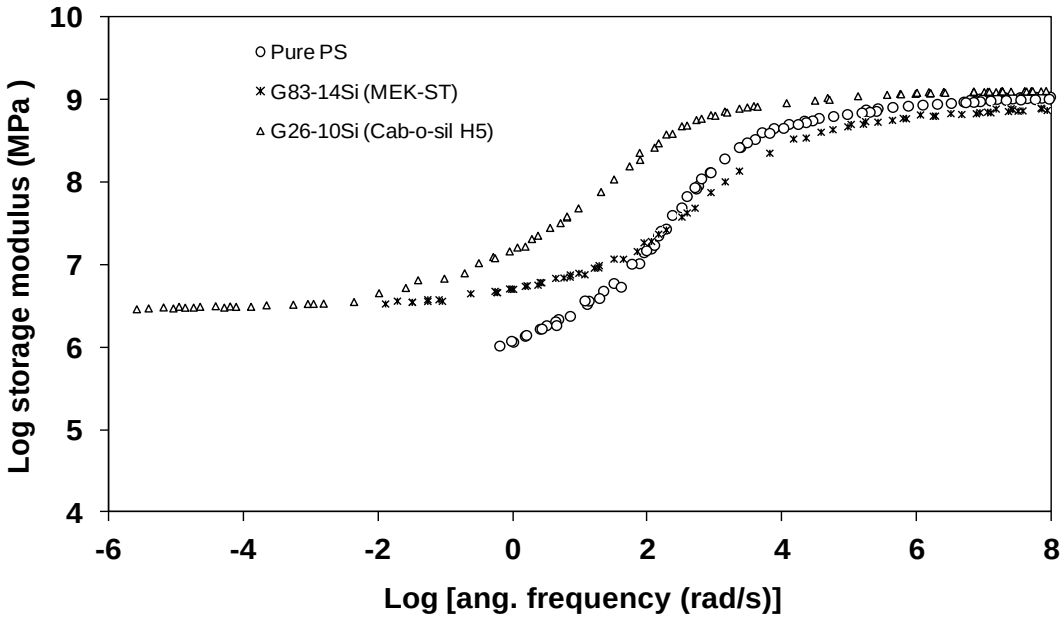

Figure 6.10: Master curves of storage modulus *vs*. frequency for pure PS and various grafted PS/ silica nanocomposites (**G83-14Si** and **G26-10Si**).

The shift factors were also analysed as a function of temperature for pure PS, **G26-10Si** and **G83-14Si** to evaluate the WLF parameters through a fit to **equation 5.2**. The parameters C_1 and C_2 for the pure polymer and the nanocomposites are listed in **Table 6.3**. **Figure 6.11** displays a plot of the shift factors of **G83-14Si** as a function of temperature. The data closely follow the fitted curve, reflecting WLF-type behaviour. Note that at higher temperature the shift factor data diverge slightly, that could be due to the time needed for a given deformation being reduced at higher temperature.[32] An excellent fit for **G83-14Si** is obtained when C_1= 9.05 and C_2 = 75.00 K at a reference

temperature of 388 K. To compare the WLF parameters (i.e. C_1 and C_2) of **G83-14Si** with those of PS reported in the literature, it is necessary to use comparable reference temperatures. If a new reference temperature, $T'_{o,}$ is chosen instead of the reference temperature (T_o), the new values C'_1 and C'_2 are given by **equations 6.2** and **6.3**.[33]

$$C'_2 = C_2 + T'_o - T_o \qquad \textbf{(6.2)}$$

$$C'_1 = C_1C_2/C'_2 \qquad \textbf{(6.3)}$$

The WLF parameters C'_1 and C'_2 of **G83-14Si** after conversion to T'_o = 373 K, are 11.31 and 60, respectively which correspond to values commonly obtained for PS at T_o = 373 K.[34] The values of C_1 and C_2 for PS and grafted PS-silica composites (**G83-14Si** and **G26-10Si)** are within the typical range reported for the majority of amorphous polymers.[35] Further details of the WLF fit are presented in **Table 6.3**.

These WLF parameters can be used to calculate approximate values of the fractional free volume, f_0, thermal expansion coefficient of the free volume, a_f, and the fractional free volume at the glass transition temperature, f_g, as expressed by **equations 5.3**, **5.4** and **5.5,** respectively (**Table 6.3**). The shift factors of the grafted nanocomposites (**G26-10Si** and **G83-14Si)** are somewhat higher compared to the neat polymer and thus a lower fractional free volume and expansion coefficient are expected. This difference could be due to the change in molecular motion in the glass transition region. The adhesion between the particles and PS molecules is strong when PS and silica nanoparticles are linked together by a covalent bond,[18] so the T_g of these composites was found to increase compared to the pure polymer T_g (**Table 6.2**). It is also observed that the increase in the T_g is more apparent when grafting PS from aggregated silica (**G26-10Si)**.

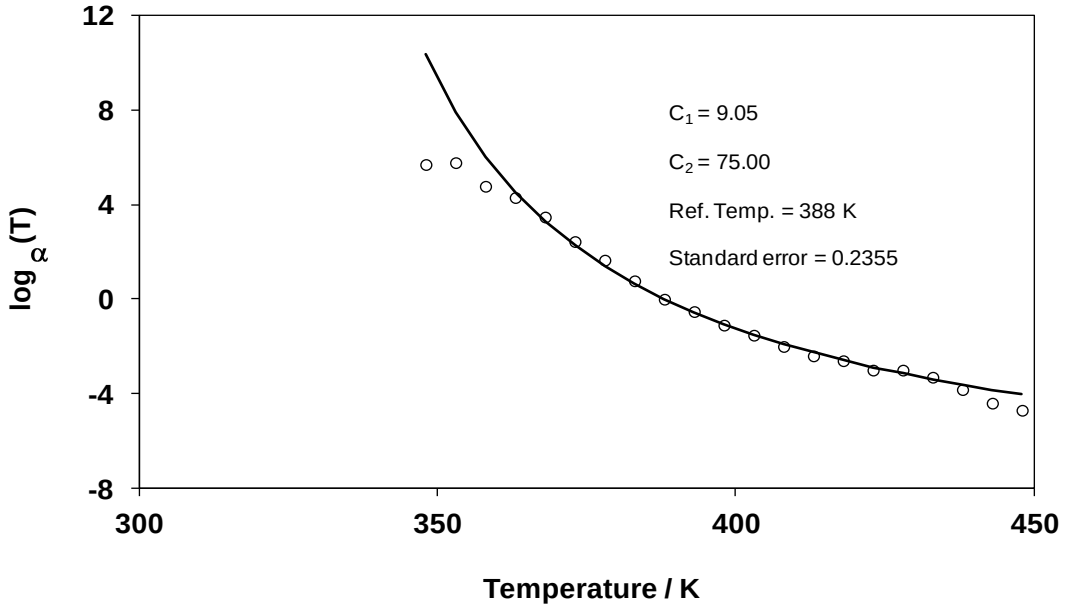

Figure 6.11: Plot of shift factor as a function of temperature for **G83-14Si**. Solid line curve represents the fit of the shift factors variation to the WLF equation.

Table 6.3 WLF fitting parameters of pure PS and grafted PS nanocomposites

Sample	C_1	C_2	Ref. Temp./K	T_g/K	f_0/K^{-1}	a_f	Ref.
PS	5.82	50.1	388	375	0.075	1.5×10^{-3}	
PS	7.14	50.0	372	372	0.060	1.2×10^{-3}	34
G83-14Si [a)]	9.05	75.0	388	383.3	0.048	6.4×10^{-4}	
G26-110Si [b)]	11.72	71.0	388	385.2	0.037	5.2×10^{-4}	

[a)] PS- MEK."G83" refers to a number-average molecular weight of 83 kg mol^{-1} for the grafted PS, "14" stands for a silica content of 14 wt%. [b)] PS-Cab-o-sil H5

Figure 6.12 shows the apparent activation energies, E_a, for PS and grafted PS nanocomposites obtained from **eq. 5.6**. For pure PS, the value of E_a is very high in the T_g region and drops significantly with increasing the temperature. The decrease of E_a in the temperature range of 370–430 K, covers an order of magnitude (370 –115 kJ mol^{-1}). However, the grafted PS silica nanocomposites show considerably higher activation energy values across a range of temperatures. For example, the value of E_a in **G83-14Si** at 430 K was only 3.2 times lower than that at 370 K. These results indicate that macromolecular motion of pure PS is more sensitive to temperature changes than when PS chains are grafted to the surface of nanoparticles (**G83-14Si** and **G26-10Si)**. In

agreement with DSC and DMTA results, the behaviour of pure PS and grafted PS silica nanocomposites are similar in the glass state region, but considerably different both in the glass transition region and in the rubbery state, with the difference being more pronounced for **G26-10Si**.

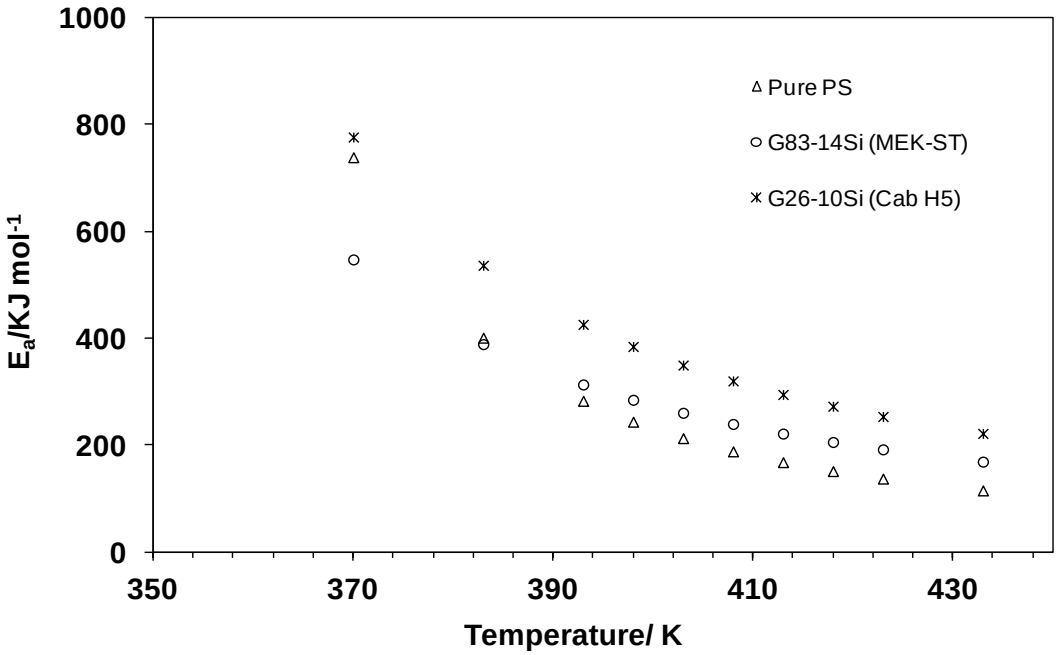

Figure 6.12: Apparent activation energy *vs*. temperature of pure PS and grafted PS silica nanocomposites (**G83-14Si** and **G26-10Si**).

6.3 Thermal and Dynamic Mechanical Properties of PSAN-silica Nanocomposites

A reliable copolymer composition is important as it affects properties such as T_g. In order to compare samples, the copolymer composition for both bulk PSAN and PSAN nanocomposites should be very similar to minimise the effect on the thermal and mechanical properties. Therefore, the monomers were copolymerised under azeotropic conditions (ca. 63 mol% styrene and 37 mol% acrylonitrile) for all samples. The preparation of bulk PSAN and PSAN nanocomposites were discussed in detail in **Chapters 2** and **3**.

6.3.1 DSC and DMTA Analysis of Dispersed PSAN/silica Nanoparticles

In this study, a serious of PSAN (63 mol% styrene and 37 mol% acrylonitrile)-silica nanoparticles with different silica type (Cab-o-sil H5 and MEK-ST) and silica contents (9.5, 12.7 and 20.0 wt%) were prepared by the dispersion of the nanoparticles in THF. The mixture was stirred for 2 days or ultrasonicated for 30 minutes (Chapter 2).

The measured glass transition temperatures for the PSAN copolymer and the nanocomposites are listed in **Table 6.4.** As shown in **Figure 6.13**, the T_g values of PSAN-Cab-o-sil H5 composites seem to be slightly lower than the T_g of neat PSAN although there is a change in the T_g between the various composites containing 7.5 wt%, 12.7 wt% or 20 wt% of silica. This result was also found with all PSAN-MEK-ST composites. Moreover, there is change in the T_g value when the samples were prepared with or without ultrasonication (**Table 6.4** and **Figure 6.14**). The nanocomposites prepared using the sonication method exhibited T_g close to neat PSAN. Overall, it seems that adding silica nanoparticles has little effect on the glass transition temperature of PSAN. This is consistent with some of the literature reports which showed only a small decrease in the glass transition of the PSAN nanocomposites.[10, 11] A plasticising residue, such as solvent residues, can also affect the T_g. This is an important factor to be considered in the dispersed samples as they are prepared by dissolving the polymer in THF, which is difficult to remove from the sample. The increase of the T_g of the samples prepared by the ultrasonication method is probably due to the good dispersion of nanosilica in the polymeric matrix.[36] From SEM images, it is evident that the dispersion Cab-o-Sil H5 in PSAN improves with ultrasonication compared to sample prepared by stirring the solutions (**Figure 6.15**).

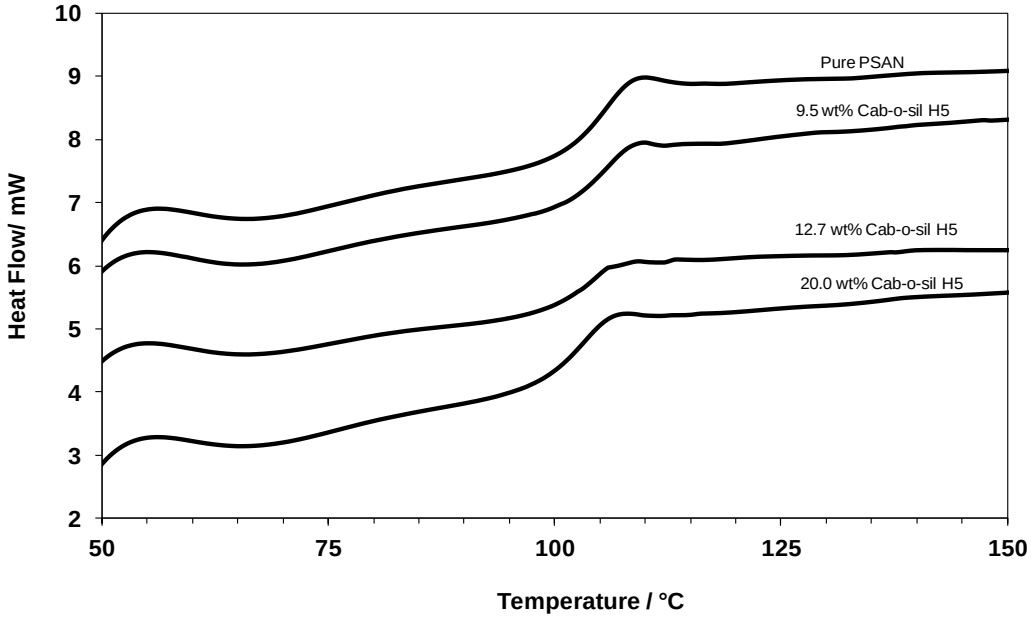

Figure 6.13: DSC traces of PSAN-Cab-o-sil H5 composites. The traces have been shifted vertically for clarity.

Table 6.4: Glass transition temperatures and heat capacity changes for various silica composites

Filler wt%	T_g / °C	ΔC_p / J g^{-1} °C^{-1}	ΔC_p / J g^{-1} °C^{-1} [d]
Pure PSAN	107	0.32	----
Cab-o-sil H5 9.5 wt% [a]	106	0.29	0.29
Cab-o-sil H5 12.7 wt% [a]	104	0.29	0.28
Cab-o-sil H5 20.0 wt% [a]	103	0.23	0.25
Cab-o-sil H5 9.5 wt% [b]	107	0.24	0.28
Cab-o-sil H5 12.7 wt% [b]	108	0.22	0.27
Cab-o-sil H5 20.0 wt% [b]	106	0.21	0.25
MEK-ST 9.5 wt% [a]	105	0.23	0.28
MEK-ST 12.7 wt% [a]	105	0.26	0.27
MEK-ST 20.0 wt% [a]	106	0.23	0.25
Error	±1	±0.01	±0.01

[a] Stirred. [b] Ultrasonication. [d] Calculated by **eq. (5.1)**.

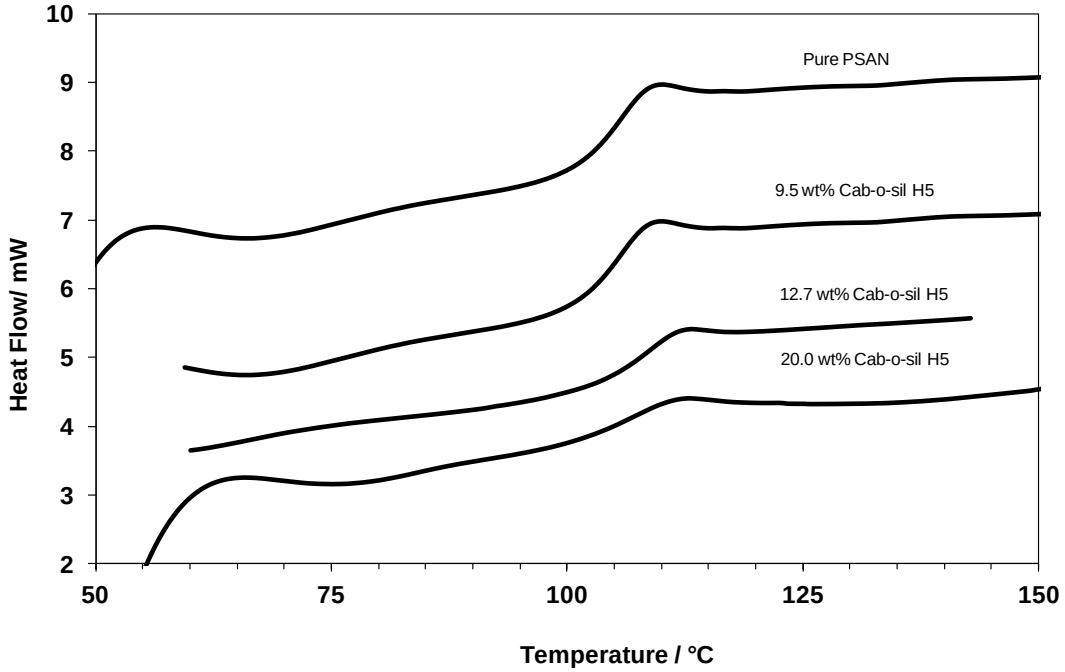

Figure 6.14: DSC traces of PSAN-Cab-o-sil H5 composites (ultrasonication). The traces have been shifted vertically for clarity

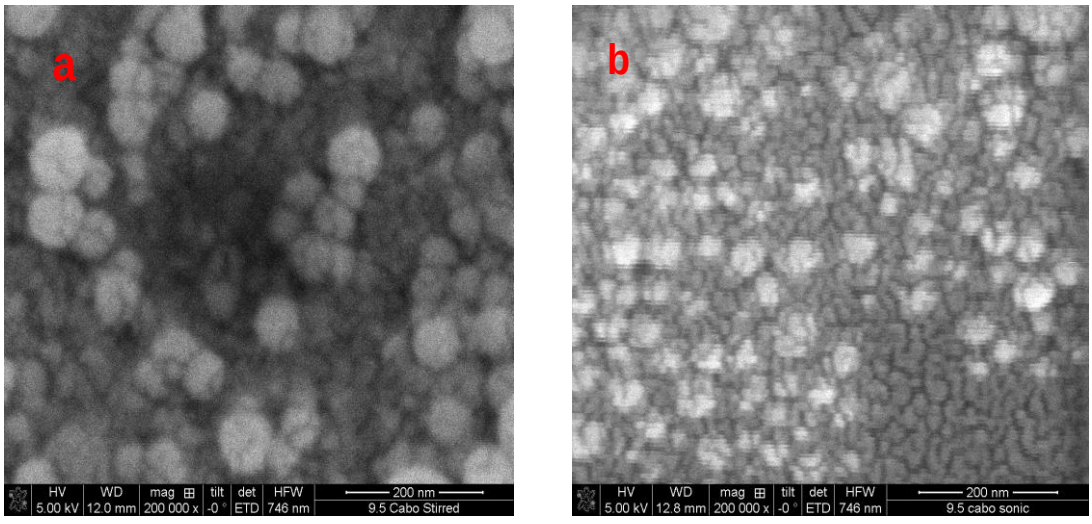

Figure 6.15: SEM micrographs of dispersed PSAN-Cab-o-sil H5 (9.5 wt%) nanocomposites prepared (a) without ultrasonication and (b) with ultrasonication.

Storage modulus *vs.* temperature curves for Cab-o-sil H5 composites (ultrasonication samples) are shown in **Figure 6.16**. The trends are similar to those reported for PMMA and PS nanocomposites. The modulus curve for unfilled PSAN shows the onset of deformation at about 120 ^{o}C, and the DMTA run stopped at 140 ^{o}C as the result of sample breakage. Addition of only 7.5 wt% Cab-o-sil H5 delayed

sample deformation significantly and made it possible to extend the DMTA measurements to 190 ^{o}C. In addition, values of plateau modulus at high temperatures show a correlation with filler content (**Figure 6.16**).

Figure 6.17 shows a direct comparison of *E′ vs.* temperature curves of Cab-o-sil H5 composites (9.5 wt%) when the samples were prepared with or without ultasonication. The ultrasonicated Cab-o-sil H5 composites display a higher overall degree of mechanical reinforcement. This may indicate a higher degree of particle dispersion (**Figure 6.15**) which leads to stronger interaction between the PSAN matrix and the unmodified Cab-o-sil H5 surface.[26, 37]

The tan δ *vs.* temperature plots (**Figure 6.18**) illustrate that the most striking difference among the curves is a broadening of the α-relaxation with increasing silica content. The tan δ size also decreases with increasing amount of filler and this is a consequence of the increasing storage modulus values with filler content, at high temperature.[38]

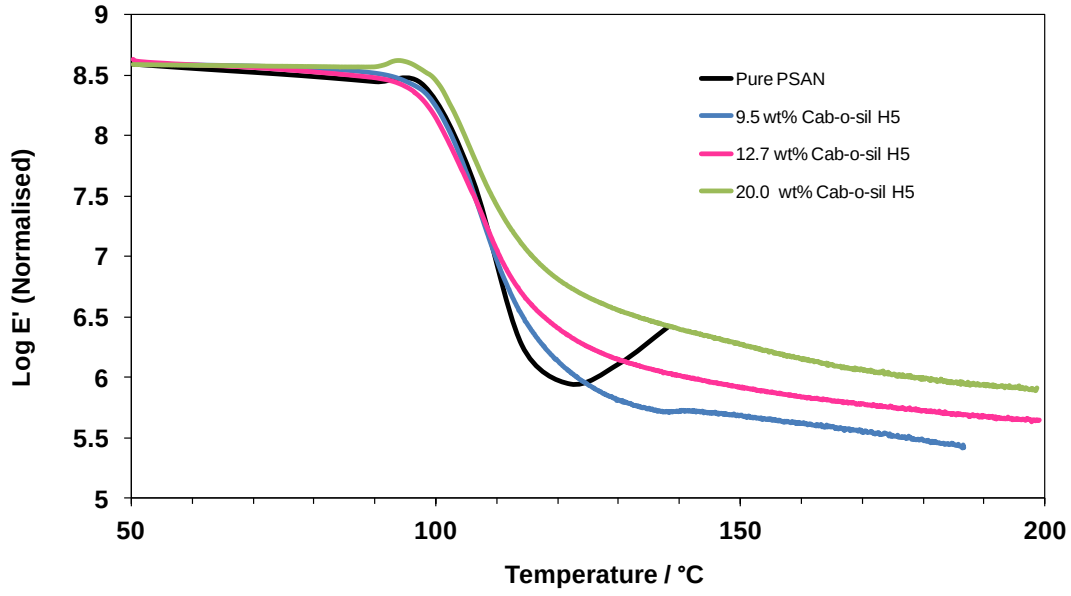

Figure 6.16: Plot of normalised storage modulus as a function of temperature for pure PSAN and dispersed PSAN-Cab-o-sil H5 composites (ultasonicated samples).

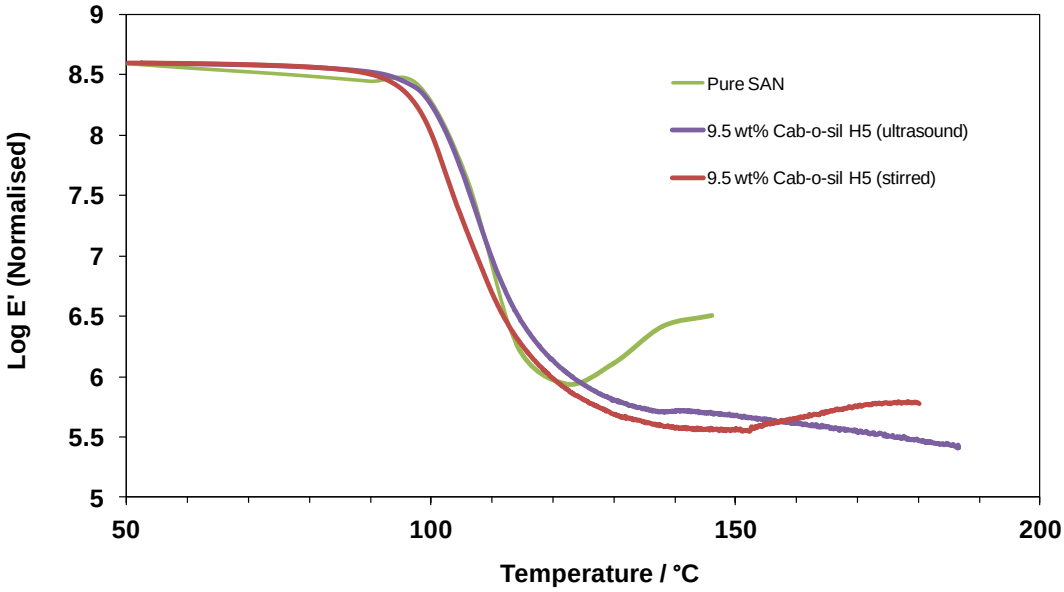

Figure 6.17: Plot of normalised storage modulus for pure PSAN and dispersed PSAN-Cab-o-sil H5 composites (9.5 wt%, using ultasonicated or without ultrasonication).

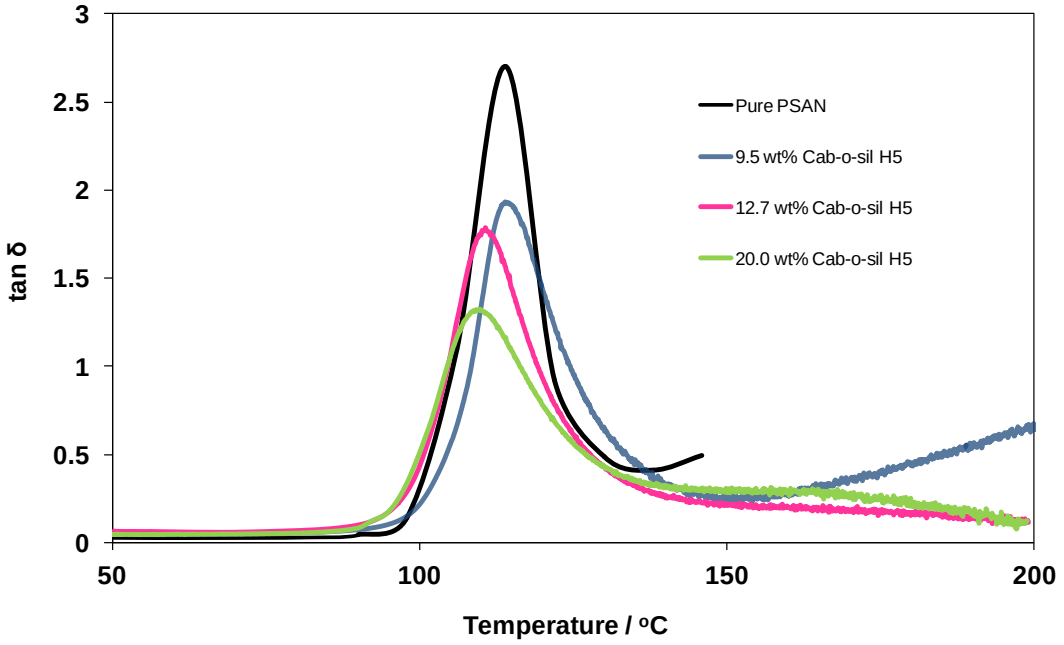

Figure 6.18: Plot of tan δ as a function of temperature for pure PSAN and dispersed PSAN-Cab-o-sil H5 composites (ultrasonicated samples).

6.3.2 DSC and DMTA Analysis of Grafted PSAN/silica Nanoparticles

PSAN-silica composites with various silica content were studied by DSC. The glass transition temperatures of grafted PSAN nanocomposites generally increased compared to neat PSAN and dispersed PSAN nanocomposites as shown by comparing **Figures 6.14** and **6.19** or **Tables 6.4** and **6.5**. This is expected based on the strong interaction between the polymer and nanofiller (covalent bond) which restricts the movement of the polymer chains[19] and is consistent with observations for PMMA and PS in this thesis (Chapter 5 and Section 6.2.2).

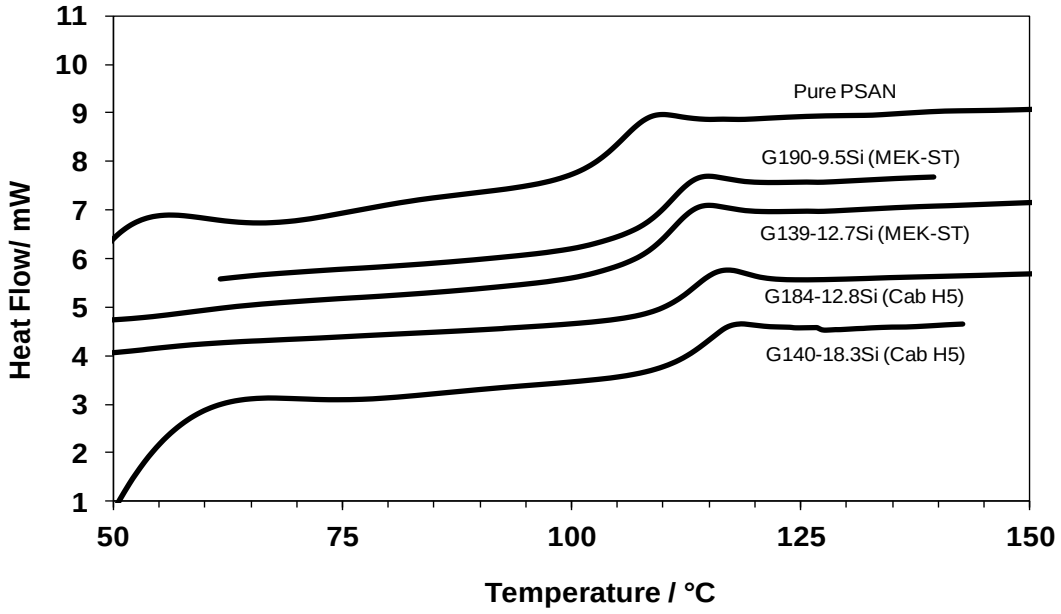

Figure 6.19: DSC traces of pure PSAN and grafted PSAN-silica nanoparticles. The traces have been shifted vertically for clarity.

Table 6.5: DSC results for various PSAN-silica composites and comparison to tan δ values corresponding to peak maximum.

Sample code	*% SiO_2*	M_w [c)] [g mol^{-1}]	T_{max} (tan δ) °C	T_g °C
PSAN	0.0	110000	114	107
G190-9.5Si [a)]	9.5	190000	116	112
G139-12.7Si [a)]	12.7	139000	122	114
G184-12.8Si [b)]	12.8	184000	115	115
G140-18.3Si [b)]	18.	140000	118	111
Error	-----	--------	±1	±1

[a)] PSAN-MEK-ST. "G190" refers to a molecular weight of 190 kg mol^{-1} for the grafted PSAN, "9.5Si" stands for a silica content of 9.5 wt%. [b)] PSAN-Cab-o-sil H5. [C)] calculated by GPC.

Figures 6.20 and **6.21** show the DMTA data (E', and tan δ) for the grafted PSAN samples prepared in this project. The normalised E' versus temperature curves once again reveal a pronounced reinforcement effect at temperatures above the glass transition. Similar to the polymer–silica mixtures studied before, the modulus of the hybrid materials containing 9.5 and 18.3% silica remained almost constant above T_g, until up to 240 °C and did not show the irreversible deformation that unfilled PSAN exhibits above 120 °C. The grafted non-aggregated silica nanoparticles samples (**G190-9.5Si** and **G139-12.7Si**) show a slightly higher storage modulus than pure PSAN before the onset of deformation; however it is the grafted aggregated silica (**G140-18.3Si)** that exhibits the greatest increase in storage modulus in the rubbery region. In addition, the tan δ *vs*. temperature plots, **Figure 6.21**, show broadening with increasing of silica content. This behaviour is similar to that observed earlier in literature.[16] As compared to the dispersed composites, grafted PSAN/silica samples display a higher storage modulus above the T_g and suppress sample deformation up to 240 °C, more than 130 °C above the glass transition of neat PSAN.

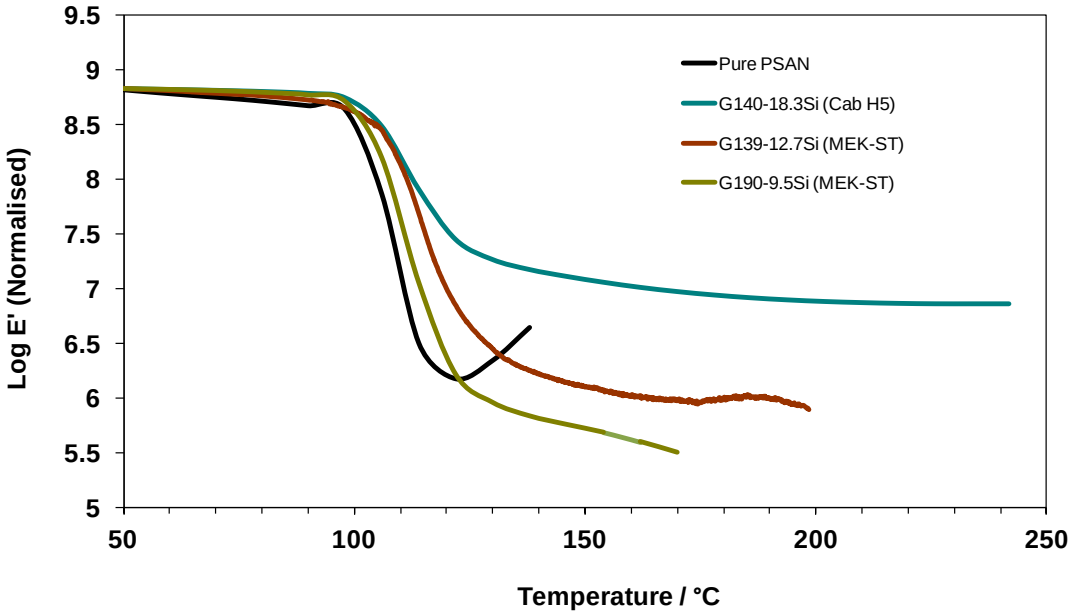

Figure 6.20: Plot of normalised storage modulus as a function of temperature for pure PSAN and grafted PSAN-silica nanoparticles prepared from MEK-ST and Cab-o-sil H5 (percentage of silica, as indicated).

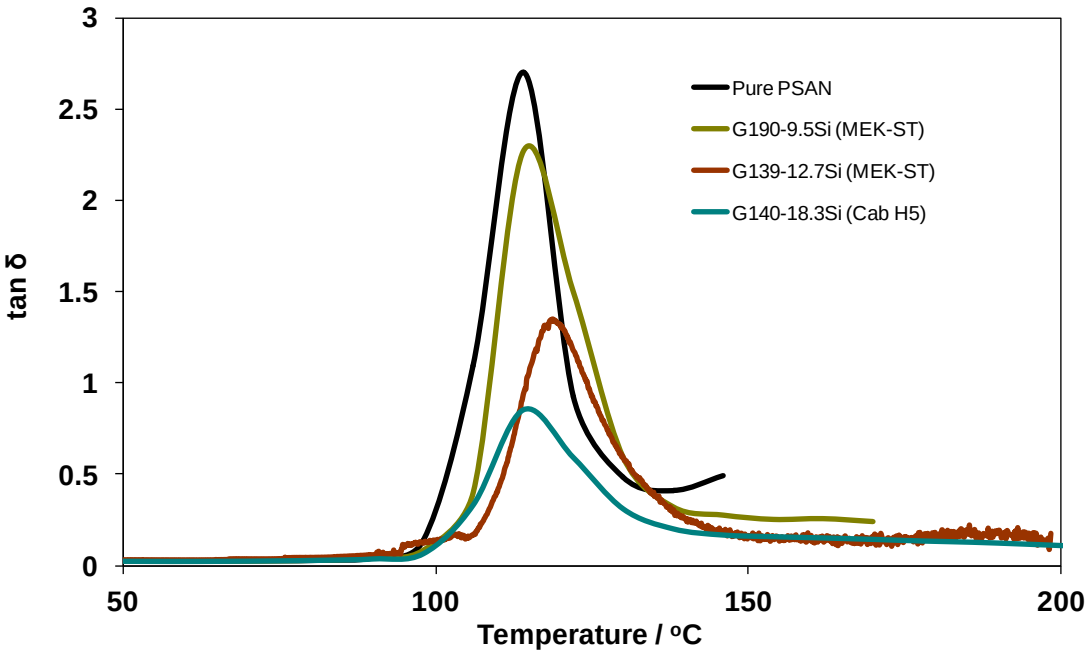

Figure 6.21: Plot of tan δ as a function of temperature for pure PSAN and grafted PSAN-silica nanoparticles prepared from MEK-ST and Cab-o-sil H5 (percentage of silica, as indicated).

To supplement the dynamic mechanical results of the pure PSAN and PSAN nanocomposites, the frequency response was studied by testing samples over a short frequency range (0.45 − 100 Hz) at a series of temperatures (66 − 200°C). An example of how the frequency-dependence of the storage modulus changes as a function of temperature is illustrated in **Figure 6.22** for pure PSAN.

The time-temperature character of the dynamic moduli in the PSAN nanocomposites was further investigated by the generating modulus─frequency master curves based on superposition principles.[28] The master curves of the storage modulus as a function of reduced frequency for both pure PSAN and grafted PSAN nanocomposites at a reference temperature of 387 K (114 °C) are plotted in **Figure 6.23.** The master curves capture the progressive improvement in mechanical reinforcement with grafting (**G140-18.3Si** and **G139-12.7Si**) and show that the frequency range over which measurements can be carried out greatly increased when the polymer is grafted to the surface of silica nanoparticles. Once again this effect is most significant when the polymer is grafted onto Cab-o-sil H5 nanoparticles (**G140-18.3Si**). Similar results have been observed for PMMA and PS nanocmposites and those results were discussed in more details in Chapters 5 and Section 6.2.2.

The parameters C_1 and C_2, WLF parameters for the pure copolymer and the nanocomposites are listed in **Table 6.6**. These parameters can be used to calculate the fractional free volume, f_0, thermal expansion coefficient of the free volume, a_f, and the fractional free volume at the glass transition temperature, f_g, as expressed by **equations 5.3**, **5.4** and **5.5** respectively (**Table 6.6**).

Figure 6.24 shows the apparent activation energies, E_a, for pure PSAN and **G140-18.3Si**, nanocomposites obtained from **eq. 5.6**. In this case the grafted aggregated composites (**G140-18.3Si)**, where the polymer is covalently attached to the surface of aggregated nanosilica the activation energies show significantly higher values across the temperature range compared to neat PSAN. The higher values for activation energy of **G140-18.3Si** is most likely caused by a stabilisation of the interphase around the silica nanopartcles by a strong chemical interaction of the polymer chains at the filler surface, aided by the aggregation of the silica particles to form a 3-D network.[31, 39] In other words, the comparison between the pure PSAN and grafted PSAN nanocomposite indicate that additional structural build-up occurred due to the strong effective

interfacial interaction between the PSAN and silica when the PSAN is grafted onto the surface of the silica.[40]

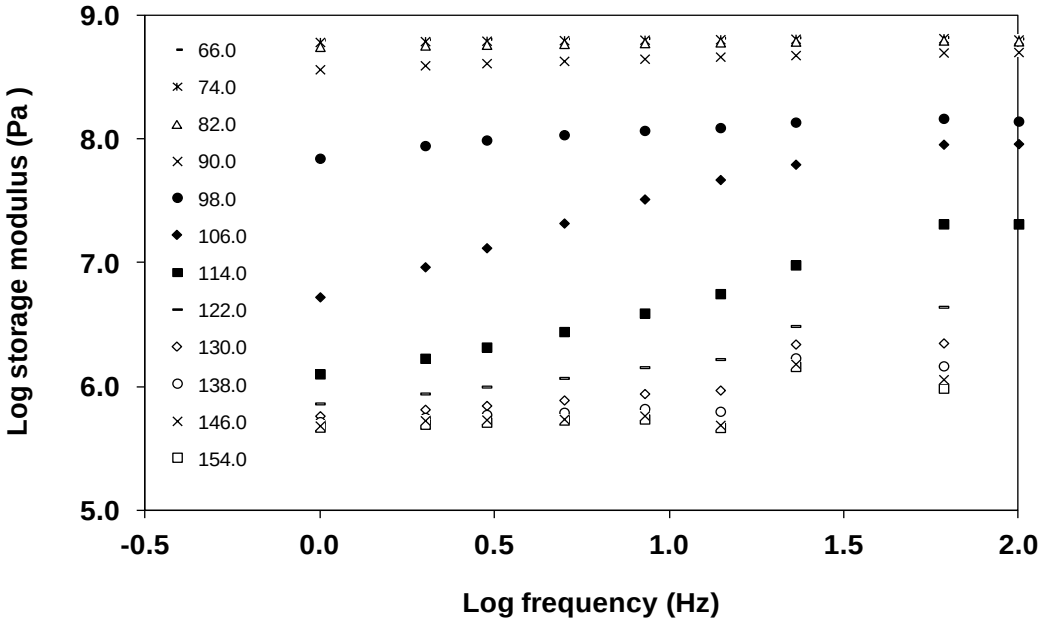

Figure 6.22: Storage modulus as a function of frequency for pure PSAN sample tested at different temperature.

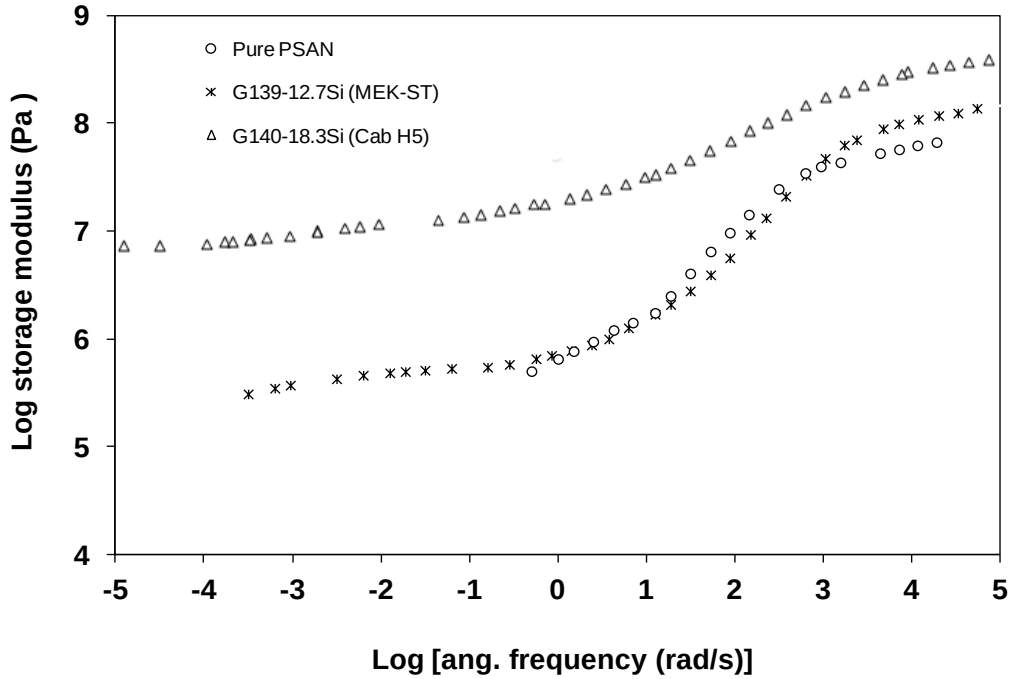

Figure 6.23: Master curves of storage modulus *vs.* frequency for pure PSAN and various grafted PSAN/ silica nanocomposites.

Table 6.6: WLF fitting parameters of pure PSAN and grafted PSAN nanocomposites.

Sample	C_1	C_2	Ref. Temp./K	T_g/K	f_0/K^{-1}	a_f	Ref.
PSAN	9.95	99.3	387	379.5	0.043	4.4 x 10^{-4}	
PSAN	7.20	146.1	443	N/A	0.060	4.1 x 10^{-4}	41
G139-12.7Si [a)]	8.97	92.93	387	386.0	0.048	5.2 x 10^{-4}	
G140-18.3Si [b)]	12.4	109.8	387	385.7	0.035	3.2 x 10^{-4}	

[a)] PSAN-MEK-ST. "G139" refers to a molecular weight of 139 kg mol^{-1} for the grafted PSAN, "12.7Si" stands for a silica content of 12.7 wt%. [b)] PSAN-Cab-o-sil H5.

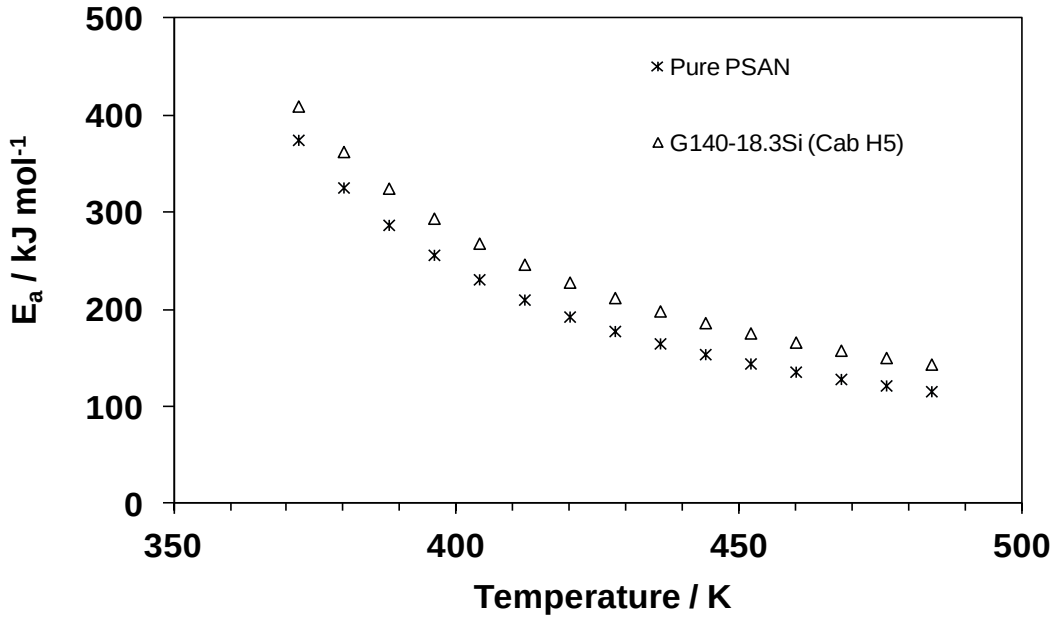

Figure 6.24: Apparent activation energy *vs*. temperature of pure PSAN and **G140-18.3Si**.

6.4 Conclusions

In summary, the influence of silica nanoparticles on the thermal, mechanical and morphological properties of PS and PSAN nanocomposites were investigated by DSC, DMTA, SEM and TEM. Whilst simple dispersion silica nanoparticles in these polymers has a negligible or little effect on the glass transition temperature, grafting the PS or PSAN from the surface of the filler nanoparticles gives materials with higher T_g compared to the neat polymer. Silica content, particle size and molecular weight all affect the thermal properties of the final composites.

Both dispersed and grafted PS and PSAN silica composites showed an increased modulus and mechanical damping properties at high temperature were also improved over neat polymers. However, the attachment of PS or PSAN chains to silica nanoparticles was particularly effective in enhancing the dynamic mechanical properties at temperature up to 130 ^{o}C above the T_g of the polymers. In addition, the storage modulus value of dispersed PSAN silica particles was also showed the increase when the composites were prepared by ultrasonication method. This is further confirmed by SEM and TEM characterisation, in which a good dispersion of particles in the PSAN was obtained.

Master curves were constructed from the storage modulus curves for pure polymers and nanocomposites, and the temperature dependence of the shift factors was found to be well described by the WLF equation. Although the apparent activation energies of neat polymers and grafted composites varied monotonically with temperature, the results indicate that molecular motion of grafted aggregated silica nanocomposites is more hindered compared to grafted non-aggregated silica nanocomposites and bulk polymer. These results suggest that it may be possible to develop mechanically reinforced hybrid materials and composites with customised mechanical property profiles at elevated temperature using cheap silica nanoparticles.

6.5 References

1. B. Xu, Y. Q. Fu, M. Ahmad, J. K. Luo, W. M. Huang, A. Kraft, R. Reuben, Y. T. Pei, Z. G. Chen and J. T. M. De Hosson, *J. Mater. Chem.*, 2010, **20**, 3442.
2. G. Havet and A. I. Isayev, *Rheol. Acta*, 2003, **42**, 47.
3. C. Triebel, P. Kunzelmann, M. Blankenburg and H. Münstedt, *Polymer*, 2011, **52**, 3621.
4. E. Kontou and G. Anthoulis, *J. Appl. Polym. Sci.*, 2007, **105**, 1723.
5. N. Jouault, P. Vallat, F. Dalmas, S. r. Said, J. Jestin and F. o. Boué, *Macromolecules*, 2009, **42**, 2031.
6. A. S. Sarvestani and C. R. Picu, *Polymer*, 2004, **45**, 7779.
7. C. Bartholome, E. Beyou, E. Bourgeat-Lami, P. Cassagnau, P. Chaumont, L. David and N. Zydowicz, *Polymer*, 2005, **46**, 9965.
8. M. A. Ver Meer, B. Narasimhan, B. H. Shanks and S. K. Mallapragada, *Acs Appl. Mater. Interfaces*, 2010, **2**, 41.
9. A. Bansal, H. Yang, C. Li, K. Cho, B. C. Benicewicz, S. K. Kumar and L. S. Schadler, *Nature Mater.*, 2005, **4**, 693.
10. P. Mélé, S. Marceau, D. Brown, Y. de Puydt and N. D. Albérola, *Polymer*, 2002, **43**, 5577.
11. V. Arrighi, I. J. McEwen, H. Qian and M. B. Serrano Prieto, *Polymer*, 2003, **44**, 6259.
12. B. J. Ash, R. W. Siegel and L. S. Schadler, *J. Polym. Sci., Part B: Polym. Phys.*, 2004, **30**, 254.
13. R. kotsilkova, D. Fagiadakis and P. Pissis, *J. Polym. Sci., Part B: Polym. Phys.*, 2005, **43**, 522.
14. G. Tsagaropoulos and A. Eisenberg, *Macromolecules*, 1995, **28**, 396.
15. Y. Y. Sun, Z. Q. Zhang, K. S. Moon and C. P. Wong, *J. Polym. Sci., Part B: Polym. Phys.*, 2004, **42**, 3849.
16. A. Kraft, V. Arrighi, P. M. E. Adams, K. Karotsis, A. McAnaw, I. J. McEwen, L. Ragupathy and C. Waring, *Polym. Prepr.*, 2007, **48**, 203.
17. P. S. Thomas, S. Thomas, S. Bandyopadhyay, A. Wurm and C. Schick, *Compos. Sci. Technol.*, 2008, **68**, 3220.
18. R. Y. Hong, H. P. Fu, Y. J. Zhang, L. Liu, J. Wang, H. Z. Li and Y. Zheng, *J. Appl. Polym. Sci.*, 2007, **105**, 2176.
19. C. J. T. Landry, B. K. Coltrain and B. K. Brady, *Polymer*, 1992, **33**, 1486.

20. P. Akcora, S. K. Kumar, V. García Sakai, Y. Li, B. C. Benicewicz and L. S. Schadler, *Macromolecules*, 2010, **43**, 8275.
21. D. A. Savin, J. Pyun, G. D. Patterson, T. Kowalewski and K. Matyjaszewski, *J. Polym. Sci., Part B: Polym. Phys.*, 2002, **40**, 2667.
22. A. P. Meera, S. Said, Y. Grohens and S. Thomas, *J. Phys. Chem. C*, 2009, **113**, 17997.
23. S. S. Sternstein and A.-J. Zhu, *Macromolecules*, 2002, **35**, 7262.
24. Z. Zhu, T. Thompson, S. Wang, Qing, E. D. von Meerwall and A. Halasa, *Macromolecules*, 2005, **38**, 8816.
25. H. M. Smallwood, *J. Appl. Phys.*, 1944, **15**, 758.
26. A. C. Comer, A. L. Heilman and D. S. Kalika, *Polymer*, 2010, **51**, 5254.
27. L. A. Pothan, Z. Oommen and S. Thomas, *Compos. Sci. Technol.*, 2003, **63**, 283.
28. M. L. William, R. F. Landel and J. D. Ferry, *J. Am. Chem Soc.*, 1955, **77**, 3701.
29. M. Mizuno, K. Nakamura, T. Konishi and K. Fukao, *J. Non-Cryst. Solids*, 2011, **357**, 594.
30. J. M. Hutchinson, *Prog. Polym. Sci.*, 1995, **20**, 703.
31. K. W. Stöckelhuber, A. S. Svistkov, A. G. Pelvin and G. Heinrich, *Macromolecules*, 2011, **44**, 4366.
32. T. K. Vaidyanathan, J. Vaidyanathan and Z. Cherian, *Dent. Mater.*, 2003, **19**, 46.
33. F. R. Schwarzl and F. Zahradnik, *Rheol. Acta*, 1980, **19**, 137.
34. J. E. Mark, *Physical Properties of Polymers Handbook*, Woodbury, New York, 1996
35. P. Cassagnau, *Polymer*, 2003, **44**, 2455.
36. Q. Wang, H. S. Xia and C. H. Zhang, *J. Appl. Polym. Sci.*, 2001, **80**, 1478.
37. A. Zhu, A. Cai, W. Zhou and Z. Shi, *Appl. Surf. Sci.*, 2008, **254**, 3745.
38. C. G. Robertson, C. J. Lin, M. Rackaitis and C. M. Roland, *Macromolecules*, 2008, **41**, 2727.
39. C. Gauthier, E. Reynaud, R. Vassoille and L. Ladouce-Stelandre, *Polymer*, 2004, **45**, 2761.
40. H. Y.Chen, E. V. Stepanov, S. P. Chum, A. Hiltner and E. Baer, *J. Plym. Sci., Polym. Phys.*, 1999, **37**, 2373.
41. J. H. Choi, J. H. Ryu and S. Y. Kim, *KOREA-AUST. RHEOL. J*, 2000, **12**, 135.

Chapter 7 - Thermal and Mechanical Properties of PBA-silica Nanocomposites and Polyester/silica Nanocomposites Resins.

Contents

7.1 Introduction

Compared to PMMA, poly(butyl acrylate) (PBA) is an industrial polymer that is used in many applications such as paints because of its good water resistance, low temperature flexibility (T_g~ −47 ^oC) and excellent weather resistance.[1] Therefore, nanocomposites of grafted PBA-silica are expected to have improved thermal and chemical resistance as well as enhanced mechanical properties such as high impact. Although few studies have been carried out on the thermal and dynamic mechanical properties of PBA-silica nanoparticles, there has been no comprehensive study about the effect of surface-grafted silica particles on thermal and mechanical properties of the nanocomposites made using both types of silica (aggregated and nan-aggreaged). Kraft *et al*.[2] have demonstrated that grafting poly(butyl acrylate) on aggreaged silica was particulary effective in improving the dynamic mechanical properties of the polymer matrix. Also studies from Carrot *et. al*. reported a small increase in the glass transition of poly(butyl acrylate) in silica composites.[3] In addition, a grafted PBA silica nanoparticle is suitable for rheological studies.[4]

This Chapter describes the thermal and dynamic mechanical properties of poly(butyl acrylate) grafted from both aggregated silica nanoparticles (Cab-o-sil H5) and colloidally dispersed silica nanoparticles (Nissan MEK-ST and MEK-ST-L) of different particle size prepared by an ATRP in miniemulsion process.

Polyester resin/silica nanoparticles are widely used in reinforced plastics in the transport and marine industries.[5] Polyester/silica nanocomposites prepared by blending have been reported to display increased mechanical properties up to a certain silica content (e.g. 2.0 wt%), but decreased mechanical performance at higher loading i.e. above 2.5 wt% silica.[6] At high filler concentration, particle–particle aggregation may dominate the mechanical response with a consequent decrease in the level of improvement. Controlling the dispersion of fillers in a polymer matrix is crucial but not always straightforward: poorly bonded particles increase brittleness and lower the composite's resistance to crack growth.[7]

To improve the dispersion of the nanoparticles and endow the compatibility between polyester matrix and nanosilica, polyester/silica nanocomposites were prepared using a mechanical and solvent-aided mixing process as described in Chapter 2. This process is advantageous since it produces a homogeneous dispersion of the filler nanoparticles in the polymer matrix (**Figure 7.1**). The dynamic mechanical properties of

a series of polyester/silica nanoparticles with different silica content (10 wt% and 20 wt%) are described in this Chapter.

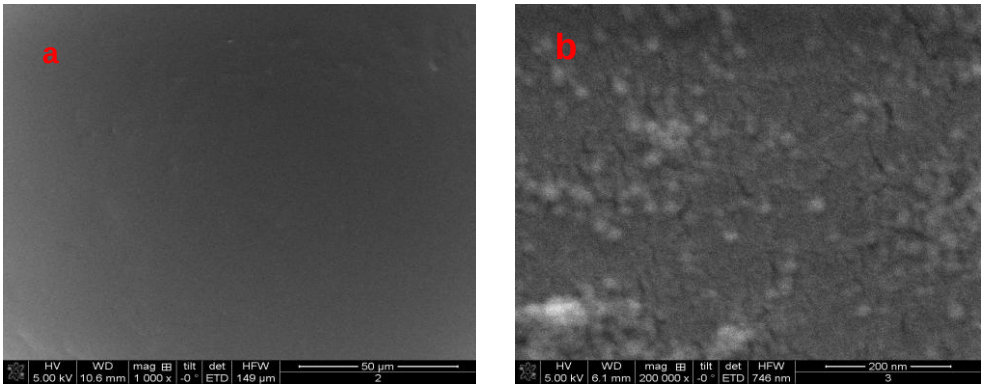

Figure 7.1: SEM micrographs of (a). Pure polyester resin and (b). Polyester-silica nanocomposites (MEK-ST 20 wt%).

7.2 DSC and DMTA Analysis of PBA/silica Nanoparticles Composites

A series of PBA-grafted silica nanoparticles with different compositions (4.5, 13.0, 20.2 and 20.6 wt%) were prepared using Cab-o-sil H5, MEK-ST and MEK-ST-L. The DSC traces of the grafted PBA nanoparticles are shown in **Figure 7.2** and glass transition temperatures reported in **Table 7.1.** As observed for other systems, grafting of PBA onto the nanoparticles slightly alters the T_g of PBA. According to the DSC measurements, the T_g values of the grafted PBA/silica nanocomposites were determined be -45.3 to -43.3 ^oC, which is close to the pure PBA T_g at -47.6 ^oC. However, there is little change in T_g with increasing filler content from 4.8 wt% (**G174-4.5Si)** to 20.6 wt% (**G193-20.6Si)** and the size and type of silica nanoparticles has no significant effect on the T_g values of the PBA matrix. For example, the T_g of both grafted PBA-aggregated silica (**G374-13.0Si)** and non-aggregated silica nanoparticles (**G193-20.6Si** and **G220-20.2Si**) are very similar. These results suggest that these changes in particle type and size have little effect on the chain mobility of the grafted PBA chains. This is in agreement with the results of Carrot et al.[3] who observed a small increase in the T_g of grafted PBA-silica composites. The authors suggested that the small difference in the glass transition could be attributed to the decrease in mobility of the grafted chains. However, Kraft *et al.*[2] observed no significant change in the T_g of grafted aggregated silica nanoparticles (Cab-o-sil H5) compared to pure PBA.

The mechanical T_g (from the tan δ maximum) values of the PBA nanocomposites are in the range of -30.7 to -32.8 °C (**Table 7.1**), as expected higher than those from DSC measurements by $5 - 12$ °C.[8] The small changes observed by DMTA are consistent with the DSC measurements.

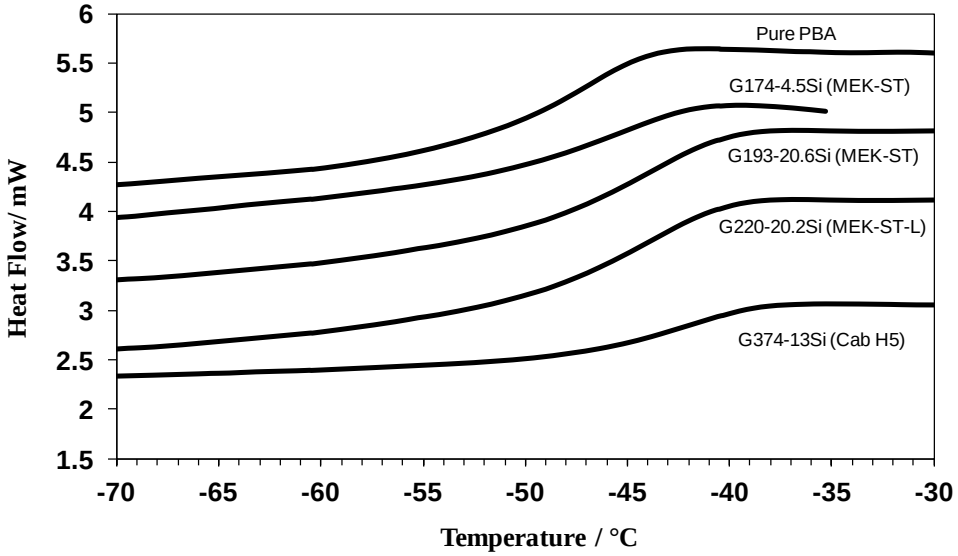

Figure 7.2: DSC traces of pure PBA and grafted PBA-silica nanoparticles. The traces have been shifted vertically for clarity.

Table 7.1: DSC results for various PBA-silica composites and comparison to T_g values obtained from tan δ maxima.

Sample	***% SiO_2***	***M_n***	***T_{max}* (tan *δ*)**	***T_g***
code		**[g mol^{-1}]**	**°C**	**°C**
Pure PBA	0.0	320000	…..	-48
G174-4.5Si [a)]	4.5	174000	-33	-45
G193-20.6Si [a)]	20.6	193000	-32	-44
G220-20.2Si [b)]	20.2	220000	-31	-44
G374-13.0Si [c)]	13.0	374000	-31	-43
Error	---	------	±1	±1

[a)] PBA-MEK-ST. "G174" refers to a number-average molecular weight of 174 kg mol^{-1} for the grafted PBA, "4.5Si" stands for a silica content of 4.5 wt%. [b)] PBA-MEK-ST-L. [c)] PBA-Cab-o-sil H5.

Although the T_g values of pure PBA are similar to those of the grafted PBA nanocomposites, the physical states of the samples, at room temperature, are different. The grafted composites are sticky solids at room temperature while pure poly(butyl acrylate) is a very viscous liquid. Although, the thermal behaviour of the grafted poly(butyl acrylate) are not improved by the addition of the nanosilica, its dynamic mechanical behaviour is however expected to be extremely different from that of the neat polymer.

Further, DMTA was used to measure the dynamic mechanical behaviour of the PBA nanocomposites. It should be mentioned that a DMTA sample could not be prepared from pure PBA as this is fluid. However, addition of only 4.5 wt% silica already allowed the sample to be prepared using a hot press. **Figure 7.3** shows the storage modulus *vs.* temperature curves for a series of PBA-silica composites with different silica content. Below the glass transition, the modulus of the polymer composites was approximately 1 GPa. It changed little until it showed a sudden drop at T_g (-45 to -43 ^oC according to DSC measurements). As usual, grafting PBA onto silica nanoparticles has virtually no effect on the modulus in the glassy region. In contrast, there is an increase in the modulus above the glass transition with increasing silica content. The storage modulus curve for 4.5 w% MEK-ST (**G174-4.5Si)** shows the onset of deformation at about $10 - 20\ ^oC$, which is absent in the composites with higher silica content (**Figure 7.3**). However, storage modulus for other composites clearly shows a large rubbery plateau which is typical of a cross-linked network. If these composites exhibited cross-links, when solvent is added, it would swell. This has been observed experimentally. The broad PDI (~2.3) is also possibly indication that the polymer is cross-linked. As observed for all aggregated nanocomposites prepared in this thesis, the highest modulus in the rubbery plateau corresponds to the aggregated silica (**G374-13.0Si)**. It is noteworthy that there is a slight difference in the modulus/temperature behaviour of PBA-MEK-ST-L **(G220-20.2Si)** and PBA-MEK-ST (**G193-20.6Si)**. MEK-ST and MEK-ST-L differ in surface area (220 and 60 m^2/g, respectively) as well as nanoparticle size (12.5 and 45 nm). There are different opinions about the effect of the particle size on the modulus of the polymer composites in the literature. Cho *et al.*[9] and Zhang *et al.*[10] demonstrated that the modulus of the composites increases with decreasing the particle size. However, other studies have shown that the increase in the storage modulus above T_g is mainly a function of the filler content.[8, 11, 12]

The T_g behaviour of the PBA/silica samples is also evaluated from the tan δ as shown in **Figure 7.4**. The tan δ peaks become smaller as the silica content increases, meaning that the behaviour progressively changes from liquid to solid like (tan δ = E''/E'). The solid-like behaviour has already been observed for filled polymers.[4, 13] Furthermore, comparing the heights of the tan δ peaks for the PBA composites at the same silica content, it is found that the peak of **G220-20.2Si** (MEK-ST-L) is higher than that for PBA-MEK-ST (**G193-20.6Si)**. This is consistent with the different surface area of these fillers; the interaction between polymer chains and filler increases with increasing surface area.[14]

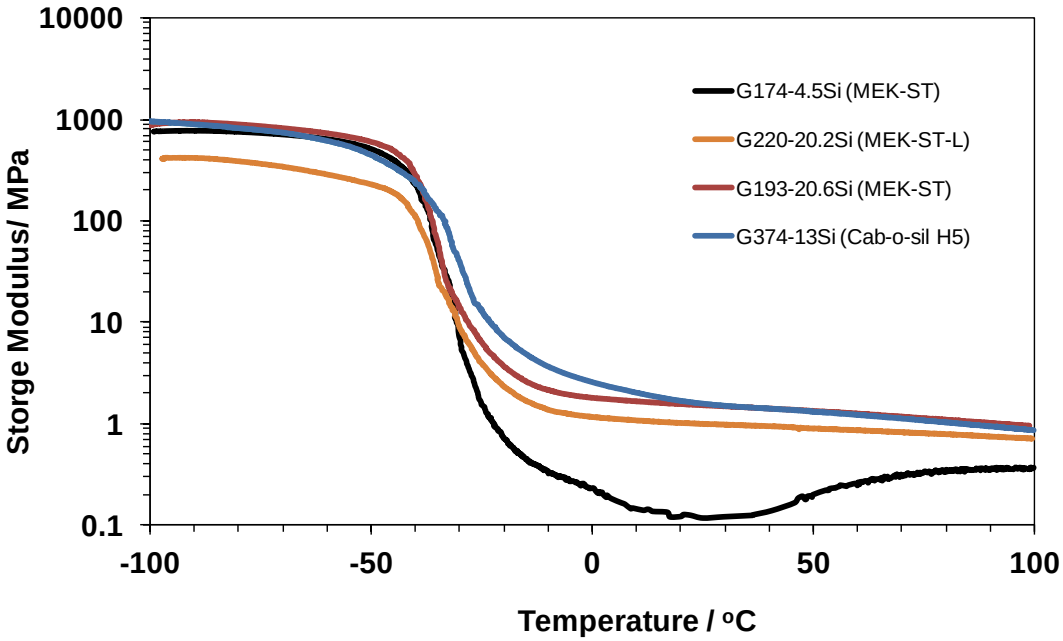

Figure 7.3: Plot of storage modulus as a function of temperature for grafted PBA-silica samples with different nanoparticles (MEK-ST, MEK-ST-L and Cab-o-sil H5) and silica content.

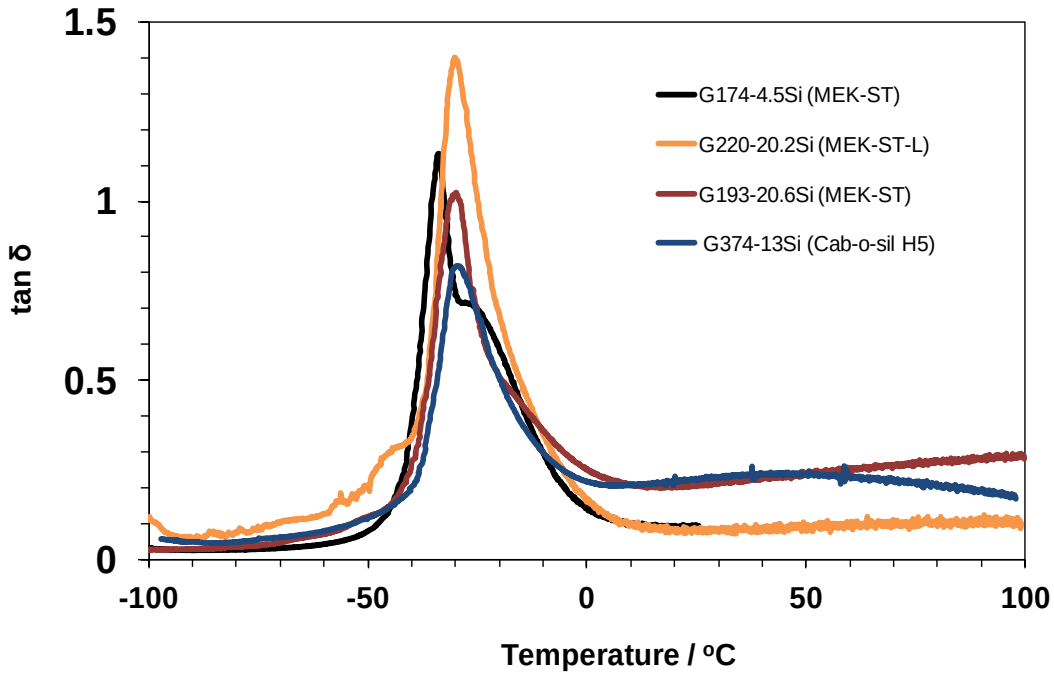

Figure 7.4: Plot of tan δ as a function of temperature for grafted PBA-silica samples with different nanoparticles (MEK-ST, MEK-ST-L and Cab-o-sil H5) and silica content.

7.3 Dynamic Mechanical Properties of Polyester/silica Nanocomposites

The effect of temperature on the dynamic storage modulus for the pure polyester resin and various nanocomposites prepared using different silica nanoparticles is shown in **Figure 7.5.** A substantial increase in the storage modulus was

observed for all polyester-silica composites resins at temperature above the glass transition. As expected, the increase in storage modulus above T_g is a function of silica content and reinforcement is once again more pronounced with aggregated silica (Cab H5 10 wt%). In addition, the polyester nanocomposites clearly show a large rubbery plateau which is typical of a cross-linked network. Below the glass transition, E' values of the composites and pure polyester resin are found to be close to each other emphasising that below the T_g the filler does not substantially alter the rigidity of the composites. A large modulus increase in the rubbery region compared to the glassy region has been also observed by Goyanes *at al.*[15] and by Vassileva and by Fridrich[16] for nano-sized filler composites. The effectiveness of silica on the modulus can be represented by a coefficient (C) as shown in **equation** (**7.1**).[17]

$$C = \frac{(E'\mathrm{g}/E'\mathrm{r})\mathrm{comp}}{(E'\mathrm{g}/E'\mathrm{r})\mathrm{resin}} \qquad (\mathbf{7.1})$$

where $E'\mathrm{g}$ and $E'\mathrm{r}$ are the normalised storage moduli in the glassy and rubbery region respectively. The lower value of the coefficient (C), the higher the effectiveness of the filler.

The measured coefficient (C) for all polyester resin-silica composites at temperature of 20 and 250 ^{o}C and frequency 1 Hz are illustrated in **Table 7.2**. As expected, the lowest value is obtained for the polyester resin with Cab-o-sil H5 (10 wt%) and the highest value for the MEK-ST sample (10 wt%). Moreover, according to values in **Table 7.2**, C of MEK-ST samples decreases with increasing silica content. This is somewhat unexpected based on Zhou *et al.*[18] and Sudirman *et al.*[5] results. These authors reported that the storage moduli of the polyester composites decrease at high filler content and attributed this to the inhomogeneous distribution of silica in the matrix. However, in the current study enhanced dispersion of silica nanoparticles in the polymer matrix was obtained by using a mechanical mixing and solvent-aided mixing technique (see Chapter 2). The morphology of nanocomposites has a large influence on their mechanical properties.[19-21] In general, highly dispersed fillers lead to improved thermal and mechanical properties. The SEM images of polyester-MEK-ST (20 wt%) shows that a good dispersion of the nanosilica in the

polyester matrix was achieved (**Figure 7.1**). This could explain the decrease in C value with increasing silica content.

Figure 7.6 displays a plot of tan δ *vs*. temperature for various polyester/silica composites. The mechanical T_g values are in the range 75 – 78 ^oC. It is apparent that there is no significant change in the main tan δ peak which is consistent with the DSC measurements. These results also indicate that no confinement of polyester chains occurred, which could restrict the segmental mobility of the matrix chains. Improvement in the interfacial bonding occurs as can be observed from the lowering in tan δ peaks. The size of the tan δ peak decreases with increasing silica content, which suggests that the mobility of the polymer chains is reduced in the hybrid materials that make up the composites. The DMTA results reveal that incorporation of both silica nanoparticles (aggregated and non-aggregated) to a polyester resin increases the mechanical properties of the nanocomposites without affecting its T_g. A similar trend was observed for banana fiber reinforced polyester composites.[22]

Table 7.2: Value of constant C and tan δ values corresponding to peak maximum and comparison to DSC glass transition.

Sample	**Silica wt%**	**C**	T_{max} **(tan** δ**)** ^oC	T_g "a" ^oC
Pure polyester resin	0.0	…	77	66
polyester resin-MEK-ST	10	0.69	78	67
polyester resin-MEK-ST	20	0.52	77	66
polyester resin-Cab-o-sil H5	10	0.23	76	66
Error	--	--	±1	±1

"a" By DSC

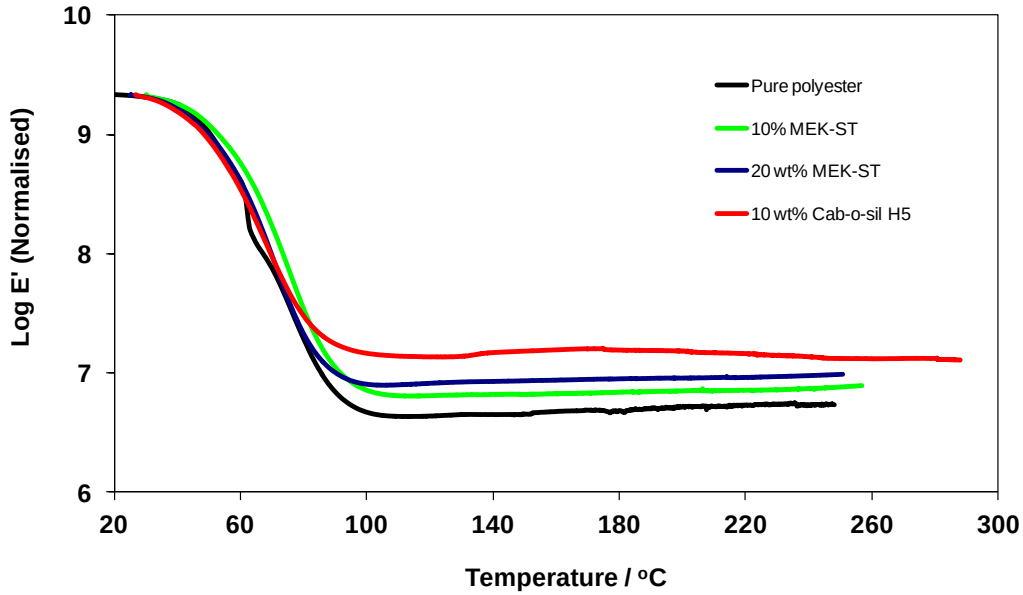

Figure 7.5: Plot of storage modulus as a function of temperature for pure polyester and dispersed polyester-silica samples with different nanoparticles (MEK-ST, and Cab-o-sil H5) and silica content.

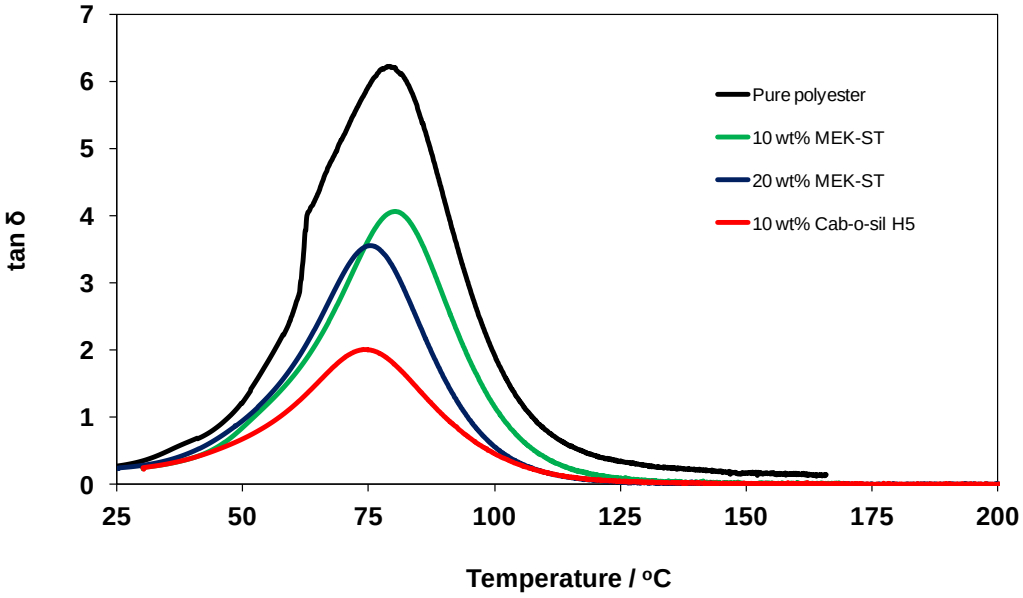

Figure 7.6: Plot of tan δ as a function of temperature for pure polyester and dispersed polyester-silica samples with different nanoparticles (MEK-ST, and Cab-o-sil H5) and silica content.

7.4 Conclusions

The reinforcement properties of two types of silica nanoparticles (aggregated and non-aggregated) were evaluated. While the T_g of PBA remained remarkably unaffected, the attachment of the PBA chains to nanosilica provided a hybrid material with virtually no high-temperature damping and an extended, reinforced, rubbery plateau at elevated temperature that is comparable to that of cross-linked polymers.

As expected, this study also demonstrated that the modulus of the nanocomposites above T_g increased with increasing nanosilica content, the reinforcement being more pronounced with aggregated silica (Cab-o-sil H5 10 wt%). In addition, particle size had little effect on the mechanical properties of PBA nanocomposites, at least in nanosilica-particle range of 12.5 ─ 40 nm in diameter.

The effect of adding nanosilica to two thermosetting resins (polyester or epoxy resin) was investigated by SEM, DSC and DMTA. It was found that the T_g values of the nanocomposites were not affected by the addition of nanosilica and were essentially similar to those of the pure resins. Morphology observations showed that the best route of dispersing the filler particles into the matrix involved mechanical mixing and a solvent-aided dispersion method. The DMTA analysis indicated that a relationship between mechanical properties and morphological structure exists in these materials. Good dispersion of silica nanoparticles plays a significant role in the reinforcement of the nanocomposites.

7.5 References

1. K. Matyjaszewski, Y. Nakagawa and C. B. Jasieczek, *Macromolecules*, 1998, **31**, 1535.
2. A. Kraft, V. Arrighi and G. N., *Polym. Mater. Sci. Eng.*, 2008, **98**, 6875.
3. G. Carrot, S. Diamanti, M. Manuszak, B. Charleux and J. P. Vairon, *J. Polym. Sci., Part A: Polym. Chem.*, 2001, **39**, 4294.
4. R. Inoubi, S. Dagreou, A. Lapp, L. Billon and J. Peyrelasse, *Langmuir*, 2006, **22**, 6683.
5. M. Anggaravidya, E. Budianto and I. Gunawan, *Procedia Chemistry*, 2012, **4**, 107.
6. Y. Chen, S. Zhou, G. Chen and L. Wu, *Prog. Org. Coat.*, 2005, **54**, 120.
7. J. Lee and A. F. Yee, *Polymer*, 2001, **42**, 577.
8. P. Dittanet and R. A. Pearson, *Polymer*, 2012, **53**, 1890.
9. J. Cho, M. S. Joshi and C. T. Sun, *Compos. Sci. Technol.*, 2006, **66**, 1941.
10. H. Zhang, Z. Zhang, K. Friedrich and C. Eger, *Acta Mater.*, 2006, **54**, 1833.
11. T. Kashiwagi, A. B. Morgan, J. M. Antonucci, M.R. Van Landingham, R. H. Harris, W. H. Awad and J. R. Shields, *J. Appl. Polym. Sci.*, 2003, **89**, 2072.
12. A. Kraft, P. M. E. Adams, V. Arrighi, J. Harkins, A. McAnaw, I. J. McEwen, S. J. Mayhew, L. Ragupathy and C. Waring, *Polym. Mater. Sci. Eng.*, 2007, **96**, 43.
13. E. Chabert, M. Bornert, E. Bourgeat-Lami, J. Y. Cavaillé, R. Dendievel, C. Gauthier, J. L. Putaux and A. Zaoui, *Mater. Sci. Eng. A*, 2004, **381**, 320.
14. G. Tsagaropoulos and A. Eisenburg, *Macromolecules*, 1995, **28**, 396.
15. S. Goyanes, P. König and J. Marconi, *Appl. Polym. Sci.*, 2003, **88**, 883.
16. E. Vassileva and K. Friedrich, *Appl. Polym. Sci.*, 2003, **89**, 3774.
17. L. A. Pothan, Z. Oommen and S. Thomas, *Compos. Sci. Technol.*, 2003, **63**, 283.
18. S. X. Zhou, L. M. Wu, J. Sun and W. D. Shen, *J. Appl. Polym. Sci.*, 2003, **88**, 189.
19. S. Ghosh, S. Goswami and L. Mathias, *J. Mater. Chem. A*, 2013, DOI: 10.1039/C1033TA10381A
20. M. Z. Rong, M. Q. Zhang, Y. X. Zheng, H. M. Zeng and K. Friedrich, *Polymer*, 2001, **42**, 3301.
21. A. Zhu, A. Cai, W. Zhou and Z. Shi, *Appl. Surf. Sci.*, 2008, **254**, 3745.
22. L. A. Pothan, Z. Oommen and S. Thomas, *Compos. Sci. Technol.*, 2003, **63**, 283.

Chapter 8 - Conclusions

Contents

8.1 Introduction

The work presented in this thesis has focused on the synthesis, characterisation and mechanical behaviour of a series of polymer nanocomposites. Methods to produce deuterated polymers have also been discussed. This chapter highlights the key findings in this thesis and the suggests future work to further understanding of effect the nanoparticles on mechanical reinforcement.

8.2 Summary

The overall conclusions are summarised in the following key points from each chapter.

8.2.1 Chapter 3

In this research, well-defined polymer nanocomposites were successfully prepared by AGET ATRP. The monomers that were successfully polymerised include methyl methacrylate, butyl acrylate, styrene and styrene-*co*-acrylonitrile. Novel ATRP initiators **1** and **2** were synthesised from commercially available compounds and then immobilised onto the surface of both aggregated (Cab-o-sil H5 and A300) and non aggregated (Nissan, MEK-ST, MEK-ST-L and IPA-ST-UP) silica nanoparticles. In ATRP both PMDETA and BPMOA served as ligands. With PMDETA as the ligand the molar mass distributions were found to be rather broad with polydispersities of 1.7 – 3.7, which indicated an uncontrolled radical polymerisation process. One reason for the poor control could be the low solubility of the copper-PMDETA complex in the organic phase (i.e. the monomer) resulting in a gradual decrease in polymerisation rate. Although the PMDETA-catalyst predominantly resided in the aqueous rather than the organic phase of the miniemulsion, it still initiated polymerisation and allowed polymer chains to be grafted from the silica surface, which was the main objective with regard to this investigation. It was possible to overcome the low solubility of the Cu-PMDETA complex by using more hydrophobic ligands such as BPMOA. With BPMOA a reduction in the polymerisation rate was observed which could be attributed to a lower radical concentration. This produced a better-controlled radical polymerisation and polymers with narrower molar mass distribution. The molar mass and polydispersity of PMMA chains grafted from silica (and subsequently cleaved) was similar to that of free PMMA formed in solution. In the case of grafted PS-silica nanoparticles the molar mass of the free polymer (3300 g mol^{-1}) was found to differ from that of the grafted PS chains (18000 g mol^{-1}). In addition, the molar mass distribution of the free polymer was slightly broader (PDI=1.24) than that of the chains grown from the surface of

silica (1.10). A possible reason for these phenomena is that all the chains in grafted PS which are attached to the particles started to grow during the early stages of the polymerisation due to the surface-bound initiator; whereas, chains formed by self-initiation in solution are continuously formed during the reaction. This result is consistent with literature reports.[1, 2] In this study the grafting density of PS obtained by the "grafting from" method was higher than the grafting densities obtained by the "grafting to" approaches reported in the literature.[3] Furthermore, ATRP of styrene with a Br-based initiator (e.g. a 2-bromoisobutyryl ester or amide initiator) is much faster and provides more control than ATRP polymerisations with a Cl-based initiator system.

In the final part of **Chapter 3**, grafting of SAN copolymers from the surface of functionalised aggregated silica as well as colloidally dispersed silica nanoparticles were discussed. For this system, the molar mass was slightly higher and molar mass distribution broader than expected for AGET ATRP polymerisation, with polydispersites of 1.6 − 2.2. The high PDI can be attributed to very small amount of Cu(II) and relatively slow deactivation. The best result was achieved when 1.0 equiv. of Cu(II) *vs*. $Sn(EH)_2$ was used. Nonetheless, the polymerisations were controlled as evidenced by the GPC results.

8.2.2 Chapter 4

A new simple method for rapid deuteration of the aromatic ring of polystyrene (PS) and poly(4-hydroxystyrene) (P4HS) under microwave irradiation was developed. Firstly, polystyrene was successfully ring-deuterated using microwave-assisted H/D exchange in "superheated" C_6D_6 at 150 °C in the presence of an ionic liquid and $EtAlCl_2$ as Lewis acid catalyst. This method was simple to carry out and shortened reaction times from several hours to 10 minutes. This approach had advantages other than time benefits. Short reaction times reduce the risk of lowering the molecular weight and broadening the molecular weight distribution. Secondly, partial H/D exchange on the aromatic ring of P4HS was achieved in D_2O–THF at 160 °C in the presence of a small amount of an acid catalyst. A ^1H NMR spectrum was recorded to determine the degree of deuteration by comparing the integrals of the hydroxyl signal, the polymer backbone signals and the aromatic region. It was found that exchange had reduced the integral of the aromatic region to ~50% after 2 × 30 minutes at 165 °C. Deuterated polystyrene was used as starting material for making deuterated poly(4-

hydroxystyrene) following a "conventional" sequence of polymer-analogous reactions: poly(4-acetylstyrene-d_4), poly(4-acetoxystyrene-d_4) and poly(4-hydroxystyrene-d_4). This method offers a cost-effective, alternative route to preparing deuterated polymers that otherwise have to be prepared from the deuterated monomers.

8.2.3 Chapters 5 and 6

The influence of different silica nanoparticles on the thermal, mechanical and morphological properties of PMMA, PS and PSAN nanocomposites were investigated by DSC, DMTA, SEM and TEM. While both DSC and DMTA measurements indicated a negligible or little effect in the glass transition temperature of polymer/silica dispersions, grafting PMMA, PS or PSAN chains from the surface of the nanoparticles gave materials with higher T_g compared to the pure polymers. As expected, filler content, particle size and molecular weight all affected the T_g of the grafted polymer. As the silica content increases, and/or the silica nanoparticle size decreases, the final composites exhibit higher T_g compared to neat polymer. Furthermore, the T_g of the grafted composites was observed to be higher than the T_g of the cleaved polymer. The largest difference in the T_g between the grafted polymer and cleaved polymer was noticed in lower molecular weight samples. This is a clear indication that, in our case, T_g changes are due to the chains being constrained at one end i.e. attached onto the surface of the silica particles.

Both dispersed and grafted PMMA, PS and PSAN silica nanocomposites showed an increased modulus and significantly lower high-temperature damping over the neat polymers. The mechanical behaviour of samples prepared by grafting chains onto non-aggregated particles such as MEK-ST (surface area = 217.6 m^2 g^{-1}, diameter = 9 to 15 nm) was found to differ considerably from that of chains bonded to aggregated silica such as Cab-o-sil H5 or Aerosil 300 (surface area = 300 m^2 g^{-1}, nominal diameter = 7 nm). Generally, it was shown that grafting leads to a constant storage modulus, at temperatures well (in some cases more than degrees) above the glass transition. By contrast, the pure polymers as well as samples prepared by dispersing the same silica particles in the polymer matrices did deform at much lower temperature. Further differences were observed depending on the state of dispersion of the particles. Evidently, a three dimensional network of silica particles is needed to achieve high modulus above T_g but grafting suppresses flow, irrespective of particle's aggregation.

These results offer a basis for designing composite materials based on polymers with controlled thermal and dynamic mechanical properties for precise application in future.

8.2.4 Chapter 7

Studies of the thermal and mechanical properties of grafted PBA-silica nanoparticles were investigated by DSC and DMTA. First of all, unlike grafted PMMA, PS and PSAN samples, T_g values of grafted PBA nanocomposites were only slightly affected by the addition of nanosilica and essentially similar to those of the pure polymer. However, the physical states of the samples, at room temperature, were different. The grafted composites were all sticky solids while pure PBA is a very viscous liquid. Therefore, the dynamic mechanical and rheological behaviour of the grafted samples was expected to be very different from that of the pure polymer. Secondly, the storage modulus of PBA composites showed a large rubbery plateau, as observed for cross-linked network. In addition, particle size had little effect on the mechanical properties of PBA nanocomposites, at least in nanosilica-particle range of 12.5 ─ 40 nm in diameter.

Polyester resin-silica composites prepared by the blending technique were also investigated in this chapter. These materials exhibited a significant improvement in mechanical properties, especially with aggregated silica. The mechanical damping at high temperature was also notably improved as evident from the tan δ *vs*. temperature plot. The morphological characterisation showed that homogeneous dispersion of silica nanoparticles into the matrix can be achieved by using mechanical and solvent-aided mixing process as shown from SEM micrographs. The above observation can be correlated with the enhancement in mechanical properties of the polyester nanocomposites.

8.3 Future Outlook

In this thesis a series of well-characterised polymer chain grafted nanoparticles have been produced. The synthetic route is simple and reproducible, making a series of future studies possible. Interesting areas of future research are highlighted below.

8.3.1 Rheological Properties of Polymer Nanocomposites

The rheological behaviour of a polymer is affected by the addition of fillers. The effect of covalently bonding chains onto nanoparticles on the flow properties is still relatively unexplored. These types of investigations are best carried out on materials with low glass transition such as the PBA samples prepared in this thesis. During the final year of the project, the synthetic route developed in this thesis was further optimised in an MChem project to prepare PBA-silica nanocomposites suitable for rheological analysis. So far only one grafted PBA sample has been tested and so future work in this area is to extend the range of grafted systems and carry out a more in-depth analysis to explain the effect of the filler on the viscosity of the polymer matrix.

8.3.2 Small-angle Neutron Scattering (SANS) of Polymer Nanocomposites

The mechanical measurements carried out on the grafted and dispersed nanocomposites have shown a series of common trends between samples. As pointed out earlier, grafting suppresses flow of the polymer chains but a three-dimensional network structure is required for reinforcement. Scattering techniques can be used to further understand how structure and morphology relate to mechanical behaviour. Both small-angle X-ray and small-angle neutron scattering (SANS) could be use as these techniques covers an appropriate length scale. SANS offers additional advantages since, through contrast variation, it is possible to investigate either the silica particles or the grafted chains. In principle SANS measurements could be carried out on any of the nanocomposite prepared in this thesis (e.g. PMMA/SAN/PS). However, deuterated samples will be needed at some stage and so PS may prove to be the best system to be studied by SANS.

8.3.3 Effect of Grafting and Particle Dispersion on the Physical Ageing

One further area of future work is physical ageing. Several studies have been reported in the literature on the effect of addition of nanoparticles on the long term properties of polymers. Enthalpy relaxation measurements on the nanocomposites prepared in this work could prove interesting particularly when comparing grafted and dispersed samples, with pure polymers.

8.4 References

1. K. Ohno, Y. Ma, Y. Huang, C. Mori, Y. Yahata, Y. Tsujii, T. Maschmeyer, J. Moraes and S. Perrier, *Macromolecules*, 2011, **44**, 8944.
2. M. N. Tchoul, M. Dalton, L.-S. Tan, H. Dong, C. M. Hui, K. Matyjaszewski and R. A. Vaia, *Polymer*, 2012, **53**, 79.
3. A. Voronov and O. Shafranska, *Langmuir*, 2002, **18**, 4471.

Appendix A1

Calculation of copolymer compositions from ^{1}H NMR integrations

The copolymer composition was calculated from ^{1}H NMR spectroscopy by comparing the integral of the aromatic proton signals at 6.66 – 7.05 ppm with the integration of the signal of the protons of the polymer backbone (styrene and acrylonitrile) at 1.15 – 2.50 ppm .

A typical calculation of the mole fraction of acrylonitrile in a PSAN close to the azeotropic composition (37 mol%) from the **^{1}H NMR** spectrum of the copolymer is set out in detail below, using PSAN-MEK-ST (12.8 wt%) as an example **(Figure A1-1)**.

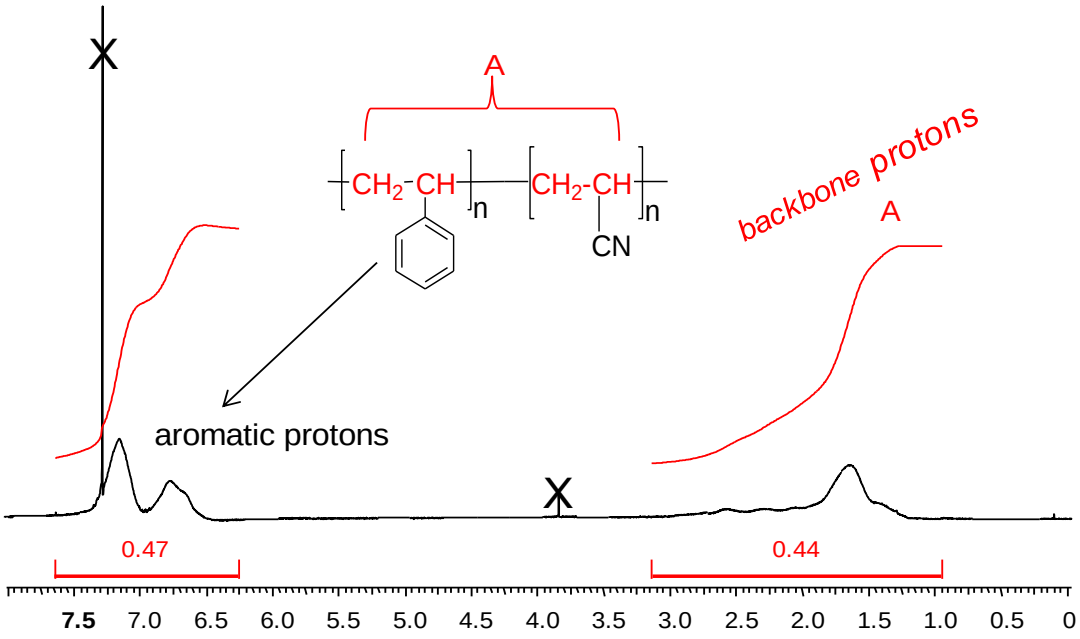

Figure A1-1: ^{1}H NMR spectrum (300 MHz, $CDCl_3$) of PSAN-MEK-ST (12.8 wt%) Solvent and impurities signals are marked by X.

The formula of the PSAN copolymers is expressed as $(C_8H_8)_x(C_3H_3N)_{1-x}$

where x is the mole fraction of styrene. The following equation was used to determine the copolymer composition

$$R = \frac{I(aliphatic)}{I(aromatic)} = \frac{0.44}{0.47} \qquad \textbf{(A1-1)}$$

where R is the ratio between the integral of the signal of the protons in the polymer backbone (styrene and acrylonitrile) in the aliphatic region and integral of the aromatic proton signals. Then the mole fraction is found by using this equation:

$$R = \frac{F_S h_S^{al} + (1 - F_S) h_{AN}^{al}}{F_S h_S^{ar} + (1 - F_S) h_{AN}^{ar}} \qquad \textbf{(A1-2)}$$

Here, h corresponds to the number of protons present in the styrene (S) or acrylonitrile (AN) repeat unit contributing to either the aliphatic h^{al} or aromatic h^{ar} region of the spectrum. F_s is mole fraction of styrene in copolymer. Considering the structure of the monomers, equation (A1-2) can be re-expressed as:

$$0.936 = \frac{3F_S + 3 \bullet (1 - F_S)}{5F_S + 0 \bullet (1 - F_S)} \qquad \textbf{(A1-3)}$$

$$0.936 = \frac{3F_S + 3 - 3F_S}{5F_S + 0}$$

Solving this equation gives:

$$F_S \approx 0.64$$

So, the mole fraction of acrylonitrile for this sample is ≈ 0.36

The reliability of this method depends, of course, on the quality of the NMR spectrum. For example, the low solubility of the modified silica nanoparticles affected the quality of the spectra by reducing the signal-to-noise ratio and broadening the signals.

Appendix A2

Calculation of copolymer compositions from elemental analysis

Elemental analysis was performed to determine both the composition of the copolymer and the percentage of silica present in the samples from the same measurement. Extrapolating backwards from the nitrogen content measured, the acrylonitrile content could be calculated. The styrene content was then calculated from the AN content.

The calculation of the mole fraction of acrylonitrile (37 mol%) in PSAN from the **elemental analysis** is set out in detail below using PSAN-MEK-ST (12.8 wt%) as an example**.** Relative atomic masses and elemental analysis results used in these calculations are listed in **Table A2-1**.

If the formula of the PSAN copolymers is expressed as $(C_8H_8)_x(C_3H_3N)_{1-x}$ where x is the mole fraction of styrene. The weight fraction of nitrogen, W_N, can be written as:

$$W_N = \frac{14.01(1-x)}{8\times12.01+8\times1.008\ \ x + (3\times12.01+3\times1.008+14.01)(1-x)} \qquad \textbf{(A2-1)}$$

$$W_N = \frac{14.01\,(1-x)}{104.144x+53.09\ 1-x}$$

Rearranging this equation leads to:

$$x = \frac{14.01-53.09\,W_N}{51.05W_N+14.01} \qquad \textbf{(A2-2)}$$

Using an experimental value of W_N = 0.0633 (in PSAN-MEK 12.8 wt%) then allows x to be determined as

~0.62

Then, the mole fraction of acrylonitrile for this sample is ~0.38

Table A2-1. Relative atomic masses and elemental analysis result for grafted PSAN-MEK-ST (12.8 wt%)

Elemental analysis results		Corrected to 100%	wt%[a)] AN content	%Silica[b)]	Relative atomic masses (g mol^{-1})
C	75.25	86.31	0.2444	12.8	12.01
H	6.42	7.36	0.1847		1.008
N	5.52	6.33	0.2398		14.01
Sum	87.19	100			

a) wt% of AN content was calculated from the percentage of C, H, and N in both styrene and acrylonitrile (Figure A2-1). Then the AN content is found by using the following equation:

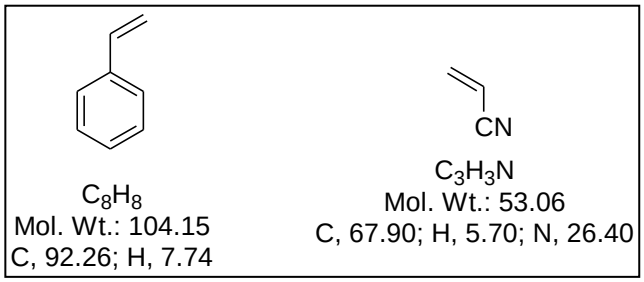

Figure A2-1: The percentage of C, H, and N in styrene and acrylonitrile comonomers.

$$C\ in\ AN\ wt\% = \frac{86.31 - 92.26}{67.90 - 92.26} = 0.2444 \qquad (\boldsymbol{A2-3})$$

$$H\ in\ AN\ wt\% = \frac{7.36 - 7.74}{5.70 - 7.74} = 0.1847 \qquad (\boldsymbol{A2-4})$$

$$N\ in\ AN\ wt\% = \frac{6.33}{26.40} = 0.2398 \qquad (\boldsymbol{A2-5})$$

b) Silica (wt%) was calculated by using equation (A2-6)

$$Silica\ wt\% = \frac{100 - 87.19}{100} \times 100 = 12.81 \qquad (\boldsymbol{A2-6})$$